



**GEO-3900**  
**Master's Thesis in Geology/Sedimentology**

**Pinchout geometry of sheet-like sandstone beds:  
a new statistical approach to the problem of lateral  
bed thinning based on outcrop measurements**

**Michal Janocko**

January, 2008  
Faculty of Science  
Department of Geology  
University of Tromsø



**GEO-3900**  
**Master's Thesis in Geology/Sedimentology**

**Pinchout geometry of sheet-like sandstone beds:  
a new statistical approach to the problem of lateral  
bed thinning based on outcrop measurements**

**Michal Janocko**

January, 2008  
Faculty of Science  
Department of Geology  
University of Tromsø



## Abstract

The pinch-out geometry of large sandbodies, such as fluvial or turbiditic palaeochannel margins and deltaic sand wedges, is of a crucial importance to the evaluation of many stratigraphic hydrocarbon traps and can generally be recognized in extensive outcrops or high-resolution seismic sections. Far more difficult to recognize and model are the digitate, feather-edge pinchouts of successions composed of sheet-like sandstone beds, such as turbidite lobes or shore-derived mid-shelf tempestites, where the individual beds may peter out at highly varied basinward distances. Both turbidites and tempestites are expected to pinch out seawards, but their actual thinning rates and pinchout geometries are little-known and unpredictable. Can the lateral variation of sheet-like bed characteristics be empirically defined?

In the present pilot study, more than 3750 closely-spaced (2-10 m lateral spacing) measurements of the lateral thickness changes in 146 turbidite and tempestite beds have been collected over lateral outcrop distances of up to 640 m. Turbidites have been measured in the Miocene Marnoso Arenacea Formation of the Northern Apennines, Italy, and the Late Cretaceous Akveren Formation of the Central Pontides, north-central Turkey, with supplementary smaller datasets from the Eocene Kusuri Formation of the Central Pontides and the Miocene Monte Fumaiolo Formation of the Northern Apennines. Tempestites have been measured in the late Miocene Karpuzçay Formation in the Manavgat Basin of Central Taurides, south-western Turkey. The spatial direction of bed thinning relative to the palaeocurrent direction has been taken into account. The datasets show that both turbidites and tempestites have a log-normal thickness frequency distribution, a trend that has been also commonly reported from bed-to-bed thickness measurements of vertical successions. In terms of an exceedence frequency plot with logarithmic scales, the log-normal distribution can be approximated by straight-line segments, which means that the bed thicknesses are self-similar (fractal) within their particular ranges. The statistical method of least-square regression has been used to identify lateral bed-thinning trends, which appear to be consistent for each genetic category of beds, but dependent upon the bed thickness range – as the downflow bed thinning rate apparently changes significantly with the bed thickness. Assuming the bed segments measured in outcrop sections represent downflow-thinning segments of unconfined (non-ponded) basin-plain turbidites and shelf tempestites, their thinning rates can be stacked together according to the local bed-thickness ranges to represent the pinchout geometry of a whole single bed. The stacking of local trends into a laterally continuous bulk trend seems to be justified by the fact that the thinner bed segments are finer-grained and composed of proportionally thinner divisions. The synthetic bulk trend appears to be a concave-upward function that flattens exponentially in the downflow direction. The range-related trend equations allow the pinchout distance of every bed in a turbiditic or tempestitic succession encountered in a well to be predicted and the net spatial pinch-out of a given bed succession to be modelled. However, the trend equations are considered to be tentative, as they require verification on a wider database.

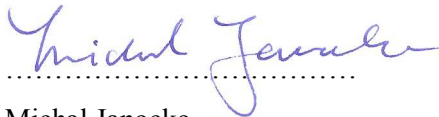
In addition, the statistical analysis revealed occurrence of bed-top undulations in both turbidites and tempestites, which are subtle to gentle and are visually unrecognizable in outcrop sections. Fourier analysis indicates statistically significant, cyclic waveform components in these undulations, with wavelengths of up to 300 m and amplitudes from a few centimetres to 60 cm. The tops of thinner beds have less pronounced and more irregular subtle undulations. The origin of the bed-top undulations is unknown, but there are several wave-like hydraulic phenomena, such as internal waves, to which they may possibly owe their formation.

## Acknowledgements

The present M.Sc. thesis reports the results of my fieldwork carried out in September-October 2006 as a part of the project 'Field reconnaissance on pinchouts' sponsored by the Hydro Research Centre, Bergen. I wish to express my gratitude to the project leader, Prof. Dr. Wojciech Nemeč (Bergen Univ.), who also acted as my external supervisor, offering both sedimentological and statistical advice and critically reading an earlier version of the thesis manuscript. I thank also Assoc. Prof. Geoffrey Corner (Tromsø Univ.), who acted as my principal supervisor and kindly took care of all the formalities related to the thesis and final examination.

For invaluable field assistance and many helpful discussions, I wish to thank Michał Warchoł, MSc (Polish Academy of Sciences, Kraków), Ediz Kirman, MSc (Ankara Univ.), Filippo d'Oriano, MSc (Florence Univ., presently at Bologna Univ.), Dr. Mehmet Cihat Alçiçek (Denizli Univ.), Dr. Volkan Özaksoy (MTA, Ankara, presently at Antalya Univ.), Dr. Massimiliano Ghinassi (Florence Univ., presently at Padova Univ.) and Dr. Carlo Messina (Bergen Univ., presently at StatoilHydro). Without their kind help, from the pre-selection of suitable outcrop sections to the reduction of physical risk in my Alpine-climb-style collecting of data on outcrop cliffs, the whole fieldwork would not be possible to carry out.

Last, but not least, I wish to thank my parents back in Slovakia for their love, unlimited encouragement and financial support given to me during the period of my studentship at the University of Tromsø.



Michal Janocko

Tromsø, 31 January 2008

# Contents

<b>1. Introduction.....</b>	<b>1</b>
<b>2. The nature of turbidites and tempestites.....</b>	<b>7</b>
2.1. Turbidites .....	7
2.2. Tempestites .....	13
<b>3. Previous studies of lateral bed-thickness changes.....</b>	<b>19</b>
3.1. Lateral trends in turbidites .....	19
3.2. Lateral trends in tempestites .....	26
<b>4. Methods and terminology .....</b>	<b>29</b>
4.1. Study methods.....	29
4.2. Terminology.....	31
<b>5. Sedimentary facies .....</b>	<b>33</b>
5.1. Turbidite facies.....	33
5.2. Tempestite facies.....	37
<b>6. The Marnoso Arenacea Formation .....</b>	<b>41</b>
6.1. Geological setting.....	41
6.2. Results .....	43
6.2.1. Bed types.....	43
6.2.2. Frequency distribution of turbidite thickness.....	43
6.2.3. Dowflow changes in bed thickness, facies, grain size, and bed-top undulations.....	45
6.2.4. Thickness changes normal to depositional dip.....	53
<b>7. The Monte Fumaiolo Formation .....</b>	<b>59</b>
7.1. Geological setting.....	59
7.2. Results .....	59
7.2.1. Bed types.....	59
7.2.2. Frequency distribution of turbidite thickness.....	60
7.2.3. Dowflow changes in bed thickness .....	62
<b>8. The Akveren Formation.....</b>	<b>63</b>
8.1. Geological setting.....	63
8.2. Results .....	66

8.2.1. Bed types.....	66
8.2.2. Frequency distribution of turbidite thickness.....	67
8.2.3. Dowflow changes in bed thickness, facies, grain size, and bed-top undulations.....	69
<b>9. The Kusuri Formation .....</b>	<b>77</b>
9.1. Geological setting.....	77
9.2. Results .....	77
9.2.1. Bed types.....	77
9.2.2. Frequency distribution of turbidite thickness.....	78
9.2.3. Thickness changes transverse to depositional dip.....	79
<b>10. The Karpuzçay Formation.....</b>	<b>81</b>
10.1. Geological setting.....	81
10.2. Results.....	83
10.2.1. Bed types.....	83
10.2.2. Frequency distribution of tempestite thickness.....	83
10.2.3. Dowflow changes in bed thickness, facies, grain size, and bed-top undulations.....	85
<b>11. Discussion .....</b>	<b>93</b>
11.1. Frequency distribution of turbidite and tempestite thickness .....	93
11.2. The downflow thinning of turbidites and tempestites .....	95
11.3. Downflow changes in grain size and facies .....	97
11.4. Predicting the pinchout geometry of turbidites and tempestites .....	98
11.5. Bed-top undulations.....	101
11.6. Thickness changes normal to palaeoflow axis .....	102
<b>12. Conclusions.....</b>	<b>103</b>
<b>References .....</b>	<b>107</b>

**Appendix**

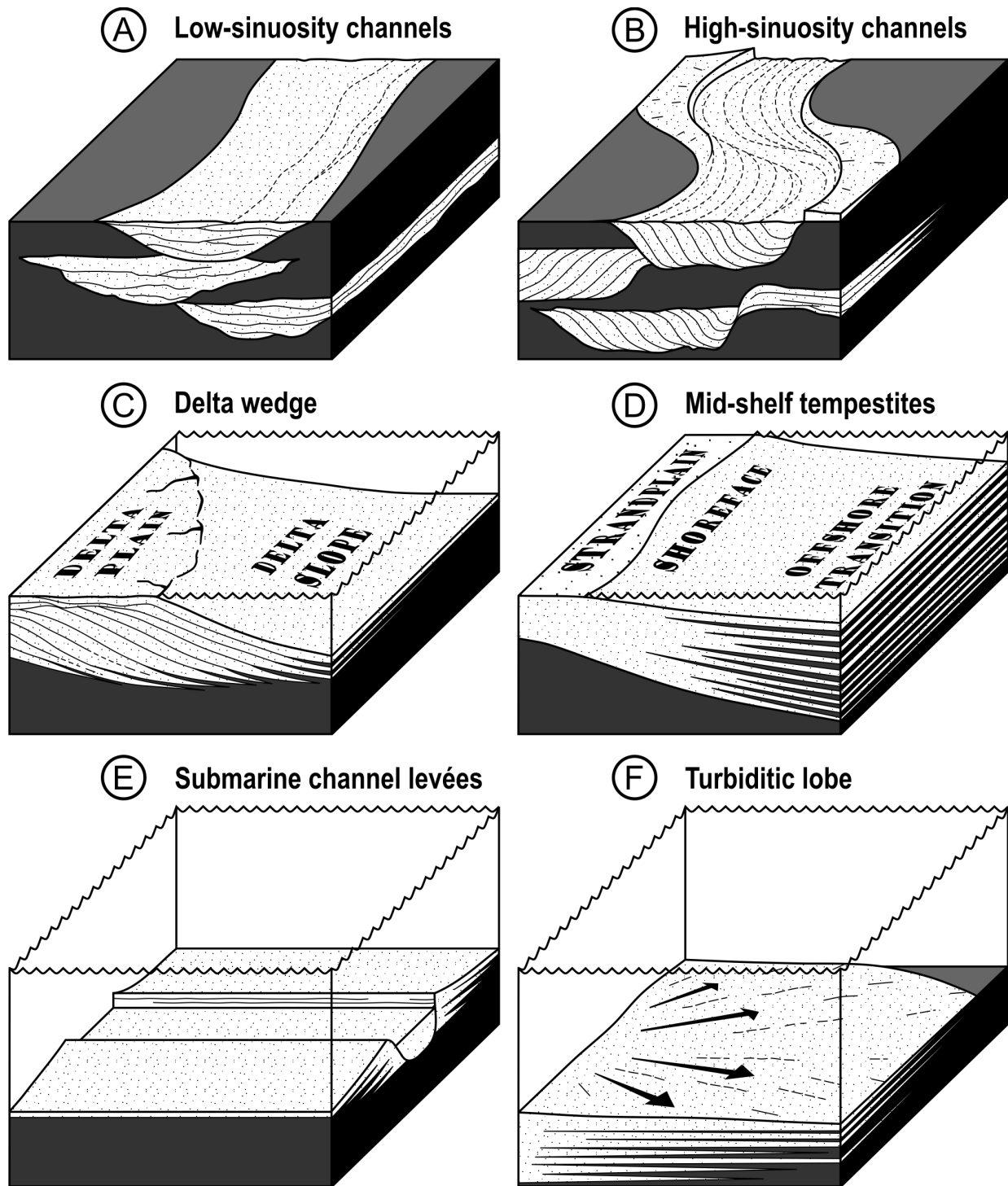
*Thickness versus Distance plots*



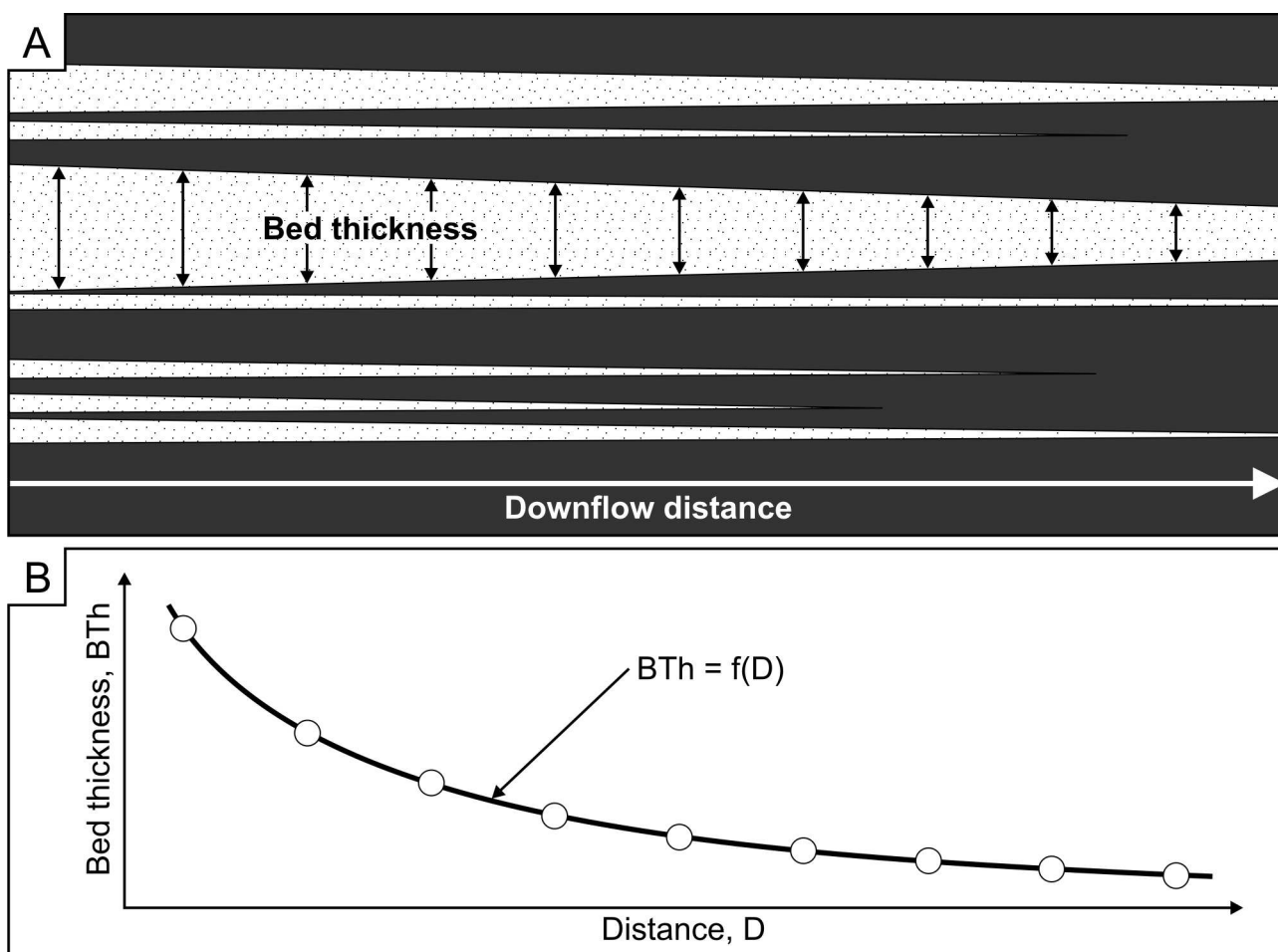
## 1. Introduction

Until less than a decade ago, the stratigraphic traps related to a lateral depositional pinchout of sandstone facies were generally classified as ‘subtle’, because their underground detection was problematic and their volume and lateral closure were uncertain. The moderate and often unimpressive reservoir volumes tentatively estimated for many such traps rendered the oil companies to rank them as ‘possible traps’ and leave for possible future consideration. However, as the global oil production has passed its peak around the turn of the century and the global consumption of oil keeps rising – the oil prices have greatly increased and so has also the interest of oil companies in a closer evaluation and possible development of subtle-trap reservoirs. An improved geological understanding of sedimentary rock successions, together with the recent advances in 3D seismic modelling and attribute analysis, have led to the recent discovery of several major reservoirs formed by depositional pinchout traps (e.g., the Tay Fm. and Maureen Fm. in the central North Sea; the Tarbert Fm. in the northern North Sea; outliers of the main Ormen Lange field in offshore mid-Norway; the Flett Fm. in the Faroe-Shetland Basin, Scotland; the Paterson Fm. in the Officer Basin, Australia; sandstone formations of the Tano Basin in offshore Ghana, Africa, and in the Hangjinqi part of the Ordos Basin in China). A great number of ‘subtle-trap’ prospects worldwide await evaluation.

Many depositional pinchouts have the form of a wedge-shaped lateral termination of an entire sandstone succession (Fig. 1A & B), as is the case with the lateral pinchout of fluvial or turbiditic palaeochannels, the lateral and distal pinchouts of fluvial mouth bars and crevasse splays or the distal pinchout of deltaic sandstone lobes. This type of *uniform* sandstone pinchout is relatively easy to recognize in seismic sections and can readily be described from large outcrop sections, and hence is not difficult to evaluate and characterize for the purpose of reservoir modelling. However, many other distal/lateral pinchouts are *diffuse*, strongly digitated in a feather-edge manner, with the individual sandstone beds separated by mudstones and pinching out at highly varied distances. Typical examples include the mid-shelf (offshore transition) successions of tempestite sandstone sheets extending several kilometres seawards from the shoreline (Fig. 1D); or the successions of sheet-like sandstone turbidites that typify non-channelized turbiditic systems as well as the terminal depositional lobes, levées and overbank deposits of channelized systems (Fig. 1E & F). These sheet-like sandstone successions are commonly a few tens to several hundreds of metres thick and several kilometres to many tens of kilometres in lateral extent, and their netto/gross sandstone volumes may thus be very considerable from a reservoir point of view. But since their lateral pinchout is non-uniform and occurs over long distances, its spatial pattern cannot be satisfactorily recognized and characterized from an outcrop section and is extremely difficult to predict in subsurface on the basis of seismic profiles and isolated wells. Simply, the sandstone beds are far beyond seismic resolution and their lateral extent cannot be directly estimated even from the most extensive outcrop sections.

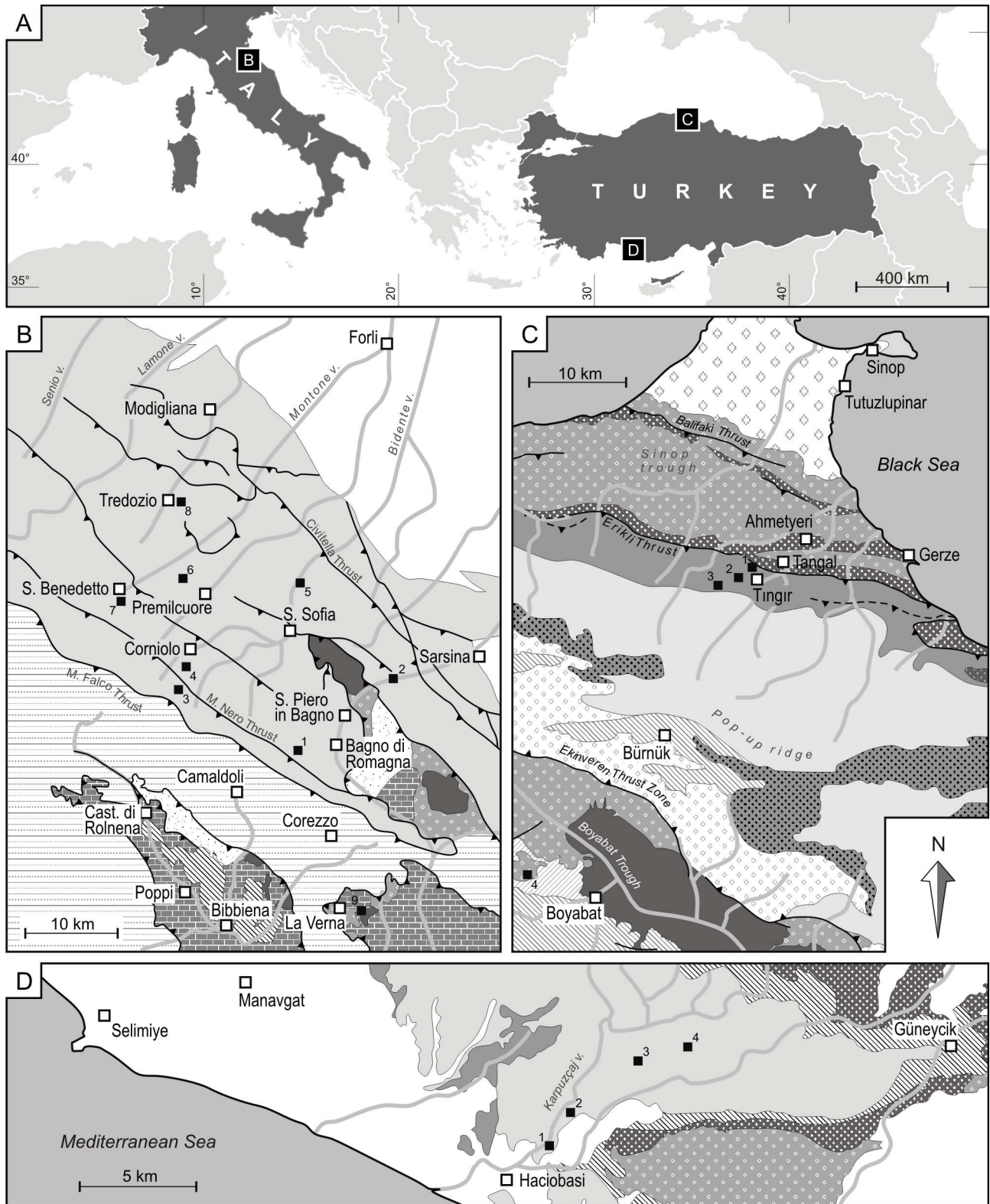


**Fig. 1.** Geometry of sandbodies formed in various depositional environments. Fluvial channel belts (**A** & **B**) are typically 2-12 m thick and a few tens to several hundred metres wide; the levées of meandering channels may be 1-2 m thick and several hundred metres in sideways extent. Deltaic sand wedges (**C**) may be a few tens of metres to several hundred metres thick and many kilometres in width and seaward extent. A similar or considerably greater extent characterizes shoreface-attached mid-shelf tempestite sandstone successions (**D**). Submarine channel sandbodies (**E**) may be several tens of metres thick and 1-2 km wide, with thick and laterally extensive levees. Turbiditic lobes (**F**) may be a few kilometres to several tens of kilometres in lateral extent. Note that the sheet-like sandstone bed successions of levees (**E**), turbiditic lobes (**F**) and mid-shelf tempestites (**D**) are characterized by a 'diffuse', highly digitate (feather-edge) pattern of lateral pinchout.






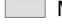

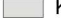




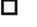



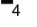
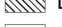





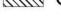








**Fig. 2.** The statistical notion evaluated by the present study is that the lateral thinning geometry of a sheet-like sandstone bed segment measured in an outcrop section (upper diagram) can be described by a characteristic trend function (lower diagram), whatever its form may be. The measured bed segments with different thickness ranges and different thinning rates can be stacked into a synthetic bulk trend characterizing a single complete “model” bed.

However, it is reasonable to expect that the limited datasets of bed-thickness measurements collected laterally in outcrop sections for beds of various thickness ranges may be mutually related by an unknown common geometrical trend (Fig. 2) and may thus be possible to interpolate by their common trend function. This notion is based on the statistical hypothesis that there is some degree of self-similarity (or fractality, see Barnsley, 1988; Feder, 1988) among the products of the same depositional process recurring in the same setting, such as the long series of turbidity currents forming a depositional lobe or the long series of storm events spreading sand to the offshore-transition zone by means of combined-flow currents. In other words, the hypothesis postulates that – in a given depositional setting and for a particular bed-thickness range – the thinning geometry of a bed produced by a large-magnitude depositional event may resemble that of a bed produced by a smaller-magnitude event. This statistical hypothesis of a partial or *range-limited* self-similarity is verified by the present study. As a result, the study postulates a new method for the estimation of



**Fig. 3.** Locality maps of the turbidite and tempestite successions selected for this study. (A) The selected study areas were in the Northern Apennines of Italy, the Central Pontides of northern Turkey and the Central Taurides of southern Turkey. The data were derived from outcrop sections of (B) the turbidites of the Marnoso Arenacea and Monte Fumaiolo formations, Northern Apennines; (C) the turbidites of the Akveren, Gürsöku and Kusuri formations, Central Pontides; and (D) the tempestites of the Karpuzçay Formation, Central Taurides.

General key	Key to B	Key to C	Key to D
 Main valley	 Recent alluvium	 Miocene - Pliocene	 Recent alluvium
 Normal fault	 Marnoso Arenacea Fm.	 Akveren Fm.	 Karpuzçay Fm.
 Thrust fault	 Monte Fumaiolo Fm.	 Gürsöğü Fm.	 Eskikoy Fm.
 Town / village	 Liguridi complex	 Yemişliçay & Kapanbogazi fm.	 Oymapinar Fm.
 Measured outcrop	 Lacustrine deposits	 Atbaşı Fm.	 Tepekli Fm.
 Fm. boundary	 Cervarola-Falterona unit	 Çağlayan Fm.	 Geceleme Fm.
	 Monte Morello Fm.	 Kusuri Fm.	
	 Canetolo complex	 Cemalettin Fm.	
		 Boyabat Fm.	
		 Bedrock	

**Fig. 3 (cont.).** Legend to the location maps in Fig. 3.

the pinchout distance of sheet-like sandstone beds, such as turbidites and tempestites, on the basis of bed-thickness datasets derived from drilling cores or vertical outcrop logs.

The datasets for the present study have been collected from a number of well-exposed turbiditic and tempestitic sandstone successions with laterally extensive outcrop sections and pre-determined palaeogeographic settings. Turbidites have been measured in the Miocene Marnoso Arenacea Formation of the Northern Apennines, Italy (Fig. 3A & B) and the Late Cretaceous Akveren Formation of the Central Pontides, north-central Turkey (Fig. 3A & C), with smaller supplementary datasets from the Eocene Kusuri Formation of the Central Pontides and the Miocene Monte Fumaiolo Formation of the Northern Apennines. Tempestites have been measured in the late Miocene Karpuzçay Formation of the Manavgat Basin, south-western Turkey (Fig. 3A & D). In total, more than 3750 measurements from 146 sandstone beds have been collected, along with systematic observations on the lateral changes in sandstone texture and primary sedimentary structures. The measurement points were spaced at 2 to 10 m, and the lateral distance spanned by the individual bed datasets was between 100 and 640 m. To ensure reliable datasets, all measurements were taken from beds that could be visually followed along an outcrop section, rather than from isolated outcrops with a subjective bed correlation.

It should be emphasized, however, that the present pilot study is little more than a preliminary attempt to find common trends in lateral bed-thinning geometry, and that the results thus need to be verified on the basis of larger datasets from a wider range of similar case studies and depositional settings.



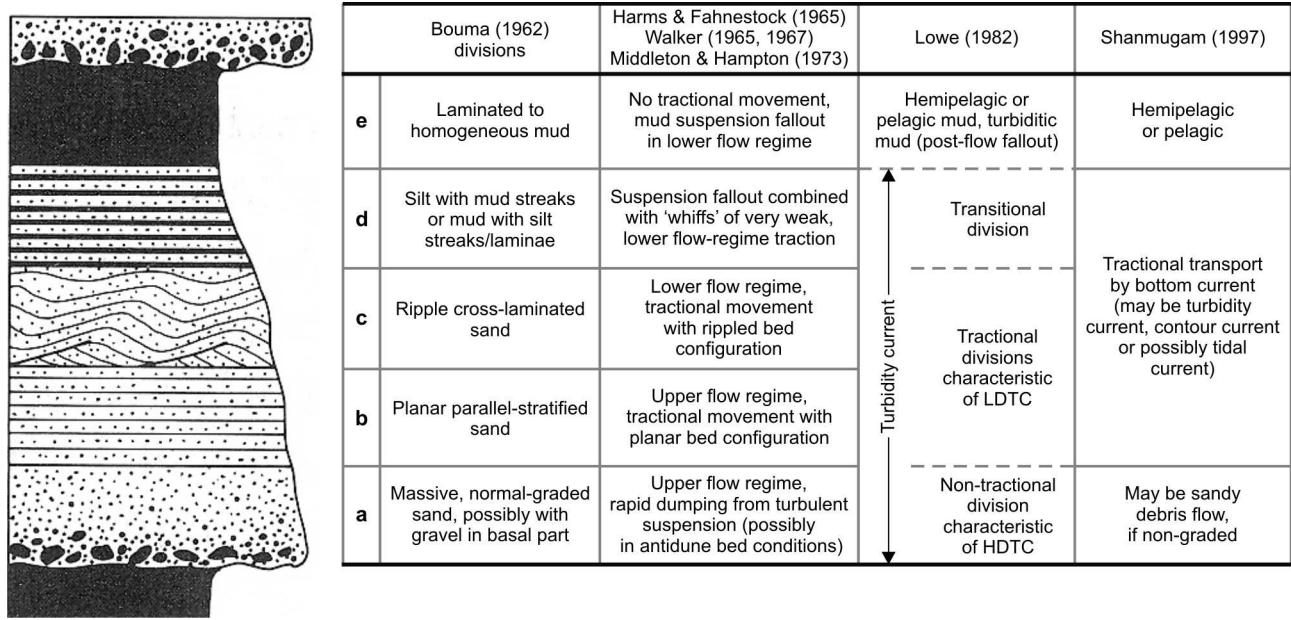
## 2. The nature of turbidites and tempestites

An extensive literature exists on the origin and depositional characteristics of turbidites (e.g., Dżułyński et al., 1959; Bouma, 1962; Mutti & Ricci Lucchi, 1972; Walker, 1978; Stow & Bowen, 1980; Hesse, 1982; Lowe, 1982; Pantin & Leeder, 1987; Middleton, 1993; Shanmugam, 1997; Kneller & Buckee, 2000; Mulder & Alexander, 2001; Talling, 2001; Felix & Peakall, 2006; Talling et al., 2007b) and tempestites (e.g., Walker, 1979; Allen, 1982; Dott & Bourgeois, 1982; Snedden & Nummedal, 1991; Myrow & Southard, 1996). In the present section, only the genesis and selected aspects of these deposits are briefly reviewed, with a focus on what may be relevant to the bed thickness variation and pinchout geometry.

### 2.1. Turbidites

Turbidites are deposits of turbidity currents (Kuenen, 1957), which are defined as subaqueous sediment-gravity flows in which the sediment particles are suspended by fluid turbulence (Middleton & Hampton, 1973). In addition to turbulence, several other mechanisms contribute to the particle support, such as the buoyancy effect of dense inter-particle fluid and particle interaction, including their hindered settling and collision-driven dispersive pressure (Middleton & Hampton, 1976; Lowe, 1982; Kneller & Buckee, 2000). The deposit of turbidity current, or turbidite, is expected to be a “graded”, fining-upward bed composed of sand and possibly gravel. Bouma (1962) recognized five component divisions of an idealized, fully-developed turbidite and labelled them in their ascending order with the letters *a*, *b*, *c*, *d* and *e*. Such a complete turbidite *abcde* is now widely referred to as the Bouma sequence (Fig. 4) and used as a standard for reference. The whole family of such complete or partial deposits (i.e., *abcde*, *bcde*, *tcde* and *tde*) are commonly called “classical” or “Bouma-type” turbidites, whereas turbidites *tde* are also known as “muddy” or “fine-grained” turbidites (Stow & Shanmugam, 1980).

The validity of the Bouma sequence as a universal standard has been widely disputed (Shanmugam et al., 1985; Hsü, 1989; Shanmugam & Moiola, 1995; Shanmugam, 1996a, b; Shanmugam et al., 1997; Shanmugam & Moiola, 1997), and even its physical interpretation has been questioned (see Fig. 4; Shanmugam, 1997, 2000). Allen (1982) and Lowe (1982) added other possible divisions, found commonly in channel-fill turbidites, and the turbidites showing evidence of very rapid non-tractional deposition (such as the Bouma *a*-division and/or the inversely-graded massive layers interpreted as basal traction carpets) are attributed to “high-density” turbidity currents (HDTCs) (*sensu* Lowe, 1982) (Fig. 5A). Accordingly, turbidites that are fully tractional (i.e., internally stratified), such as beds *bcde* or *tcde*, are considered to be products of “low-density” turbidity currents (LDTCs) (Fig. 5B).



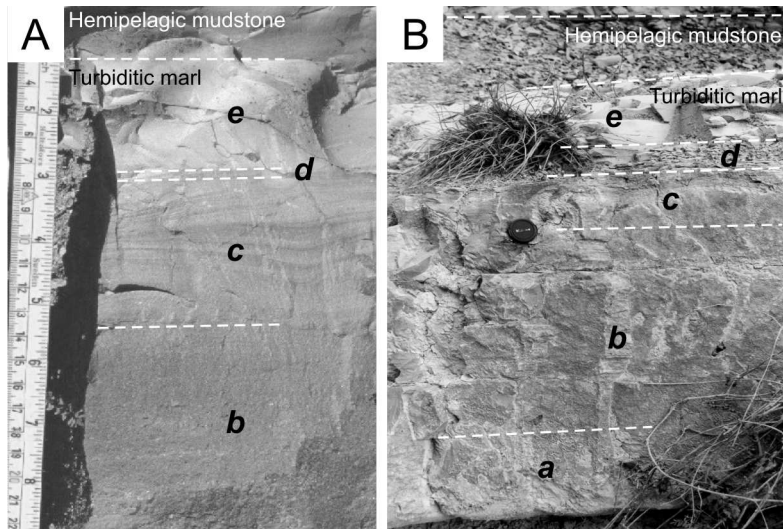
**Fig. 4.** The complete Bouma sequence comprising divisions *a*, *b*, *c*, *d* and *e*. The table summarizes the main internal characteristics of the individual divisions, as given by Bouma (1962), and the genetic interpretations given subsequently by of Harms and Fahnestock (1965), Walker (1965, 1967), Middleton & Hampton (1973), Lowe (1982) and Shanmugam (1997).

The sheet-like turbidites measured in the present study are classical turbidites, although their grading is commonly poorly developed due to the narrow grain-size range and also the massive division *a* commonly constitutes most of the bed thickness, possibly in part due to syndepositional liquefaction (see also Vrolijk & Southard, 1997). In Lowe's (1982) classification, the deposits studied are products of high- to low-density turbidity currents. The bed segments measured vary from thin (<25 cm) to moderately thick (>50 cm) and thick (>100 cm).

The local thickness of turbidite in an outcrop is generally considered to depend upon the runout distance of a particular turbidity current in the basin. The runout, or distance from the source, depends upon several factors, such as: (1) the turbidity current's original volume; (2) the current's competence and capacity; (3) the mineral composition and grain-size range of the sediment carried by the current; (4) the concentration of sediment in the current's profile and the related flow rheology; and (5) the effect of basin-floor topography on the current (e.g., flow acceleration/deceleration due to varied seafloor gradient, and possibly lateral confinement, stripping or ponding of flow).

*Flow volume* – The volume of turbidity current is thought to be determined by the magnitudes of the triggering event (Sinclair and Cowie, 2003), although the erosion and entrainment of sediment by turbidity current may considerably increase the initial flow volume. A variety of triggering mechanisms have been described from deep-water settings. Mechanisms such as slope oversteepening, slope undercutting during sea-level changes and seismic destabilization have been invoked as causes of surge-type currents, with an





**Fig. 5.** Example of turbidity current deposits from the Akveren Formation, Central Pontides. **(A)** Deposit of a low-density turbidity current (sensu Lowe, 1982) consisting of tractional divisions *b*, *c*, *d* and suspension-fallout division *e*. **(B)** Deposit of a high-density turbidity current containing a massive (non-structured) division at the base signifying rapid non-tractional deposition. Note the clear contact between the turbiditic marls (divisions *e*) and the overlying hemipelagic mudstones.

abrupt release of a finite sediment volume and with the flow thickness reflected directly in the thickness of its deposit (Kneller & Branney, 1995; Mulder & Alexander, 2001). Other triggering mechanisms, such as wave action during storms, retrogressive slumping or hyperpycnal river effluent, can produce more sustained, long-duration and quasi-steady turbidity currents, with the thickness of the resulting deposit not necessarily related to the current's actual thickness (Kneller & Branney, 1995). The thickness frequency distribution of turbidites has been approximated by power-law functions and considered to reflect the magnitude frequency distribution of the triggering events (Rothman et al., 1994; Beattie & Dade, 1996; Carlson & Grotzinger, 2001; Sinclair & Cowie, 2003).

*Flow competence and capacity* – Flow competence (i.e., the grain-size calibre and amount of sediment the flow can entrain) and flow capacity (i.e., the amount of sediment the flow can transport) are considered to be proportional to the flow volume and to be the primary controls on the thickness of deposit produced by turbidity current (Kneller & Branney, 1995). The flow competence to transport the largest particles is an indirect function of the velocity of flow, or a more direct function of the flow's sediment concentration and turbulence intensity, whereas the flow capacity for sediment transport is related to the flow power, or the energy available per unit time (Hsü, 2004).

*Character of sediment* – The thickness of turbidite is a function of grain size (Potter & Scheidegger, 1966; Rupke, 1976; Sadler, 1982; Zeng & Lowe, 1997), which in turn seems to be a function of the sediment concentration in a turbidity current, flow thickness and bottom slope (Scheidegger & Potter, 1965; Sadler, 1982). Grain size is thought to decrease downflow with the turbidite thickness in a concave-upward fashion, although this relationship may not apply if the sediment in source area is relative fine-grained and well-sorted, with a narrow grain-size range (Sadler, 1982). Calcareous particles have a lower specific density than siliciclastic particles of same size, and hence are easier entrained and kept in suspension. Coarse calcareous

material in turbidity current can undergo fragmentation during transport, thus increasing the proportion of fines in the flow, and can also undergo post-depositional brecciation in the deposit during its compaction, which may affect turbidite thickness (Seguret et al., 2001).

*Flow rheology* – Rheology is a discipline of physics at the crossroads with soil/fluid engineering (with “soil” meaning natural clastic sediment), concerned with the response of materials to shear stress. In rheology, every material (whether a sediment, fluid or their mixture) is described by its constitutive relationship between the applied shear stress and the resulting shear-strain rate. It is generally assumed that a turbidity current, much like a flowing water, has the rheological behaviour of a Newtonian fluid (i.e., the shear-strain rate increases linearly with the applied shear stress, which means a constant, strain rate-independent viscosity). In reality, this assumption is most probably incorrect for the majority of turbidity currents, because their viscosity depends directly on the volumetric concentration of sediment, which is obviously non-uniform in the flow profile and also depends strongly on the intensity of turbulent shear strain; and since the concentration and viscosity increase with a decreasing shear strain, the turbidity current is effectively a non-Newtonian “pseudoplastic” fluid (W. Nemeč, pers. comm. 2007).

There are also other rheological changes to consider. When the current decelerates and the sediment concentration in its lower part increases, the increasing flow viscosity may suppress turbulence and cause rapid sediment damping (deposition of Bouma *a*-division, Fig. 4); or a non-turbulent basal traction carpet may form and be carried along by the shearing force of the current until the carpet’s thickness becomes too great or flow power too low for pervasive laminar shear to occur and the carpet undergoes frictional plastic “freezing” (Lowe, 1982). The formation and freezing of traction carpet may occur repetitively in a turbidity current, and the reforming carpets in some flows may contain mud disseminated from the settling mud clots or flow-entrained mud clasts and thus be subject to a combined cohesive-frictional plastic freezing (the “slurry flow” of Lowe & Guy, 2000). At the distal-most reaches of the current, where the sand-depleted and mud-rich flow wanes, the intensely settling mud may suppress turbulence and render the flow laminar, or a non-shearing “rigid plug” may develop in its upper part, above the basal part subject to laminar shear (Baas & Best, 2002, 2007; Baas et al., 2005). In the case of river-generated hyperpycnal flows and limited entrainment of ambient water, the depletion of sediment load may lead, instead, to the turbidity current’s “lofting”, whereby the current or its part becomes a Newtonian fluid similar to the ambient water and eventually lifts up from the basin floor due to buoyancy reversal (Hesse et al., 2004). Flow lofting may be caused by a rapid deceleration of ponded turbidity current, causing excess fallout of mud fraction (Sparks et al., 1993) and resulting in an unusually thick mud capping (Sinclair and Cowie, 2003).

The rheological behaviour of turbidity currents may thus be complex, depending on the flow stage, mud content and grain-size composition, and this fact seems to be reflected in the apparent frustration of some authors with a detailed rheological classification of these flows (e.g., Shanmugam, 1997, 2000).

Nevertheless, a turbidity current will move and spread in the basin as a “fluidal flow” (Lowe, 1982; Nemeč, 1990), although the rate of its sediment-load depletion and hence also the spatial thickness distribution of the resulting deposit may depend on whether the fluid is actually Newtonian or non-Newtonian (W. Nemeč, pers. comm. 2007).

Recently, Talling (2001) has indicated that the thickness frequency distributions of the individual Bouma divisions in a sedimentary succession reflect the thickness frequency distribution of the entire turbidite beds. His study, from sheet-like turbidites of depositional lobes, points to a common spatial pattern of sediment-load depletion, basically independent of the current’s stage or flow regime.

*The effect of basin-floor topography* – The processes of flow ponding, stripping and lofting, as well as the erosional amalgamation of successive deposits, may have great impact on turbidite bed thickness and may also lead to erroneous interpretations of deposits in terms of their location within a turbiditic system. Flow ponding occurs when turbidity currents are trapped within a topographic confinement or in front of a topographic barrier, and this phenomenon commonly results in a dramatic thickening of deposits and/or thick sheet-like sand-mud couplets (Sinclair, 1992; Sinclair and Tomasso, 2002). Flow stripping, in turn, is a process where the finer, more dilute portion of the flow is able to detach itself from the flow and escape to be deposited elsewhere, often causing a local increase in the sand/mud ratio of the deposits. Flow stripping typically occurs on the backslopes of moderate topographic barriers or obstacles, where it may have a significant effect on the thickness of turbidite beds deposited on the upstream side of the obstacles. A typical example of this phenomenon is the inner Taveyannaz Basin of eastern Switzerland, where the thin beds in the upper part of the succession show abrupt grain-size reduction towards their tops and have been interpreted to be remnants of thicker bypassing flows subject to flow stripping (Sinclair, 1992; Sinclair and Tomasso, 2002; Sinclair and Cowie, 2003). Considerable flow stripping may also occur at sharp channel bends (Nakajima & Satoh, 2001; Fildani et al., 2006). The process of erosional amalgamation, caused by the flow response to depositional topography, generally results in an abnormal thickening of beds. Because this phenomenon drastically alters the bed-thickness frequency distribution of turbidite successions and typically occurs in base-of-slope settings, it has been used through exceedence frequency analysis as a signature of such depositional settings (Rothman et al., 1994; Rothman & Grotzinger, 1996).

Since all turbidity currents inevitably decelerate when spreading on the basin floor, the vast majority of these currents must be subject to a hydraulic jump, which means a transition from supercritical (Froude number  $Fr > 1$ ) to subcritical flow ( $Fr < 1$ ), where the flow becomes fully depositional. Topographic features, such as a break in slope or channel outlet, can localize the hydraulic jump and affect the bulk pattern of bed thickness distribution.

In other topographic settings, turbidity currents can locally accelerate and produce characteristic large-scale depositional bedforms referred to broadly as sediment waves (e.g., Normark et al., 1980; Howe, 1996;

Piper et al., 1999; Wynn et al., 2000a, b). Depending on the grain-size composition and geometric character of these bedforms, they have been variously referred to sand waves (Kenyon & Belderson, 1973; Karl et al., 1986), mud waves (Flood, 1988; Lewis et al., 1998), abyssal antidunes (Fox et al., 1968), giant ripples (Ewing et al., 1968), depositional ridges (Johnson & Schneider, 1969) and lower continental-rise hills (Rona, 1969). The sediment waves typically have wavelengths of 0.5-6 km and heights of up to 70 m, with crests commonly oriented parallel or subparallel to the strike of depositional slope (Normark et al., 1980; Lewis et al., 1998; Wynn et al., 2000b; Nakajima & Satoh, 2001), and therefore are considered to be most flow-transverse features.

These features have been reported from a wide range of depositional settings, including backslopes of channel levées (e.g., Normark et al., 1980; Lewis et al., 1998; Piper et al., 1999; Nakajima & Satoh, 2001; Fildani et al., 2006), channels (Malinverno et al., 1988; Lewis et al., 1998; Morris et al., 1998), proximal depositional lobes (e.g., Howe, 1996), as well as from the toes of deep-water Gilbert-type deltas (Bornhold & Prior, 1990; Nemeč, 1990) and the open slopes flanking volcanic islands (Schmincke et al., 1973; Wynn et al., 2000a, b). Processes responsible for the formation of these bedforms remain unclear and most of the interpretations stem from scaled laboratory experiments. The majority of sediment waves studied in outcrops and seismic sections have been attributed to “cyclic steps” (Parker & Izumi, 2000; Taki & Parker, 2005; Sun & Parker, 2005) or “chutes-and-pools” (Schmincke et al., 1973; Fralick, 1999) produced by spatial recurrence of hydraulic jumps; or to internal waves occurring at the interface of two fluids with different densities and moving relative to each other, such as a turbidity current ploughing its way under the ambient seawater (Hand et al., 1972; Normark et al., 1980; Howe, 1996, p. 231, model 1; Wynn et al., 2000b, p. 1193). Hand et al. (1972) and Vrolijk & Southard (1997) suggested that internal waves could also form as a result of internal density-layering of a turbidity current, which might explain the occurrence of sediment waves in certain parts of the deposit and not necessarily throughout its lateral extent. Density-layering of turbidity currents has been reported from laboratory experiments (e.g., Felix & Peakall, 2006).

Another possible explanation invokes internal waves propagating along the pycnocline in seawater, causing hydrostatic pressure fluctuations (cyclic loading) on the seafloor and hence effecting the deposition of sediment from turbidity currents. In order to be significantly affected by this high-moving internal waves, the turbidity currents would have to be low-concentration, low-velocity flows (Normark et al., 1980), such as those triggered by storms over the edges of shelves and distally-steep carbonate platforms or by the shoaling of internal waves over continental or deltaic slopes (Wunsch, 1969; Southard & Cacchione, 1972; Cacchione & Wunsch, 1974; Kao et al., 1985; Nemeč, 1995).

A slightly different concept explaining the formation of sediment waves stems from the lee-wave model of Flood (1988). Although this model originally referred to oceanic contour currents, it has also been invoked for turbiditic sediment waves (e.g., Howe, 1996, p. 231, model 2) and large-scale bedforms formed

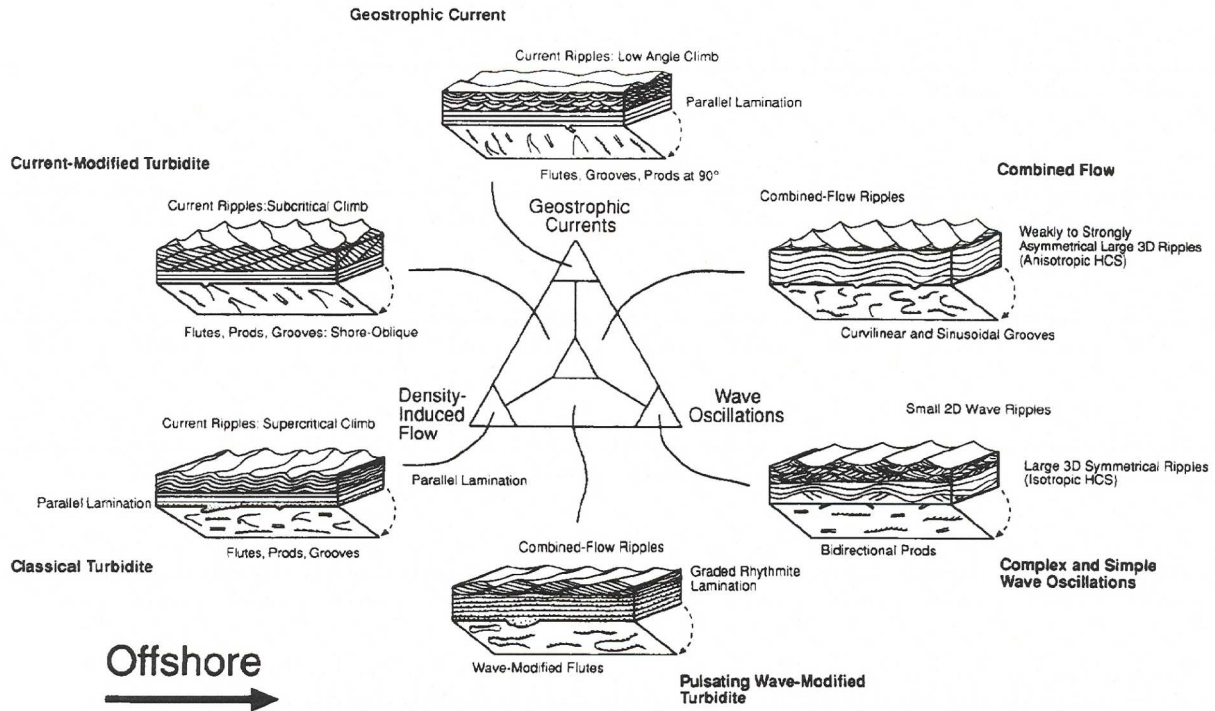
behind topographic obstacles due to hydraulic jump in a density-layered turbiditic current (Castro & Snyder, 1993; Wynn et al., 2000b). Experiments conducted by Pantin & Leeder (1987) and Edwards et al. (1994) suggested yet another mechanism that may theoretically be responsible for large-scale turbiditic bedforms. The experiments involved reflected turbidity currents and showed that internal solitons (solitary waves) generated by the reflection of a density flow from an obstacle may create large-scale bedforms, often with the shape and internal stratification of antidunes.

## 2.2. Tempestites

Tempestites (from the Latin word *tempestus* and old English noun *tempest*, which mean storm) are sheet-like sand beds formed by storms outside the inner-shelf shoreface zone. Mid-shelf successions of tempestitic sandstone sheets intercalated with mudstones may be several hundred metres thick. The exact mechanism of tempestite formation have long been disputed, with a generally notion that multiple processes may be involved. Since storm waves, much like the fairweather ones, tend to comb sand shorewards, a unidirectional seaward current has been widely invoked to explain the incursion of sand to mid-shelf zone. This notion gave rise to the concept of “combined-flow” conditions, a combined action of storm waves and unidirectional current (Harms et al., 1982; Snedden & Nummedal, 1991). The processes considered by various authors included: storm waves; wind-driven littoral currents; storm waves combined with ebbing tidal currents; storm-surge ebb currents; rip currents; tsunamis; and storm-generated density underflow currents (Hayes, 1967; Kelling & Mullin, 1975; Scott et al., 1978; Walker, 1979; Morton, 1981; Snedden et al., 1988; Snedden & Nummedal, 1991; Johnson & Baldwin, 1996). The evidence of these processes comes mainly from observation on modern shelves, whereas their distinction in the ancient sedimentary record remains to be highly problematic.

Early depositional models derived from ancient tempestites focused mainly on gravity and excess-weight forces, along the line of interpretation for deep-water turbidites. These models have been criticized by oceanographers, who can see little evidence for turbidity currents on shelves and, instead, point to the importance of storm-generated geostrophic currents. These are currents of seaward-returning water, compensating for the storm “coastal setup” (i.e., the piling of excess water mass by storm waves against the coastline) and turning gradually from cross-shelf to shelf-parallel flow direction under the influence of Coriolis force (Walker, 1979). The near-bottom sediment concentrations measured by oceanographers on modern shelves are generally too low for autosuspension, and hence the role of excess-weight forces is probably minor in the deposition of tempestites.

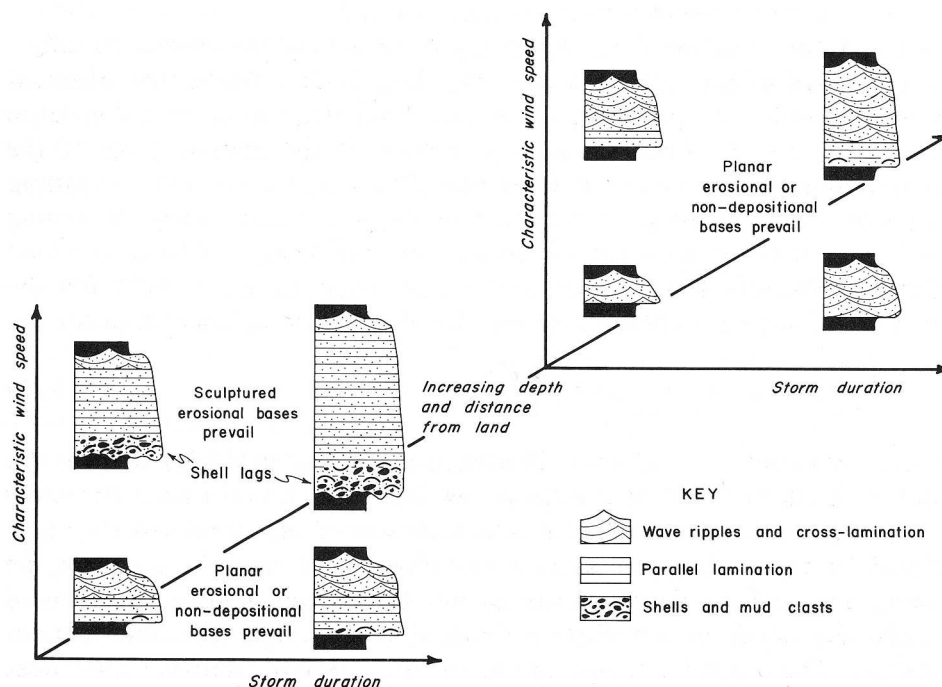
However, the tempestites formed on modern mid-shelves by the largest known storms appear to be little more than 10-15 cm thick (e.g., see Snedden et al., 1988; Snedden & Nummedal, 1991), whereas the



**Fig. 6.** Tempestite model of Myrow & Southard (1996), attributing different varieties of deposits to different combinations of storm-related processes. The end-member processes are gravitational flow due to excess weight, unidirectional geostrophic current and oscillatory wave action.

tempestites in ancient mid-shelf successions are commonly several decimetres or even more than a metre thick (e.g., Bourgeois, 1980; Dott & Bourgeois, 1982). This fact and the highly varied internal character of ancient turbidites have led some authors to suggest that the present-day wave climate of the world's shelves may be incomparable to the ancient climates and that the origin of ancient tempestites may thus be best explained by nonactualistic processes, with excess-weight forces possibly as an important factor (e.g., Duke, 1985; Duke et al., 1991). One of the most recent attempts to explain the wide range of sedimentary structures found in tempestites is by Myrow & Southard (1996), who used a ternary diagram (Fig. 6) to invoke combinations of three end-member processes: geostrophic currents, oscillatory waves and density-induced flow. A wide range of hydraulic conditions is thus envisaged as possibly resulting for storm events, and this notion may serve as a guide to the interpretation of modern and ancient tempestites. Myrow & Southard (1996) also suggested possible introduction of sediment by river floods, earthquakes and other catastrophic processes to explain the relatively great maximum bed thicknesses of many ancient tempestite successions.

Allen's (1982) model, shown in Fig. 7, may serve as an additional guide to the variation in tempestite beds. According to this model, tempestites are seaward-thinning sheets of allochthonous sand with sharp erosional bases that often exhibit offshore-directed scours, rill- and flute-marks. Grain-size grading, or upward fining, is expected to be more pronounced in the upper part or near the top, rather than in the lower



**Fig. 7.** Hypothetical variation in tempestites postulated by Allen (1982). The three-dimensional graph shows how a single storm deposit evolves as a function of characteristic wind speed and storm duration with increasing depth and distance from the shoreline.

part of the bed. The lack of grading is thought to reflect stable full-storm stage of deposition. Basal lags of shells and/or foreshore-derived fine gravel may also occur. The bed top is characteristically sharp, with an abrupt change from sand to mud, which contrasts with the gradational tops of turbidites (cf. Fig. 4). The internal stratification in the inner-shelf segment of tempestite would typically comprise planar parallel-stratification overlain by hummocky or swaley cross-stratification and covered with wave-ripple cross-lamination at the top. The mid-shelf bed segment will be thinner, finer-grained and possibly better graded (provided that the sand is not too well-sorted), internally composed of planar parallel-stratification and wave-ripple cross-lamination, possibly with climbing ripples. The outer-shelf bed equivalent will be a layer of laminated, silty hemipelagic mud, usually homogenized by bioturbation (Allen, 1982).

The controls on the thickness of tempestite beds are thought to be somewhat similar to those on turbidites. They include: (1) the volume of sediment entrained and spread seawards by storm; (2) the textural and mineralogical character of nearshore sediment source; (3) the hydraulic competence and capacity of storm event; (4) the hydraulic mode and spatial pattern of sediment dispersal; (5) the magnitude of oscillatory waves; and (6) shelf floor topography. Some of these factors are discussed briefly below.

*Entrained sediment volume* – The volume of sediment entrained by storm depends chiefly upon the magnitude of the storm event and the availability and erodibility of sediment in the nearshore zone (foreshore to shoreface). This relationship has recently been considered in quantitative terms by Storms et al.

(2002), with the implication that a close correspondence can be expected between the storm's capacity to entrain sediment and its competence to spread the sediment seawards.

*Wave oscillations* – Oscillatory waves and their parameters play crucial role in the entrainment of sediment and formation of tempestites (Storms et al., 2002). A new light has recently been shed on this issue by the experiments of Dumas & Arnott (2006) on the formation of hummocky cross-stratification. Isotropic 3-D hummocky bedforms were generated under long wave periods (~8–10 s) and moderate oscillatory velocities ( $U_o$  ~50–90 cm/s) with very weak (<5 cm/s) to no unidirectional flow. Hummocks became anisotropic with the addition of only a small unidirectional current (5–10 cm/s), and began to resemble unidirectional dunes when the unidirectional current was increased above 10 cm/s. Synthetic aggradation of the hummocky bedforms at high (4.2 mm/min) and low (1 mm/min) rates generated stratification resembling hummocky and swaley cross-stratification, respectively. Based on these findings, the authors suggest that hummocky cross-stratification optimally forms above (but close to) storm wave base where aggradation rates during storms are high enough to preserve hummocks but unidirectional current speeds are sufficiently low to generate low-angle, isotropic cross-stratification. Swaley cross-stratification is hypothesized to be deposited between fairweather and storm wave base, but in shallower water, where aggradation rates are low enough to cause preferential development and filling of erosional swales.

If the shelf water is not too shallow and/or wave energy is not strong enough to disperse sediment throughout the water column, the near-bottom turbulence added by waves can enhance density underflow. Such flows have been referred to as “wave-modified turbidity currents” (Myrow & Southard, 1996), but should better be considered as “density-modified” storm ebb surges or geostrophic currents. The turbulence added by waves reduces deposition from suspension, maintaining elevated density and hence allowing for gravitational driving force (Myrow & Southard, 1996). In contrast, when large waves are mixing strongly the entire water column, they can disrupt the efficiency and lateral continuity of seaward sediment transport.

*Shelf topography* – Shelves are generally very gently-sloping ( $0.01$ - $0.1^\circ$ ) areas of low topographic relief, smoothed by hemipelagic sediment accumulation, although some shelves are more inclined ( $1$ - $3^\circ$ ) and/or have pre-existing topography that may have a considerable effect on storm sand dispersal (Snedden & Nummedal, 1991). Modern storm-dominated shelves abound in relict large sand bodies (shoal retreat massifs, linear sand ridges, low-relief sand shoals) formed during the Holocene transgression, and these deposits are presently reworked or maintained as local depocentres by storm activity (Boggs, 2001). Large bedforms, in the form of sand patches, sand waves and sand ridges/ribbons, are common on tide-dominated shelves. On narrow shelves, an impinging contour current or shelf-wide littoral current may contribute to along-shelf sediment dispersal.

The seaward dispersal of sand by storm events has commonly been modelled on the basis of geometry (i.e., with the eroded sediment volume distributed seawards to the storm wave base as a wedge) or using the



physical law of diffusion. Similar models have been widely used for sand dispersal by turbidity currents. The results may not necessarily be unrealistic, although neither of these model types has much relevance when it comes to the actual processes that control sediment transport and a process-based modelling should preferably be used (Storms et al., 2002). The sand transport by storm obviously involves different processes, but it may be enhanced by gravity force and may to some extent resemble the dispersal of turbiditic sand. Notably, the thickness of deposit and the seaward distance of dispersal can be expected to be proportional to the storm magnitude, or to the volume of sediment entrained by the storm.



### 3. Previous studies of lateral bed-thickness changes

#### 3.1. Lateral trends in turbidites

The lateral continuity of sandstone beds in “flysch” successions has been a subject of interest long before the term “turbidite” was coined by Kuenen (1957). An example of such work is the long-distance (12 km) bed-by-bed correlation of sandstones in the Turonian Kemtchi Formation of the Caucasus Flysch by Vassoevich (1948), later extended to a lateral distance of more than 200 km by Grossheim & Vassoevich (1960) and Grossheim (1961). Although these deposits were not originally attributed to turbidity currents, they were obviously turbidites, as pointed out by Hesse (1974) among others. Correlations of basin-plain and channel-fill turbidites after the pioneering studies of Kuenen (1957) and Bouma (1962) showed that the lateral changes in grain size and bed thickness are, indeed, significant over long distances (Dźułyński & Walton, 1965; Hesse, 1965; Ryan et al., 1965; Belderson & Laughton, 1966; Conolly & Ewing, 1967; Dean & Anderson, 1967; Enos, 1969; Griggs et al., 1969; Lovell, 1969; Bornhold & Pilkey, 1971; Bartolin et al., 1972). The pinchout rate and distance of the individual beds in these studies varied from one case to another. For example, Enos (1969) showed that the majority of turbidite beds in the Ordovician Cloridorme Formation of Quebec peter out in downcurrent direction within a distance of 10 km. Similar results were obtained from lateral bed correlations in the Tenmile Creek Formation of Ouachita Mountains, where Picha & Niem (1974) reported bed pinchouts over a distance of 20-40 km; and from the correlations of piston cores in the Columbus Basin, Bahamas, where the individual turbidites could be mapped to extend from the basin origin to their pinchout over an area of  $7.7 \times 10^5 \text{ km}^2$ . In contrast, Hesse (1965; 1974) managed to correlate some turbidites in the Early Cretaceous Gault Formation, Eastern Alps, over a distance of 115 km; Griggs et al. (1969) reported turbidites extending over 170 km from the Cascadia Deep-Sea Channel in offshore Oregon; and Conolly & Ewing (1967) correlated turbidites in piston cores for more than 200 km in the Puerto Rico Trench.

Most of these early studies were concerned primarily with turbidite bed correlation and lateral extent, without systematic measurement of bed thicknesses and statistical assessment of their lateral trends. Studies in which the lateral changes in bed thickness were measured and can be statistically assessed are reviewed in Table 1. The lateral bed-thickness trend indicated by these studies was sigmoidal in shape (i.e., the sandstone bed thins at a relatively high rate with distance in the most proximal and distal segments, but has a fairly uniform thickness over its main, intermediate segment) or was concave-upward in the main, middle segment, but flatter and fairly uniform in the most proximal and most distal segments. Other beds had a

linear thinning trend, with a more rapid, convex-upward distal termination; or were thinning in a concave-upward manner throughout their lateral extent.

Long-distance correlations conducted during the last 40 years have been more detailed and shed more light on the issue of lateral turbidite thinning. Correlations over distances of up to 120 km have been done in outcrop sections (Ricci Lucchi & Valmori, 1980; Amy & Talling, 2006), while correlations based on piston cores in modern basins spanned distances of more than 1200 km (Wynn et al., 2002). The bed-thickness trends range from sigmoidal (Rupke, 1976; Hirayama & Nakajima, 1977; Amy et al., 2004; Talling et al., 2007a) to convex-upward/linear (Hesse, 1982; Smith & Møller, 2003) and to simple concave-upward (Hirayama & Nakajima, 1977; Amy & Talling, 2006; Talling et al., 2007a, b) (see Table 1). Beds in submarine channel levees are thought to thin in a concave-upward manner (Skene et al., 2002; Kane et al., 2007). Importantly, studies by Hesse (1974), Hirayama & Nakajima (1977) and Talling et al. (2007a, b) indicate that the lateral thinning trend is directly related to the actual thickness range, with thicker turbidites showing a different trend than the thinner ones. However, there seems to be little consensus.

For example, a statistical assessment by Hesse (1974, his Table 3) indicated that thinner turbidites (< 1 m in thickness) pinch out more rapidly and are less continuous than the thicker turbidites in the same succession. An exactly opposite trend was indicated by the datasets of Hirayama & Nakajima (1977) and Talling et al. (2007a, b), showing thinner turbidites (< 40 cm in thickness) over long distances to have a lower thinning rate than that of the thicker turbidites. This trend is evidenced by a concave-upward and roughly exponential trend of lateral bed thinning documented by these authors. Talling et al. (2007a) distinguished between small-, medium- and large-volume deposits in the Marnoso Arenacea Formation and demonstrated that the last two had a slightly different thinning trend than the first ones. The small-volume turbidites could be satisfactorily approximated by a concave-upward trend, whereas the large- and medium-volume turbidites had a fairly uniform thickness in their extensive proximal segments and a concave-upward thinning trend in the distal segments.

The most detailed studies of lateral variation in turbidite beds have thus far been done in extensive single outcrops. Enos (1969) managed to walk out some beds in the Ordovician Cloridorme Formation of Quebec over distances of up to 3 km. However, no detailed data on bed thickness trends were published from this study. Parkash (1970) traced eight beds in the same outcrop over a distance of 3.2 km, finding no systematic downcurrent change in either thickness or grain size. Browne et al. (1996, 2000) walked out 15 moderately thin beds (20-60 cm thickness) over an outcrop length of 230 m (with 8 measurement stations) in the Mt. Messenger Formation, northern Taranaki, New Zealand. Their observations are as follows: "Beds up to 35 cm thick can be expected to pinch-out over the horizontal distance of the outcrop (230 m); beds that persist are at least 25 cm thick, and are more likely to be continuous if they are 35 cm thick. Over a horizontal distance of 100 m, approximately 50% of the sandstone beds can be correlated, but over a distance of 200 m,

**Table 1.** Summary of previous work referring to lateral bed-thickness changes of turbidites and tempestites. Asterisk (\*) denotes studies in which the thickness trends were measured from published data (e.g., isopach maps, correlated sections, graphs) or assumed from descriptions in the text. The presented thickness trends refer only to seaward-thinning segments of turbidites and tempestites. For a more detailed description of the listed studies see text.


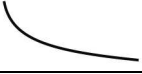





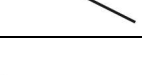






CASE STUDIES OF TURBIDITE PINCHOUTS				
Reference	Location	Trend	Trendline shape	Comments
Bornhold & Pilkey (1971)*	Columbus basin, Bahamas	sigmoidal		5 beds correlated over ~25 km.
		concave-upward		
Bennetts & Pilkey (1976)*	Hispaniola-Caicos Basin	convex-upward		One bed correlated over ~50 km.
Rupke (1976)*	Eocene flysch, southwestern Pyrenees	sigmoidal		Trend based on a reconstructed mega-bed (only the thinning portion of the bed considered – approx. 15 km long).
Hirayama & Nakajima (1977)*	Kazusa Group, Otaday Formation, Boso Peninsula, Japan	sigmoidal		Trends based on 16 beds correlated over ~38 km. Only portions of beds between their max. thickness and pinchout were considered.
		concave-upward		
Hesse (1982)	Gault Formation, Eastern Alpine Flysch	linear		10 beds correlated over ~106 km.
DeVries & Lindholm (1994)	Cerro Toro Formation, Chile	concave-upward		Individual beds walked out over a distance of 150 m. Beds are a part of a submarine channel-levee.
Browne et al. (1996, 2000)*	Mt Messenger Formation, North Taranaki, New Zealand	convex-upward		Individual beds walked out over a distance of 230 m.
Edbrooke & Browne (1996)*	Whakataki formation, Wairarapa	convex-upward		Individual beds walked out over a distance of 500 m.
Smith & Møller (2003)*	Ormen Lange field, offshore Norway	convex-upward		Cores correlated over ~50 km. Trend based on decrease of percentage sand with distance.
Amy et al. (2004)*	Peira Cava Basin, Alpine foreland basin	sigmoidal		5 beds correlated over ~10 km. Flows were probably obstructed by lateral slope!
Amy & Talling (2006)	Marnoso Arenacea Formation, Apennines, Italy	concave-upward		Beds (30 m thick interval) correlated over a distance of ~120 km.
Kane et al. (2007)	Rosario Formation, Baja California, Mexico	power-law		Submarine channel-levee. Trend based on mean sandstone thickness from proximal to distal outcrops (relative to channel belt) over a distance of 1.5 km.

Table 1. (Continued).










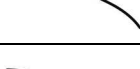


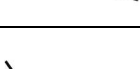




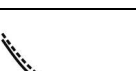





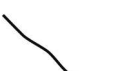











CASE STUDIES OF TURBIDITE PINCHOUTS				
Reference	Location	Trend	Trendline shape	Comments
Talling et al. (2007a)	Marnoso Arenacea Formation, Apennines, Italy	concave-upward (small-volume deposits)		Beds correlated over a distance of ~120 km. Trends shown here do not take into account the affect of flow ponding and show only the thinning sandstone portions of the beds.
		sigmoidal (intermediate-volume deposits)		
		sigmoidal (large-volume deposits)		
Talling et al. (2007b)	Marnoso Arenacea Formation, Apennines, Italy	concave-upward		Beds correlated over a distance of ~120 km. Trend shown pertains to thin turbidites (<40 cm, small-volume deposits of Talling et al. 2007a)
EXPERIMENTAL AND NUMERICAL STUDIES OF TURBIDITE PINCHOUTS				
Reference	Type of study	Trend	Trendline shape	Comments
Rukavina (1965)	experimental	concave-upward		Flume system.
Lüthi (1981)*	experimental	concave-upward		Unobstructed flow.
Middleton & Neal (1989)	experimental	sigmoidal		Flume system.
Bonnecaze et al. (1993)*	experimental	sigmoidal/ concave-upward		Unobstructed flow. Trend based on assumption: density of deposit (mass per unit area) = thickness of deposit.
Dade et al. (1994)	numerical model	convex-upward		Unobstructed flow.
Bonnecaze et al. (1995)*	experimental	sigmoidal		Unobstructed flow. Trend based on assumption: density of deposit (mass per unit area) = thickness of deposit.
Dade & Huppert (1995)*	experimental	sigmoidal/ concave-upward		Flume system. Trend based on assumption: density of deposit (mass per unit area) = thickness of deposit.
Zeng & Lowe (1997)	numerical model	concave-upward /sigmoidal		Unobstructed flow.
Gladstone et al. (1998)*	experimental	sigmoidal/ concave-upward		Unobstructed flow. Trend based on assumption: density of deposit (mass per unit area) = thickness of deposit.

Table 1. (Continued).

EXPERIMENTAL AND NUMERICAL STUDIES OF TURBIDITE PINCHOUTS				
Reference	Type of study	Trend	Trendline shape	Comments
Hallworth & Huppert (1998)*	experimental	sigmoidal		Unobstructed flow. Trend based on assumption: density of deposit (mass per unit area) = thickness of deposit.
Woods et al. (1998)	experimental & numerical	close to linear (exponential function)		Unobstructed flow. The trend is best approximated by an exponential decay.
Pratson et al. (2000)	numerical model	sigmoidal → concave-upward		Unobstructed flow. Solid line: steep slope (5.25°); dashed line: gentle slope (2.25°)
		concave-upward /sigmoidal → sigmoidal		Unobstructed flow. Solid line: short slope (5 km); dashed line: long slope (40 km)
		sigmoidal → concave-upward		Unobstructed flow. Solid line: small initial size of flow/current (500 x 2 m); dashed line: large initial size of flow/current (2000 x 2 m)
Alexander & Mulder (2002)	experimental	concave-upward		Unobstructed flow.
Choux & Druitt (2002)	experimental	roughly concave-upward		Flume system. Trend based on several curves. The reader is referred to their Fig. 4 for exact shapes of the trendlines.
Felix (2002)	numerical model	concave-upward		Simulation of the Great Banks 1929 event.
Al Ja' Aidi et al. (2004)*	experimental	concave-upward		Unobstructed flow.
Amy et al. (2004)*	experimental	concave-upward		Obstructed and unobstructed flow.
Gray et al. (2005)	experimental	concave-upward		Unobstructed flow. Trendline shown is an approximate mean of four different thinning trends (corresponding to four different slope angles). Trendline is taken from a log/linear plot; on a linear/linear plot the concave trend shown would be even more pronounced.
Lamb et al. (2006)	experimental	sigmoidal		Obstructed (ponded) flow.

**Table 1.** (Continued).

CASE STUDIES OF TEMPESTITE PINCHOUTS				
Reference	Location	Trend	Trendline shape	Comments
Myrow & Hiscott (1991)	Chapel Island Formation, southeast Newfoundland	concave-upward		Tempestite model based on outcrop observations.
Trincardi & Field (1991)*	Tyrrhenian Sea margin	concave-upward		Inferred from isopach maps of multi-bedded sand bodies.
Brenchley et al. (1993)	Bell Island Group, Beach Formation, eastern Newfoundland	concave-upward		Trend based on a plot of length versus frequency distribution of beds. Beds were probably deposited in a semi-confined setting.
Wheatcroft & Borgeld (2000) *	northern California shelf	concave-upward		Trend derived from isopach maps of three different flood events.
Bentley et al. (2002) *	northern Gulf of Mexico	concave-upward		Trend assumed from an isopach map of the Hurricane Camille event bed.
Murray et al. (2002) *	Palos Verdes shelf	concave-upward		Trend measured from an isopach map.
Wheatcroft & Drake (2003) *	northern California shelf	concave-upward		Trend inferred from text. Flood event.
Wheatcroft et al. (2006)	northern Adriatic Sea	concave-upward		Flood event.
NUMERICAL STUDIES OF TEMPESTITE PINCHOUTS				
Reference	Type of study	Trend	Trendline shape	Comments
Zhang et al. (1999)	numerical simulation	concave-upward		Pinchout distance of a 3 cm thick bed = 5 km from the point of max. thickness.
Scully et al. (2002) *	analytical model	concave-upward		Trend based on plots of tons/m versus distance.

this percentage drops to about 30%.” The outcrop section was approximately perpendicular to the depositional axis, and hence their datasets probably represent bed trends transverse, rather than parallel, to a depositional fan lobe. Edbrooke & Browne (1996) traced laterally 34 sandstone and 33 mudstone beds for almost 500 m (with 10 measurement stations) in the mid-Miocene Whakataki Formation, Wairarapa, New Zealand. The outcrop section was approximately parallel to the depositional axis. about 90% of beds could be correlated over a distance of 200 m and about 80% of beds over a distance of 400-500 m. Beds that pinched out within the outcrop section had maximum thicknesses mainly less than 5 cm, whereas beds



thicker than 5 cm could be correlated throughout the outcrop. These studies indicate that thin beds peter out at higher rates, which is in agreement with the long-distance correlation study of Hesse (1974).

Experimental work on bed thickness has yielded more consistent results than the outcrop studies, although the laboratory deposits were very thin. Experimental laboratory setups varied from large (10 x 6 m) to small (1 x 1 m) rectangular tanks with slopes of 0° to 30°. Turbidity currents were generated by either lock release or continuous fluid discharge, and were relatively dilute (<15 vol. % of sediment), contain sediment analogues such as silica grains/flour, glass or plastic beads. The resulting deposits thinned out gradually towards their termini in a concave-upward manner (Rukavina, 1965; Lüthi, 1981; Bonneau et al., 1993; Dade & Huppert, 1995; Gladstone et al., 1998; Woods et al., 1998; Alexander & Mulder, 2002; Choux & Druitt, 2002; Al Ja'Aidi et al., 2004; Amy et al., 2004; Gray et al., 2005; Lamb et al., 2006). However, studies by Bonneau et al. (1993), Dade & Huppert (1995), Gladstone et al. (1998) and Lamb et al. (2006) showed a segment with fairly uniform thickness in the most proximal parts of the deposits (Table 1). This zone of uniform thickness was extended in the studies by Bonneau et al. (1995) and Hallworth & Huppert (1998), rendering the thickness trends to be approximately sigmoidal in shape. The experiments of Middleton & Neal (1989) are an exception, showing a more or less uniform thickness of deposits throughout their lateral extent, with an abrupt termination, often concave-upward in shape. This experiment was conducted in a horizontal flume channel (0.15 x 6 m) and is therefore difficult to compare with the unconfined flows used in the other experiments. However, its outcome corresponds with the aforementioned outcrop observations by Browne et al. (1996, 2000), Edbrooke & Browne (1996) and Hesse (1974).

Attempts were made to develop process-based numerical models predicting turbidite thickness, based on the flow parameters of turbidity current. Dade et al. (1994) proposed a model for a non-eroding turbidity current surge moving down a uniform slope. Their model took into account the effects of ambient water entrainment, deposition of sediment, bottom friction and slope gradient. The deposit thickness was predicted to diminish as an inverse square root of the downstream distance for the surge moving downslope due to its negative buoyancy; and once the negative buoyancy of the surge was eliminated by sediment fallout, the thickness of the deposit declined exponentially in a convex-upward manner. The overall shape of the thickness trendline was thus close to linear, with an abrupt convex-upward termination (Table 1). Zeng and Lowe (1997) developed a process-based computer model that can generate synthetic turbidites based on various parameters known from experimental and outcrop studies. The simulated turbidite bed reported in their paper had an overall concave-upward trend with a slight convex-upward terminal part. Woods et al. (1998) used both experimental and numerical simulations to study deposition of ash flows. Their numerical model for turbulent suspension flow successfully compared with their experimental observations and yielded a nearly linear trend best expressed as an exponential function. Pratson et al. (2000) used a mathematical model to analyse the effects of initial flow volume, flow density, slope length and slope gradient on the

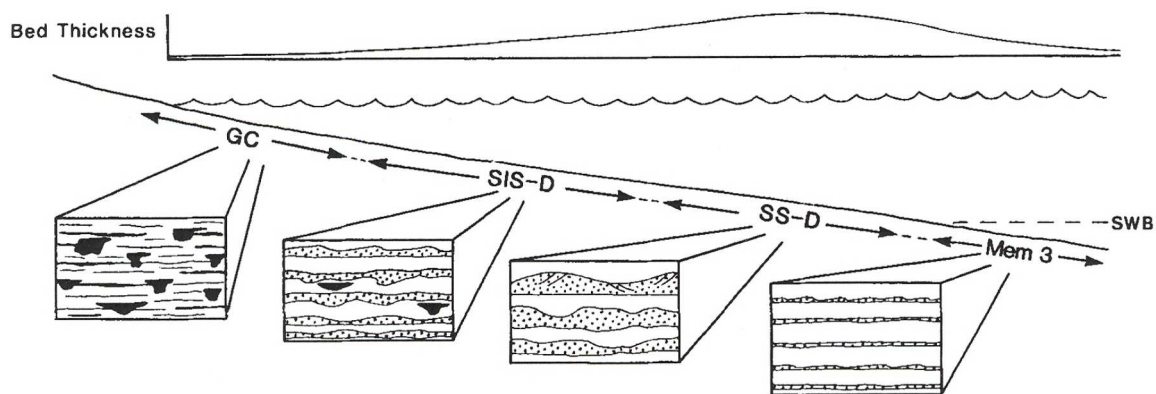
geometry of the resulting deposit of turbidity current. The observed geometries demonstrate that almost every shape predicted by experiments, numerical models or derived from outcrop studies to this day could, in fact, be obtained from the model (see trends shown in Table 1).

Observations by Kuenen (1951), Meischner (1962, 1964), Middleton (1967), Lovell (1969, 1971), Eder (1971), Sadler (1982), Amy & Talling (2006) and Talling et al. (2007a) indicate a more rapid thinning of turbidites in their proximal, thicker segment, often referred to as the “proximal limb”. These studies suggest that the longitudinal profile of turbidite bed is lenticular, thickening quickly in the proximal part and, after reaching the point of maximum thickness, thinning more gently further downcurrent.

### **3.2. Lateral trends in tempestites**

The lateral, seaward thickness variation of tempestite beds has thus far been little studied. Most of the published data come from the recent studies of modern shelves, with research focused more on processes than on the detailed geometry of deposits. In general, both the thickness and grain size of storm beds have been reported to decrease seawards (Aigner & Reineck, 1982; Allen, 1982; Tamura & Masuda, 2005; and references therein), because the storm-generated combined flow wanes in this direction, with a number of processes possibly improving the sediment sorting (Swift et al., 2003). Trincardi & Field (1991) studied high-resolution side-scan sonar profiles from the shelf of Tyrrhenian Sea, and though their observations were from sandbodies considerably thicker than a single storm bed, the spatial distribution of sand indicated a concave-upward thinning trend. Myrow & Hiscott (1991) proposed a depositional model for tempestite beds of the Chapel Island Formation, southeastern Newfoundland, and suggested that the beds initially thicken and then thin with distance from the shoreline (Fig. 8). In this model, both the thickening and the thinning bed segments are characterized by a concave-upward thickness trend. The geometries of storm beds reported from the the Beach Formation of the Bell Island Group, eastern Newfoundland (Brenchley et al., 1993), differ from those mentioned above. These storm beds have a strikingly short seaward extent, between 2 and 40 m, and thicknesses of up to 30 cm. The geometry of their seaward thickness profile tends to be lenticular, because their bases are commonly concave-upward and the top surfaces are often convex-upward. However, the stacking pattern of these deposits indicates a semi-confined marine environment, quite different from “normal” open shelves and the depositional setting considered in the present study.

Zhang et al. (1999) used a numerical model to simulate storm deposition on a 20-km wide (seaward width) continental shelf on the basis of the seafloor gradient and storm-wave parameters of the Eel shelf, northern California. He concluded the storm bed thickness would decrease in a concave-upward manner with distance from the shoreface, but would increase again at a distance of around 6 km and reach its maximum around 10 km away; farther seawards, the thickness would decrease in a concave-upward manner and the



**Fig. 8.** Tempestite model for the Chapel Island Formation, southeast Newfoundland, as proposed by Myrow (1992) and Myrow & Hiscott (1991). A typical tempestite bed shows a bed-thickness trend that first increases and then decreases away from the shoreline. The proximal setting is one of bypass and erosion (gutter cast facies: GC). Passing seaward, gutter casts die out and bed thickness increases (siltstone-dominated facies: SIS-D). Rare hummocky cross-stratification is formed in the thicker sandstone beds further out on the shelf (sandstone-dominated facies: SS-D). Below storm wave base (SWB), distal tempestites resemble classical turbidites (member 3).

bed would peter out around 15 km away from the shoreline. The maximum thickness of the modelled deposit was only 3 cm. A year later, Wheatcroft & Borgeld (2000) published thickness data on three storm-spread river-flood deposits from the Eel shelf, supporting the numerical predictions of Zhang et al. (1999). The numerical model of Scully et al. (2002) for the deposition on the Eel shelf showed somewhat different results. The expected geometry of the deposit resembled closely that predicted by Zhang's et al. (1999) and measured by Wheatcroft & Borgeld (2000), the model suggested that the sediment deposition would not occur until 7 km away from the Eel River mouth.

Bentley et al. (2002) mapped out the distribution of a major hurricane event bed in the northern Gulf of Mexico, showing that the bed thickness follows approximately the same trend as predicted for and observed on the Eel shelf. The distribution of grain sizes, however, appears to be highly varied and unpredictable, although the sand involved is relatively fine-grained. The occurrence of maximum bed thickness in proximal mid-shelf zone and a concave-upward seaward thickness decrease were also demonstrated statistically by Murray et al. (2002) from the Palos Verdes shelf and by a more recent study from the Eel shelf by Wheatcroft & Drake (2003). The distribution and geometry of sand spread by storm during the autumn 2000 Po River flood on the northern Adriatic shelf was mapped by Wheatcroft et al. (2006). The resulting deposit was up to 20 cm thick and spread offshore to a distance of around 9 km, and appeared to thin seawards in a concave-upward manner. The datasets discussed above are summarized in Table 1.



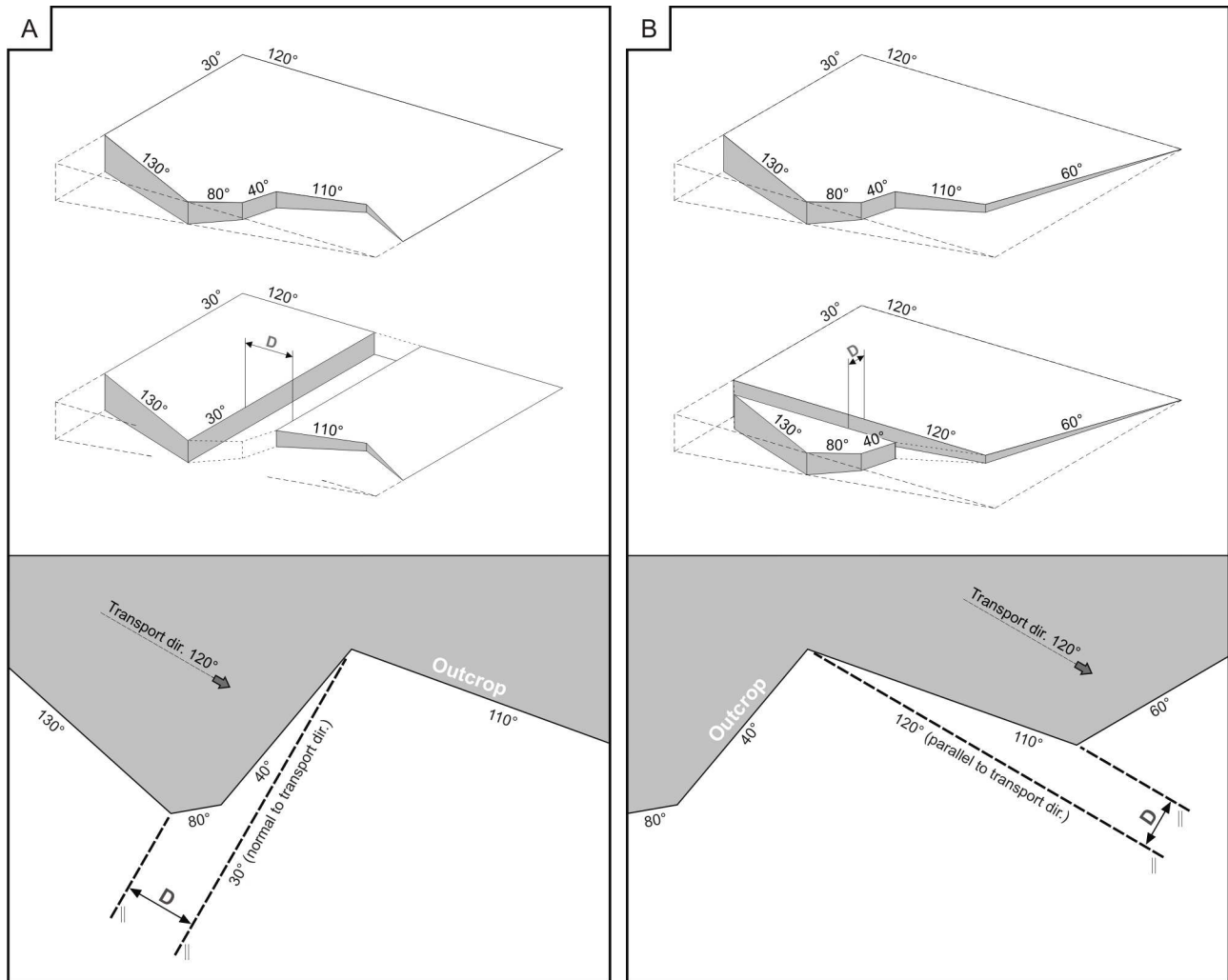
## 4. Methods and terminology

### 4.1. Study methods

In the present study, the lateral thickness changes of 146 turbidite and tempestite beds have been measured in five different formations (see Fig. 3). The measurement points were spaced at 2-10 m and the bed segments measured were up to nearly 500 m long. At every measurement point, the measured bed was also described in terms of its local grain-size range (grading), sedimentary structures (Bouma and tempestite divisions and their thicknesses), sole marks (especially flutes and their spatial direction) and the character of base and top boundaries. Grain size was determined by using a magnification glass and grain-size comparator. In order to minimize error, the measurements and observations were taken in well-preserved bed segments, with clear base and top. Only sandstone beds underlain and overlain by mudstone were selected, and amalgamated beds were discarded. The accuracy of thickness measurements, for both the beds and their divisions, was held at 0.1 cm for thin beds, but was reduced to 0.5 cm for beds thicker than 10 cm, which allowed for a comparable percentage of error. Rock weathering and gradational turbidite tops were the main source of error, although uncertain bed profiles had been avoided.

Outcrop sections approximately parallel or perpendicular to the palaeocurrent direction were measured in order to obtain 3-D datasets. Where the outcrop strike varied significantly over considerable distances, the outcrop section was divided into segments approximately parallel and/or perpendicular to the palaeocurrent direction or the data points were projected onto one of these directions. The distance between two segments approximately parallel to the palaeocurrent direction was measured as the distance between two normals to the depositional dip (Fig. 9A). Similar approach was used for calculation of the distance between two segments perpendicular or strongly oblique to the palaeocurrent direction, with the gap length calculated as the distance between two parallels to the palaeocurrent direction (Fig 9B). In this approach, it was assumed that the turbidite in the outcrop section thins in one preferential direction and that sideways thickness changes on the outcrop scale are negligible. The distances between tangent lines normal or parallel to the outcrop segments were measured in ArcGis®.

The thickness frequency distribution of the measured beds has been analysed by several graphic and numerical methods. Graphical tests include linear frequency histogram, logarithmic frequency histogram, log-log exceedence frequency plot (i.e., a logarithmic plot of bed thickness values,  $t$ , against the number of thickness values greater than or equal to  $t$ ) and probability-probability plot (comparing the cumulative frequency of a given variable,  $t$ , to the cumulative frequency of a theoretical reference distribution). Statistical tests included: the significance test of the Pearson correlation coefficient for linear fit on a



**Fig. 9.** Figure illustrates the necessary corrections that had to be made to account for large variations in outcrop strike. It is assumed the turbidite at the outcrop location thins in a single direction; lateral changes (normal to paleo-transport direction) in bed thickness in single outcrops are considered negligible in comparison to the overall volume of the deposit. **(A)** Example of how the distance between two individual segments roughly parallel to the paleocurrent direction was measured. The wedge-shaped geometrical body is a schematic representation of a turbidite bed with no lateral changes in thickness at the outcrop scale. The distance ( $D$ ) between two normals tangent to the segments is measured in ArcGis<sup>®</sup> and the missing measurements within this interval are transposed as missing values in the bed-thickness dataset. **(B)** Similar approach is used in calculating the distance between two segments perpendicular or strongly oblique to the paleocurrent direction. The distance between these two segments is calculated as the distance between two parallels to the paleocurrent direction. Note: Corrections for outcrop strike were only needed on three outcrops in the Marnoso Arenacea Formation, Italy.

probability plot (the plot of bed thickness values against their cumulative frequency) and the Anderson-Darling, Kolmogorov-Smirnov, Ryan-Joiner and Shapiro-Wilk distribution tests (see Levene 1960; Shapiro & Wilk, 1965; Lilliefors, 1967; Ryan & Joiner, 1976). Using a Minitab<sup>®</sup> implementation tool for individual distribution identification, the bed-thickness datasets were tested against fourteen theoretical distributions: normal, lognormal, three-parameter lognormal, gamma, three-parameter gamma, exponential, two-parameter

exponential, smallest extreme value, Weibull, three-parameter Weibull, largest extreme value, logistic, loglogistic and three-parameter loglogistic.

Least-square regression (see Kahane, 2001) was used to define lateral bed-thickness changes. All datasets were verified to meet the following regression criteria: the homoscedasticity and normality of residuals and the absence of unusual and influential data. Beds that failed to fulfil these assumptions were excluded from the analysis. Outlier data were removed until the regression criteria were met. In order to assess what function approximates best the lateral thickness changes of a particular bed, regression trendlines offered by Microsoft Excel<sup>®</sup> were fitted to the datasets and their goodness of fit was evaluated on the basis of the coefficient of determination ( $R^2$ ). After the evaluation of regression trends, regression lines were fitted to the bed datasets to approximate the gradient of the bed lateral thinning. Beds with strongly nonlinear lateral thinning trends that did not meet the criteria of linear regression, were split into straight-line segments for further analysis.

The method of Fourier transform (see Folland, 1992) was used to study bed-top undulations. The Fourier transform converts a waveform dataset measured in the time domain or, as in the present case, a one-dimensional space domain, into the frequency domain. This is accomplished by breaking down the original waveform into a series of sinusoidal terms, each with a unique magnitude, frequency and phase. This process effectively converts a waveform that is difficult to describe mathematically into a more manageable series of sinusoidal functions which, when added together, represent exactly the original waveform. Plotting the amplitude of each sinusoidal term against its frequency gives a power spectrum, which reflects the relative contribution of particular sinusoids in the original waveform in the frequency domain (also known as the periodogram). The frequency spectra of beds belonging to the same thickness class were quantitatively assessed by calculating the mean dominant frequency peaks (i.e., their x- and y coordinates in periodogram), which were later used to construct harmonic functions of the undulations. The statistical methods were implemented with the use of SPSS<sup>®</sup>, Minitab<sup>®</sup> and Microsoft Excel<sup>®</sup> software.

## **4.2. Terminology**

Sedimentary facies are basic types of deposits distinguished descriptively on the basis of their bulk characteristics, such as texture, structure, biogenic features, colour and other feature (Harms et al., 1982). The individual facies are given short descriptive/interpretive names and letter-code labels, with the description of each facies clearly separated from its interpretation in the report.

The present study deals with turbidite and tempestite sandstone beds, which are typical “event” deposits – products of brief depositional phenomena separated by long periods of mud fallout. These event deposits show considerable between-bed and within-bed (lateral) variation, and the distinction of facies pertains to

sandstone bed types distinguished on the basis of their component divisions (i.e., vertical changes in sediment structure and/or texture). In the case of turbidites, facies nomenclature refers to the well-known Bouma divisions, with the letter symbol “T” denoting a turbidite bed as such and the italic subscripts *a*, *b*, *c*, ... denoting the bed’s component divisions (Fig. 4). In the case of tempestites, the arbitrary letter symbol “S” is used to denote a storm bed and the following italic subscripts are used to denote the sandstone bed’s component divisions: *m* = massive (non-stratified) division; *p* = planar parallel-stratified division; and *r* = ripple cross-laminated division (with symmetrical or asymmetrical wave-ripple structures).



## 5. Sedimentary facies

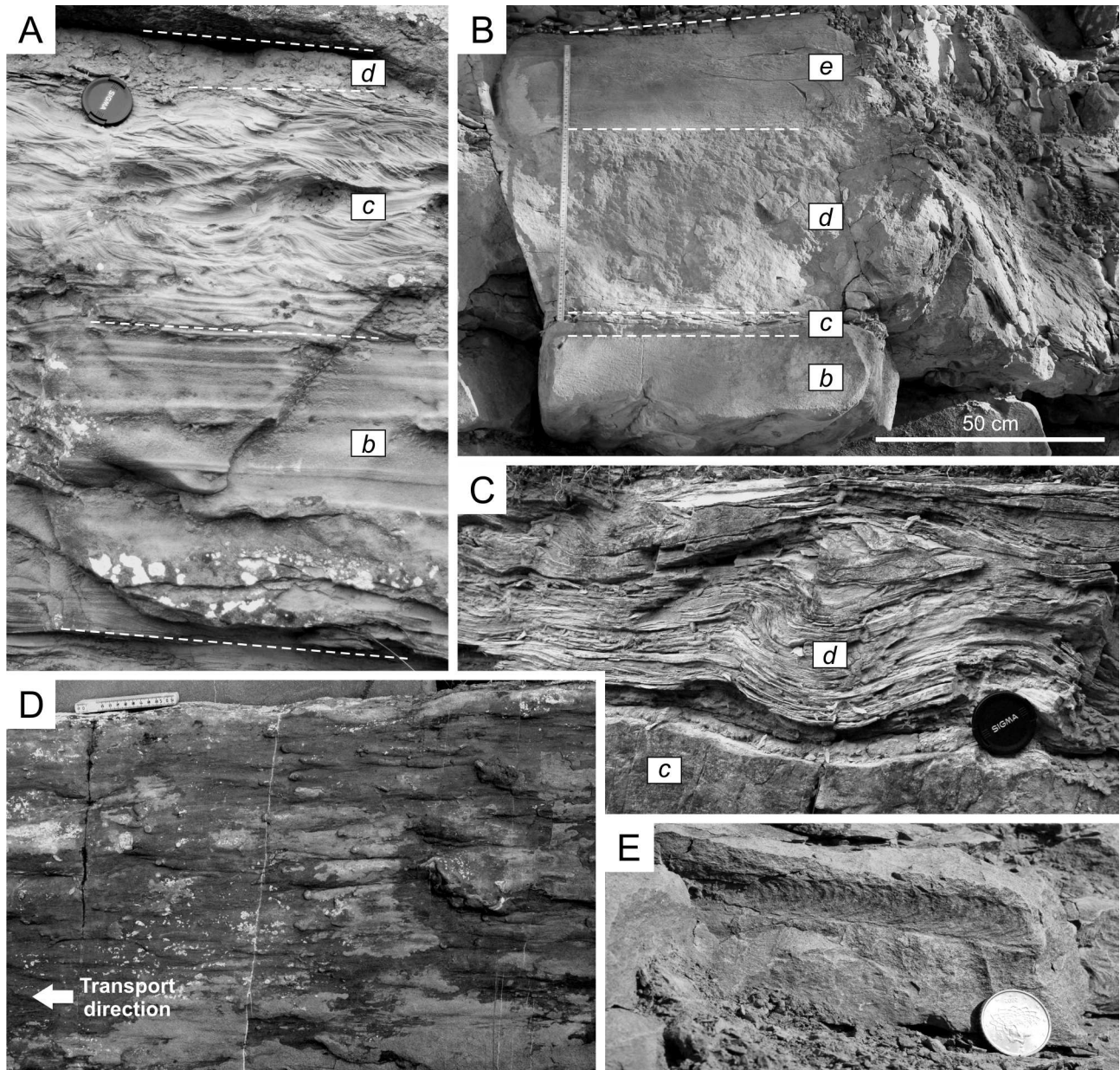
The following descriptions and interpretations of facies refer to the sandstone beds measured in the present study and do not exhaust the entire spectrum of sedimentary facies in the respective formations. For more comprehensive descriptions of the facies that constitute these various formations, the reader is referred to the regional literature reviewed in a subsequent section.

### 5.1. Turbidite facies

The turbidite beds measured in the outcrop sections commonly represent three types (facies) of classical, Bouma-type turbidites: *Tabcde*, *Tbcde* and *Tcde* (cf. Fig. 4). In addition, certain beds contain divisions of negligible thickness, constituting the following bed-type variants (divisions in parantheses are of negligible thickness): *Tabc(de)*, *Tab(cde)*, *Ta(b)c(de)*, *Ta(bcde)*, *Tbcd(e)*, *Tbc(de)*, *Tb(cde)*, *Tb(c)d(e)* and *Tc(de)*. Beds of Facies *Tabcde* are generally the thickest and coarsest-grained, with the thicknesses between 75 and 133 cm and grain sizes between coarse and very fine sand and with silty to muddy topmost divisions. Beds of Facies *Tbcde* have thickness between 10 and 100 cm and grain sizes between coarse/medium and very fine sand, whereas those of Facies *Tcde* are 2.5-40 cm thick and composed mainly of fine/very fine to very fine sand; their capping divisions are similarly silty to muddy. Facies *Tabcde* constitutes ~5% of the beds, or bed segments, measured in the Marnoso Arenacea Formation, ~9% in the Kusuri Formation, ~70% in the Monte Fumaiolo Formation and is absent from the turbidites measured in the Akveren Formation. Facies *Tbcde* constitutes ~60% of the bed segments measured in the Marnoso Arenacea Formation, ~70% in the Akveren Formation, ~91% in the Kusuri Formation, and is absent from the turbidites measured in the Monte Fumaiolo Formation. The occurrence percentage of Facies *Tcde* in the particular formations is following: ~30% of the beds measured in the Akveren Formation, ~30% in the Monte Fumaiolo Formation, ~35% in the Marnoso Arenacea Formation and 0% in the Kusuri Formation. The component divisions of these turbidite facies are described briefly and interpreted below, with an emphasis on their similarities and differences observed in the various formations. Photographs of the facies belonging to the particular formations are shown in Figs. 10, 11 and 12.

**Turbidite division a** – This is the so-called basal “massive” division of Bouma-type turbidites (cf. Fig. 4), and it is present only in the turbidite facies *Tabcde* and its variants.

*Description:* This basal division in the studied beds consists of non-stratified, poorly to well-graded, very coarse or coarse to medium sand, locally containing scattered mudstone clasts (from less than 1 cm to a few decimetres in length). The colour of this division in the Marnoso Arenacea formation is generally whitish-



**Fig. 10.** Outcrop photographs illustrating lithofacies of turbidites measured in the Marnoso Arenacea Formation. (A) Bed of Facies *Tbcde*, variant *Tbcd(e)*. Note the gradational transition in structures from division *b* to *c* and from *c* to *d*. (B) Bed of Facies *Tbcde*. Note the significant difference in the thickness of the separate Bouma divisions when compared to the turbidite shown in A. The total thickness of beds in A and B is approximately the same. (C) Detail of a convoluted silt-interval (division *d*) overlying rippled sandstone (division *c*). Bed of Facies *Tcde*. (D) Flute casts occurring at the base of beds. Flow direction is in this case from left to right. (E) Detail of a burrow in planar parallel-stratified sandstone.

grey to light yellowish-grey, whereas in the Monte Fumaiolo and Kusuri formations it is light grey to grey. This division occurs typically in the thickest beds (> 30 cm) and its thickness ranges from 10 to 50 cm.

*Interpretation:* Division *a* represents rapid dumping of sand directly from turbulent suspension (Allen, 1982; Kneller and Branney, 1995), possibly with the development of a transient, upward-freezing “moving

bed” (Kneller and Branney, 1995; Vrolijk and Southard, 1997). This non-tractional mode of sand deposition is attributed to the suppression of near-bed turbulence by excess sediment concentration (Lowe, 1982, 1988) and signifies a “high-density” type of turbidity current (*sensu* Lowe, 1982).

**Turbidite division *b*** – This is the planar parallel-stratified, or “flat-laminated”, division of Bouma-type turbidites (cf. Fig. 4), and it is present in facies *Tabcde* and *Tbcde*.

*Description:* This division consists mainly of medium to fine sand and shows planar parallel stratification, and occasionally with gently undulating (wavy) internal surfaces of scour and/or stratification. In the beds measured in the Marnoso Arenacea Formation, this division is either non-graded or showing a step-like, non-uniform ‘jerky’ pattern of normal grading (Fig. 10A). In the beds measured in the other formations, the upward fining of this division is usually gradual and better pronounced. Division *b* is common in relatively thin sandstone beds (<40 cm) and in the upper parts of thick (>50 cm) sandstone beds. The thickness of division *b* ranges mainly from 2 to 30 cm, but is up to 100 cm in some of the thickest beds.

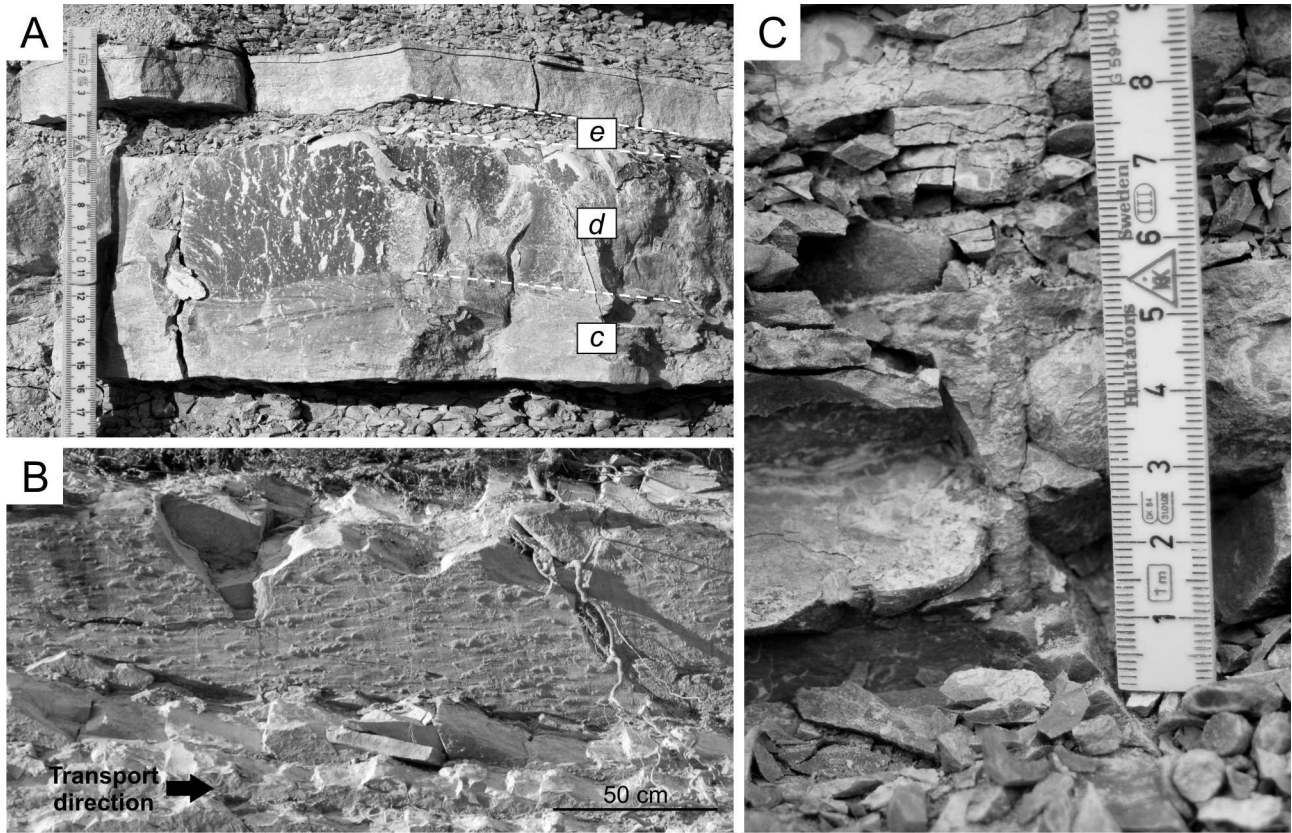
*Interpretation:* Planar parallel-stratified sand signifies tractional deposition from transport in the upper, supercritical flow regime, with the “upper-stage” plane bed configuration (Harms et al., 1975). The non-uniform, jerky pattern of abrupt grain-size changes in this division in the Marnoso Arenacea turbidites indicates short-term fluctuations of flow power, possibly with brief episodes of substrate erosion and sediment bypass. The undulatory scours and/or strata sets may represent incipient phases of standing-wave antidune formation (Allen, 1982; Alexander et al., 2001).

**Turbidite division *c*** – This is the cross-laminated, or small-scale cross-stratified, division of Bouma-type turbidites (cf. Fig. 4), which occurs in all the three facies in the present case.

*Description:* This division consists of fine or very fine sand, commonly grading upwards into silt, and shows current-ripple cross-lamination (or small-scale trough cross-stratification), locally representing climbing ripples. In the Marnoso Arenacea turbidites, this division is commonly convoluted, hydroplastically deformed. The upper and lower contacts are typically gradational, though locally fairly sharp. Division *c* occurs in both thin (<40 cm) and relatively thick beds (>50 cm), and its thickness varies from 1 to 20 cm, occasionally up to 50 cm.

*Interpretation:* The cross-laminated bed division represents tractional deposition of sand to coarse silt from transport in the lowermost part of the lower, subcritical flow regime, with a rippled bed configuration (Harms et al., 1975; Allen, 1982). The trough-shaped sets of cross-laminae indicate 3-D current ripples, probably linguoid or cusped (Allen, 1982). Climbing ripples indicate bedform migration in the conditions of intense sediment fallout from suspension (Harms et al., 1975).

**Turbidite division *d*** – This is the upper and somewhat enigmatic division of Bouma-type turbidites (cf. Fig. 4). This fine-grained division in the present case, as in many other turbiditic formations described in the literature, is generally thin and poorly distinguishable from the overlying mudstone due to their fissility and



**Fig. 11.** Outcrop photographs illustrating lithofacies of turbidites measured in the Akveren Formation. **(A)** Bed of Facies Tcde consisting of ripple cross-laminated sandstone (division *c*) capped by turbiditic marl (division *d*). Note the undulatory top of the rippled interval and the weathered transition from division *d* to the overlying turbiditic marl. **(B)** Flute casts occurring at the base of beds. Flow direction in this case being from left to right. **(C)** Detail of a burrow penetrating a thin, ripple cross-laminated bed.

joint weathering. Therefore, division *d* was not included in the bed-thickness measurements in all such turbidites. However, several turbidites in the Marnoso Arenacea Formation had well-developed and relatively thick division *d* (see Fig. 10B & C), and the latter was therefore included in the measurements of bed thickness.

*Description:* In the Marnoso Arenacea Formation, division *d* consists of non-graded or very weakly graded silt and shows planar or slightly undulatory parallel lamination, generally diffuse and often convoluted (Fig. 10B & C). This division is fissile, has gradational upper and lower boundaries and commonly contains plant detritus. The thickness of division *d* in the beds of this formation ranges between 13 and 50 cm, corresponding to ~20-71% of the bulk thickness of a turbidite. In the Akveren Formation, division *d* is relatively thin and composed of whitish- or light greenish-grey silty marl, massive, less fissile and often burrowed, with gradational upper and lower boundaries (Fig. 11A). Division *d* is negligibly thin in the turbidite beds measured in the Kusuri and Monte Fumaiolo formations.

*Interpretation:* The origin of division *d* remains to be uncertain, because small-scale laboratory experiments thus far failed to reproduce this kind of deposit (cf. Fig. 4). A “lower-stage” (lower flow-regime) plane-bed transport was initially invoked by many authors, until it has eventually been confirmed by laboratory experiments that this transport mode is limited to coarse and very coarse sand (Harms et al., 1972, 1975). Most authors are presently inclined to attribute this upper division to the waning of a dilute, weak and sand-depleted tail of turbidity current, with the deposition from suspension fall-out, possibly by a rhythmic shedding of sediment (Kerr, 1991) and occasionally combined with transient “whiffs” of weak tractional dispersal, responsible for the smudging of silt on muddy substrate (Middleton, 1993). The massive character of the marlstone *d*-divisions in the Akveren Formation is probably due to diagenesis, which had obliterated primary lamination by turning the fine-grained calcareous deposit into a micritic limestone.

## 5.2. Tempestite facies

The succession of sheet-like sandstone beds of the Karpuzçay Formation shows many features diagnostic of deposition in an offshore-transition environment, such as shallow-marine sublittoral assemblages of benthic foraminifers and ichnofauna as well a lateral shoreward transition to, and interfingering with, shoreface sandstone succession (Larsen, 2003). The sandstone beds are coarse- to fine-grained, have sharp bases and sharp tops, as is typical of tempestites, but are dominated by planar parallel stratification, generally lack hummocky cross-stratification and also seldom show well-developed wave-ripple cross-lamination. The beds measured are on average 13 cm thick and represent facies *Smp(r)*, *Sm(r)*, *Sp(r)* and *Sr*, with the ripple cross-laminated division *r* ranging from well-developed to thin and locally absent. About 24% of bed-thickness measurements are from beds containing the massive division *m*, 57% of measurements are from beds of facies *Sp(r)*, and 19 % of measurements are from beds that consist entirely of the tempestite division *r*. The component divisions of these tempestite facies are illustrated in Fig. 12 and described briefly and interpreted below.

**Tempestite division *m*** – Basal massive division occurs mainly in thicker beds, and though expected in tempestites (e.g., Bourgeois, 1980; Dott & Bourgeois, 1982; Myrow & Southard, 1996) – its occurrence and graded character have misled earlier researchers into considering the Karpuzçay Formation to be a turbidite succession (see review by Larsen, 1999, 2003).

*Description:* The massive (non-stratified) division consists of well-sorted, coarse to medium sand, shows normal grading and locally contains an admixture of plant debris and microscopic shell detritus (Fig. 12A; Larsen, 2003). This division forms the lower part of thicker (>30 cm) beds, has a sharp, erosional base and also fairly sharp upper boundary, and ranges in thickness from 5 to 30 cm. The colour of this sandstone division varies from light yellowish-grey to whitish-grey.

*Interpretation:* The origin of basal massive division in tempestites is attributed to syndepositional liquefaction and/or a non-tractional deposition by rapid direct fallout from turbulent suspension (Dott & Bourgeois, 1982; Lowe, 1988). The first portion of sand deposited on the seafloor may originally be stratified, but becomes homogenized by liquefaction due to the cyclic loading by storm waves (division *m*) and subsequently overlain, with some erosion, by the later portion of stratified sand (division *p*) deposited by a waning storm. The alternative explanation is that, as the sediment suspension generated by storm begins to settle, the concentration of particles near the seafloor increases and the water turbulence there becomes intermittently suppressed, which causes rapid dumping of the near-floor volume of unsupported particles. Both these notions are consistent with the fact that division *m* invariably consists of the bed's coarsest sediment, which would be expected to fallout fastest from suspension and concentrate near the seafloor immediately after the storm peak.

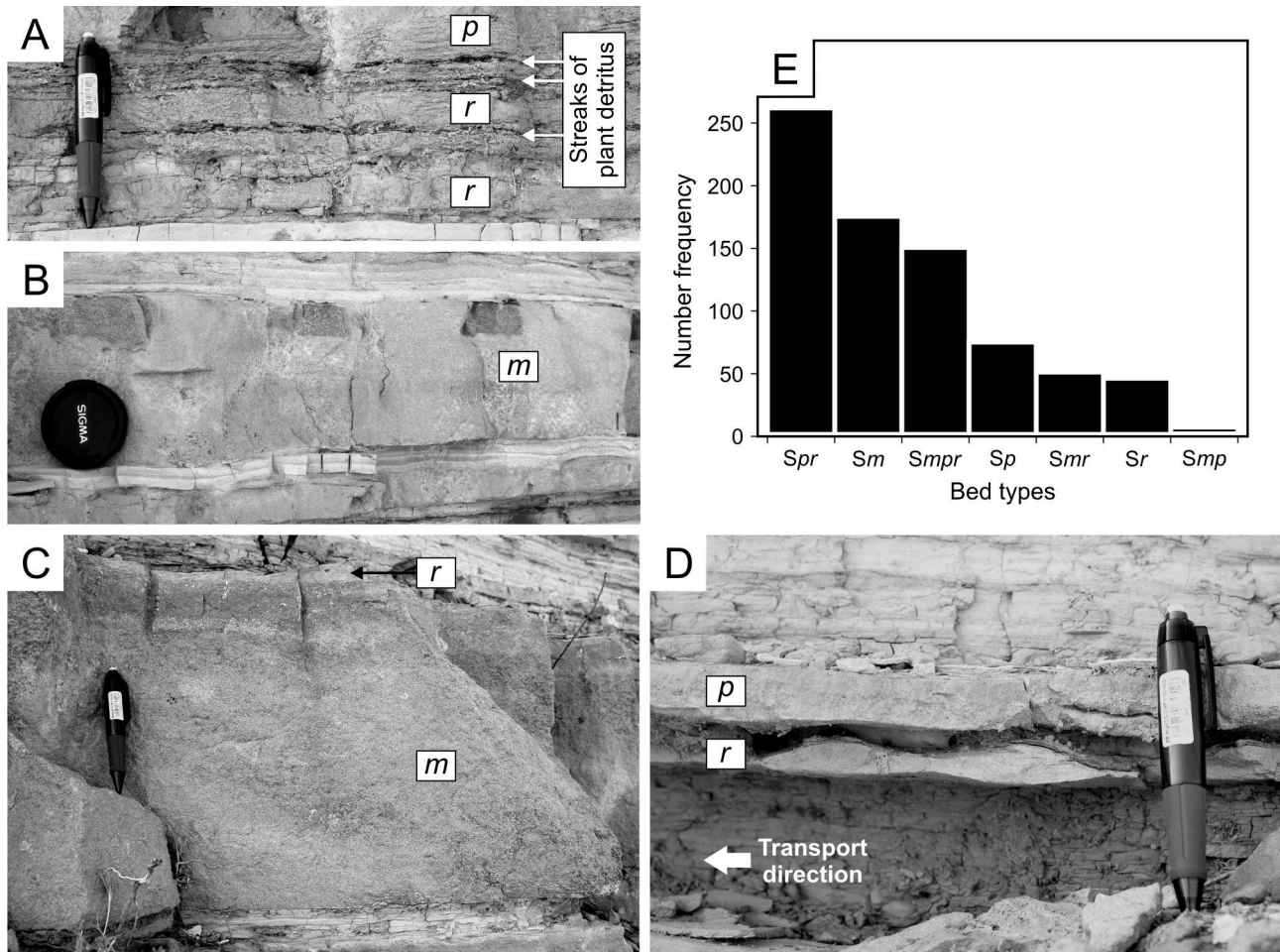
**Tempestite division *p*** – This division, composed of planar parallel strata, abounds in tempestites (Fig. 6; see Bourgeois, 1980; Allen, 1982; Dott & Bourgeois, 1982; Myrow & Southard, 1996) and commonly predominates in the sandstone beds of the Karpuzçay Formation.

*Description:* This division consists of medium to very fine sand, planar parallel-stratified, occasionally showing undulatory (wavy) internal surfaces of truncation and/or stratification. The sandstone colour is light yellowish- to whitish-grey. Streaks of concentrated plant detritus and/or shell debris occur locally. The thickness of this division ranges from 3 to 40 cm, spanning the bulk of the bed profile in many cases. The lower boundary is sharp in facies *Sp(r)*, but sharp to diffuse in facies *Smp(r)*. The upper boundary is texturally gradational in beds *Smpr* and *Spr*, but sharp, with a direct mudstone capping, in beds *Smp* and *Sp*.

*Interpretation:* In a storm-related combined-flow regime, planar parallel stratification may have only two origins: the action of waves with orbital velocities too high to form wave ripples (Komar, 1976), or a powerful storm-generated current carrying sand by plane-bed transport in the upper flow regime (Harms et al., 1975; Myrow & Southard, 1996). In the present case, the shelf may have been inclined at up to 3° (E. Larsen, pers. comm. 2007) and the storm-ebb surges would likely be sand-laden and thus “density-modified”, greatly enhanced by gravity (see earlier section 2.2). The lack of hummocky cross-stratification supports the notion of relatively strong unidirectional currents. Dune bedforms have a considerable time-lag (Allen, 1982) and would not form if the current waned relatively quickly, passing the hydraulic field of dune stability too fast. Therefore, the notion of powerful storm-generated currents is favoured here.

**Tempestite division *r*** – The wave-ripple cross-laminated division, although generally weathered and often poorly developed in the present case, is the least difficult to explain, because it figures in virtually all tempestite models – from Bourgeois (1980), Allen (1982) and Dott & Bourgeois (1982) to Myrow & Southard (1996) (e.g., see Fig. 5).

*Description:* This topmost bed division consists of well-sorted, fine to very fine sand showing wave-



**Fig. 12.** Outcrop photographs of beds measured in the Karpuzçay Formation. (A) Thin-bedded sandstone tempestites intercalated with layers containing large amounts of plant detritus and shell debris. (B) A typical tempestite bed displaying sharp contacts with the under- and overlying mudstone. Bed of Facies *Sm*. (C) Bed of Facies *Smr* consisting of massive (non-structured) sandstone with a rippled top. (D) Thin-bedded tempestites of Facies *Sr* consisting of symmetrical wave ripples. (E) The occurrence frequency of the particular facies present in the measured beds.

ripple cross-lamination. Symmetrical wave ripples are common (Fig. 12D), along with asymmetrical ripples and occasional combined-flow ripples showing broad rounded crests and narrow V-shaped troughs (see Yokokawa et al., 1995). No clear evidence of climbing ripples has been found. This division is 0.3 to 20 cm thick and occurs mainly in thin beds (<30 cm), but also in the topmost parts of thicker beds (>30 cm).

*Interpretation:* The occurrence of ripple cross-lamination at the tops of the beds, directly above a planar parallel-stratified division, supports the notion of a rapid mode of hydraulic energy decline, which would explain further the lack of dune bedforms despite strong unidirectional currents (see interpretation of the previous bed division). The ripples were formed by either purely oscillatory waves or a waning, weak combined flow.





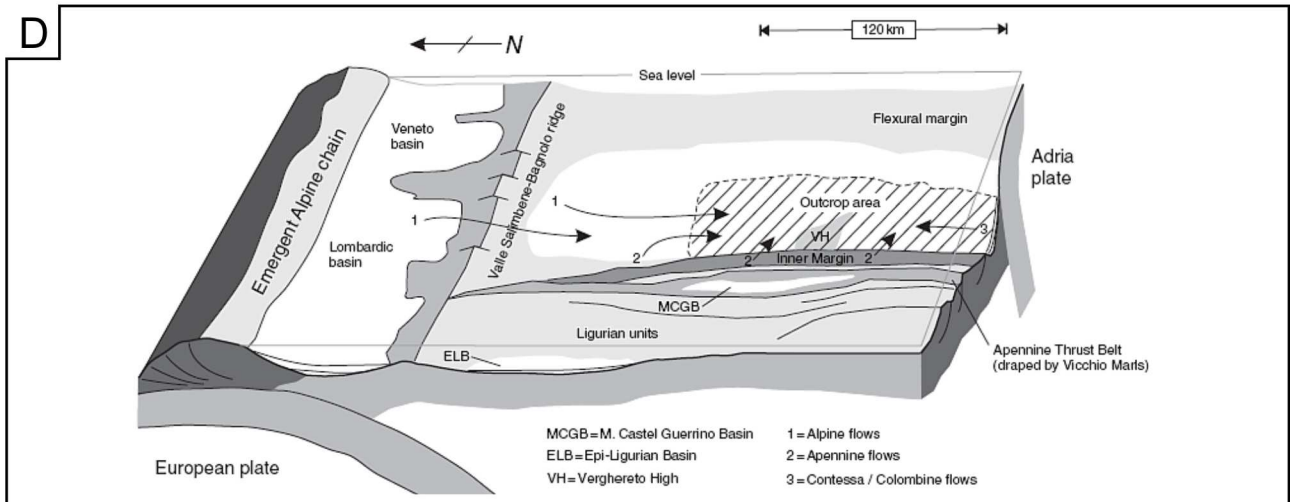
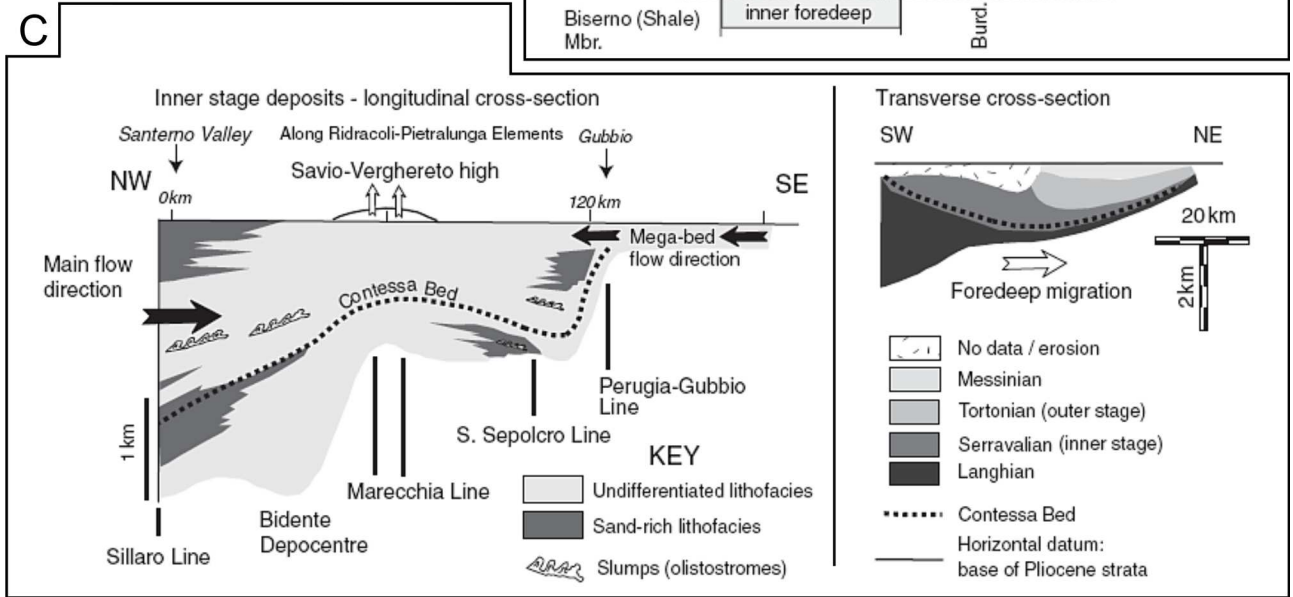
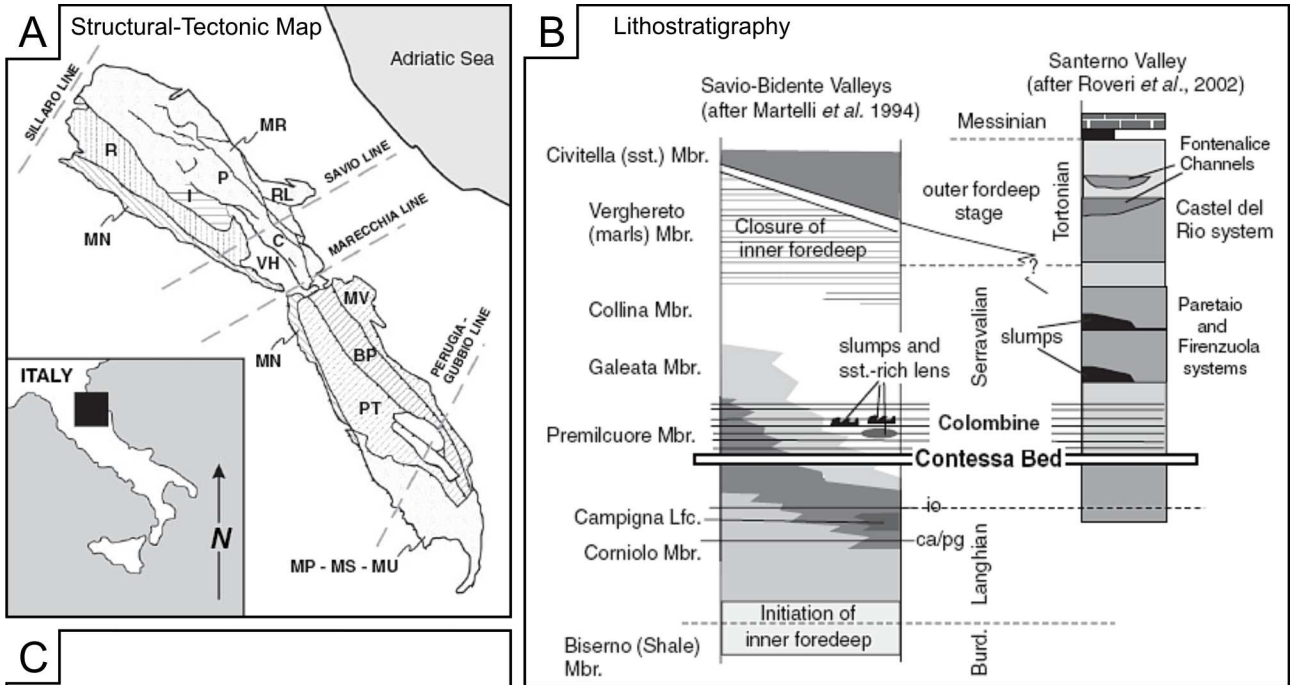
## 6. The Marnoso Arenacea Formation

### 6.1. Geological setting

The Late-Burdigalian to Tortonian, over 3500 m thick Marnoso Arenacea Formation was deposited in an elongate foreland basin adjacent to the Apennine thrust belt (Ricci Lucchi & Valmori, 1980; Ricci Lucchi, 1981, 1986; Talling, 2001; Amy & Talling, 2006; Talling et al., 2007a, b). The formation represents one of several foredeep turbidite basins that migrated towards the north-east during the Serravallian, as a result of thrust-front migration related to the subduction of the Adria plate beneath the overriding African plate. Deposition within each foredeep was typically dominated by mud-rich sedimentation, gradually replaced by marls, which dominate the upper parts of the basin-fills and drape the flexural margins. These thrust-top and foredeep basins were eventually overthrust by west-derived Ligurian and Subligurian units with oceanic affinity (Ricci Lucchi, 1981, 1986; Zattin et al., 2002). Deposition within the Marnoso Arenacea foredeep is generally subdivided into an older (Late Burdigalian to Serravallian) ‘inner stage’ and a younger (Serravallian to Tortonian) ‘outer stage’ (e.g., Amy & Talling, 2006). The inner-stage deposits were deposited in a relatively wide (> 60 km) and unchannelized foredeep and form the north-west (i.e., ‘inner’) part of the Marnoso Arenacea outcrop (Fig. 13C; Ricci Lucchi & Valmori, 1980). The transition to the outer stage is marked by the disruption of the foredeep by thrust faults. The outer-stage strata form the north-eastern (i.e., ‘outer’) part of the outcrop area and are characterized by a locally channelized deposition within a narrower basin.

The turbidite deposits studied in this work belong to the inner stage of the Marnoso Arenacea foredeep. This basin is a typical foreland basin with its basin fill pinching out towards the north-east flexural ramp and its cross section orientated normal to the paleo-thrust front (Fig. 13C). It is filled mostly by submarine flows sourced from the north-east, with an Alpine or subsidiary Apennine provenance, as indicated by the lithic component of sandstone beds (Gandolfi et al., 1983). Alpine sourced flows traversed the Valle Salimbene-Bagnolo Ridge, which separated the Marnoso Arenacea foredeep from the shallower-water Lombardic Basin (Fig. 13D; Ricci Lucchi, 1981). Currents occasionally entered the Marnoso Arenacea foredeep from the south-east, depositing limestone-rich ‘mega-turbidites’ (Ricci Lucchi & Valmori, 1980).

The deposits of the Marnoso Arenacea Formation crop out for a distance of ca 170 km along the basin axis to the south-east of the Santerno Valley (Fig. 13A). The strata are buried beneath Ligurian and Epiligurian units and alluvial sediments further to the north-west, as indicated by bore holes and seismic profiles in the area (see references in Argnani & Ricci Lucchi, 2001). Inner-stage deposits also thin markedly to the south of the Perugia-Gubbio Line (Ricci Lucchi & Valmori, 1980). The studied strata are exposed in



---

river canyons and road-cut sections, they are oriented both parallel and perpendicular the paleotransport direction and range in lateral extent from 100 to 500 m. Examples of some of the measured outcrops are illustrated in Fig. 14.

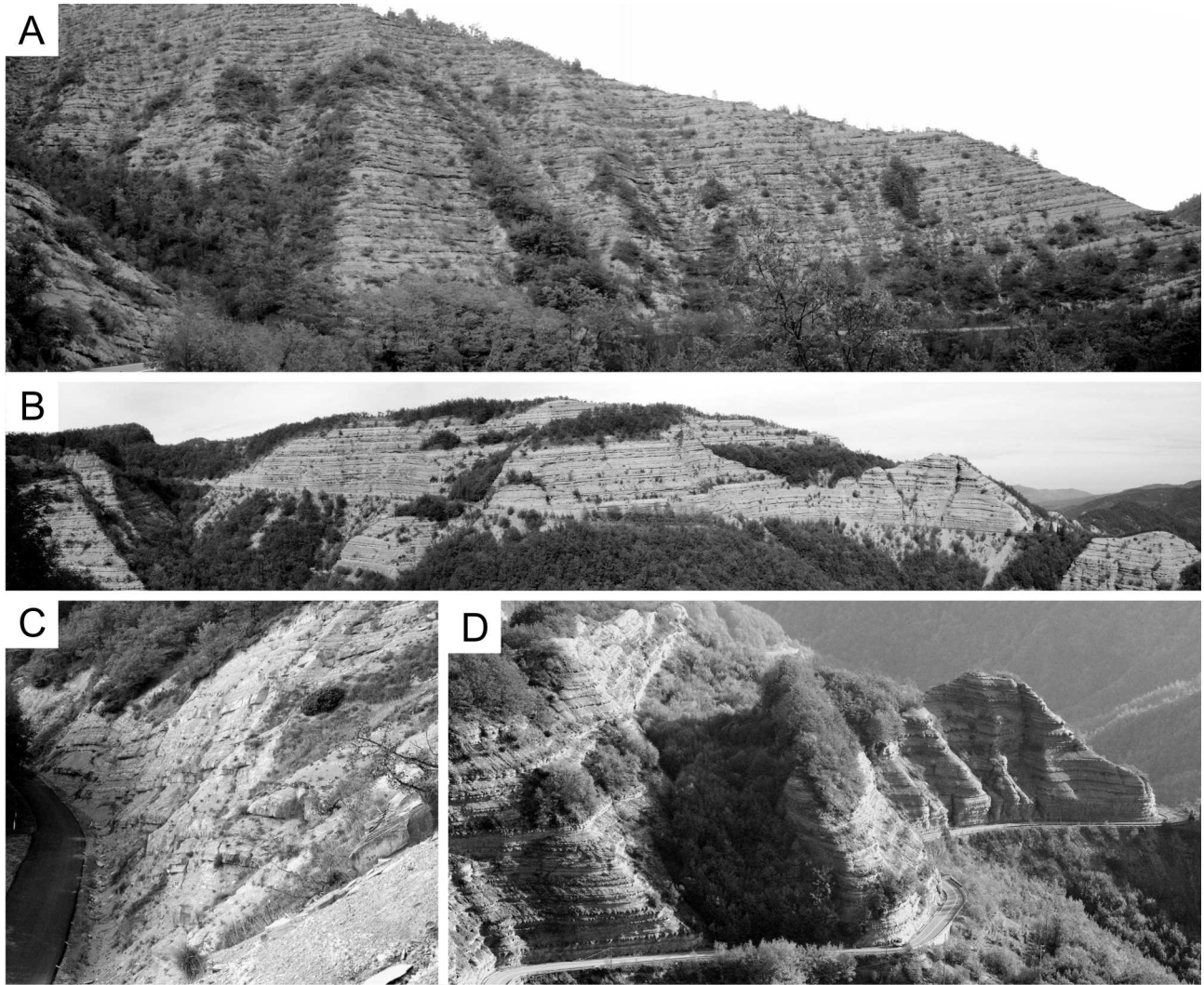
## **6.2. Results**

### **6.2.1. Bed types**

Marnoso Arenacea sandstones represent classical Bouma-type turbidites of depositional fan lobes deposited in a deep-marine setting (Ricci Lucchi & Valmori, 1980; Ricci Lucchi, 1981, 1986). The measured turbidites are of siliciclastic composition and have extremely sheet-like geometries. A total of 65 sandstone beds have been measured in this formation. Beds typically show normal grading, have well developed flute casts at their bases, and range in grain size from coarse or very fine sand to silt. The individual sandstones are intercalated with relatively thin mudstone beds (<30 cm). Eight different facies variants can be distinguished in this formation: *Tabcd(e)*, *Tabc(de)*, *Tab(cde)*, *Tbcd(e)*, *Tbc(de)*, *Tb(cde)*, *Tcd(e)* and *Tc(de)*. The lateral change in the separate Bouma divisions is not visually observable in the measured outcrops, although the change in divisions from thick to thin beds indicates the individual Bouma divisions pinch out successively from *a* to *d* in the dowflow direction, as will be described in section 7.2.3. below. The respective thickness-ranges of the individual Bouma divisions are as follows; division *a*: 10-50 cm, division *b*: 10-100 cm, division *c*: 2.5-50 cm, division *d*: 20-50 cm. The total thickness of beds varies from 2.4 to 133 cm.

### **6.2.2. Frequency distribution of turbidite thickness**

A total of 1767 measurements were recorded from the 65 measured beds in the Marnoso Arenacea Formation. Mean and median values of the obtained thickness population are calculated to be 31.315 and 20 cm, respectively. Numerical and graphical tests applied in this study indicate bed thickness in the Marnoso



**Fig. 14.** Photographs of the measured outcrops in the Marnoso Arenacea Formation. (A) Outcrop near the village of Corniolo. (B, D) Outcrops below the passo di Monchioli, uproad from the town of Bagno di Romagna. (C) Outcrop northwest from the village Premilcuore.

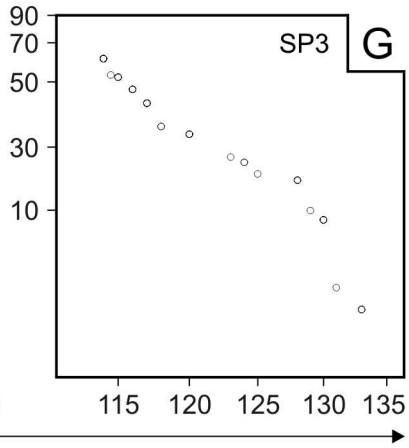
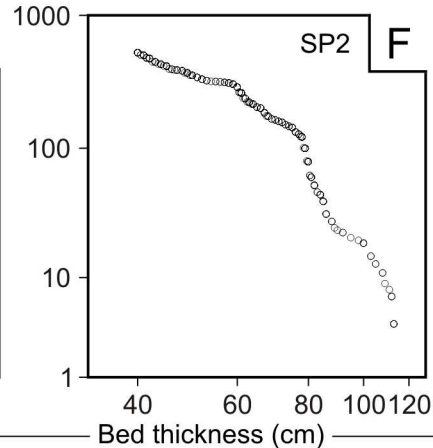
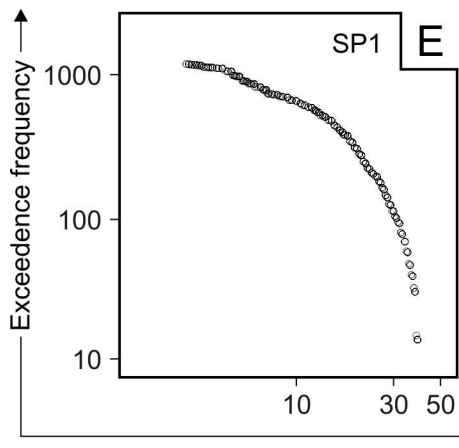
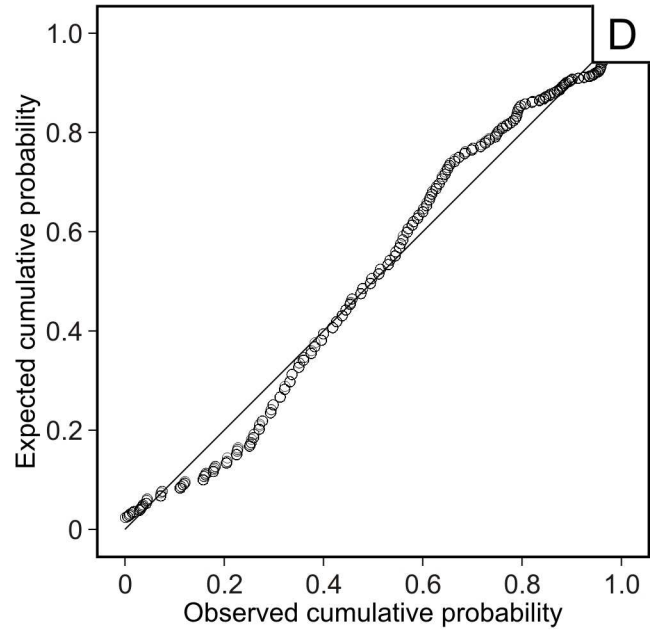
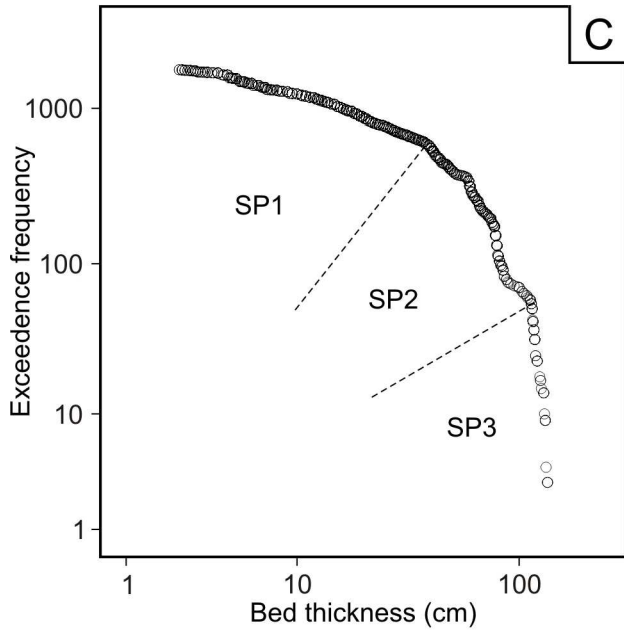
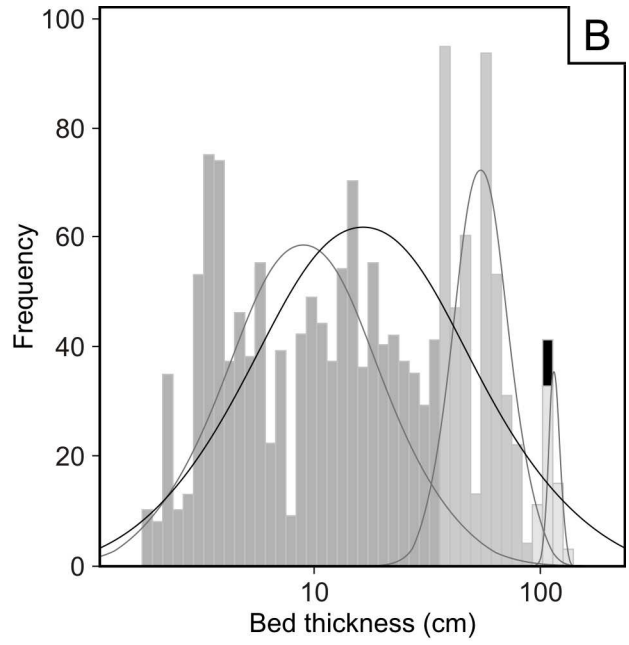
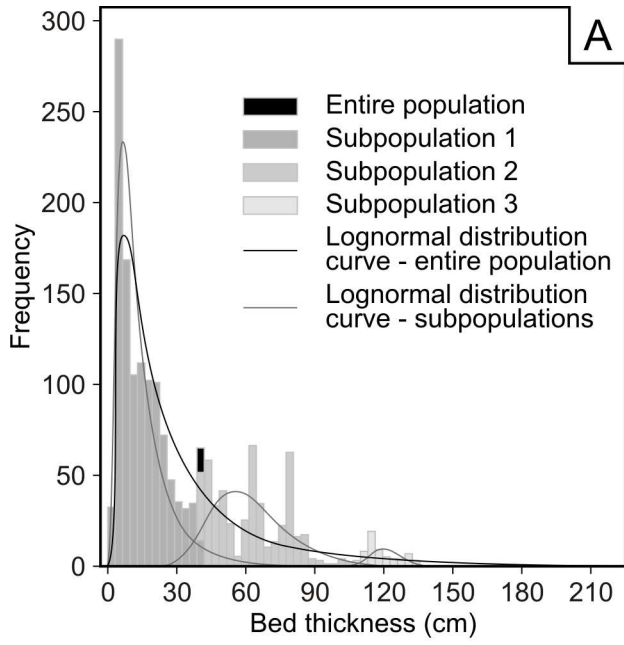
Arenacea Formation follows a lognormal distribution. The method of exceedence frequency (EF) plot, probability-probability plot, and frequency histograms were chosen to define the frequency distribution graphically. The deviation from a straight-line power-law relationship and the convex-up shape of the EF-curve on a plot with logarithmic axes indicates a lognormal distribution (Fig. 15C). The EF-curve consists of several straight-line segments separated by inflexion points. Such distributions have been previously interpreted as segmented power-laws (e.g., Rothman & Grotzinger, 1996; Chen & Hiscott, 1999; Sinclair & Cowie, 2003); however, as pointed out by Sylvester (2007) and indicated by the results in this study, the individual segments when re-plotted display a lognormal trend on a log-log exceedence frequency plot (Fig. 15E, F & G). This signifies the overall lognormal distribution is a summation of three separate lognormal distributions, corresponding to thin-, medium-, and thick-bedded turbidites. A good approximation to a

lognormal distribution is also indicated by the data trend on a probability-probability (P-P) plot (Fig. 15D). P-P plot compares the cumulative probabilities of a given variable to the cumulative probabilities of a theoretical reference distribution. If the given variable matches the reference distribution, the points cluster around a straight line. Three distributions were tested on a P-P plot: normal, lognormal, and exponential distribution, out of which lognormal gave the best results (Fig. 15D). Frequency histograms support the observations of exceedence frequency and probability-probability plots (Fig. 15A & B). The overall distribution is skewed to right meaning thin-bedded turbidites dominate over thick-bedded turbidites. The three distinct subpopulations observed on the EF-curve are also very well defined on linear histogram, each consisting of several minor lognormally-distributed subpopulations (Fig. 15A). The distribution takes on a Gaussian shape when plotted on a logarithmic histogram (Fig. 15B).

Estimation method of least squares (failure time on rank) and maximum likelihood was applied to test numerically what distribution best approximates the data. Pearson correlation coefficient for the linear fit on a probability plot and the Anderson-Darling test statistic were used to define the goodness of fit. Fourteen different distributions were tested: normal, lognormal, three-parameter lognormal, gamma, three-parameter gamma, exponential, two-parameter exponential, smallest extreme value, Weibull, three-parameter Weibull, largest extreme value, logistic, loglogistic, and three-parameter loglogistic. This analysis shows the data are best approximated by a lognormal distribution with the Pearson correlation coefficient of 0.98 and Anderson-Darling test statistic of 20.786. Numerical tests applied to the data did not yield statistically significant values. The following tests were applied: Kolmogorov-Smirnov test, Anderson-Darling test, and Shapiro-Wilk test with Lilliefors significance correction (does not assume data were drawn from a lognormal distribution). Probability values for all these tests showed the deviation from a lognormal distribution is significant. However, as correctly pointed out by Talling (2001) any numerical goodness-of-fit test will result in rejection of the null hypothesis when the number of observations is very large (NIST/SEMATECH, 2007).

### **6.2.3. Dowflow changes in bed thickness, facies, grain size, and bed-top undulations**

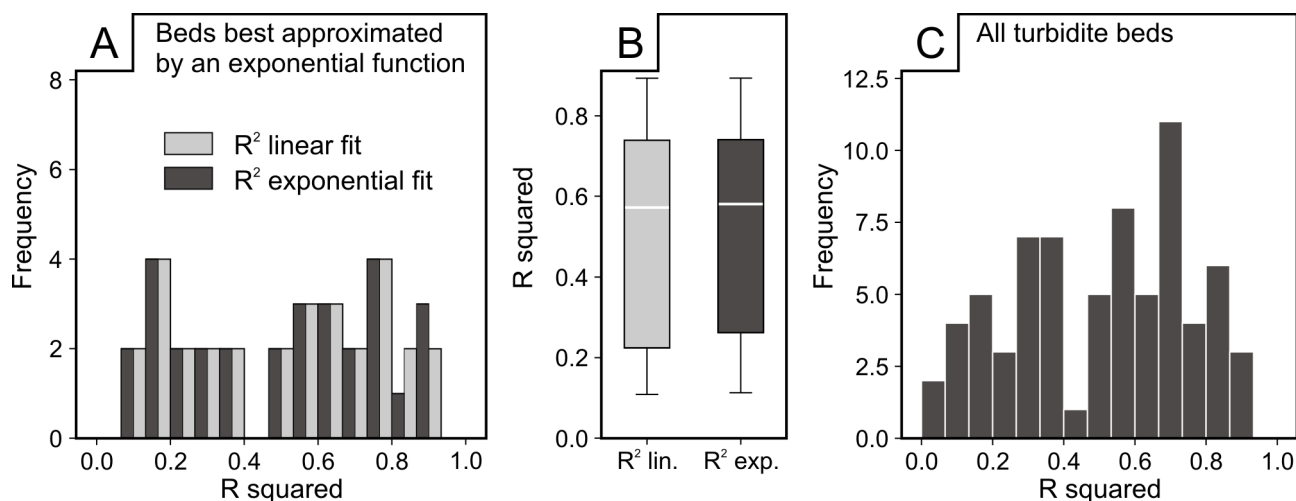
Out of 65 beds measured in the Marnoso Arenacea Formation 50 were measured parallel to the paleotransport direction and 15 were measured perpendicular to the paleotransport direction. The local thicknesses of measured beds range from 2.4 cm to 133 cm and the lateral/distal extent of beds in single outcrops varies from 50 to 410 m. Least square regression was applied to define the lateral and distal bed-thickness changes. Results have shown that 40 of all measured beds are best approximated by a linear function having the form of  $y = bx + c$ , where  $y$  is the bed thickness,  $x$  is the distance from the starting measuring point,  $b$  is the gradient of the regression line and  $c$  is the intercept. The rest of the beds (25 beds)



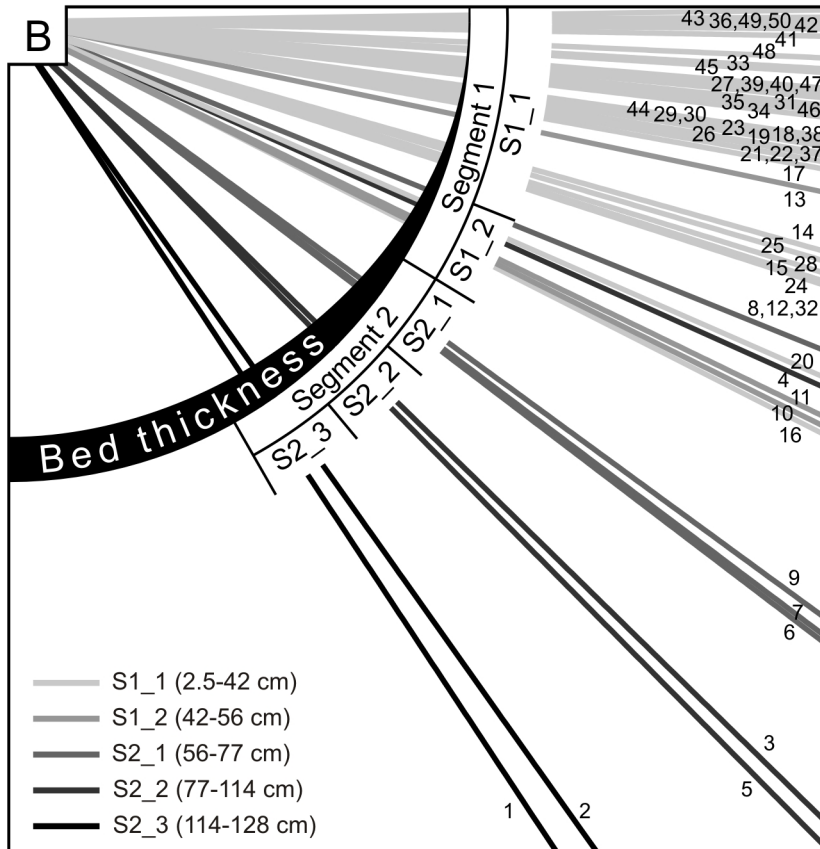
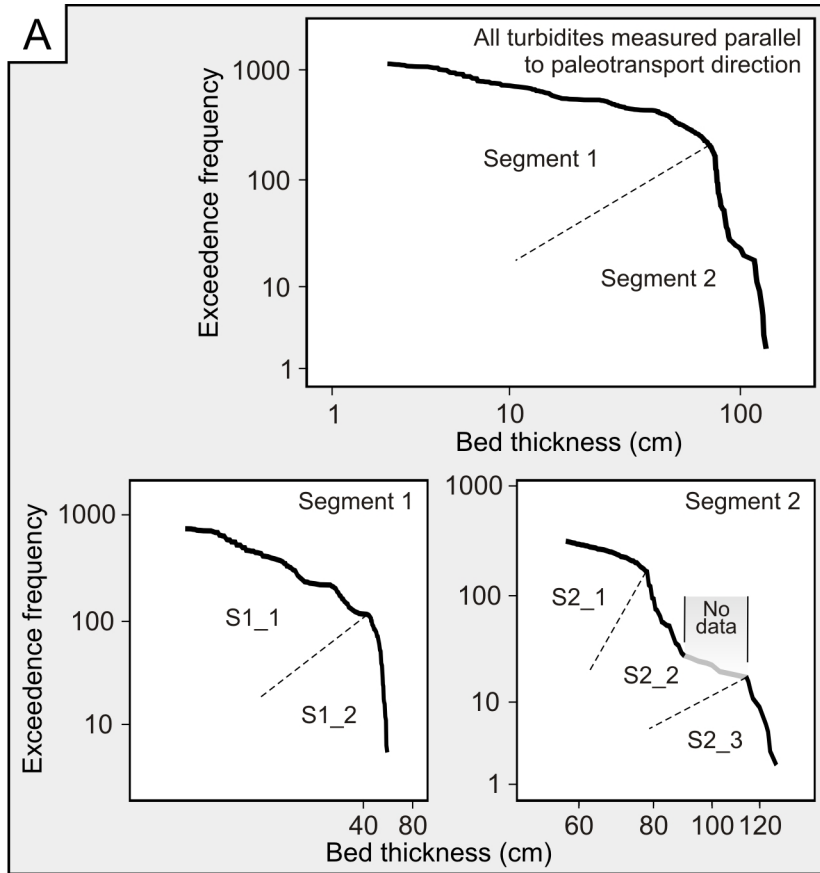
**Fig. 15.** Frequency distribution of turbidite thickness in the Marnoso Arenacea Formation. The thickness population of turbidites in this formation consists of 1767 measurements in 65 beds. **(A)** Frequency histogram shows the distribution is skewed to the right, meaning thin-bedded turbidites prevail. **(B)** Frequency histogram of the log-transformed bed thickness indicates the overall distribution consists of three minor lognormal distributions. The same trend can be observed in C. **(C)** Exceedence frequency plot of data. The overall distribution forms a segmented convex-up EF-curve. This distribution consists of three minor straight-line segments separated by inflexion points. Such distributions have been previously interpreted as segmented power-laws, however, as shown in E, F and G re-plotting the individual segments shows they are distributed lognormally. **(D)** The distributions and the observed segments in B are confirmed by data trends on a logarithmic P-P plot, on which the data points have a tight fit to a straight line. **(E, F & G)** Thickness subpopulations derived from the segments of the overall EF-curve display a convex-up curve on a log-log EF-plot, suggesting they follow similar distribution as the thickness population they come from.

are best approximated by a negative growth exponential function of the form  $y = ce^{bx}$ , where  $c$  and  $b$  are constants,  $e$  is the base of the natural logarithm, and  $y$  and  $x$  are the bed thickness and the downflow/transverse distance, respectively. Because linear regression is more practical and allows for determination of constant thickness-change gradient, beds best approximated by an exponential function were fitted linear regression trendlines for further analysis. Approximating exponential data by linear trendlines yields in this case satisfactory results; the change in the coefficients of determination  $R^2$  from exponential to linear fits is insignificant as indicated by the change of the mean  $R^2$  from 0.5099 to 0.5033 and by the change of the median  $R^2$  from 0.5812 to 0.5726. Graphical representation of this correlation together with the distribution of the overall  $R^2$  in the Marnoso Arenacea Formation is shown in Fig. 16.

Turbidite beds measured parallel to the paleotransport direction range in thickness from 2.4 to 128 cm and are lognormally distributed as indicated by the EF-curve in Fig. 17A. This frequency distribution can be subdivided into five thickness classes based on the geometry of the EF-curve: 2.5-42 cm, 42-56 cm, 56-77 cm, 77-114 cm, and 114-128 cm. Downflow thickness-changes of these beds approximated by linear



**Fig. 16.** **(A)** Frequency histogram showing the distribution of  $R^2$  for linear and exponential regression fits in beds that diminish in thickness exponentially. **(B)** Box-whisker plot of  $R^2$  for linear and exponential fits. The caps at the end of each box indicate the minimum and maximum values; the box is defined by the lower and upper quartiles and the line in the center of the box is the median. **(C)** Histogram showing the distribution of  $R^2$  (linear fit) for all 65 beds measured in the Marnoso Arenacea Formation.



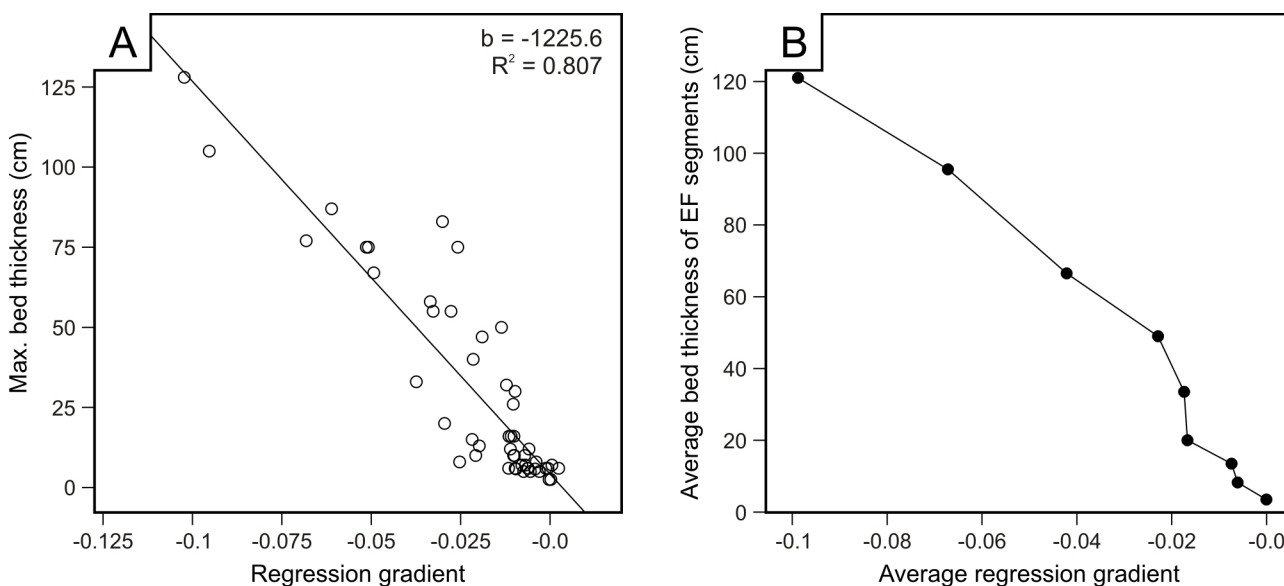
**C**

Bed #	Max. thickness (cm)	Regression gradient	Bed #	Max. thickness (cm)	Regression gradient
1	128	-0.1023	27	12	-0.0059
2	105	-0.0953	28	10	-0.0208
3	87	-0.0661	29	10	-0.0102
4	83	-0.0301	30	10	-0.01
5	77	-0.0682	31	10	-0.0071
6	75	-0.0514	32	8	-0.0253
7	75	-0.0508	33	8	-0.0039
8	75	-0.0258	34	7	-0.0079
9	67	-0.0493	35	7	-0.0069
10	55	-0.0335	36	7	0.0005
11	55	-0.0327	37	6	-0.0116
12	55	-0.0277	38	6	-0.0098
13	50	-0.0136	39	6	-0.0063
14	47	-0.019	40	6	-0.0061
15	40	-0.0215	41	6	-0.0012
16	33	-0.0374	42	6	-0.0006
17	32	-0.0122	43	6	0.0024
18	30	-0.0098	44	5.8	-0.0095
19	26	-0.0103	45	5.8	-0.0042
20	20	-0.0295	46	5	-0.0074
21	16	-0.0115	47	5	-0.0055
22	16	-0.0109	48	5	-0.003
23	16	-0.0101	49	2.5	-0.0003
24	15	-0.0218	50	2.5	0.0002
25	13	-0.0198			
26	12	-0.0111			

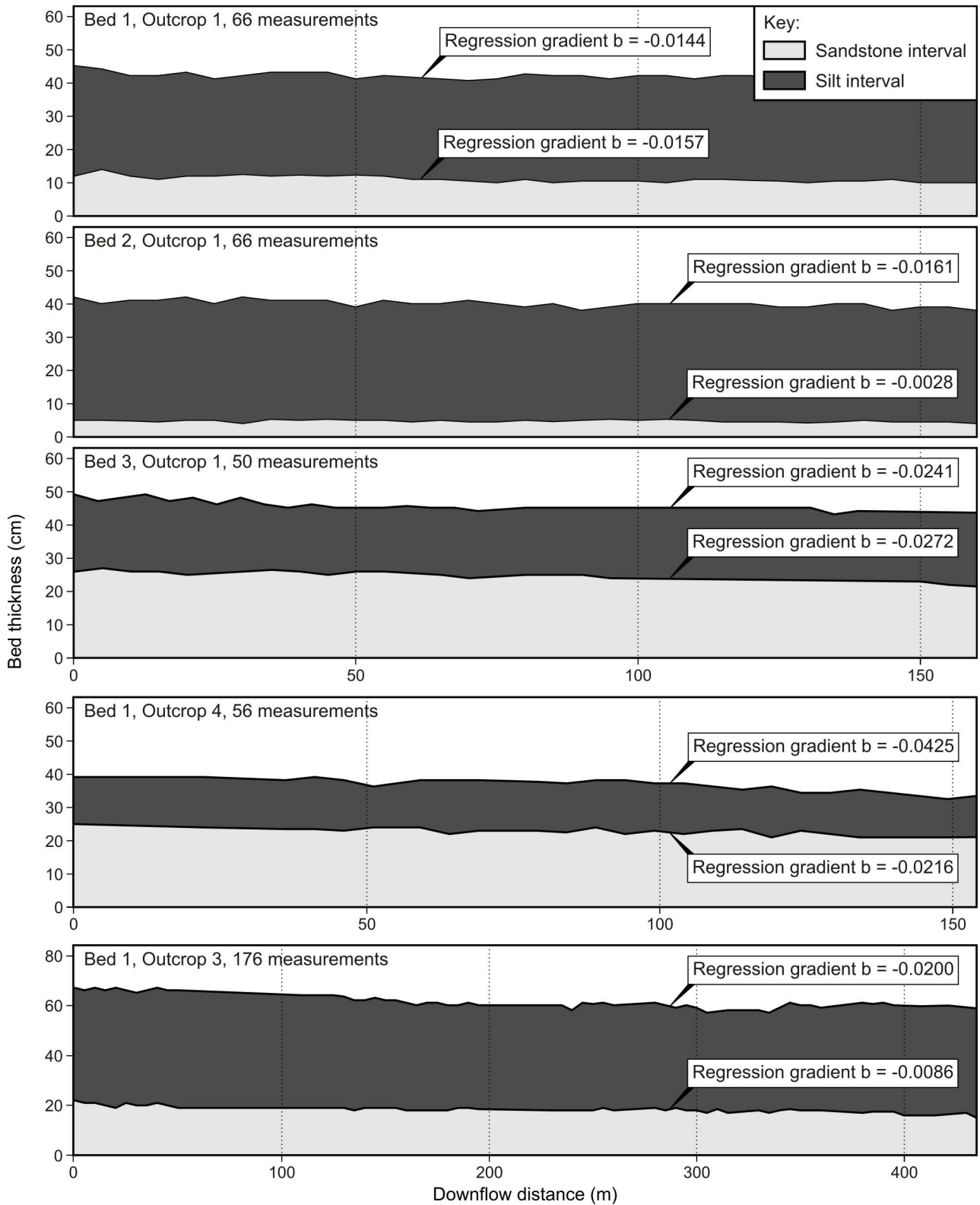


**Fig. 17.** (A) Exceedence frequency plots with logarithmic axes for all turbidites measured parallel to paleotransport direction. The overall distribution curve can be divided into two separate straight-line segments representing the two main thickness subpopulations. These subpopulations when re-plotted display a lognormal trend on the EF-plot and can be further subdivided into five minor segments. (B) Regression gradients (thinning rate) for all the beds measured parallel to paleotransport. Each bed is represented by its regression line. The intercepts of the regression equations are set to a common value to make the thinning rates of beds comparable on a single plot. The shading of the lines corresponds to the particular thickness classes defined from the EF-curves. Each bed is numbered (from thickest to thinnest) with their exact regression gradients listed in (C). See Appendix for *distance* versus *thickness* plots of the individual beds.

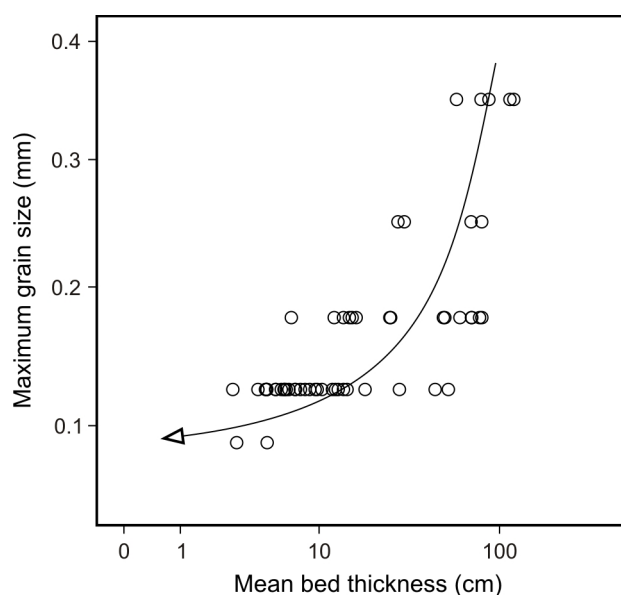
regression coefficients (gradients of regression lines) range in number from -0.1023 to 0.0024 (Fig. 17C). The wide spectrum of regression gradients indicates the thinning rate of turbidite beds in Marnoso Arenacea varies significantly and cannot be expressed by a single linear function. Assuming the pinchout geometry of a single turbidite bed is nonlinear in shape and the thickness of a bed diminishes downcurrent, the local thinning gradient should theoretically be a function of the local bed thickness. Quantitative and qualitative comparisons between thinning gradients and bed thicknesses support this presumption and are illustrated in Fig. 17B and Fig. 18. Fig. 18A shows the relationship between the maximum bed thicknesses (of bed-segments measured in single outcrops) and their corresponding thinning gradients is significant with the goodness-of-fit  $R^2$ -value being higher than 80 %. Furthermore, the intervals of lateral thinning rates constituting the overall spectrum shown in Fig. 17B are consistent with the segments seen on the EF-curve defining the specific thickness classes (Fig. 17A). Results indicate the local bed thickness in the Marnoso Arenacea Formation decreases with increasing local thinning gradient. This trend becomes even more



**Fig. 18.** (A) Plot showing the relationship between the regression gradient and the local bed thickness in Marnoso Arenacea beds measured parallel to paleotransport. Note the regression gradient increases with decreasing local bed thickness. The  $R^2$ -value for the linear regression fit indicates this relationship is statistically significant. (B) The relationship between bed thickness and thinning rate becomes very evident when the mean thinning gradient is plotted against the average bed thickness of the particular EF-segments.

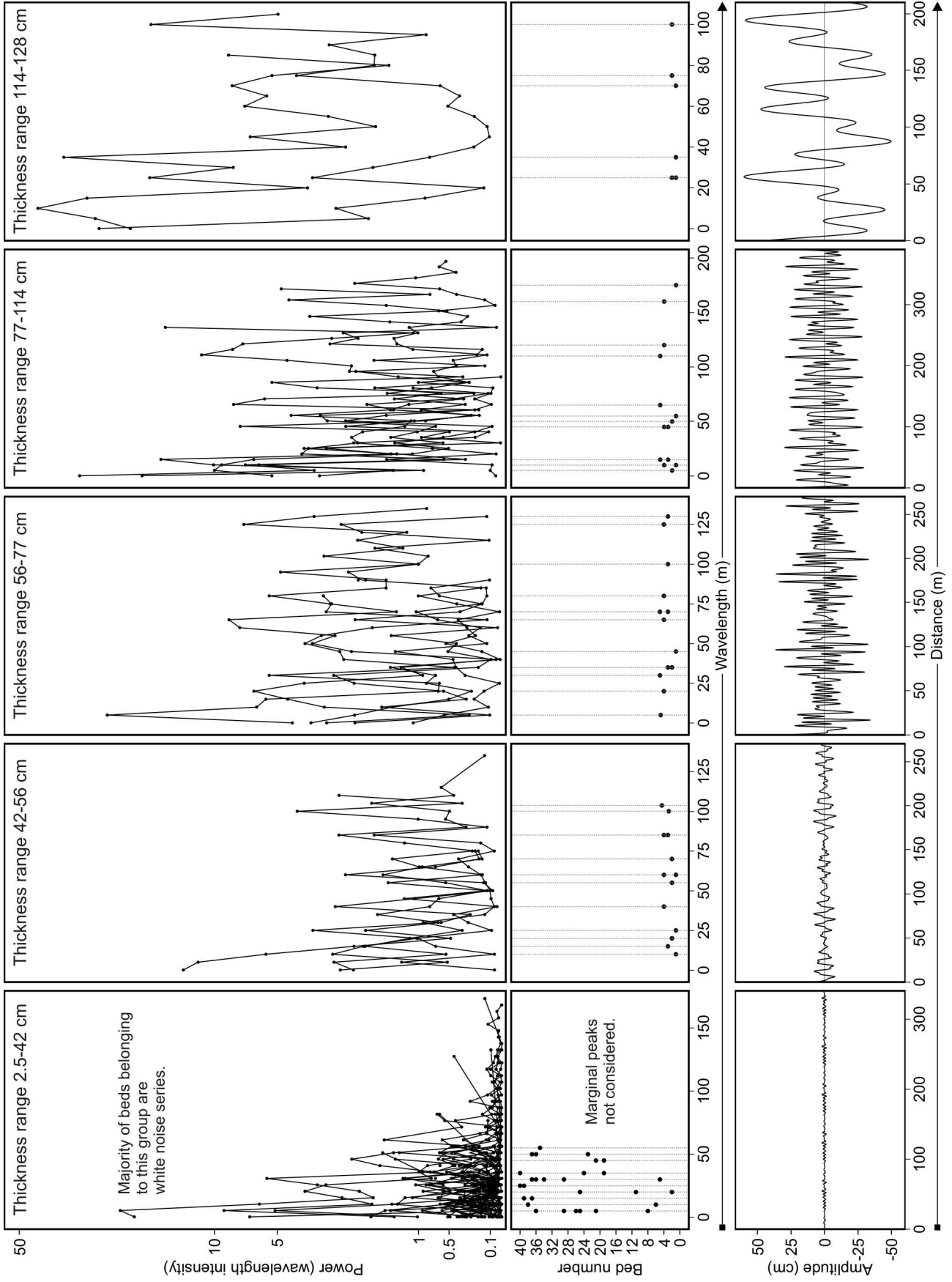


**Fig. 19.** Five Marnoso Arenacea beds in which both the sandstone and the siltstone interval were measured. These systematic measurements indicate the thinning rate of the siltstone interval (Bouma division *d*) within a turbidite bed is independent of the thickness and the thinning rate of the underlying sandstone interval, and also, the total thickness of the bed.



**Fig. 20.** Change in maximum grain size from thick to thin beds in the Marnoso Arenacea Formation. Maximum grain size is found to diminish with decreasing local bed thickness in a concave-upward fashion. Note: plot with logarithmic axes.

pronounced when the mean thickness of the EF-segments is plotted against their corresponding average thinning gradients (Fig. 18B). The spectrum of thinning rates, when stacked according to the thickness classes derived from the EF-curve (under the assumption that bed thickness decreases continuously downflow), implies the pinchout geometry of a single turbidite bed is of concave-upward shape (Fig. 23). The pinchout distance of such a theoretical turbidite bed with its maximum thickness being 128 cm would be approximately 96.5 km. This distance is roughly consistent with the extent of beds derived from long-distance bed-to-bed correlations in the Marnoso Arenacea Formation by Amy and Talling (2006). The thinning rate of the silt interval (Bouma division *d*) within a turbidite bed derived from measurements of five beds in Marnoso Arenacea seems to be independent of the thickness and the thinning rate of the underlying sandstone interval, and also, the total thickness of the bed (Fig. 19). However, the change in lithology from thick to thin beds indicates the separate Bouma divisions pinch out in the downcurrent direction successively from division *a* to division *d* and overall have lenticular pinchout geometries (Fig. 24). Grain-size trends of the measured beds are comparable to that of Sadler's (1982) with the maximum grain size diminishing with decreasing bed thickness in a concave-upward fashion (Figs. 20 & 23). The analysis of bed-top undulations in the studied beds suggests their geometries do show certain periodicities and hence are worth investigating mathematically. An exception are the thin-bedded turbidites (<42 cm) in which the bed thickness variations seem to be almost purely random without any autocorrelation structure as indicated by their frequency spectrums examined on cumulative periodograms. Despite this indication, an effort has been made to differentiate between the different wavelength-frequencies in order to best approximate the actual undulations. The dominant wavelengths of the bed-top waveforms for the specific thickness classes defined from the EF-curve are as follows: thickness class 2.5-42 cm: 5, 15, 30, 35, 50 meters; thickness class 42-56



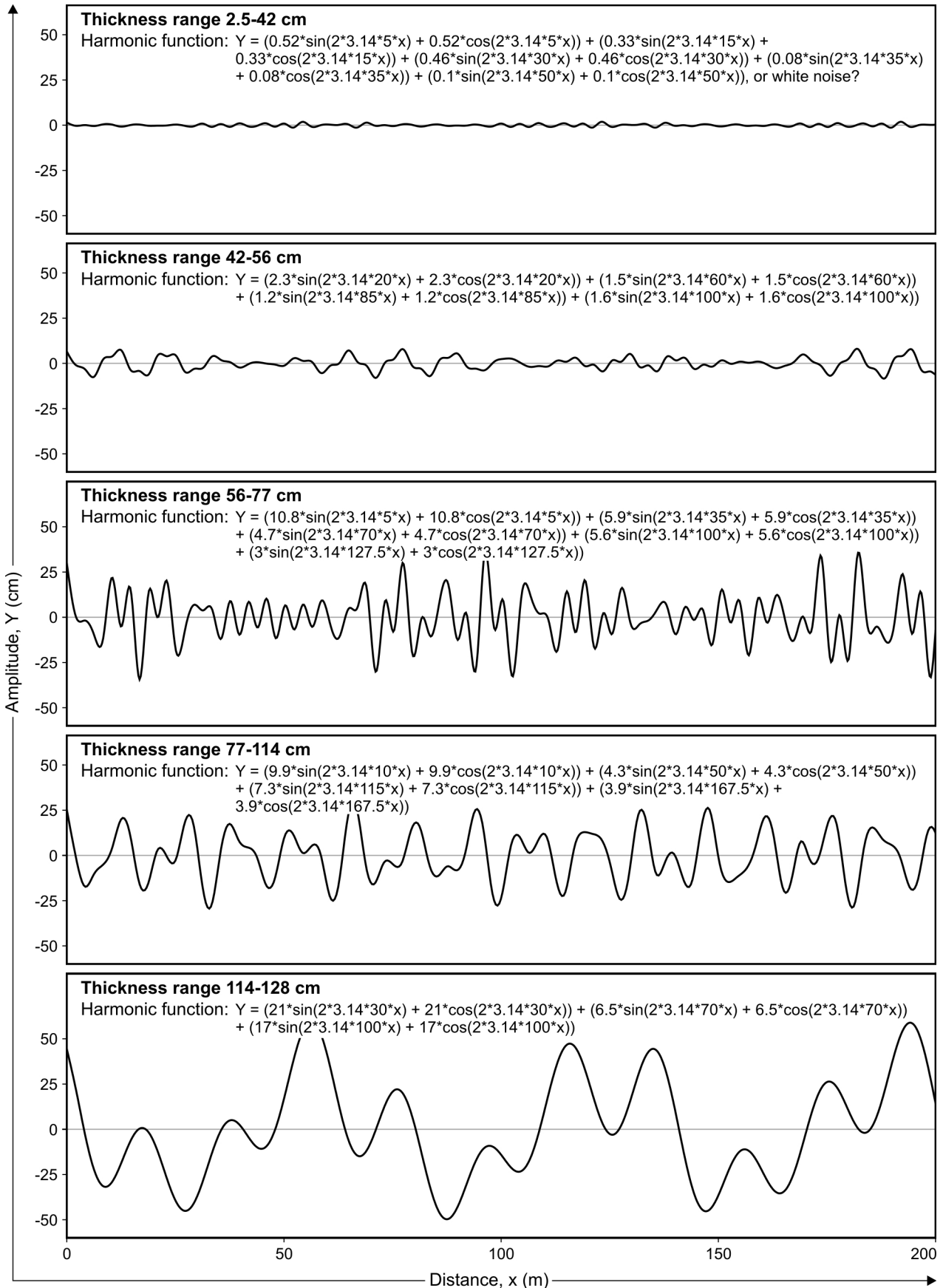
**Fig. 21.** Figure illustrating the analysis of bed-top undulations in the Marnoso Arenacea Formation. Frequency spectrums of the individual beds plotted on periodograms (top) were compared within the particular thickness ranges derived from the EF-curve. Dominant peaks of the frequency spectrums were picked out (middle) and their corresponding wavelengths and power were used to model harmonic functions representing the actual bed-top undulations (bottom). Periodograms show that the power of the wavelengths increases with bed thickness, and also, the dominant frequency spectrum shifts from low to high wavelengths with the increase in bed thickness. This trend is more pronounced in the modelled undulations (bottom). The wavelength and downflow distances (x-scale) vary for the particular thickness ranges and depend on the measured length of the beds.

---

cm: 20, 60, 85, 100 meters; thickness class 56-77 cm: 5, 35, 70, 100, 127.5 meters; thickness class 77-114 cm: 10, 50, 115, 167.5 meters; thickness class 114-128 cm: 30, 70, 100 meters. The length of the wavelengths is observed to increase with bed thickness, while their abundance decreases (i.e., the waveform becomes simpler, random noise is filtered out) (Figs. 21, 22 & 23). The amplitude of the waveforms decreases with bed thickness with the maximum amplitude for the 114-128 thickness class being approximately 60 cm.

#### **6.2.4. Thickness changes normal to depositional dip**

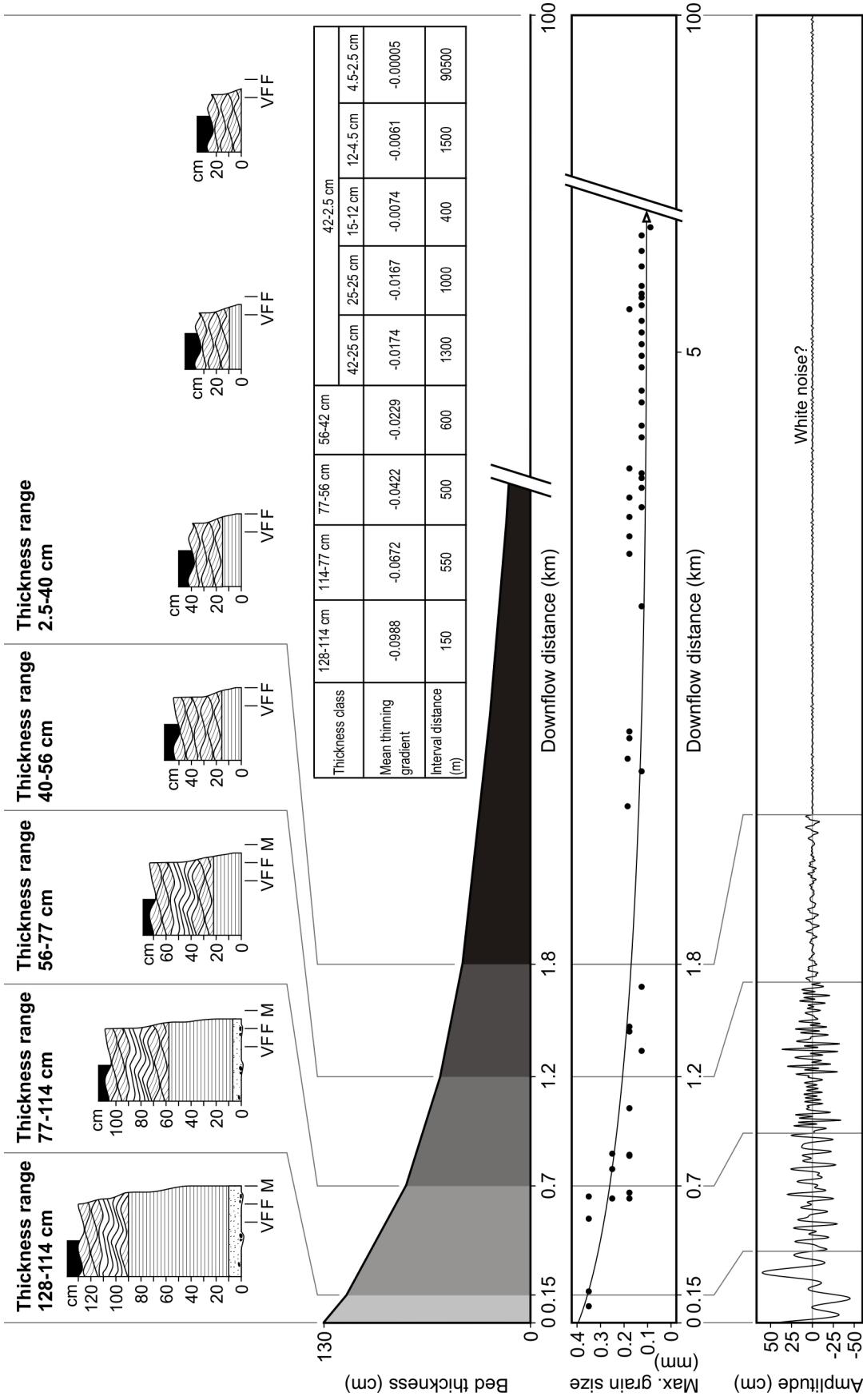
Beds measured perpendicular to the paleotransport direction constitute only a small dataset in this study, and therefore, statistical analyses and conclusions drawn about the thinning rates of these beds might be subject to error. The thickness frequency distribution of the beds seems to be best approximated by a Gaussian theoretical distribution as indicated by the frequency histogram and the normal P-P plot in Fig. 25A & B; the Pearson correlation coefficient for the linear fit on a probability plot of 0.964, and the Anderson-Darling and Kolmogorov-Smirnov test statistic of 4.163 and 0.104, respectively. The exceedence frequency curve of these measurements maintains its convex shape on a plot with logarithmic axes, similar to beds measured parallel to the paleotransport direction. Four thickness classes can be distinguished from the EF-curve: 3-30 cm, 30-59 cm, 59-127 cm, and 127-133 cm. Although these thickness classes differ considerably from the classes distinguished in beds measured parallel to the paleotransport direction, the regression gradients defining the thinning rate of beds follow roughly the same trend – the maximum thickness of beds decreases with increasing regression gradient (Fig. 25C & D). This relationship, approximated by a linear regression line has a confidence value of 68.5 % and a regression gradient of -236, indicating the beds measured perpendicular to paleotransport thin at a higher rate than the beds measured parallel to the depositional dip (with a regression gradient of -1225,6 – Fig. 18A). Four beds (26 % out of all beds) do not follow this trend and can be considered outliers. However, because the thickest bed measured (max. thickness 133 cm) is the only bed in the class 127-133 cm, and it does not have a comparison in the dataset of beds measured parallel to the paleotransport direction, it cannot be considered an outlier and its thinning rate is to be representative



**Fig. 22.** Modelled bed-top undulations and their corresponding harmonic functions for the thickness classes derived from the EF-curve.. Note the wavelengths and amplitudes of the waveforms increase with bed thickness. The complexity of the harmonic functions increases with decreasing bed thickness as more random noise is introduced into the series. For the thickness range 2.5-42 cm most of the beds test as white-noise series, hence it can be said the obtained harmonic function does not define the actual bed-top undulations very well.

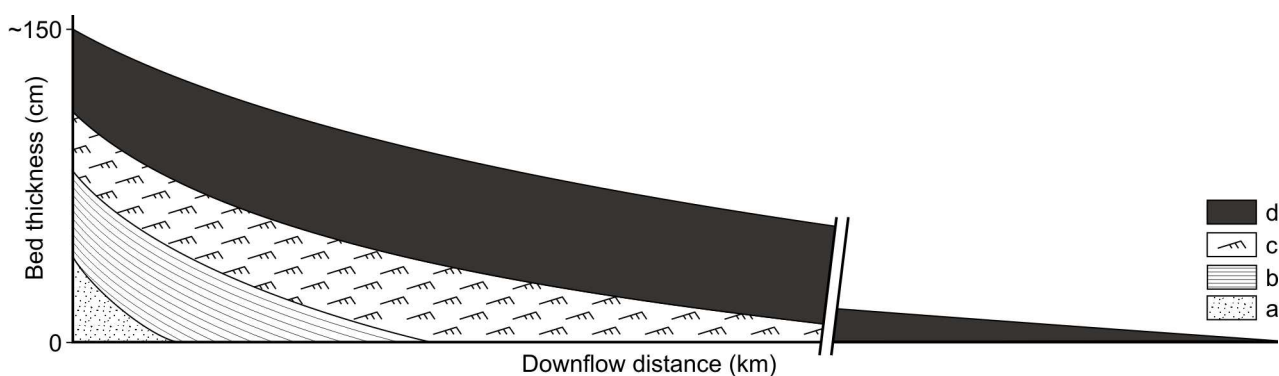
---

of the particular thickness class. Thereby, assuming a turbidite bed thins continuously from its centre towards its lateral margin, the lateral pinchout geometry of a single bed would be of a roughly concave-upward shape with a gentle dipping proximal extremity (Fig. 25E). The lateral pinchout distance from the centre of a 133 cm thick turbidite would be in this case approximately 9.5 km. However, because of the assumed fan shape of the Marnoso Arenacea turbidites, this distance cannot be taken to represent the lateral thinning trend along the entire downflow axis of a single turbidite.



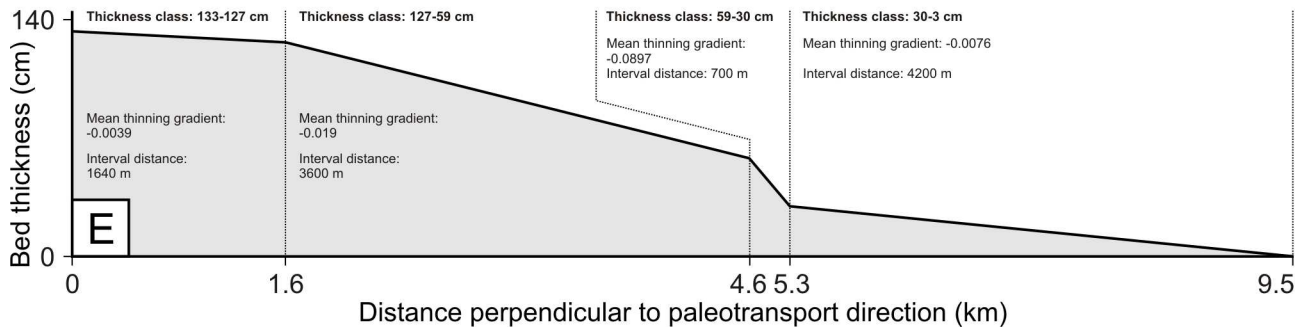
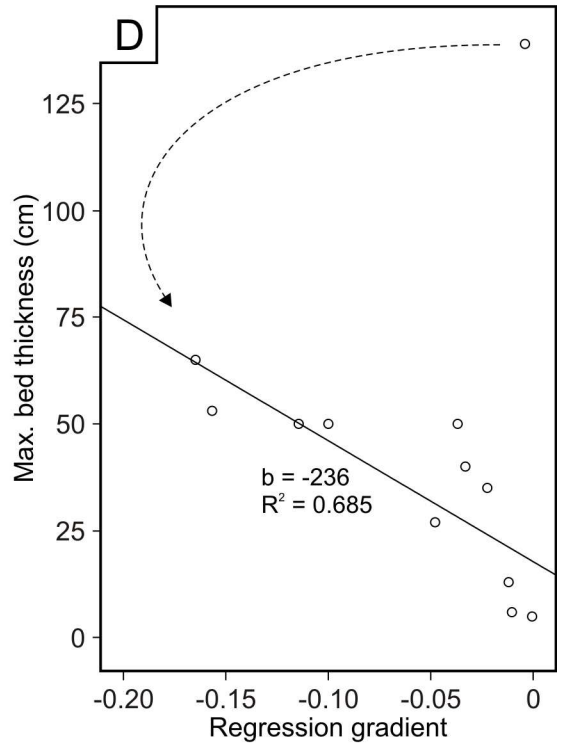
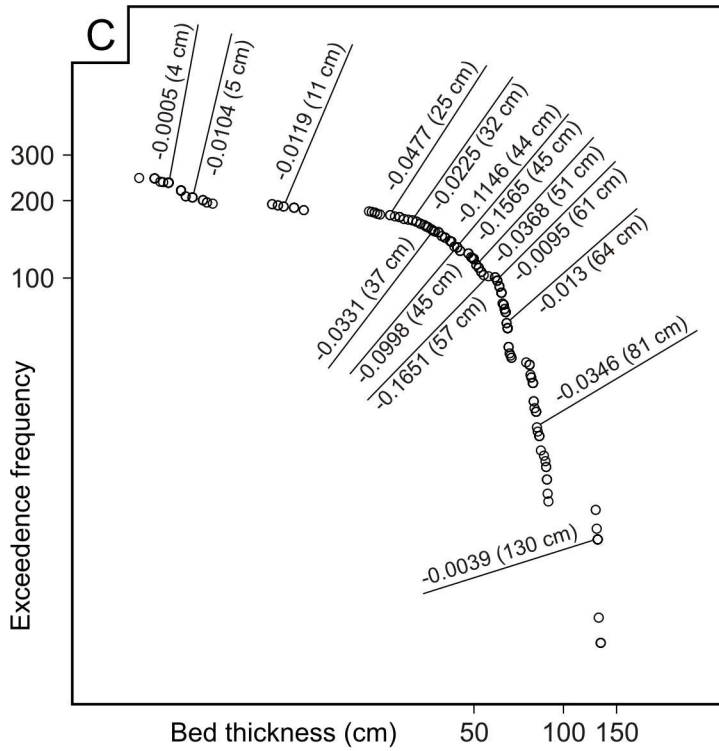
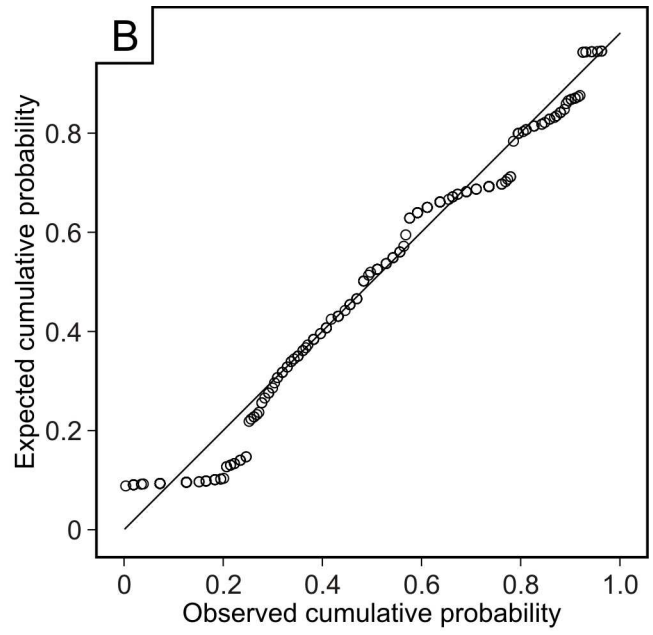
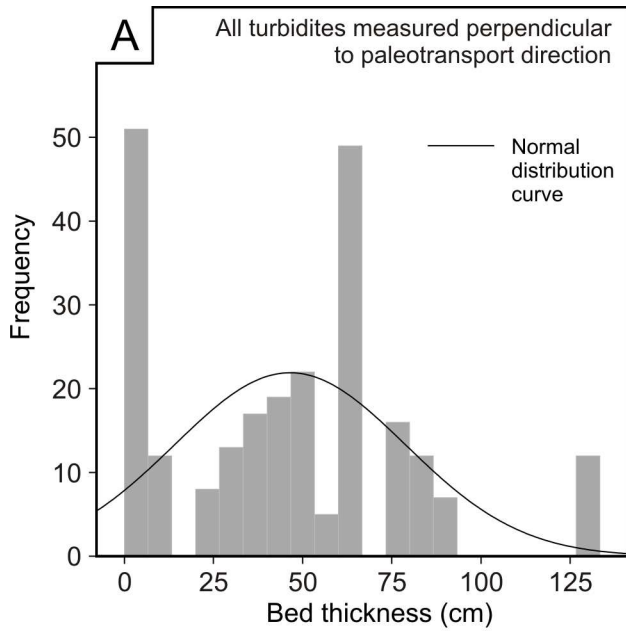
**Fig. 23.** Downflow changes in bed thickness, facies, grain size, and bed-top undulations for the Marnoso Arenacea Formation turbidites. These trends are based on the assumption that a turbidite bed thins continuously in the downflow direction from the point of its maximum thickness (i.e., locally thick beds are more proximal than locally thin beds). Stacking together the mean thinning rates for the particular thickness classes defined from the EF-curve yields pinchout geometry of a concave-upward shape (upper middle). The concave-upward trend is followed by the maximum grain size and to a certain degree also by the individual Bouma divisions (top). Bed-top undulations decrease in wavelength and amplitude with decreasing bed thickness, thereby also with increasing downflow distance. For a more detailed description of the overall trends see text.





**Fig. 24.** Schematic representation of pinchout geometries for the particular Bouma divisions. These geometries are based on the division changes from thick to thin beds. Note the pinchout geometries of the individual intervals are of lenticular shape meaning they will experience thickening in the most proximal areas. In the distal parts the divisions will peter out in a concave-upward fashion.

**Fig. 25 (next page).** Thickness frequency distribution and lateral thinning rates of Marnoso Arenacea beds measured perpendicular to the paleotransport direction. (A) Frequency histogram indicating a Gaussian distribution of the measurements. The distribution is slightly skewed to the right. (B) Normal P-P plot showing a good fit of the data to a straight line, meaning the normal distribution fits the data very well. (C) Exceedence frequency plot of the data with lateral regression gradients added to illustrate the change in thinning rate with local bed thickness. The EF-curve has a convex shape and can be segmented into four straight-line segments (Note: plot with logarithmic axes). (D) Plot illustrating the change of regression gradient with maximum bed thickness. The regression line approximating the trend of beds below 75 cm has a gentler gradient than the regression line in Fig. 18A, suggesting the beds measured perpendicular to paleotransport thin more rapidly than beds measured parallel to the paleotransport direction. The thickest bed (133 cm) does not follow this trend; however, because it is the only bed within that specific thickness range it cannot be considered an outlier. A theoretical trend from the thickest bed to the subsequently thinner beds is indicated by the dashed arrow. (E) Pinchout geometry of a single turbidite bed perpendicular to paleotransport. The stacking of the thinning rates for the individual thickness classes indicates the bed will thin at a low rate in its most proximal areas before it starts tapering out in a roughly concave-upward fashion. Because of the assumed fan shape of the Marnoso Arenacea turbidites, this distance cannot be taken to represent the lateral thinning trend along the entire downflow axis of a single turbidite.



## 7. The Monte Fumaiolo Formation

### 7.1. Geological setting

The Early Serravalian Monte Fumaiolo Formation is a succession of shallow marine bioclastic sediments and represents a marginal equivalent of Marnoso Arenacea which was deposited in the Umbria-Marche domain (north-western part of the Adriatic plate) during the collision of the Adriatic and European plates (Sestini et al., 1986). The sediments of Monte Fumaiolo were deposited behind the inner thrust front, and over the Ligurid nappes which have an oceanic domain (Ricci Lucchi and Valmori, 1980; Ricci Lucchi, 1981; 1986). Little has been published on the sedimentology of this formation and the depositional setting of a Gilbert-type delta can only be inferred from the large fore- and bottom-sets observed at the outcrop of La Verna. The measured outcrop (Fig. 26) represents deltaic sandstone lobes pinching out in prodeltaic shelf mudstones. For location of the outcrop in northern Apennines see Fig. 3B.

### 7.2. Results

#### 7.2.1. Bed types

A total of three beds were measured in the Monte Fumaiolo Formation. These three beds have a siliciclastic composition, show normal grading, and range in grain size from coarse to very fine sand. They are separated by a very thin layer (<5 cm) of siltstone, which otherwise dominates the outcrop (Fig. 26). The beds have probably been deposited by sand dumped by a bypassing turbidity current in the hydraulic-jump conditions at the base of a steep delta slope (W. Nemeč, pers. comm. 2007). Only two facies variants are recognized in this succession:  $Ta(b)c(d)$ , and  $Tc(d)$ . The downflow pinching of the  $Tac$  beds results in the loss of the  $a$  division, hence these beds turn into  $Tc$ -type turbidites in their most distal extremities. The thickness of the  $a$ -division ranges from 10 to 25 cm, while the thickness of the  $c$  division is generally less than 5 cm. The Bouma division  $b$  in the measured bed-segments is of negligible thickness. The overall thickness of the measured beds ranges from 0.3 to 29.5 cm.



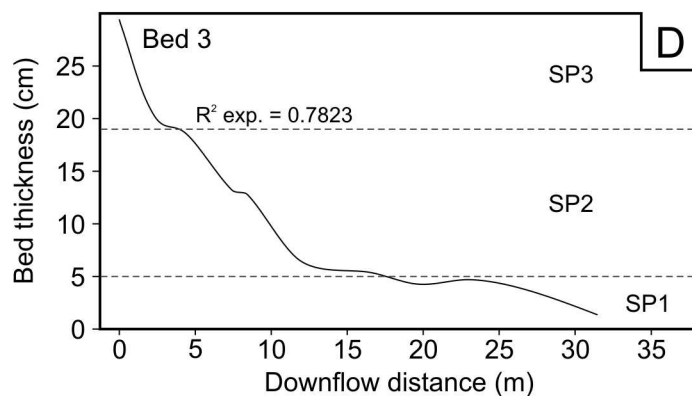
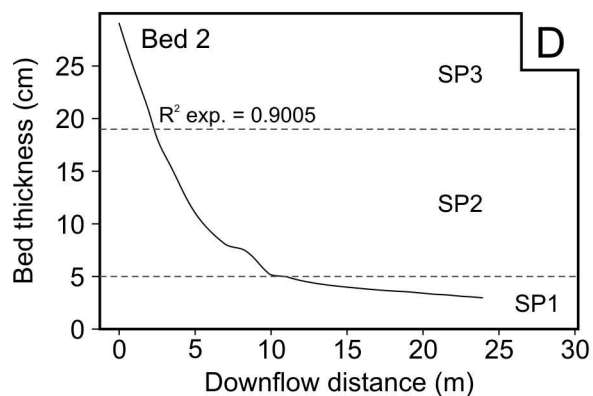
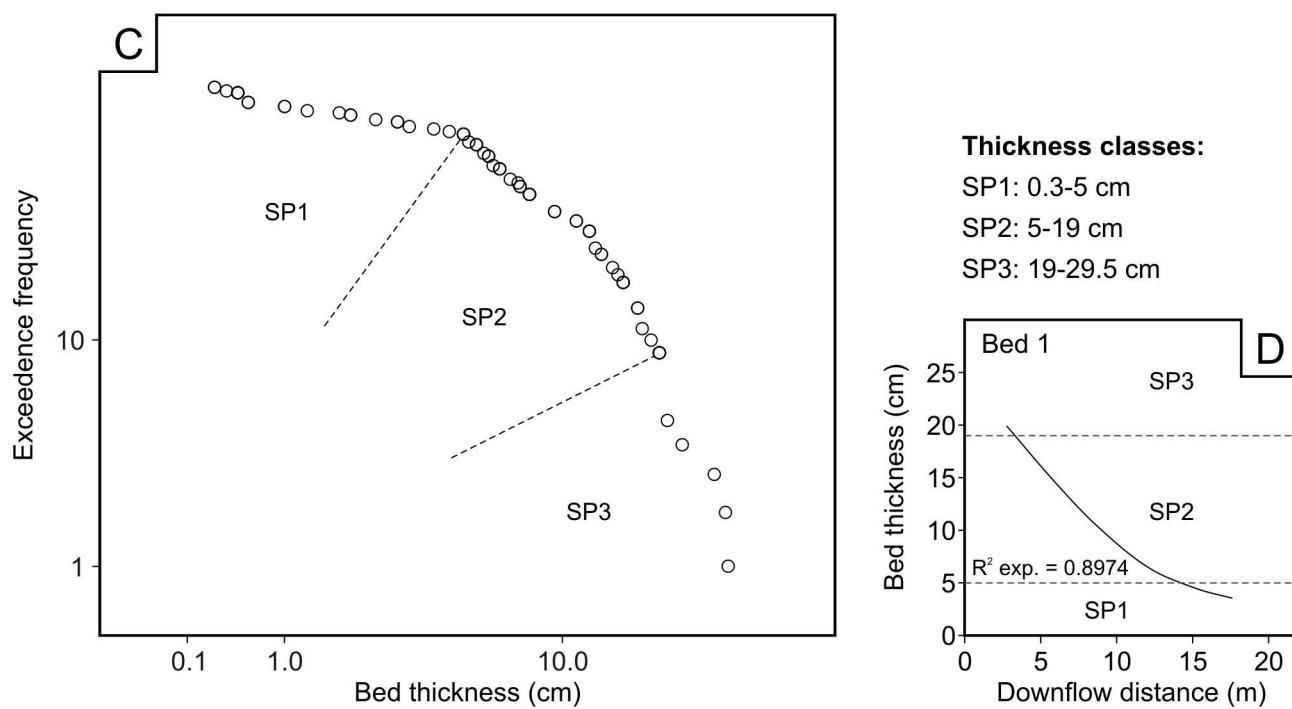
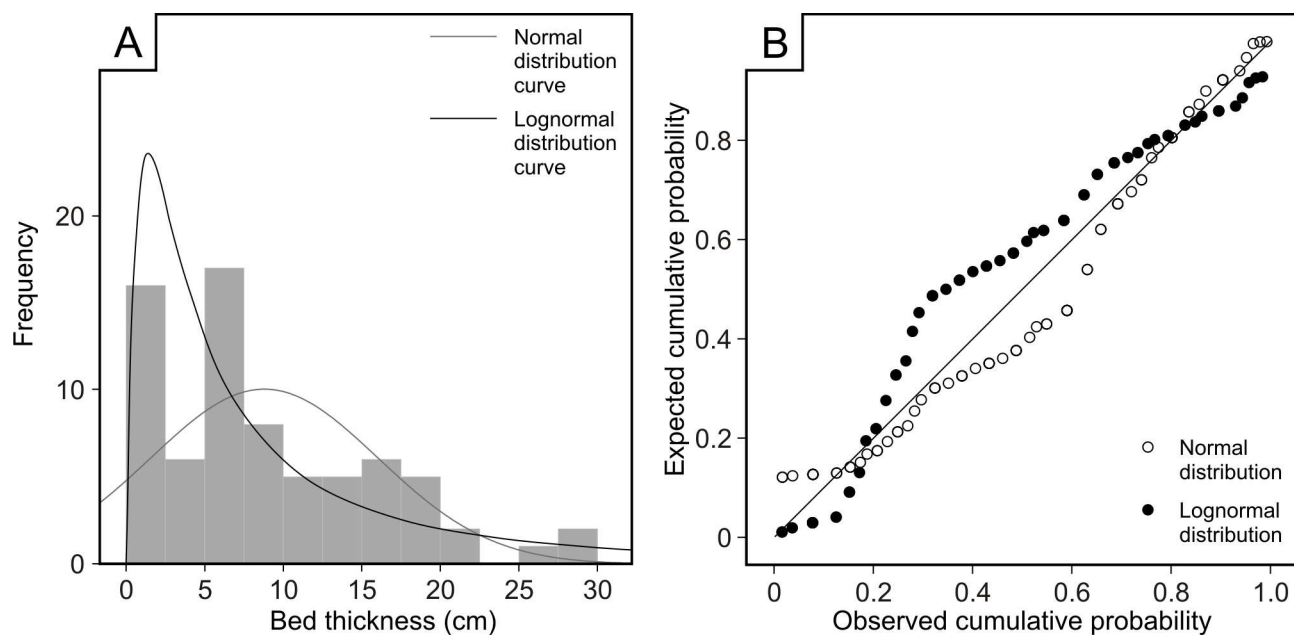
**Fig. 26.** Figure showing beds measured in the Monte Fumaiolo Formation, northern Apennines. The measured beds represent deltaic sandstone lobes pinching out in prodeltaic shelf mudstones. Outcrop on the photograph is approximately 70 m long and is located below the Franciscan convent of La Verna. The view is along the depositional strike.

### 7.2.2. Frequency distribution of turbidite thickness

The three measured beds in the Monte Fumaiolo Formation correspond to 73 measurements. The mean and median thickness is 8.797 and 6.5, respectively. Graphical and numerical tests indicate the thickness frequency distribution of the measured beds is best approximated by a Gaussian (normal) test distribution. However, because the difference between its fit to a Gaussian test distribution and a lognormal test distribution is very small, these turbidites can also be considered to have a lognormal thickness distribution. The frequency histogram of the data shows the distribution is slightly skewed to the right suggesting a lognormal trend (Fig. 27A). The normal distribution trend becomes more pronounced on a P-P plot where the fit to a straight line is better for the Gaussian distribution (Fig. 27B). This trend is also indicated by numerical distribution tests. The Pearson correlation coefficient for the normal distribution is 0.956,

---

**Fig. 27.** Thickness frequency distribution and lateral thinning rates of the measured beds in the Monte Fumaiolo Formation. The thickness population consists of 73 measurements in 3 beds. (A) Frequency histogram shows the distribution is slightly skewed to the right and can be approximated by Gaussian and lognormal test distribution equally well. (B) P-P plot for the Gaussian and the lognormal distribution. Normally distributed data seem to have a better fit the straight line. (C) The exceedence frequency curve is of concave-upward shape and can be segmented into three straight-line segments defining the particular thickness classes (Note: plot with logarithmic axes). (D) Line plots of the three measured beds in the Monte Fumaiolo Formation. All three beds have concave-upward pinchout geometries with inflexion points corresponding to the segment boundaries observed on the EF-curve. Note the pinchout distance for these beds is much shorter than in the other studied formations.



whereas for the lognormal distribution it is only 0.950. Anderson-Darling test statistic for the Gaussian and lognormal distribution is calculated to be 2.011 and 2.924, respectively. The EF-curve has a convex-up shape on a plot with logarithmic axes and can be divided into three straight-line segments defining the particular thickness classes (Fig. 27C). These classes consist of the following thickness intervals: 0.3-5 cm, 5-19 cm, and 19-29.5 cm.

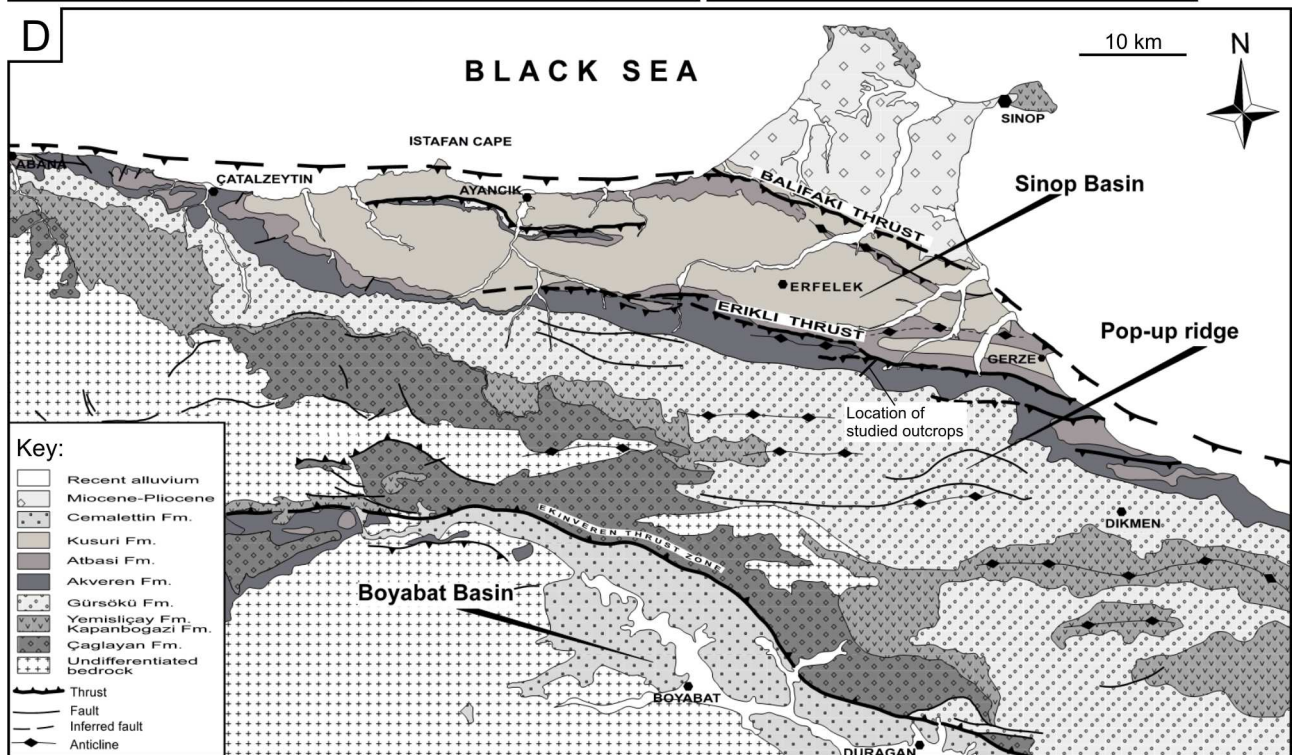
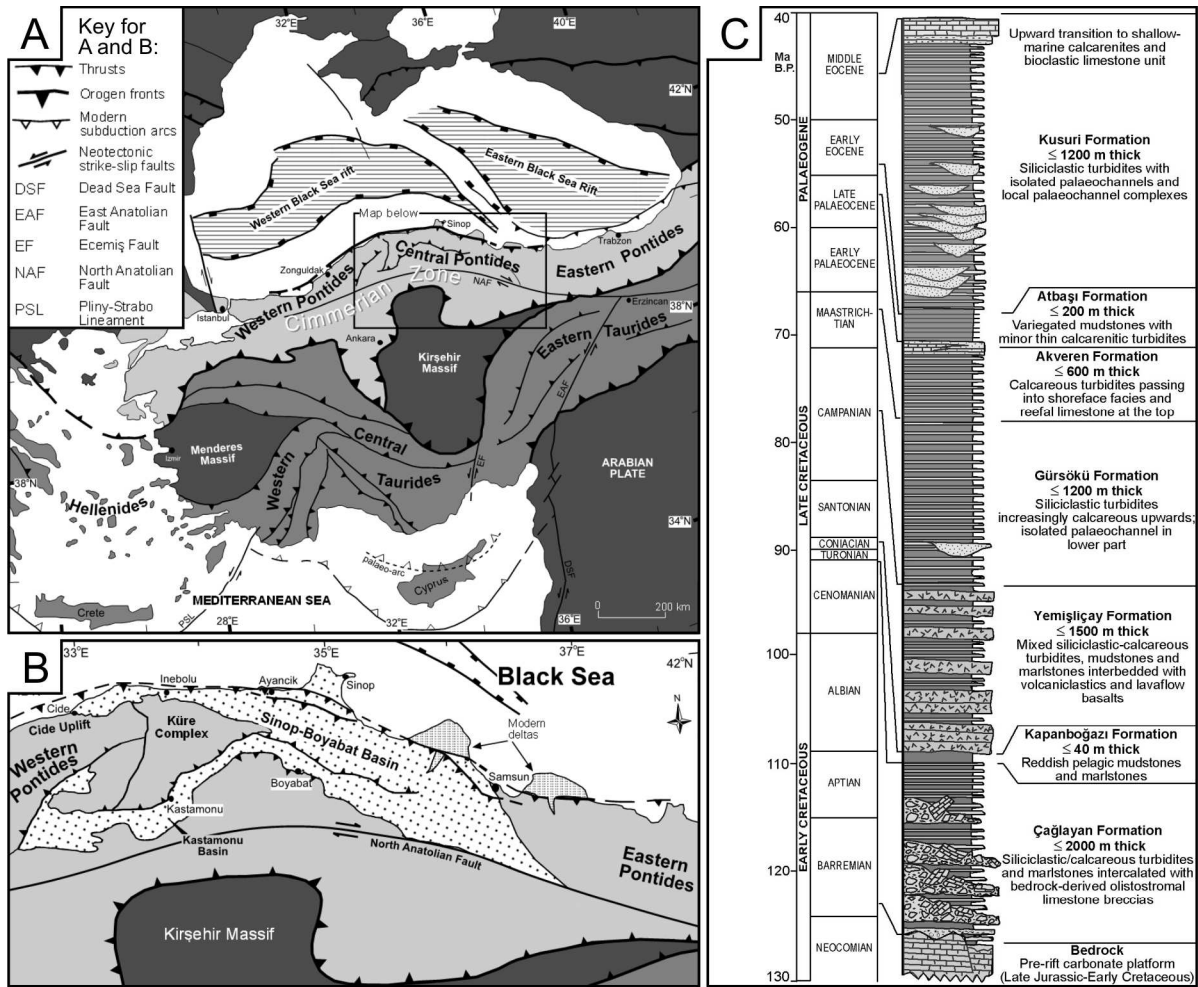
### **7.2.3. Dowflow changes in bed thickness**

Measured beds range in thickness from 29.5 cm to 0.3 cm. All three beds pinch out within the transect of the outcrop (~70 m), however, when the thickness values drop under 0.3 cm the beds are difficult to follow. Therefore a cut-off value of 0.3 cm has been established for these beds. The lateral thinning trend of the beds is best approximated by a negative growth exponential function of the form  $y = ce^{bx}$ , where  $c$  and  $b$  are constants,  $e$  is the base of the natural logarithm, and  $y$  and  $x$  are the bed thickness and the downflow distance, respectively. The mean  $R^2$  value for the exponential fits is 0.86. All three measured beds possess two subtle inflexion points in their downflow thinning trends (Fig. 27D). These inflexions seem to correspond to the segment boundaries of the EF-curve (Fig. 27C).

## 8. The Akveren Formation

### 8.1. Geological setting

The Akveren Formation occurs in the fill of the Sinop-Boyabat Basin located in the Central Pontides of northern Turkey. The Pontide orogenic belt of Anatolia resulted from the suturing of Africa-derived microcratons that were successively accreted to the Cimmerian margin of Eurasia during the Alpine orogeny (Şengör, 1987; Okay & Tüysüz, 1999; Görür & Tüysüz, 2001). The accretion process was diachronous and spatially non-uniform, resulting in a highly differential development in the western, central and eastern segments of the Pontide orogenic zone (Okay & Şahintürk, 1997). The northward emplacement of the Central Pontide nappes was caused by the large Kırşehir Massif (Fig. 28A), which indented the margin and underwent counter-clockwise rotation (Görür et al., 1984; Kaymakçı et al., 2003). The northward subduction of Neotethys under the Cimmerian margin was accompanied by backarc extension that led to the formation of the Black Sea rift system along a former intra-Cimmerian suture in the Early Cretaceous time (Robinson et al., 1996; Yılmaz et al., 1997; Nikishin et al., 2003). The Sinop-Boyabat Basin (Fig. 28B) formed as an extensional graben, ‘hanging’ structurally between the strongly subsiding Western Black Sea Rift to the north and the Central Pontide accretionary zone to the south. The basin underwent two main rifting phases before becoming subject to orogenic compression in the late Campanian and being decoupled from the extensional Black Sea regime in the late Maastrichtian time. In the earliest Eocene, the basin was split axially into two subparallel troughs by a structural pop-up ridge formed by the northward Erikli thrust and the antithetic, southward Ekinveren back-thrust. The southern wedge-top (‘piggyback’) trough, referred to as the Boyabat Basin, was initially subneritic but underwent rapid shallowing, whereas the northern foredeep trough, referred to as the Sinop Basin, remained bathyal and hosted the Kusuri turbiditic system (foreland terminology after DeCelles & Giles, 1996, and Ori & Friend, 1986). The Sinop Basin underwent contraction and was affected by blind thrusts, until the northernmost Balıfakı thrust (Fig. 28D) turned the foredeep into another wedge-top basin in the early Middle Eocene. The blind thrusts related to the compressional uplift were oriented parallel to the basin’s axis and had presumably a significant effect on the sedimentation in the basin, acting as barriers and/or conduits of turbiditic flows coming from W-SW (Fig. 29). Both basins were then tectonically inverted in the Late Eocene, although alluvial sedimentation in the Boyabat Basin probably persisted into Oligocene (Aydın et al., 1995b). Large parts of the basins were uplifted to  $\geq 1000$  m above sea level, resulting in good overall exposure. Coastal cliffs, river canyons, road-cut sections and abandoned quarries afford excellent outcrops in the Sinop Basin. The easternmost part of the basin is non-preserved, eroded due to the strong uplift of the Eastern Pontides, whereas the northwestern part extends offshore,

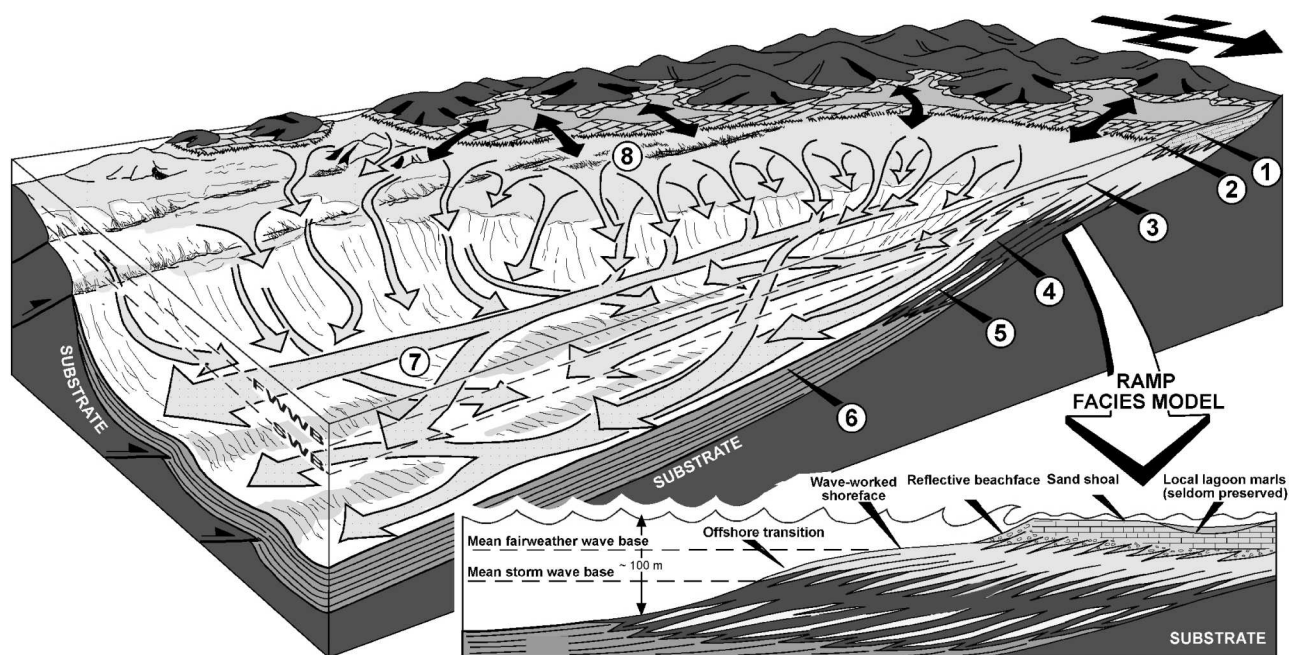




**Fig. 28.** (A) Tectonic map of Anatolia and surrounding areas, showing the Pontide and Tauride orogenic belts enveloping the Kırşehir Massif. (B) Simplified map of the Central Pontides, showing the location of the Sinop-Boyabat Basin (after Janbu et al., 2007). (C) Stratigraphy of the Sinop-Boyabat Basin (after Leren et al., 2007). (D) Geological map of the Sinop-Boyabat Basin, showing the areal distribution of the basin-fill formations in C.

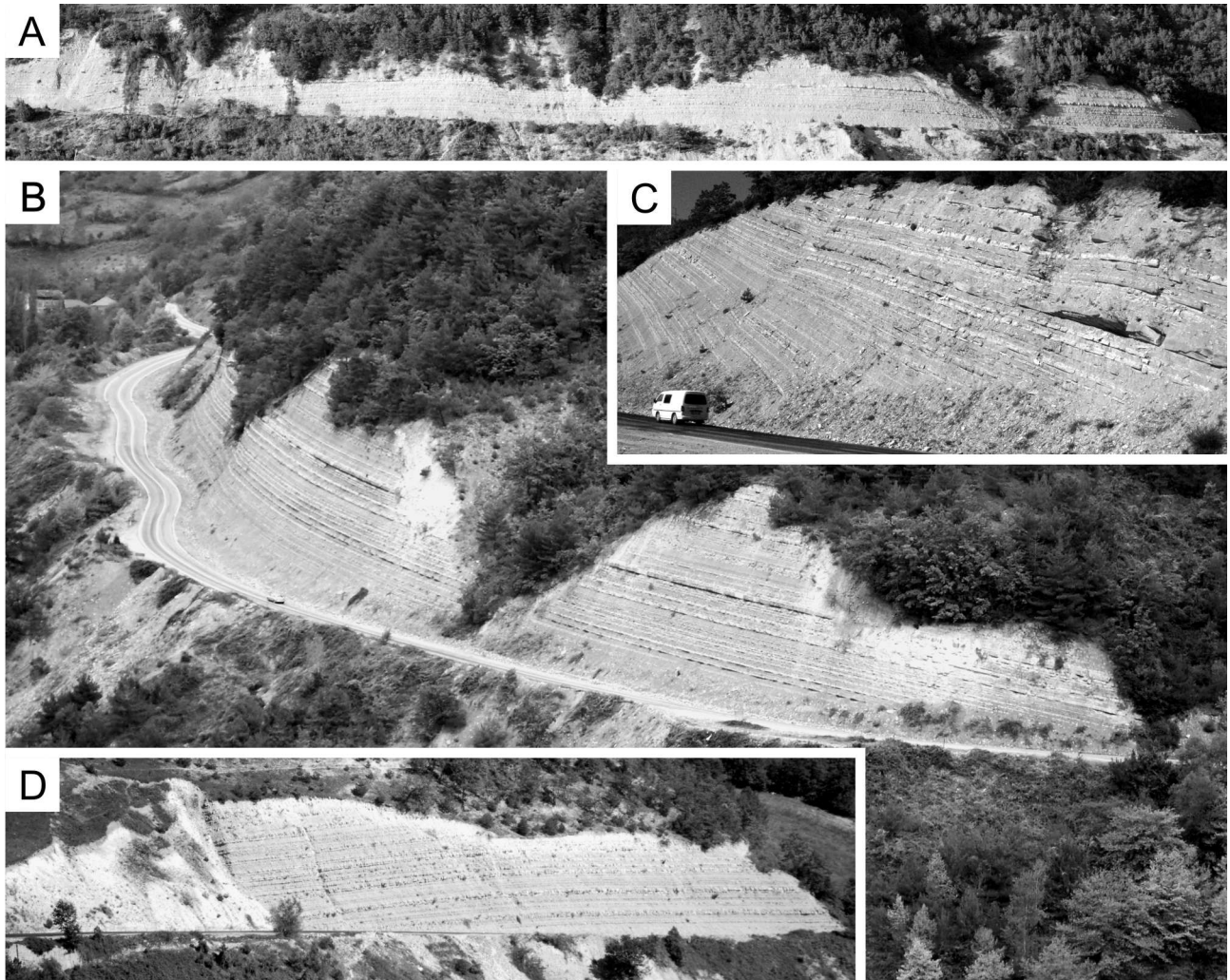
where it has not been explored.

The studied Akveren Formation is reported to be up to 600 m thick (Aydın et al., 1995a), Maastrichtian to Late Palaeocene in age (Leren, 2003), consists of alternating calcarenites, calcareous mudstones, marlstone and massive bioclastic limestones and has a gradational contact with the underlying Gürsöku Formation. The calcarenite beds are turbidites, although the topmost part of the formation is recognized to be a succession of calcarenitic tempestites. The Akveren-Formation outcrops chosen for this study are exposed along the asphalt road southwest of the village Tingir and are shown in Fig. 30.



- ① Shoal-water reefal platform made of bioclastic limestones, with local marly lagoons; swept by waves and tidal currents, and heavily eroded by storms.
- ② Reflective gravelly shoreline, turning into dissipative during storm setup.
- ③ Inner ramp (shoreface) zone, supplied almost continuously with abundant sand; pronounced aggradation results in low surface gradient, probably  $\sim 1^\circ$ .
- ④ Mid-ramp (offshore transition) zone, supplied with sand only during storms; limited aggradation and steeper gradient (possibly  $< 3\text{--}5^\circ$ ), with bypass chutes generated by storm rip currents and backsurges.
- ⑤ Outer ramp (offshore zone), episodically accumulating sand, but otherwise acting mainly as a sand bypass zone with gradients of probably  $< 1^\circ$ .
- ⑥ Basin-floor (deep-water) zone of turbiditic sedimentation with gradients of probably  $< 0.1^\circ$ .
- ⑦ Basin-floor topography with episodically subtle ridges (blind-thrust anticlines) promotes mainly linear, non-radial sand dispersal towards the E/SE, but some turbidity currents episodically spread obliquely across the basin.
- ⑧ Thrust-induced uplift along the southern margin causes an apparent forced regression, with waves eroding most of the shoreface deposits and also much of the offshore-transition deposits.

**Fig. 29.** Depositional model for the ramp-sourced, calciclastic basin-floor turbiditic system of the Akveren Formation; generalized palaeogeographic scenario and sediment dispersal pattern for the late Maastrichtian time (schematic, not to scale). After Leren et al. (2007).



**Fig. 30.** Photographs of the measured outcrops in the Akveren Formation, Central Pontides. The road-cut sections are exposed near-by the village of Tingir, Northern Turkey. For the locations of the measured outcrops in the Sinop Basin see Fig. 3C. (A & B) Outcrop number 1, (C) outcrop number 3, (D) outcrop number 2.

## 8.2. Results

### 8.2.1. Bed types

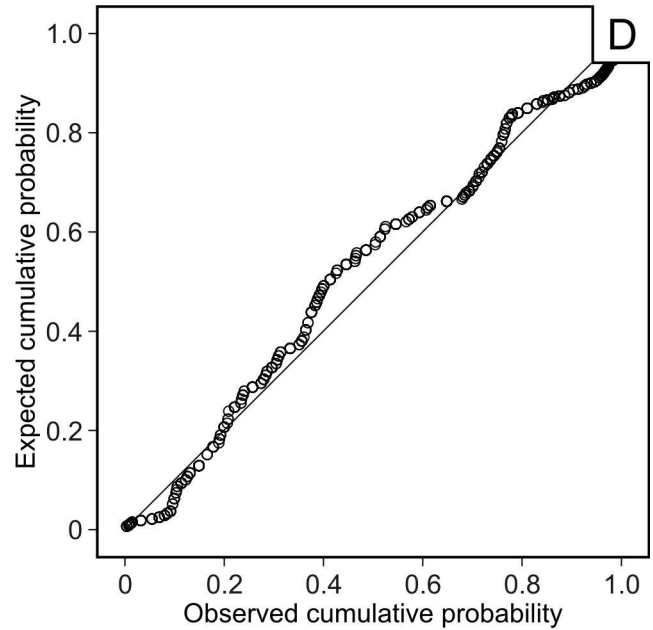
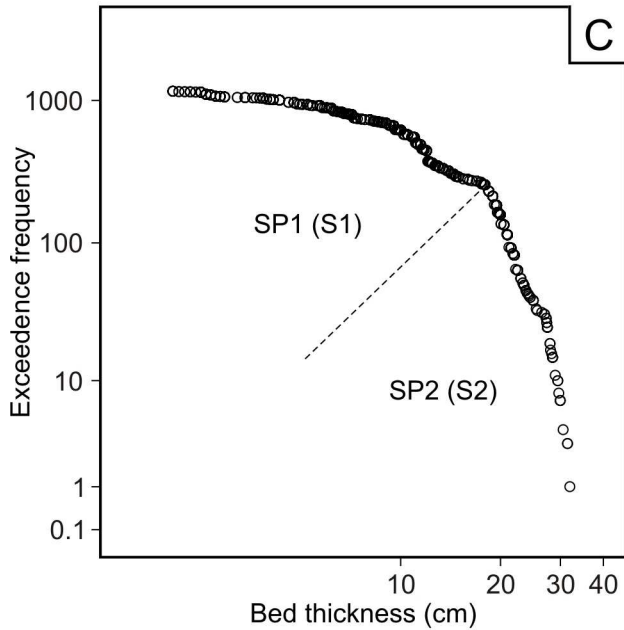
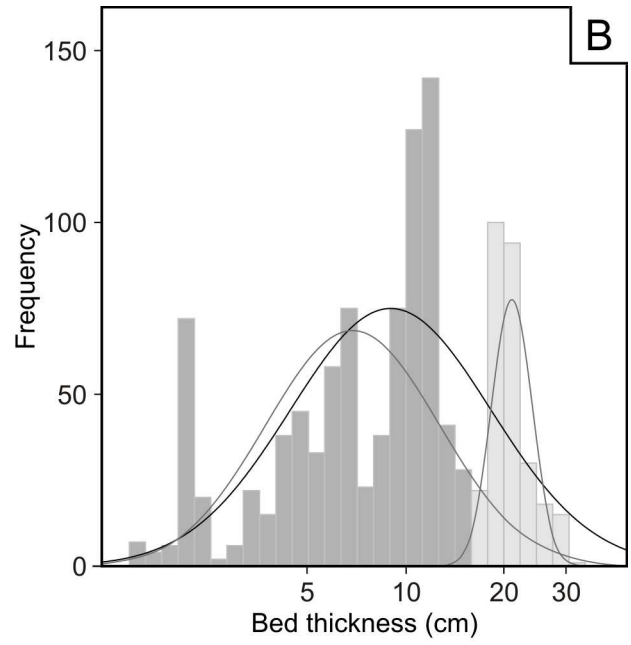
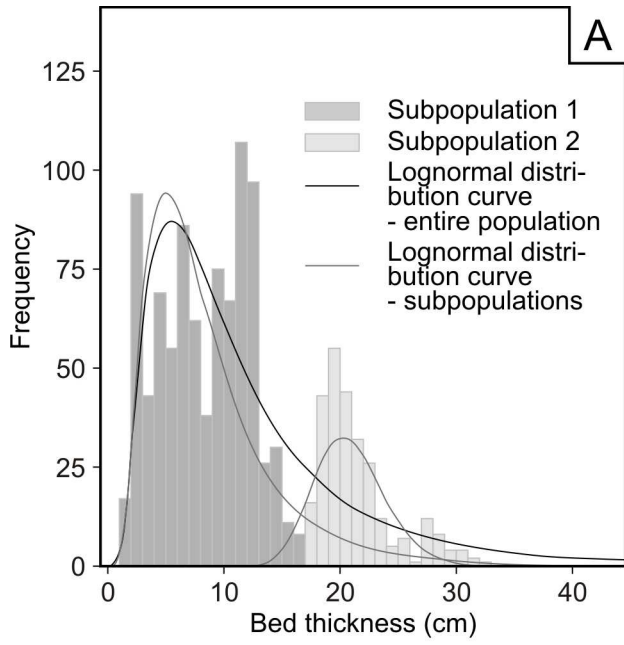
Sandstone beds with marlstone cappings measured in the Akveren Formation are of calciclastic composition, they show normal grading, and range in grain size from fine to very fine sandstone. These beds are separated by grey-coloured, calcareous mudstones, typically ranging in thickness from 5 to 30 cm. The sandstone and marlstone beds have been interpreted by Leren (2003) as deep-water turbidites with a carbonate platform as a source. Six facies variants are distinguished in the 40 measured beds:  $Tbcd(e)$ ,  $Tbc(de)$ ,  $Tb(c)d(e)$ ,  $Tb(cde)$ ,  $Tcd(e)$  and  $Tc(de)$ . The thickness-ranges of the particular Bouma divisions are as follows;  $b$ : 2-20 cm,  $c$ : 1.5-

10 cm, and *d*: 5-25 cm. The lateral evolution of the separate Bouma divisions is not visually observable in the measured outcrops, although the change in divisions from thick to thin beds indicates the individual Bouma divisions pinch out successively from *b* to *d* in the dowflow direction, as will be described later in the text. The overall thickness of these beds ranges from 1.5 to 32 cm.

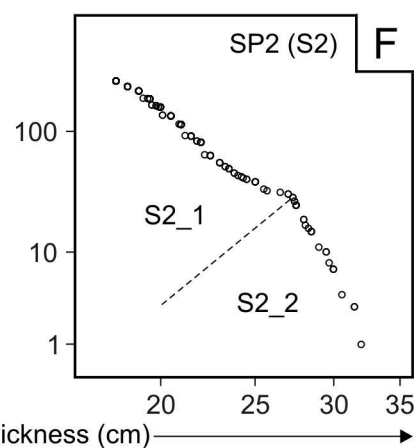
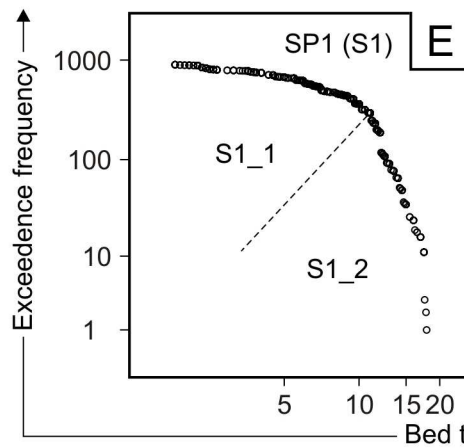
### 8.2.2. Frequency distribution of turbidite thickness

Sandstone beds within the chosen stratigraphic interval of the Akveren Formation can be classified as thin-bedded turbidites (sensu Talling et al., 2007b), ranging in thickness from 1.5 to 32 cm. The total number of measured beds equals 40 (corresponding to 1157 thickness measurements) with the mean and median thickness being 11.116 and 10.0 cm, respectively. Distribution tests detailed below indicate the thickness population of the measured beds in the Akveren Formation is distributed lognormally. The thickness frequency spectrum is dominated by thin-bedded turbidites and consists of two distinct subpopulations as shown by the frequency histogram in Fig. 31A. The frequency distribution of the subpopulation 18-32 cm is similar to the overall distribution with its spectrum slightly skewed to the right, while the subpopulation 1.5-18 cm has more of a bell-shaped normal trend (Fig. 31A). The overall distribution is best approximated by a Gaussian fit when plotted on a logarithmic frequency histogram (Fig. 31B). Exceedence frequency curve of the measurements has a convex shape on a plot with logarithmic axes and can be divided into two roughly straight-line segments (Fig. 31C). The thickness-ranges of these two segments correspond to the subpopulations distinguished on the frequency histogram in Fig. 30A. These two subpopulations also display a convex-up trend on logarithmic EF-plots and can be further segmented into four minor thickness classes: 1.5-10 cm, 10-18 cm, 18-27 cm, and 27-32 cm (Fig. 31E & F). The lognormal distribution of the overall thickness population is also confirmed by the lognormal P-P plot on which the data-points have a good fit to a straight line (Fig. 31D).

Results of numerical distribution tests are in agreement with the indications of EF, P-P, and histogram plots described above. Out of fourteen theoretical distributions (normal, lognormal, three-parameter lognormal, gamma, three-parameter gamma, exponential, two-parameter exponential, smallest extreme value, Weibull, three-parameter Weibull, largest extreme value, logistic, loglogistic, and three-parameter loglogistic) the Akveren dataset tests as being best approximated by a three-parameter lognormal distribution with Pearson correlation coefficient of 0.988 and the Anderson-Darling test statistic of 7.710. The second best approximation is the standard lognormal distribution (Pearson correlation coefficient being in this case 0.976, and the Anderson-Darling test statistic being 16.482). Probability values for the Kolmogorov-Smirnov, Anderson-Darling and Ryan-Joiner (similar to Shapiro-Wilk test) tests are statistically significant; meaning the lognormality of the thickness distribution is not exactly accurate.



**Thickness classes:**  
 S1\_1: 1.5-10 cm  
 S1\_2: 10-18 cm  
 S2\_1: 18-27 cm  
 S2\_2: 27-32 cm

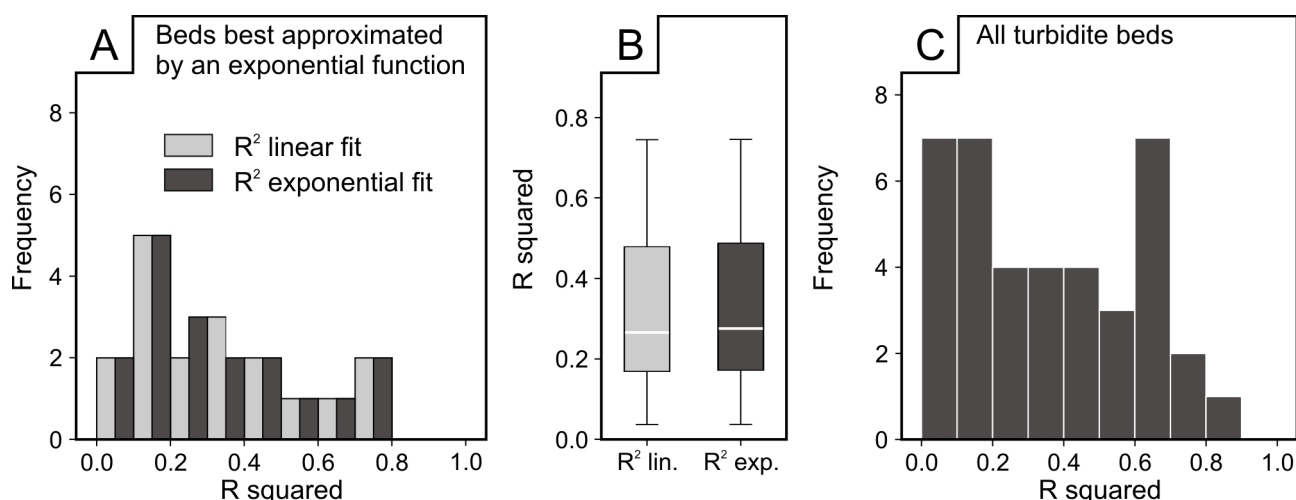


**Fig. 31.** Frequency distribution of turbidite thickness in the Akveren Formation. The thickness population consists of 1157 measurements (40 beds). **(A)** Linear frequency histogram shows the distribution is skewed to the right indicating lognormality. Two distinct subpopulations can be clearly defined from the linear histogram: 1.5-18 cm and 18-32 cm. **(B)** Logarithmic frequency histogram confirms the notion of a lognormal distribution as the overall distribution curve takes on a near-Gaussian shape. **(C)** Exceedence frequency plot of the measurements. The convex-shaped EF-curve seems to consist of two straight-line segments which are consistent with the two subpopulations observed on the frequency histogram (Note: plot with logarithmic axes). **(D)** Lognormal P-P plot shows the data points have a tight fit to a straight line and are therefore approximated by a lognormal distribution very well. **(E & F)** Subpopulations derived from the EF-curve and the frequency histogram have a convex shape on EF-plot with logarithmic axes and can be subdivided into four minor thickness classes based on the geometries of the EF-curves.

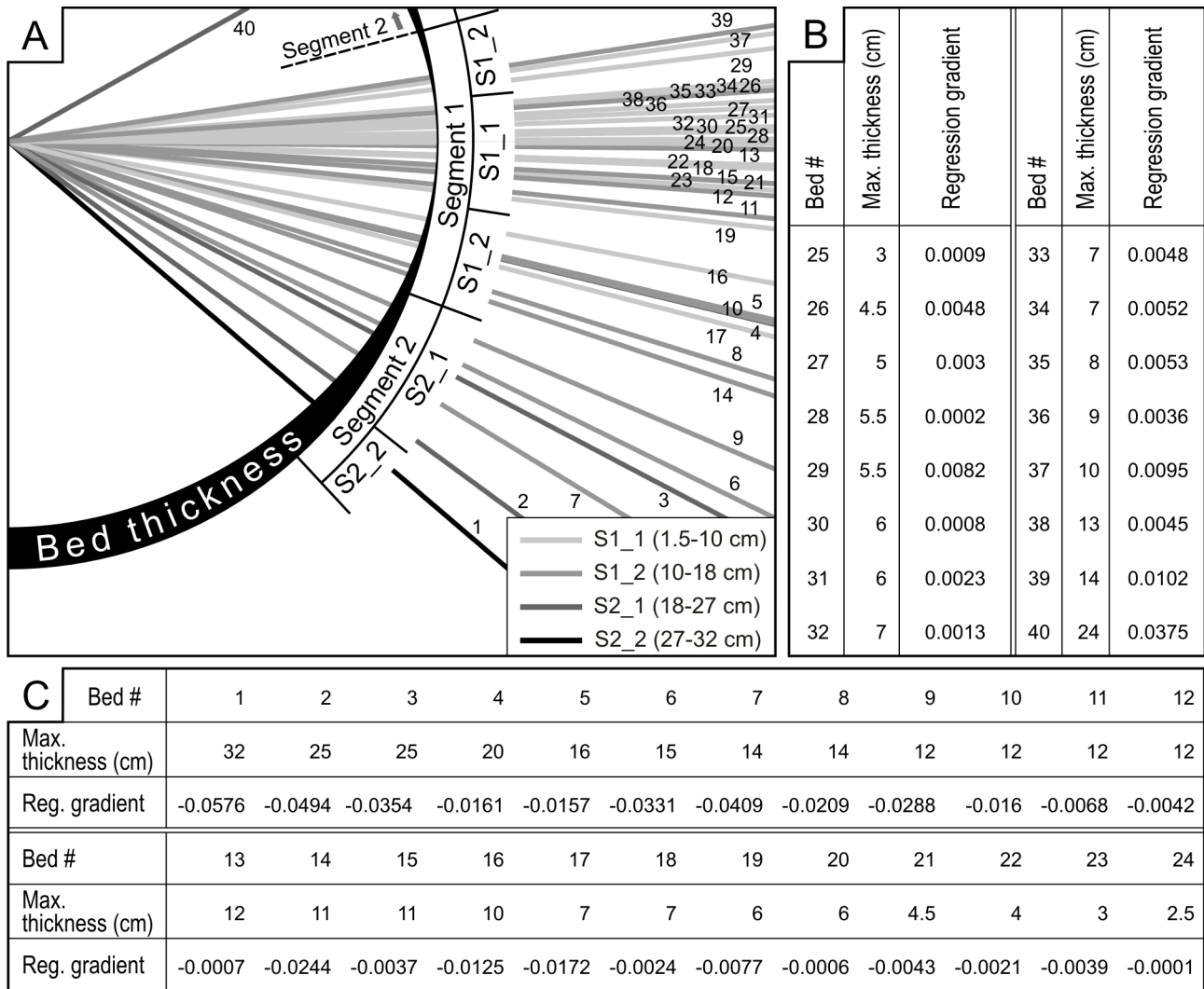
However, as pointed out under 7.2.3., any numerical goodness-of-fit test will result in rejection of the null hypothesis when the number of observations is very large (Talling, 2001; NIST/SEMATECH, 2007; Sylvester, 2007).

### 8.2.3. Dowflow changes in bed thickness, facies, grain size, and bed-top undulations

Lateral extent of the individual beds measured in single outcrops varies from 68 to 484 m, with all studied outcrops oriented approximately parallel to the paleotransport direction. 24 of the measured beds (60 %) decrease in thickness in the downflow direction, while 16 of the measured beds (40 %) are observed to thicken downflow. Using least square regression, 22 beds (55 %) are best approximated by a linear trendline and 18 (48 %) are best expressed by an exponential regression line. In order to obtain regression-line gradients for the exponential thickness trends, linear trendlines were fitted to the data causing a decrease in the mean coefficient of determination  $R^2$  from 0.3351 to 0.3292 and the median  $R^2$  from 0.2754 to 0.2647



**Fig. 32.** **(A)** Frequency histogram showing the distribution of  $R^2$  for linear and exponential regression fits in beds that diminish in thickness exponentially. **(B)** Box-whisker plot of  $R^2$  for linear and exponential fits. The caps at the end of each box indicate the minimum and maximum values; the box is defined by the lower and upper quartiles and the line in the center of the box is the median. **(C)** Histogram showing the distribution of  $R^2$  (linear fit) for all 40 beds measured in the Akveren Formation.

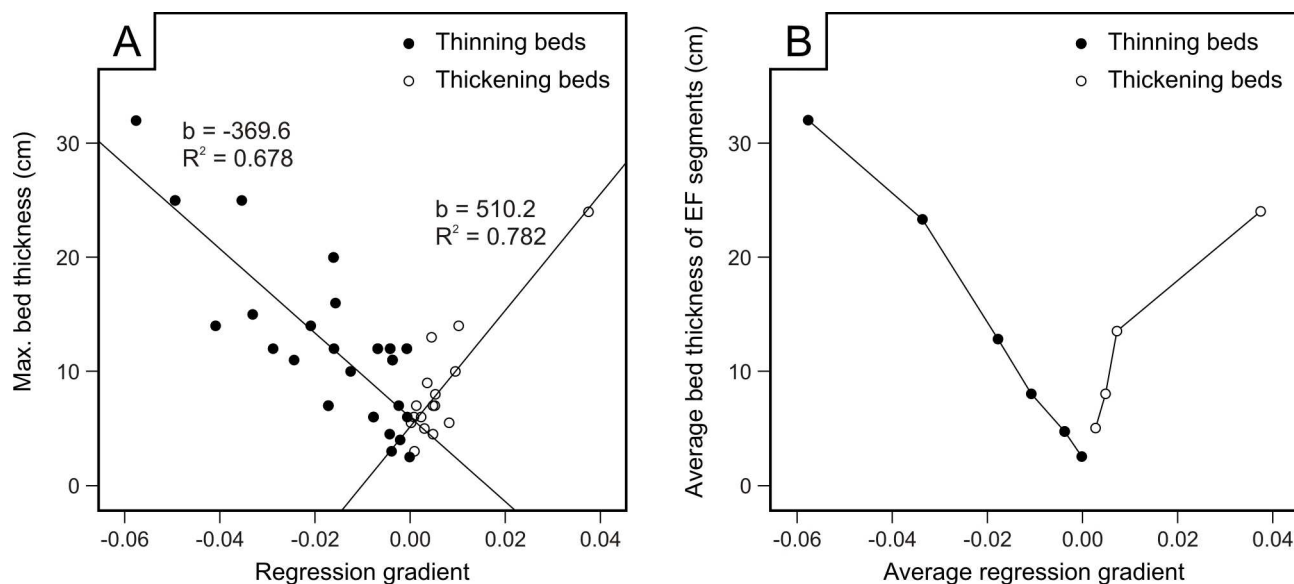


**Fig. 33.** (A) Regression gradients (thinning rate) for the beds measured in the Akveren Formation. Each bed is represented by its regression line. The intercepts of the regression equations are set to a common value to make the thinning rates of beds comparable on a single plot. The shading of the lines corresponds to the particular thickness classes defined from the EF-curves in Fig. 31C, E & F. The exact regression gradients for thickening and thinning beds are listed in (B) and (C), respectively. In B beds are numbered from thinnest to thickest, while in C the numbering is reversed. See Appendix for *distance versus thickness* plots of the individual beds.

(Fig. 32A & B). The overall distribution of  $R^2$  is slightly skewed towards the lower end of the spectrum with its mean and median being 0.3644 and 0.333, respectively (Fig. 32C).

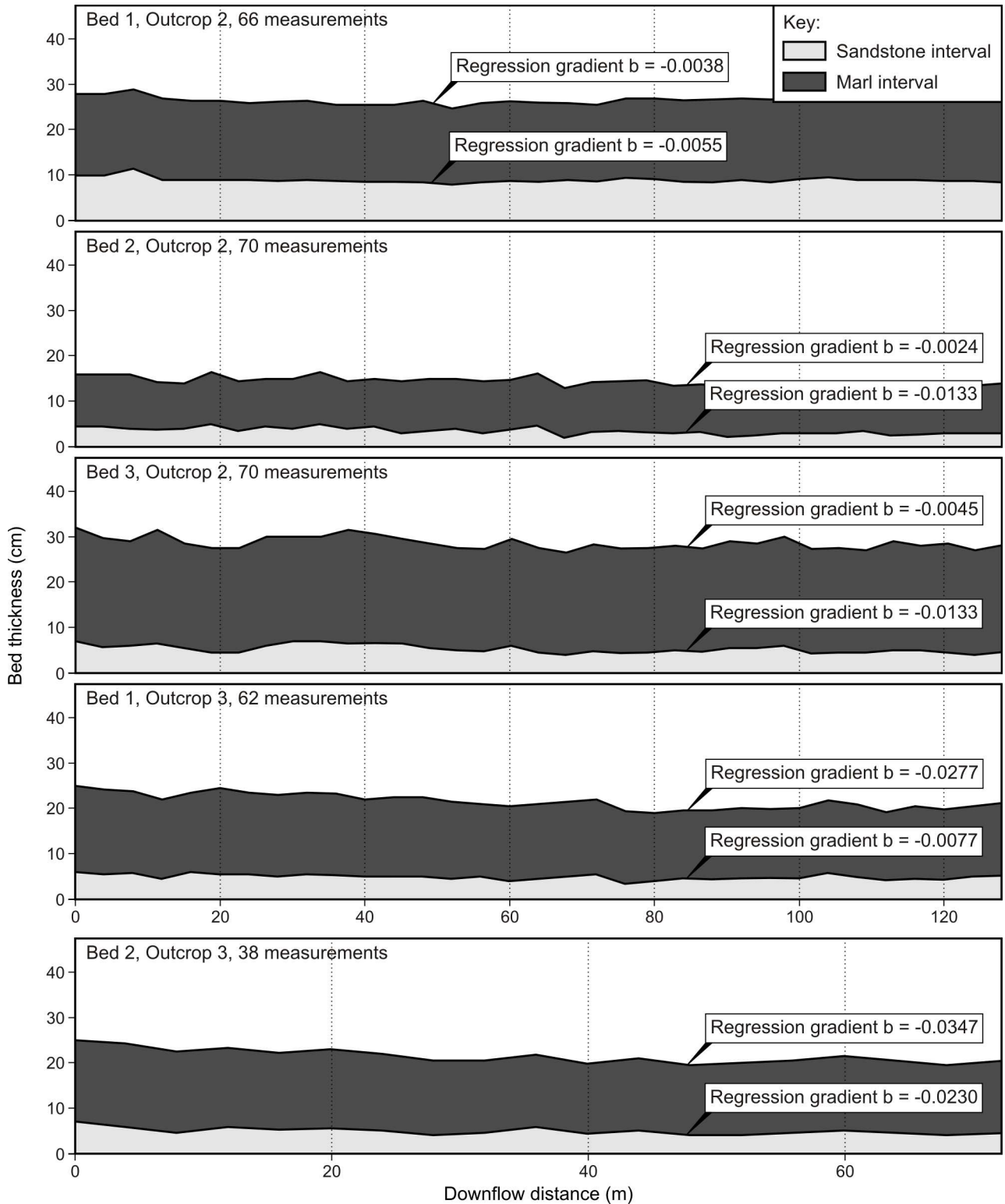
Gradients of regression trendlines approximating downflow bed thickness changes constitute a wide spectrum, ranging in number from -0.0576 to 0.0375 (Fig. 33). Because a large percentage of beds in the Akveren Formation is thickening in the downflow direction this gradient spectrum has been divided into a positive and a negative sector corresponding to thickening and thinning beds, respectively. As mentioned in

section 9.2.1., turbidites in the Akveren Formation have probably been subjected to partial ponding in synclinal depressions caused by blind-thrust anticlines, which implies that both thinning and thickening



**Fig. 34.** (A) Maximum bed thickness of thinning beds in the Akveren Formation decreases with increasing regression gradient at a rate of -369.6, and increases with the regression gradient in thickening beds at a rate of 510.2. Note that the rate for the thinning beds is considerably lower than that for the Marnoso Arenacea turbidites suggesting the beds in the Akveren Formation thin more rapidly downcurrent. (B) The relationship between bed thickness and thinning rate becomes very evident when the mean thinning gradient is plotted against the average bed thickness of EF-segments.

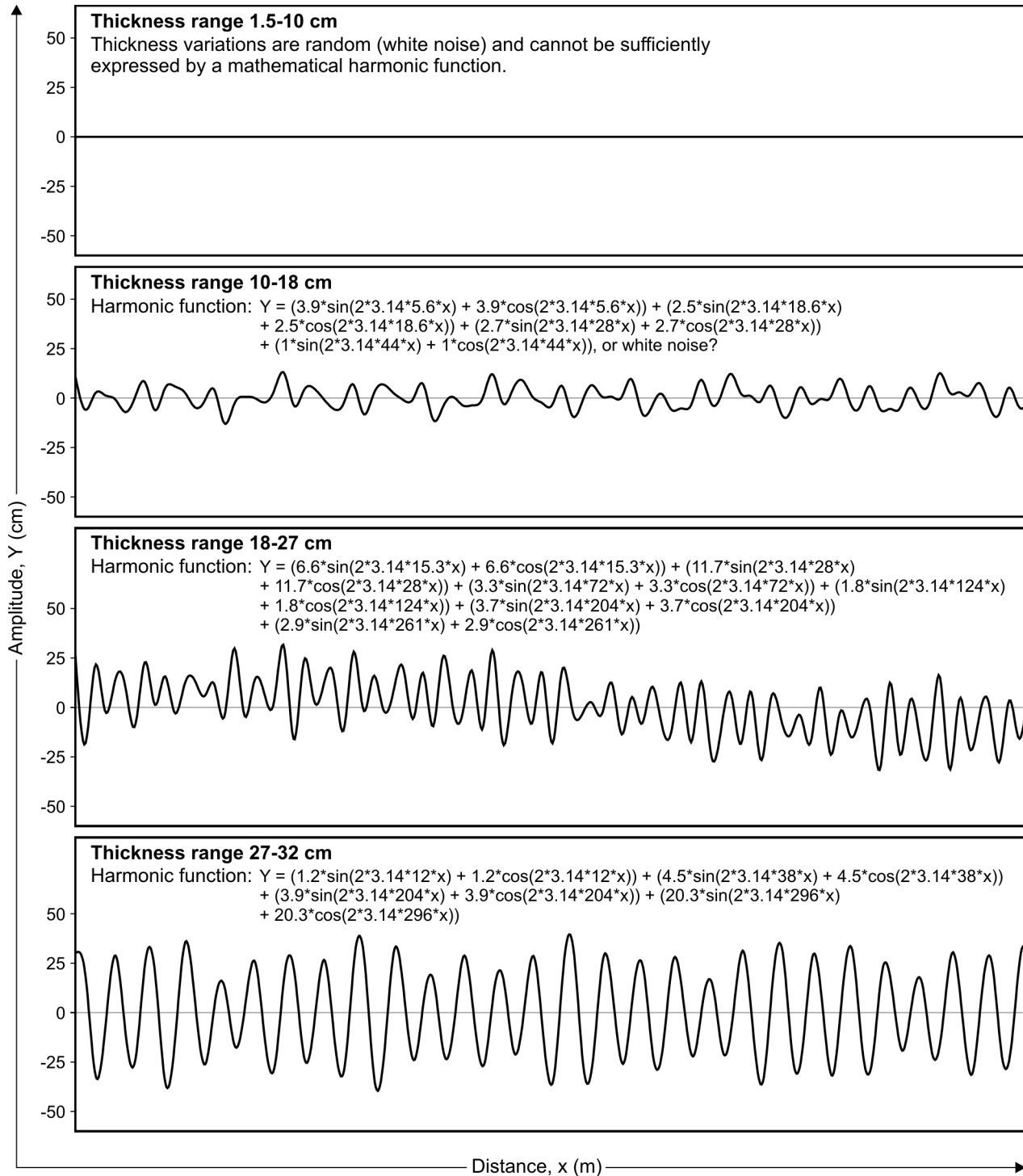
outcrop segments of beds could theoretically represent separate parts of a single turbidite. Assuming both thinning and thickening turbidites have nonlinear downflow thickness trends as indicated by the wide spectrum of regression gradients, the local thinning gradient of a single bed can be expressed as a function of the local bed thickness. This relationship in the Akveren Formation is proven to be statistically significant by the linear-fit  $R^2$ -value of 0.678 for the thinning beds and 0.782 for the thickening beds (Fig. 34A). Thinning beds seem to diminish in thickness more rapidly in the downflow direction than thickening beds in the upflow direction, as indicated by a higher absolute value of the regression coefficient for thickening beds (Fig. 34A). For both, thinning and thickening turbidites in the Akveren Formation the change in the downflow thickness is more significant than for turbidites in the Marnoso Arenacea Formation (which have a regression coefficient of -1225.6, see Fig. 18). The difference in the rate of thinning and thickening is also illustrated in Fig. 34B, where mean thickness of the EF-segments is plotted against their corresponding average thinning gradients. Stacking the regression gradients for the thinning beds and assuming the measured bed-intervals represent downflow-thinning segments of unconfined basin-plain turbidites, the pinchout geometry of these beds would be of concave-upward shape. The pinchout distance for such a bed with a maximum thickness of 32 cm would be, according to the obtained thinning gradients, approximately 39 km (Fig. 37). Pinchout geometries of the separate Bouma divisions based on their change from thick to



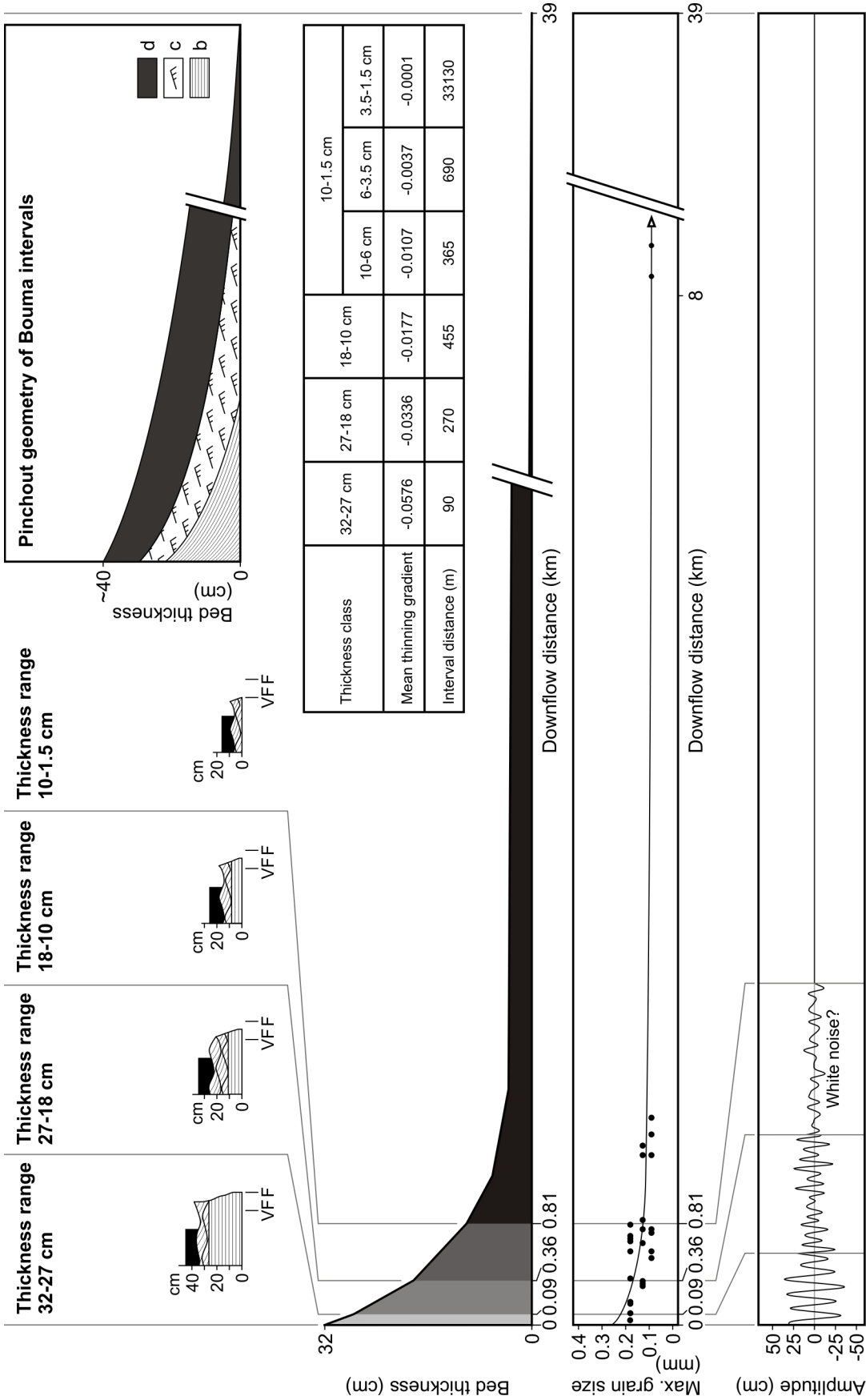
**Fig. 35.** Five beds from the Akveren Formation in which both the sandstone and the marlstone interval was measured. These systematic measurements indicate the thinning rate of the marl interval (Bouma division  $d$ ) within a turbidite bed is independent of the thickness and the thinning rate of the underlying sandstone interval, and also, the total thickness of the bed.



thin beds are similar to those in the Marnoso Arenacea turbidites, with every division typified by a proximal thickening and a distal thinning, resulting in an overall lenticular downflow geometry (Fig. 37). However, as in the Marnoso Arenacea Formation, closely-spaced measurements of individual beds indicate the thinning rates of the Bouma-divisions  $d$  are independent of the thickness and the thinning rate of the underlying sandstone intervals, and also, the total thickness of the bed (Fig. 35). Grain size trend resembles the overall thickness change, decreasing exponentially from thick to thin beds (Fig. 37). The Fourier analysis of bed-thickness variations suggests bed-top undulations are present in the studied beds; however, majority of beds thinner than 18 cm (82.5 % of all beds) test as white noise series meaning their thickness variations are caused by a random process. Also in the thickest beds there is a great proportion of white noise. If a comparison is made with the Marnoso Arenacea turbidites, the thickness range of beds measured in the Akveren Formation corresponds roughly to the thinnest set of beds in the Marnoso Arenacea (thickness class 2.5-42 cm), where almost 100 % of beds test as white noise series. Albeit many of the beds in the Akveren Formation might only be white noise series, an effort has been made to differentiate between the different wavelength-frequencies in order to best approximate the actual undulations. The dominant wavelengths of the bed-top waveforms for the specific thickness classes defined from the EF-curve are following: thickness class 1.5-10 cm: only random noise; thickness class 10-18 cm: 5.6, 18.6, 28, 44 meters; thickness class 18-27 cm: 15.3, 28, 72, 124, 204, 271 meters; thickness class 27-32 cm: 12, 38, 204, 296 meters. The length of the wavelengths is observed to increase with bed thickness, while their abundance decreases (i.e., the waveform becomes simpler, random noise is filtered out) (Fig. 36, 37). The amplitude of these waveforms decreases with decreasing bed thickness; the maximum amplitude for the 27-32 thickness class is approximately 40 cm.



**Fig. 36.** Modelled bed-top undulations and their corresponding harmonic functions for the Akveren Formation. Note the wavelengths and amplitudes of the waveforms increase with bed thickness. The complexity of the harmonic functions increases with decreasing bed thickness as more random noise is introduced into the series. For the thickness range 1.5-10 cm all of the beds test as white-noise series.



**Fig. 37.** Figure summarizing the thickness, grain size, facies, and bed-top undulation changes in the Akveren Formation turbidites that thin downflow. These trends are based on the assumption that a turbidite bed thins continuously in the downflow direction from the point of its maximum thickness (i.e., locally thick beds are more proximal than locally thin beds). When the mean thinning rates for the particular thickness classes defined from the EF-curve are stacked together, the pinchout geometry of a single turbidite bed is of concave-upward shape (upper middle). The concave-upward trend is followed by the maximum grain size and to a certain degree also by the individual Bouma divisions (top). Bed-top undulations decrease in wavelength and amplitude with decreasing bed thickness, thereby also with downflow distance. For a more detailed description of the overall trends see text.



## 9. The Kusuri Formation

### 9.1. Geological setting

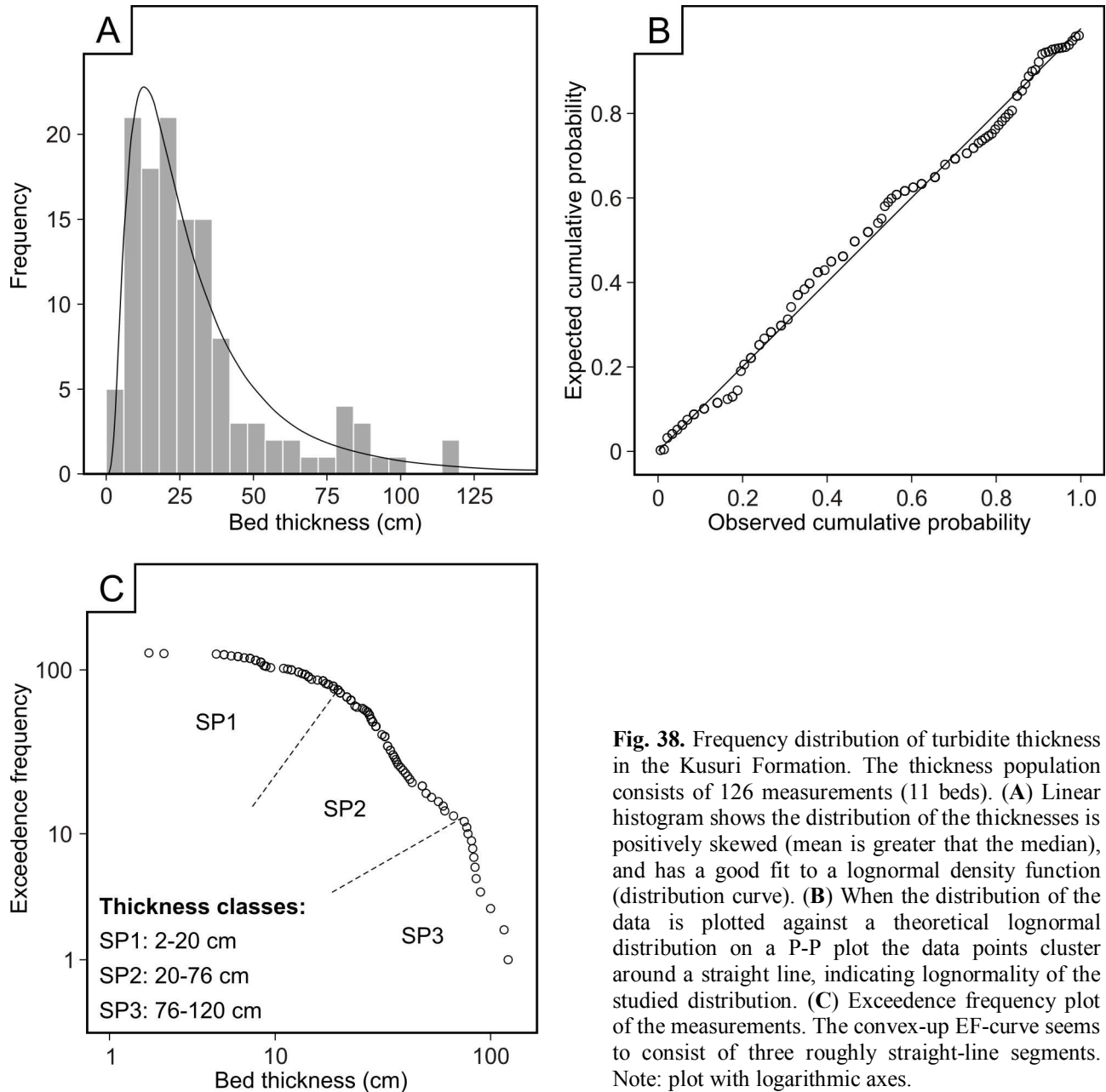
The Late Maastrichtian to Middle Eocene Kusuri Formation crops out in the Sinop-Boyabat Basin (Fig. 28D) located in the Central Pontides of northern Turkey (for the description of the tectonic evolution of Central Pontides and the Sinop-Boyabat Basin the reader is referred to section 9.1. above). This  $\leq 1200$  m thick turbiditic succession is a record of abundant supply of siliciclastic sediment from the east, attributed to a fluvio-deltaic system draining the adjacent, emerged Eastern Pontide foreland. In section it consists of a mud-rich lower part dominated by sheet-like turbidites and a sand-rich middle part containing solitary and multi-storey palaeochannels (Fig. 28C). The mud-rich upper part of the succession contains sheet-like turbidites that are increasingly calcareous, with a rapid upward transition to neritic calciclastic tempestites and littoral bioclastic limestones at the top.

In the Early Eocene, the axial pop-up ridge split the original Sinop-Boyabat Basin into the foredeep Sinop Basin and the ‘piggyback’ Boyabat Basin (Fig. 28D; Leren, 2003). This study focuses on the Early-Eocene to Middle-Eocene part of the Kusuri Formation which is exposed in the Boyabat Basin as a series of vertically-stacked inter-fingering turbiditic lobes.

### 9.2. Results

#### 9.2.1. Bed types

The eleven beds measured in the Kusuri Formation are of siliciclastic composition, they typically show normal grading, and range in grain size from very coarse to very fine sand. The individual beds are intercalated with mudstones, ranging in thickness from 1 to 30 cm. The measured outcrop represents a transverse section through a small system of turbiditic lobes deposited in a deep-water setting (W. Nemeč, pers. comm. 2007). Six facies variants are recognized in this outcrop: *Ta(bcde)*, *Tab(cde)*, *Ta(b)c(de)*, *Tb(cde)*, *Tbc(de)* and *Tc(de)*. The thickness-ranges of the separate Bouma divisions are as follows; *a*: 30-80 cm, *b*: 5-40 cm, and *c*: 2-10 cm. Remaining divisions are of negligible thickness. The internal character of beds is generally hard to recognize in the full length of beds due to their heavy weathering. The overall thickness-range of beds is 2 to 120 cm.



**Fig. 38.** Frequency distribution of turbidite thickness in the Kusuri Formation. The thickness population consists of 126 measurements (11 beds). **(A)** Linear histogram shows the distribution of the thicknesses is positively skewed (mean is greater than the median), and has a good fit to a lognormal density function (distribution curve). **(B)** When the distribution of the data is plotted against a theoretical lognormal distribution on a P-P plot the data points cluster around a straight line, indicating lognormality of the studied distribution. **(C)** Exceedence frequency plot of the measurements. The convex-up EF-curve seems to consist of three roughly straight-line segments. Note: plot with logarithmic axes.

### 9.2.2. Frequency distribution of turbidite thickness

The eleven beds measured in the Kusuri Formation correspond to 126 thickness measurements. The mean and median value for the obtained thickness range is set to be 29.76 and 23, respectively. The frequency distribution of turbidite thickness is unambiguously lognormal as indicated by the right-hand skewness of the distribution on a linear histogram (Fig. 38A), convex shape of the exceedence frequency curve on a plot with logarithmic axes (Fig. 38C), linear trend on a lognormal P-P plot (Fig. 38B), and statistically insignificant probability values of the Anderson-Darling and Kolmogorov-Smirnov distribution tests being 0.181 and

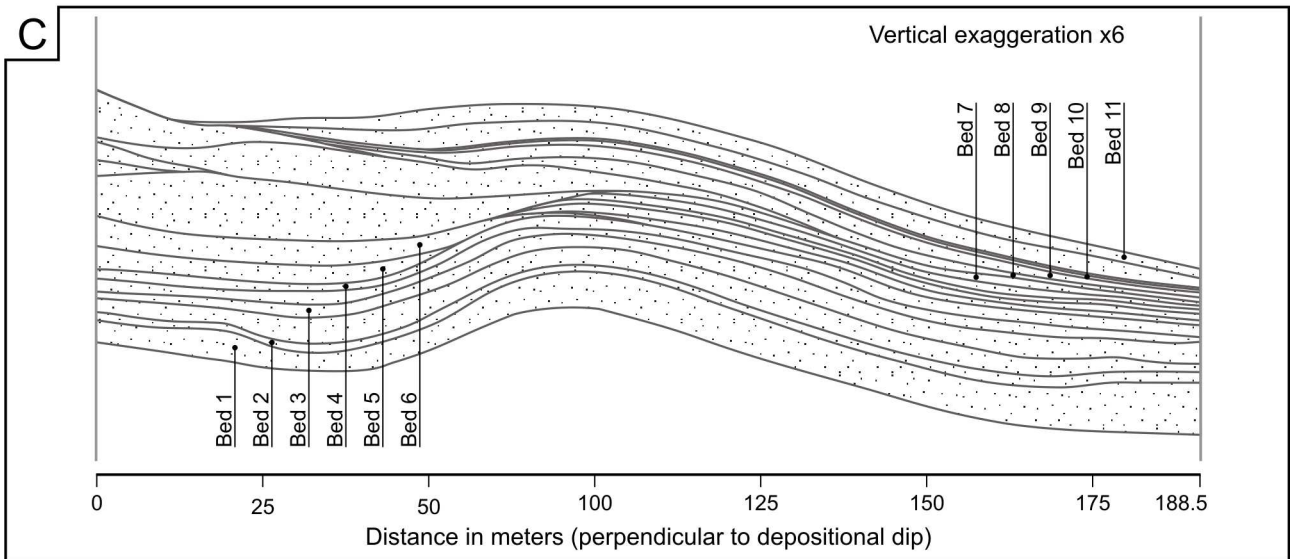
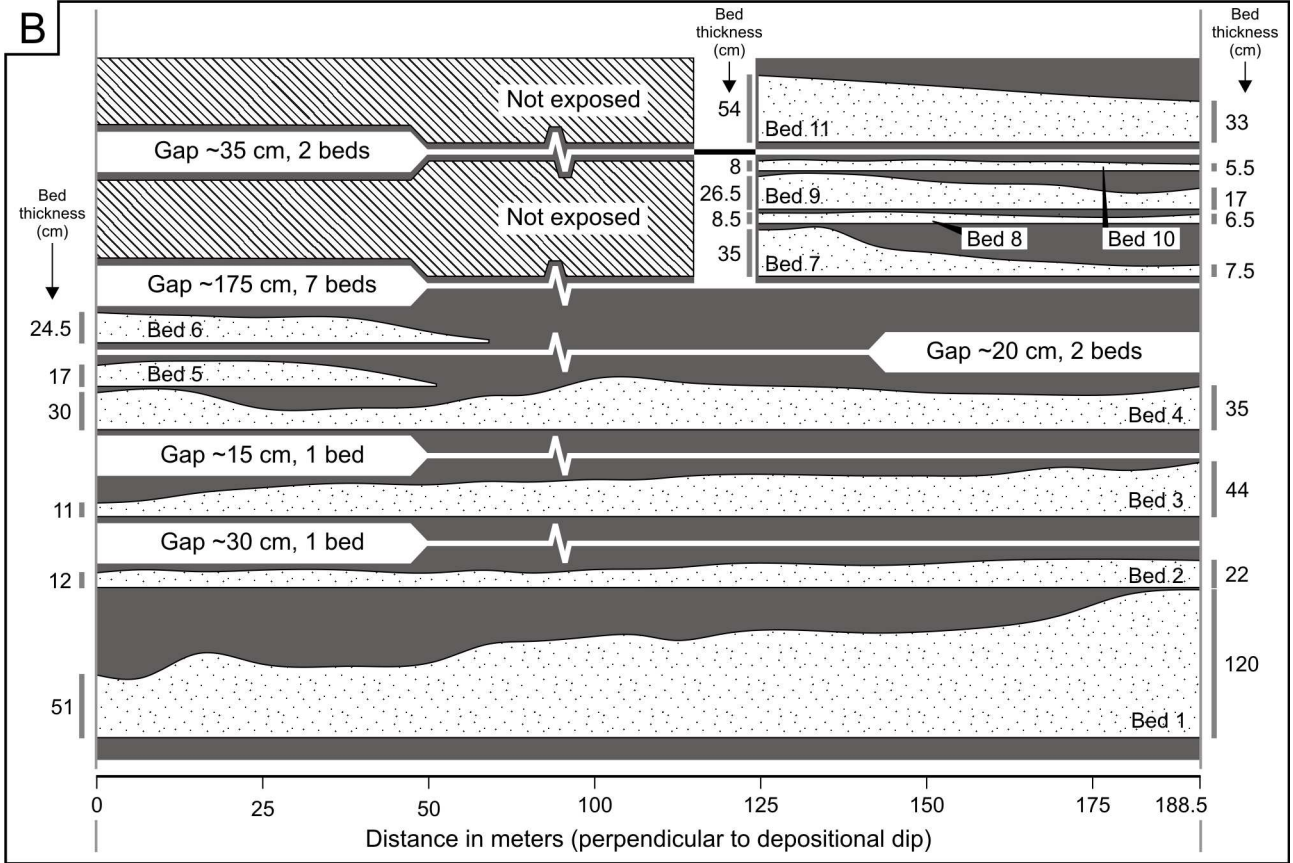
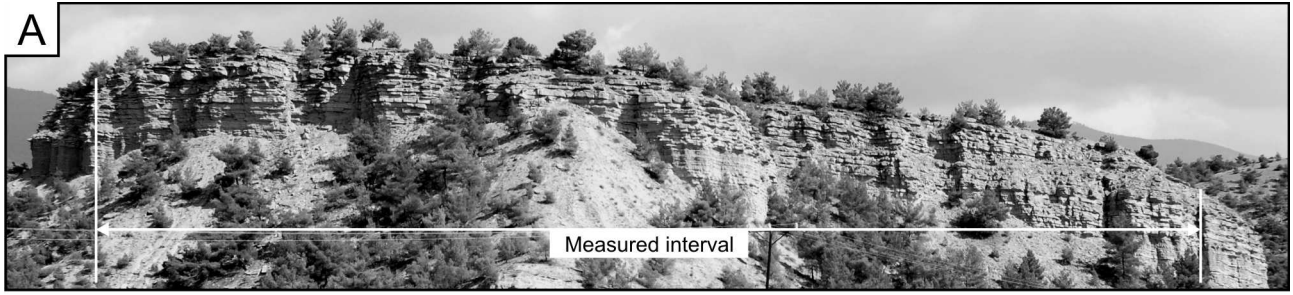
0.15, respectively. The exceedence frequency curve consists of three roughly straight-line segments, making it possible to divide the overall thickness population into three separate thickness classes: 2-20 cm, 20-76 cm, and 76-120 cm (Fig. 38C). Each of the three classes is distributed lognormally and passes the Anderson-Darling test for a lognormal distribution with a probability value of 0.012 for the thickness class 2-20 cm, 0.073 for the thickness class 20-76 cm, and 0.024 for the thickness class 76-120 cm ( $\alpha$ -level for the test being in this case 0.01). The overall thickness distribution is thus a composite distribution consisting of three separate lognormally-distributed thickness subpopulations.

### 9.2.3. Thickness changes transverse to depositional dip

The measured outcrop is approximately 200 meters long and represents a transverse-to-oblique section through a succession of vertically-stacked inter-fingering turbiditic lobes (W. Nemeč, pers. comm. 2007). Majority of the measured beds experience a dramatic reduction in thickness throughout the distance of the transect, suggesting the exposed lobes are of limited areal extent. Closely-spaced thickness measurements show the cross-sectional profiles of the studied lobes are alternately of concave-upward and convex-downward shape (Fig. 39B). Systematic measurements coupled with photomosaic observations suggest the lobe cross-sectional geometries are more a product of the confinement to the pre-existing paleo-seafloor topography (Fig. 39C) rather than a product of the depositional processes in terms of internal physical processes within the turbiditic flows. There seems to be no apparent relationship between the local bed thickness and the corresponding thinning rate as beds have both concave-upward and convex-downward cross-sectional geometries. Pinchout geometries of the separate Bouma divisions have not been recognized in these beds due to lack of their exposure and heavy weathering of the beds. Grain size tends to fine towards the edges of the individual lobes and is coarsest at the bottom of thick segments (generally in the middle parts of the lobes).

---

**Fig. 39 (next page).** Lateral thickness changes of beds measured in the Kusuri Formation. The studied outcrop represents a transverse-to-oblique section through a succession of vertically-stacked inter-fingering turbiditic lobes. **(A)** Photograph of the outcrop. The approximate length of the measured interval is ~ 200 meters. **(B)** Cross-sectional profiles of beds derived from closely-spaced (5-10 m) measurements. Bases of beds are flattened-out in order to enhance the geometrical trends of thinning. Pinchout geometries seem unpredictable, ranging in shape from convex to concave profiles. The depicted gaps represent intervals of beds that were not measured. **(C)** Lobe geometries inferred from systematic measurements of beds and from detailed photographs of the outcrop. This cross-section is in part corrected for the fault in the middle of the outcrop. Note the inter-fingering of lobes and their confinement to the uneven pre-existing topography.



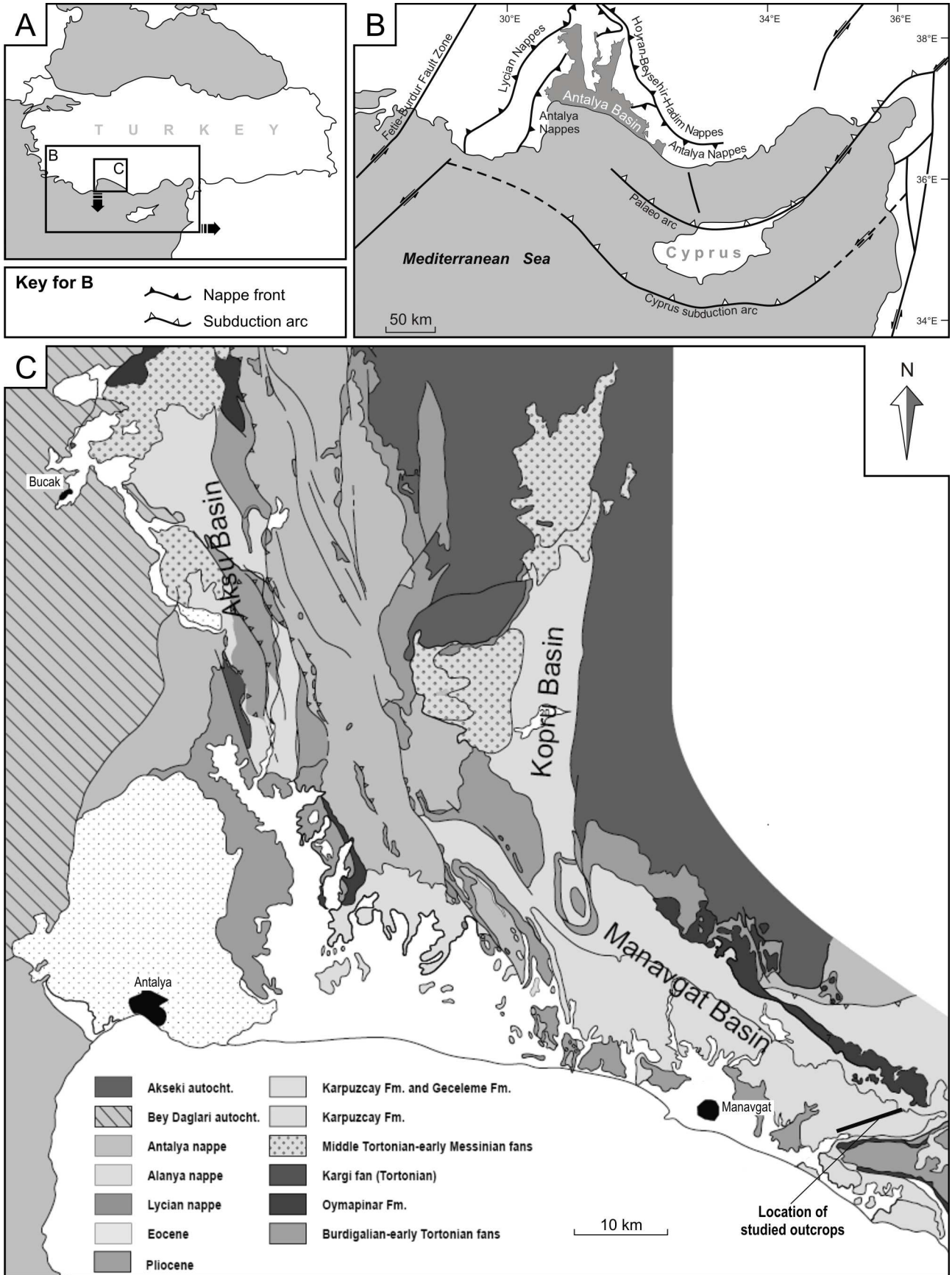


## 10. The Karpuzçay Formation

### 10.1. Geological setting

The Karpuzçay Formation is an open-marine tempestitic succession interspersed with tsunamites occurring in the Manavgat Basin, which is an eastern sub-basinal compartment of the large Neogene Antalya Basin in southwestern Turkey (Fig. 40; Dreyer et al., in prep.). The Manavgat Basin developed as a SE-trending graben, oblique to the adjoining Köprü graben, with a submerged southern footwall and a high-relief northern margin defined by a series of en echelon normal faults and a high-relief rocky coast. The Manavgat Basin was open to the palaeo-Mediterranean Sea and hosted a neritic to littoral environment, subject to long-fetch storm waves and fringed with a gravelly shoreline and coastal cliffs. The basin-fill stratigraphy is illustrated in Fig. 41 and described and discussed by Larsen, Wathne et al. (in prep.). The Karpuzçay Formation studied in this paper ranges in age from Late-Serravallian to Early Messinian and is approximately 400 m thick. It is dominated by sand-rich offshore-transition deposits, contrasting the underlying Geceleme Formation consisting mainly of mud-rich sublittoral deposits. The marked increase in storm sand delivery to the sublittoral environment from the Geceleme Formation to the Karpuzçay Formation was accompanied by a rapid progradation of local fan deltas, including the Katırınemeği fan-delta complex in west-central part of the basin (Fig. 41). The isolated fan deltas, with axes 10 to 20 km apart, were formed as hanging-wall coastal systems along the basin's high-relief northern margin. This abrupt increase in terrestrial sediment supply is attributed to a major forced regression (Dreyer et al., in prep.), possibly caused by a eustatic sea-level fall (Haq et al., 1988). The relative sea-level fall caused incision of coastal rivers and activated an abundant fluvial supply. The resulting fan deltas prograded rapidly across the narrow, wave-dominated littoral zone and further into sublittoral environment, of which deposits are investigated in this study.

The tempestite deposits of Karpuzçay Formation are well exposed in extensive road-cut sections oriented roughly perpendicular to the basin margin, ca. 15 km away from the westward pinchout of the Katırınemeği fan delta (asphalt road between the villages Hacıobası and Kızılkaya south of the town of Manavgat; see Fig. 3D). The minimal tectonic deformation and the lateral extent of the individual outcrops reaching in some cases 400 m makes these outcrops an excellent place to study lateral bed pinchouts (see Fig. 42 for examples of some of the studied outcrops).



**Fig. 40.** (A) Location map for B and C. (B) Location of the Antalya Basin in southwestern Turkey. (C) Simplified map of the Antalya Basin, showing its Aksu, Köprü and Manavgat compartments. Note the location of the studied outcrops in the southwestern part of the Manavgat Basin.

---

## 10.2. Results

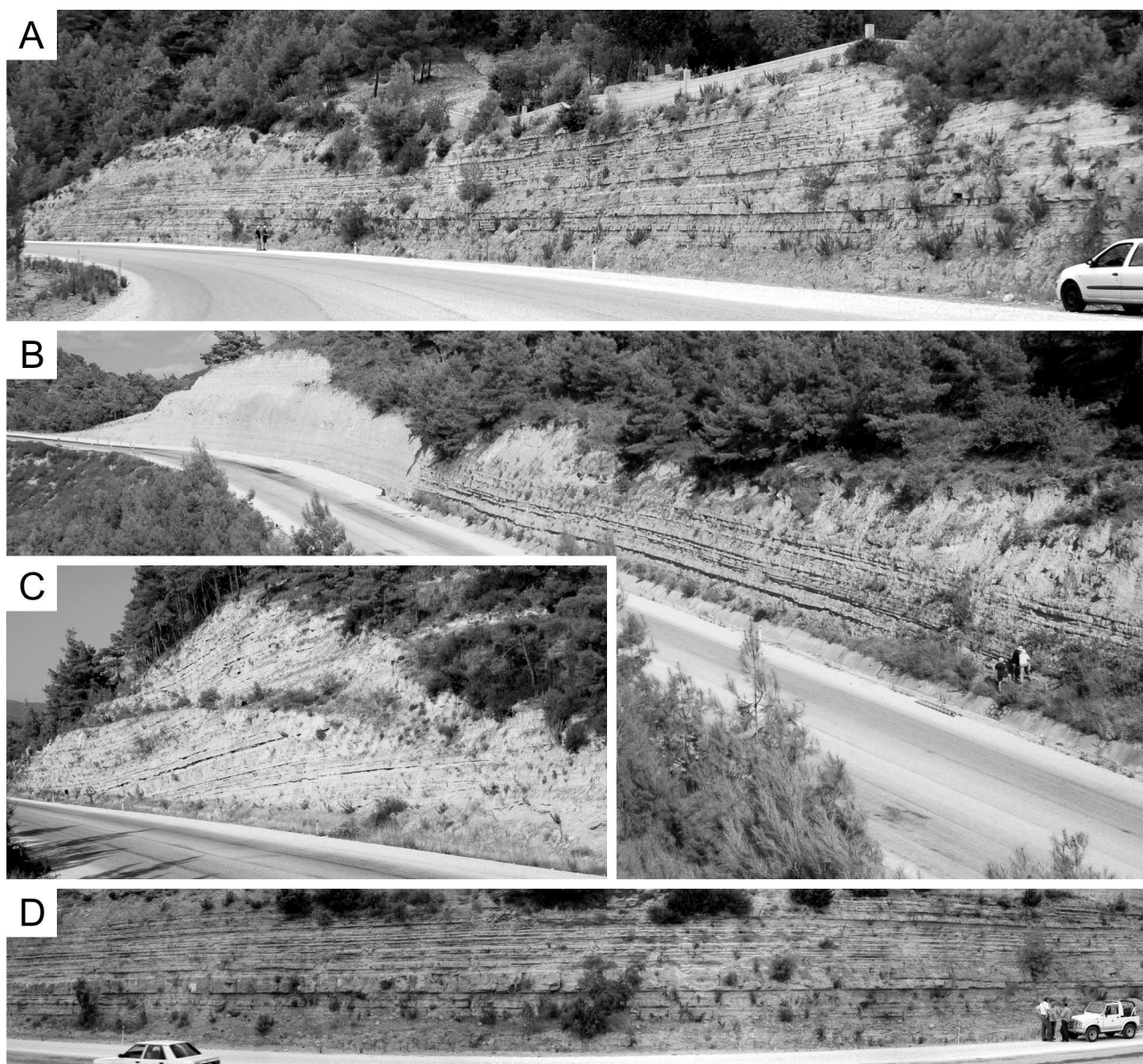
### 10.2.1. Bed types

Sandstone beds measured in the Karpuzçay Formation have sheet-like geometries, are siliciclastic in composition, show normal grading, have sharp tops and bases, and range in grain size from coarse to very fine sand. They are intercalated with thin mudstone beds (<30 cm), often containing very thin layers of siltstone (<1 cm) and plant detritus and/or shell debris. The asymmetrical ripples, local gutter casts and sporadic tool marks in the sandstone beds indicate transport direction towards the SW and WSW, which means seawards, straight or obliquely away from the shoreline. These beds have been previously interpreted as episodic, discrete incursions of shore-derived sand deposited below fair-weather wave base, and their generation has been attributed to storms (Wathne et al., in prep.). The following facies variants are comprised in the measured beds:  $Sm(pr)$ ,  $Smp(r)$ ,  $Sm(p)r$ ,  $Smpr$ ,  $Sp(r)$ ,  $Spr$ , and  $Sr$ . Frequency distribution of these bed-types occurring in the Karpuzçay Formation is shown in Fig. 12E. The lateral variation in division thickness can vary significantly throughout the length of the outcrops. The respective thicknesses of the individual divisions are following: division  $m$ : 5-30 cm, division  $p$ : 3-40 cm, division  $r$ : 0.3-20 cm. The total thickness of the 21 measured beds varies from 0.3 to 40 cm.

### 10.2.2. Frequency distribution of tempestite thickness

The obtained thickness population consists of 637 measurements, ranges from 0.3 to 40 cm, and has a mean and median value of 12.9 and 10.5, respectively. The frequency distribution of turbidite thickness is determined to be lognormal based on graphical and numerical tests described below. Linear histogram shows the distribution is skewed to the right and has a good fit to the lognormal density distribution curve (Fig. 43A). Taking a logarithm of the thickness data results in a normal distribution with a mean of 10.3 cm and a standard deviation of 2.08 cm (Fig. 43B). Lognormality of the data is also suggested by the exceedence frequency curve, which has a convex-up shape on a log-log plot and consists of three roughly straight-line segments separated by two inflexion points having the value of 5 and 25 cm. These three segments display convex-shaped EF-curves when re-plotted on a logarithmic plot (Figs. 41E, F & G), which suggests lognormality and allows for further segmenting in order to achieve a more detailed identification of



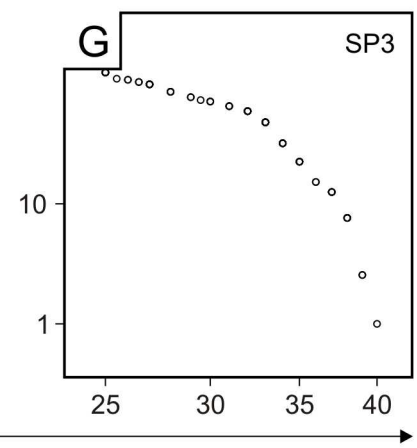
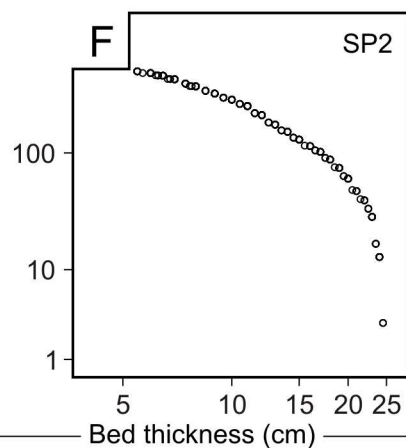
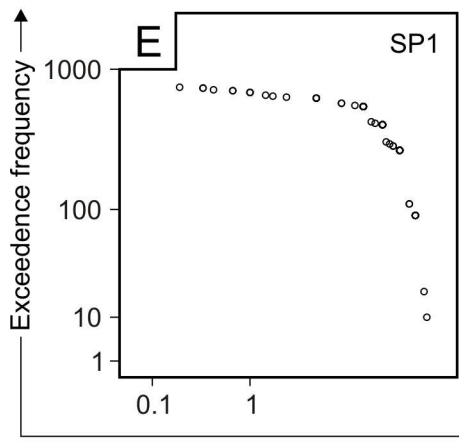
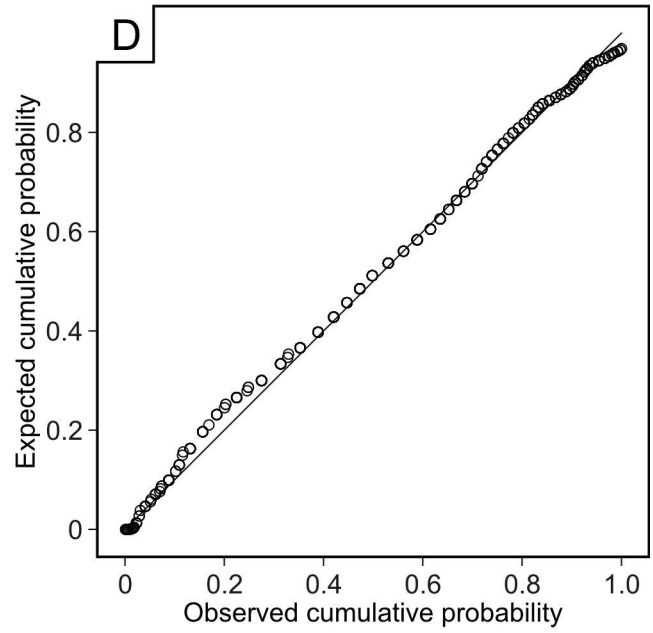
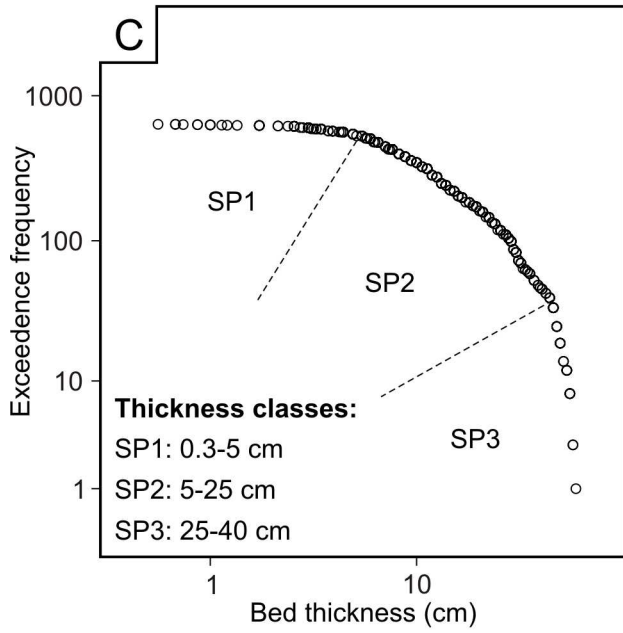
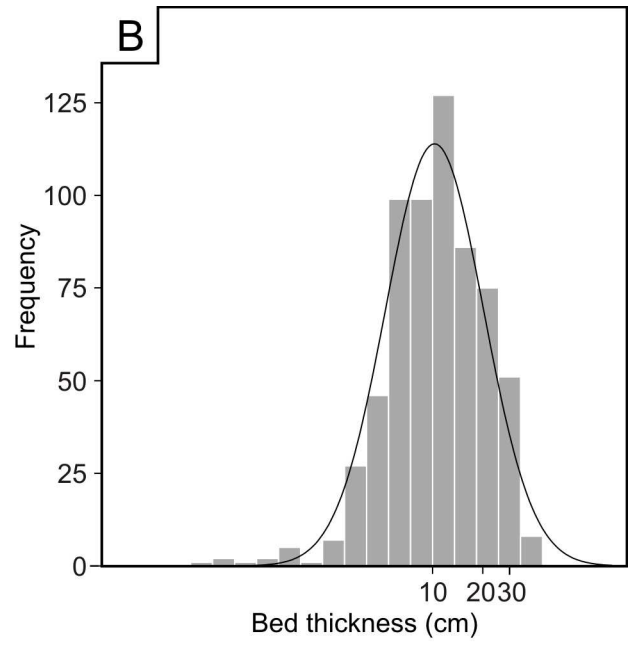
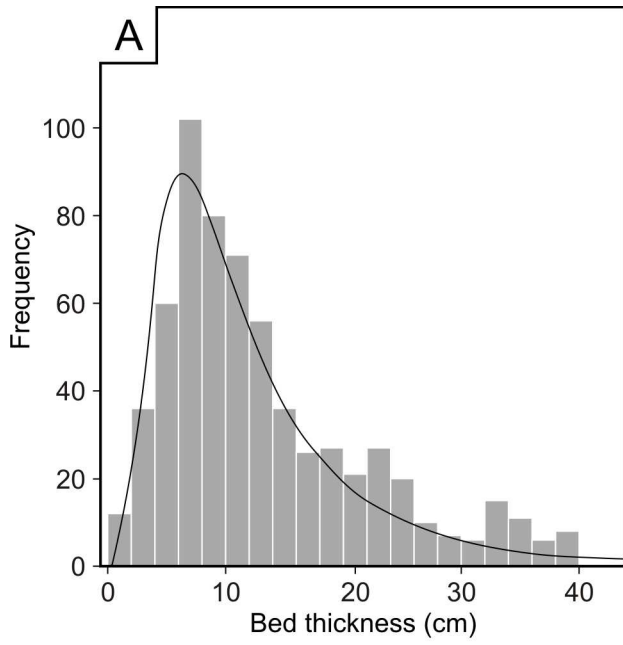


**Fig. 42.** Photographs of the measured outcrops in the Karpuzçay Formation. The road-cut sections are exposed along the asphalt road between the villages Hacıobası and Kızılkaya south of the town Manavgat. For the locations of the measured outcrops see Fig. 3A. (A & D) Outcrop number 4, (B), outcrop number 2, (C) outcrop number 3.

the linear fit on a probability plot being 0.995 and the Anderson-Darling test statistic being 1.848.

### 10.2.3. Dowflow changes in bed thickness, facies, grain size, and bed-top undulations

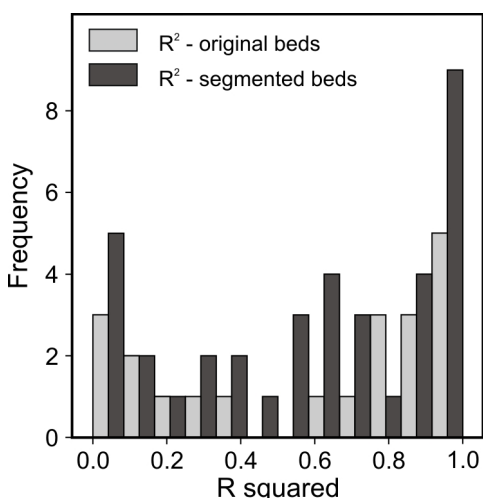
The reduction in bed thickness over the measured length intervals (up to 310 m) is generally more significant in comparison to the turbidites of Marnoso Arenacea and Akveren formations. 13 beds (62 %) are best approximated by a linear regression line, while the remaining 8 beds (38 %) have a best fit to an exponential



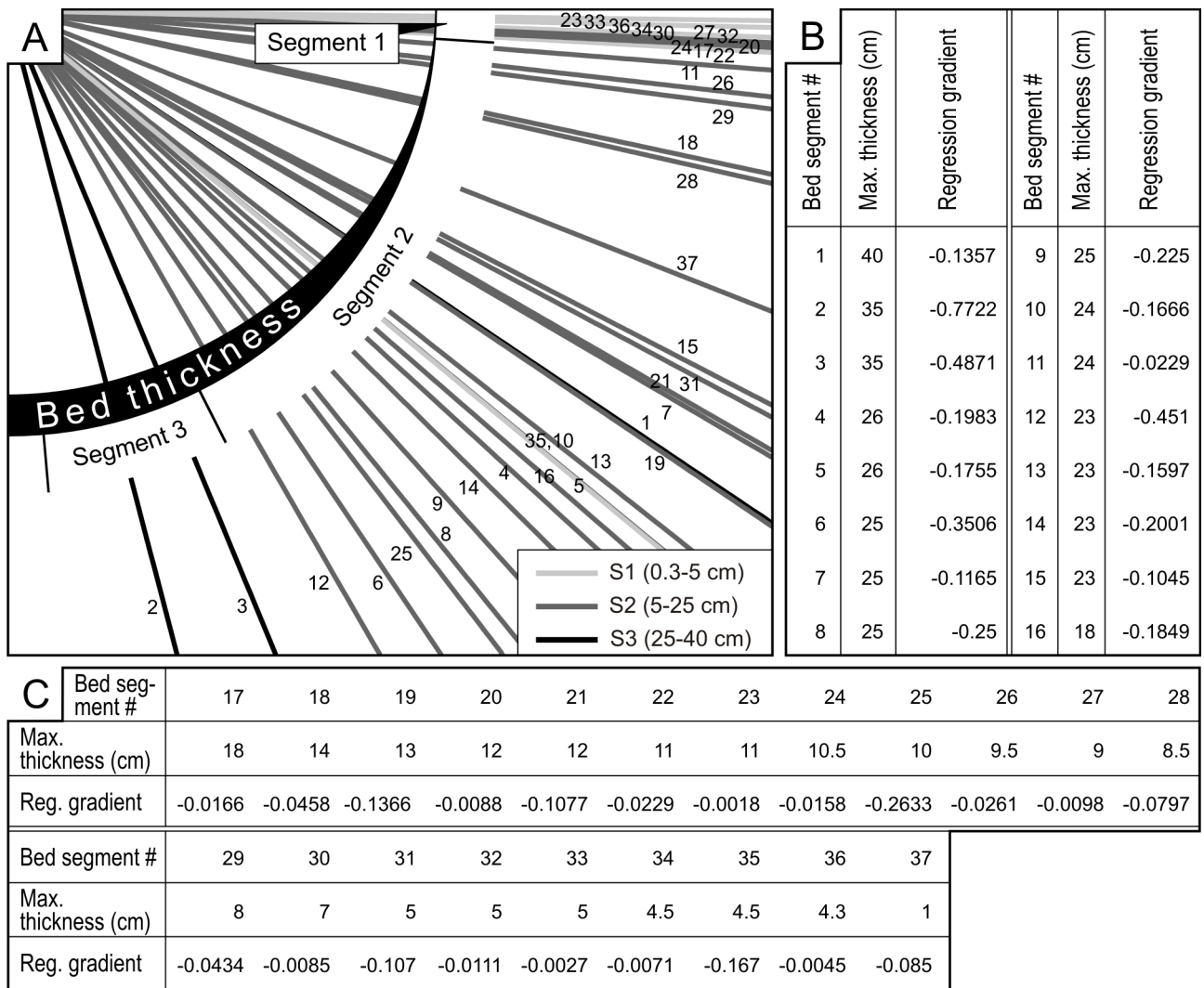
**Fig. 43.** Frequency distribution of tempestite thickness in the Karpuzçay Formation. The thickness population of all measured tempestites consists of 637 measurements in 21 beds. **(A)** Frequency histogram shows the distribution is skewed to the right, meaning thin-bedded tempestites prevail. **(B)** The log-transformed bed thicknesses approximate to a Gaussian distribution on a frequency histogram, indicating a lognormal distribution. **(C)** Exceedence frequency plot of data. The overall distribution forms a convex-up curve on a log-log EF-plot and consists of three minor straight-line segments separated by inflexion points. **(D)** Lognormal P-P plot shows the data points have a tight fit to a straight line and are therefore approximated by a lognormal distribution very well. **(E, F & G)** Thickness subpopulations derived from the segments of the overall EF-curve display a convex-up curve on a log-log EF-plot, suggesting they follow a similar distribution as the population they come from.

function. Due to the rapid reduction in downflow thickness, beds spanning a wide range of thicknesses had to be broken into segments corresponding to the particular thickness classes derived from the EF-curve. This process had a significant effect on the  $R^2$  values for some of the beds. Because thinning rate changes with bed thickness (as will be explained later in the text), the segmentation of beds allowed for better approximation of thinning trends (thus higher  $R^2$ -values) without using nonlinear regression functions. However, a strong negative effect of the process was the cut-back of the dependent variable (in this case the downflow distance), which resulted in an increased variance and thus a decrease in the  $R^2$ -values. The result is a slight increase in the mean coefficient of determination  $R^2$  from 0.5803 to 0.6001, which overall is not a dramatic change (Fig. 44).

Regression gradients representing downflow bed-thickness changes range from -0.0018 to -0.7722 (Fig. 45B & C). This gradient spectrum is extremely wide when compared to the Marnoso Arenacea and Akveren turbidites. A subsequent suggestion, as in the previous formations, is that this gradient spectrum cannot be expressed by a single linear function, and can be thought to imply that the regression gradient is directly related to the local bed thickness. The relationship between the regression gradient and the local bed thickness has a linear-fit  $R^2$ -value of 0.414 and cannot be considered significant (Fig. 46A). However, the low coefficient-of-determination value might only be a consequence of scarce data; the mean thickness of the EF-segments plotted against their corresponding average thinning gradients proves this relationship has a



**Fig. 44.** Due to the rapid reduction in downflow thickness, beds spanning a wide range of thicknesses had to be broken into segments corresponding to the particular thickness classes derived from the EF-curve. This figure illustrates the effect this segmentation had on the  $R^2$  values defining the goodness of fit. The segmented beds show a slight increase in the  $R^2$  values, indicating the measured beds are

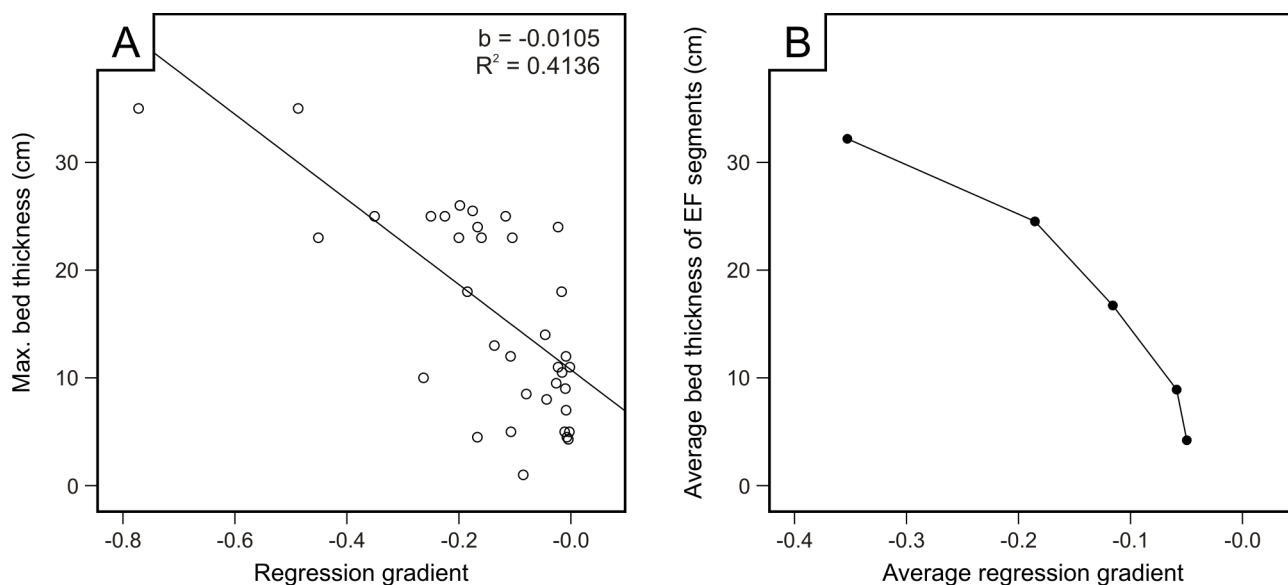


**Fig. 45.** (A) Regression gradients (thinning rate) for the bed-segments measured parallel to paleotransport. Each bed-segment is represented by a regression line. The intercepts of the regression equations are set to a common value to make the thinning rates of bed-segments comparable on a single plot. The shading of the lines corresponds to the particular thickness classes defined from the EF-curves. Each bed segment is numbered (from thickest to thinnest) with their exact regression gradients listed in (B) and (C).

certain trend and is not to be considered negligible (Fig. 46B). Thus, the thinning rate (regression gradient) increases with decreasing bed thickness (i.e., locally thick beds thin more rapidly than locally thin beds) and the overall pinchout geometry of a single tempestite bed is thought to be of concave-upward shape (Fig. 49). Using this concept, a 40 cm thick tempestite bed would pinch out within a distance of 2400 meters (Fig. 49). The individual tempestite divisions seem to have lenticular pinchout geometries, as shown by the change in lithology from thick to thin beds (Fig. 49).

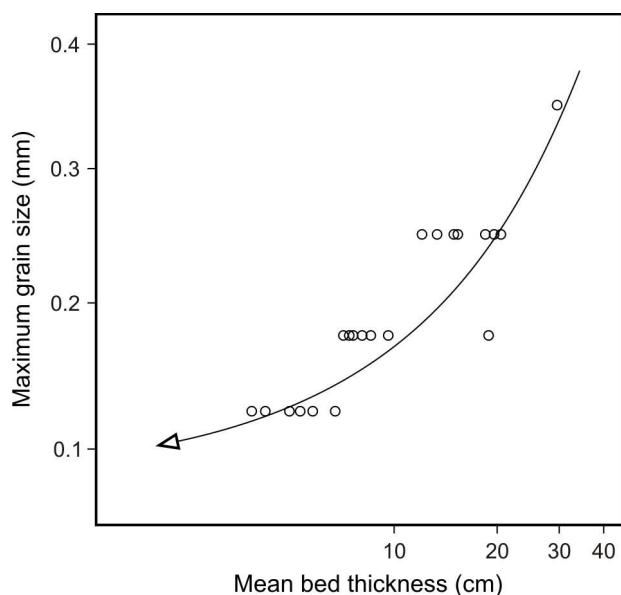
Grain size does not show any apparent change throughout the measured segments of the beds, but is found to decrease exponentially from thick to thin beds as in the case of Marnoso Arenacea and Akveren turbidites (Fig. 47). Periodic thickness variations that could be considered bed-top undulations are present in



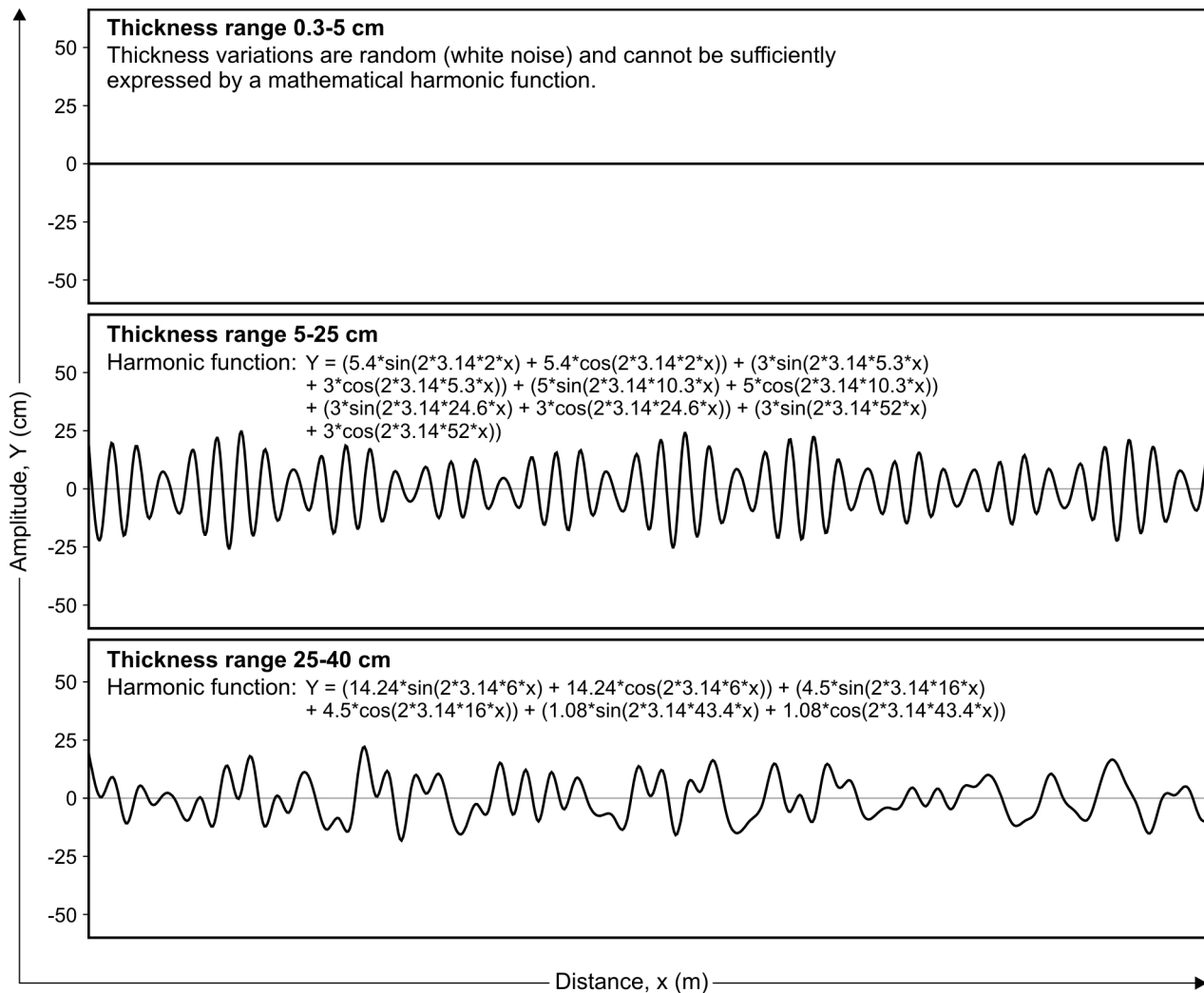


**Fig. 46.** (A) Maximum bed thickness of tempestites in the Karpuzçay Formation decreases with increasing regression gradient at a rate of -0.0105. Note that this rate is considerably lower than that for the Marnoso Arenacea and Akveren turbidites suggesting the beds in the Karpuzçay Formation thin more rapidly downcurrent. (B) The relationship between bed thickness and thinning rate becomes very evident when the mean thinning gradient is plotted against the average bed thickness of EF-segments.

the studied tempestite beds, and are found to be even more pronounced than in some of the studied turbidites. According to the frequency spectrums of beds plotted on cumulative periodograms only a few beds test as white noise series, meaning the mathematical approximation of bed-top undulations is in this case appropriate. This does not apply to beds thinner than 5 cm, in which the bed-thickness variations seem to be purely random without any autocorrelation structure. The dominant wavelengths of the bed-top waveforms for the specific thickness classes defined from the EF-curve are as follows: thickness class 0.3-5 cm: only

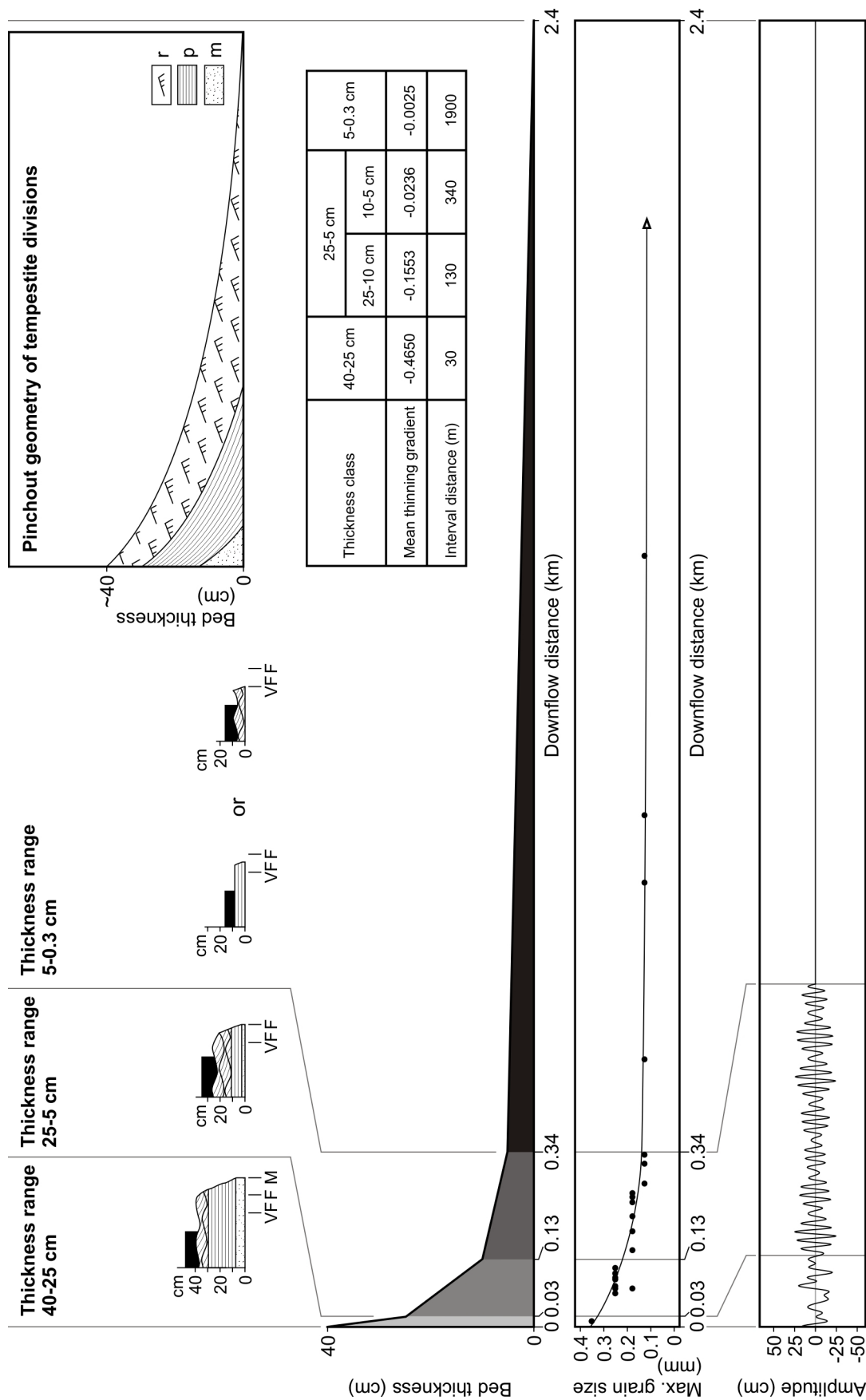


**Fig. 47.** Change in maximum grain size from thick to thin beds in the tempestites of the Karpuzçay Formation. Maximum grain size is found to diminish with local bed thickness in a concave-upward fashion. Note: plot with logarithmic axes.



**Fig. 48.** Modelled bed-top undulations and their corresponding harmonic functions for the thickness classes derived from the EF-curve. The presence and abundance of short wavelengths is found to decrease with decreasing bed thickness (i.e., the waveform becomes simpler, random noise is filtered out). No apparent change in amplitude of the bed-top undulations is detected from the thickness class 25-40 cm down to the thickness class 5-25 cm, however, the introduction of shorter wavelengths in class 5-25 cm and white noise in class 0.3-5 cm signifies the waveform signal dies out with decreasing bed thickness, implying a decrease in the waveform amplitude from thick to thin beds.

random noise; thickness class 5-25 cm: 2, 5.3, 10.3, 24.6, 52 meters; thickness class 25-40 cm: 6, 16, 43.4, meters. The presence and abundance of short wavelengths is found to decrease with bed thickness (i.e., the waveform becomes simpler, random noise is filtered out) (Fig. 48, 49). No apparent change in amplitude of the bed-top undulations is detected from the thickness class 25-40 cm down to the thickness class 5-25 cm, however, the introduction of shorter wavelengths in class 5-25 cm and white noise in class 0.3-5 cm signifies the waveform signal dies out with decreasing bed thickness, implying a decrease in the waveform amplitude from thick to thin beds. The maximum amplitudes in the studied beds range up to 25 cm.



**Fig. 49.** Figure summarizing the thickness, grain size, facies, and bed-top undulation changes in the tempestites of the Karpuzçay Formation. These trends are based on the assumption that a tempestite bed thins continuously in the downflow direction from the point of its maximum thickness (i.e., locally thick beds are more proximal than locally thin beds). When the mean thinning rates for the particular thickness classes defined from the EF-curve are stacked together, the pinchout geometry of a single tempestite bed is of concave-upward shape (upper middle). The concave-upward trend is followed by the maximum grain size and to a certain degree also by the individual tempestite divisions (top). Bed-top undulations decrease in wavelength and amplitude with bed thickness, thereby also with downflow distance. For a more detailed description of the overall trends see text.



## 11. Discussion

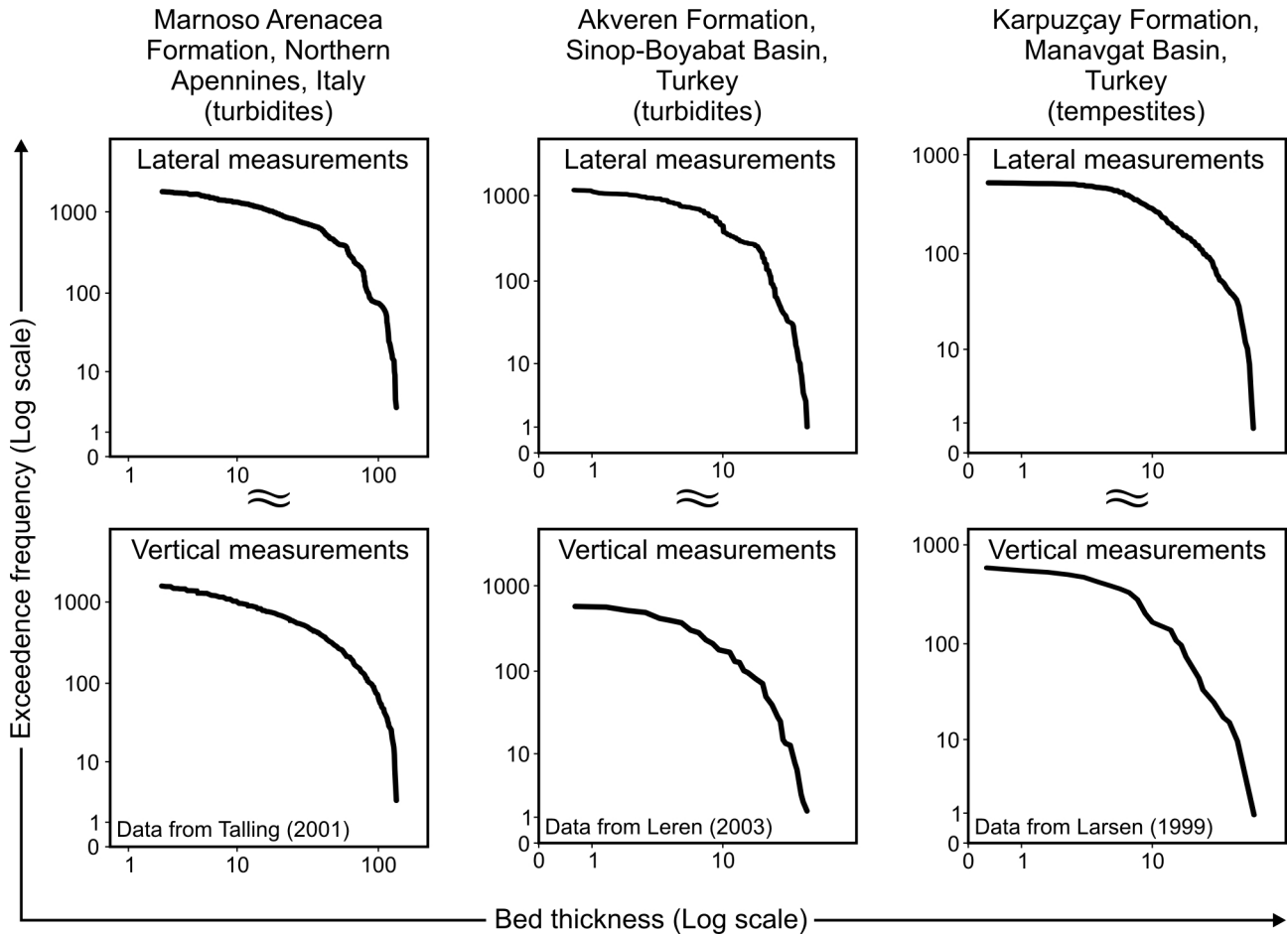
### 11.1. Frequency distribution of turbidite and tempestite thickness

Deep-water turbidites and mid-shelf tempestites measured in this study are characterized by a lognormal thickness frequency distribution (Figs. 15, 27, 31, 38 & 43). Bed-to-bed thickness measurements in vertical outcrop sections of these deposits show similar type of thickness frequency distribution (Fig. 50), which suggests that the EF-plot of vertically measured bed thicknesses may approximate the EF-plot of lateral bed-thickness changes.

Lognormal frequency distribution of turbidite thicknesses has also been reported from other studies (e.g., McBride, 1962; Enos, 1969; Ricci Lucchi & Valmori, 1980; Murray et al., 1996; Talling, 2001; Sylvester, 2007; Talling et al., 2007a). The same type of distribution is indicated by turbidite thickness datasets analysed by Beattie & Dade (1996), Chen & Hiscott (1999), Carlson & Grotzinger (2001) and Sinclair & Cowie (2003), with the data forming a convex-up curve when plotted on a log-log EF-plot, although these authors chose to consider the apparent straight-line segmentation of the curve as an evidence of a segmented power-law distribution, rather than lognormal distribution. The reasoning was that, since a variable with power-law distribution is expected to form a straight line in a log-log EF-plot, the segmented plot would necessarily be a mixture of two or more power-law distributions.

However, it has been pointed out by Talling (2001) and confirmed by Longhitano & Nemec (2005) and Sylvester (2007) that the apparent straight-line segmentation of a log-log EF data plot is merely an artefact of lognormal distribution. Simply, a lognormal data population, when displayed as a log-log EF-plot, tends to split into approximately straight-line segments, or subpopulations. This does not mean, however, that the subpopulations follow strictly a power law. As demonstrated in the present study (Figs. 15, 31 & 43), when the individual straight-line segments of the EF plot are re-plotted separately, they all form convex-upward curves and hence represent lognormal, rather than power-law subpopulations.

Nevertheless, the segmentation of lognormal frequency distribution in a log-log EF-plot is an attractive property, allowing us to divide the lognormal population objectively into some “natural” subpopulations and each of them to be approximated as a straight-line (or power-law) distribution. In other words, the lognormal EF-curve can be conveniently considered as a “range-limited”, bimodal or polymodal power-law distribution and be approximated as such. The main advantage of this approximation is that: (1) the lognormal population can be objectively divided into subpopulations; and (2) the frequency distribution for each of the bed-thickness ranges can be described satisfactorily by the corresponding straight-line’s gradient (known as the “fractal number”; see Feder, 1988).



**Fig. 50.** Figure showing the similarity between exceedence frequency curves defined from lateral and vertical (bed-to-bed) measurements of turbidites and tempestites. This similarity suggests the EF-plot of vertically measured bed thicknesses may approximate the EF-plot of lateral bed-thickness changes. Vertical thickness data come from the measurements of Talling (2001), Leren (2003) and Larsen (1999).

The thinner turbidites (<40 cm) measured in the Marnoso Arenacea Formation and Akveren Formation, and the tempestites measured in the Karpuzçay Formation, show very similar thickness distributions. Their log-log EF-plots show a marked inflexion point corresponding to the bed-thickness value of ~25 cm (Figs. 15, 31 & 43). These distributions can thus be considered as bimodal and approximated with straight lines as two power-law subpopulations, even though the approximation could theoretically be improved by distinguishing more straight-line segments.

Bimodality of turbidite thickness frequency distributions has previously been ascribed hypothetically to the difference between deposits of low- and high-density turbidity currents (Talling, 2001) or considered to reflect the difference between deposits of turbidity currents controlled flow competence and flow capacity (Hiscott, 1994; Kneller & McCaffrey, 2003). These conceptual notions might possibly be applied also in the present case, with the hypothetical implication that the deposition of both deep-water turbidites and mid-shelf tempestites is controlled, at least to some extent, by similar factors.

However, this interpretation is not followed here, because – as pointed out above – the dataset bimodality is apparently little more than an artefact of the curve's crude, first-order approximation by a power-law approach. The convex-upward curve in all cases could as well be divided into a larger, or almost infinite, number of straight-line segments if a more exact approximation were to be achieved. This means that bimodality is not an intrinsic, unique property the dataset distribution itself, but rather a result of the way in which we choose to approximate it – no matter how useful this approximation may possibly be for other purposes, as discussed further below.

## **11.2. The downflow thinning of turbidites and tempestites**

Consistent basinward thinning of turbidites and tempestites has been evidenced by long-distance correlations (Bornhold & Pilkey, 1971; Hirayama & Nakajima, 1977; Myrow & Hiscott, 1991; Trincardi & Field, 1991; Wheatcroft & Borgeld, 2000; Bentley et al., 2002; Murray et al., 2002; Wheatcroft & Drake, 2003; Amy & Talling, 2006; Wheatcroft et al., 2006; Talling et al., 2007a, b), by experimental studies (Rukavina, 1965; Lüthi, 1981; Bonnecaze et al., 1993; Dade & Huppert, 1995; Gladstone et al., 1998; Woods et al., 1998; Alexander & Mulder, 2002; Choux & Druitt, 2002; Al Ja'Aidi et al., 2004; Amy et al., 2004; Gray et al., 2005; Lamb et al., 2006) and by numerical modelling (Zeng & Lowe, 1997; Zhang et al., 1999; Pratson et al., 2000; Scully et al., 2002). The outward-thinning wedge shape of turbidite beds was reproduced experimentally and numerically for the “collapsing”, or “depletive” (sensu Kneller & Buckee, 2000), unconfined currents in which the flow velocity, sediment concentration and sediment-depletion rate decrease away from the source; or more strictly, from the near-scour zone of hydraulic jump, beyond which the current becomes fully depositional.

The present study has demonstrated that the lateral thinning rate of any given turbidite or tempestite bed depends on the bed's local thickness range: the relatively thick bed segments measured appear to thin faster than the thinner segments (Figs. 17, 18, 27, 33, 34, 45 & 46). From the perspective of a turbidity current's unconfined spreading and decay on a basin floor, it can be assumed that the thin beds in an outcrop section represent the “distal” mode of sediment depletion, whereas the thicker beds represent more “proximal” modes. The fact that there are thinner and thicker beds in any particular outcrop sections means obviously that there were smaller and larger turbidity currents involved; but since the physical nature of these currents was basically the same, we may assume that also their downflow pattern of sediment-load partitioning would be the same. In other words, the deposits of large and small turbidity currents have different volumes and basinward extent, but their gross geometry is expected to be similar. Although this notion is not claimed here to be strict, it serves widely as the basis for virtually all laboratory experiments, where it is assumed that the small-scale flows and their deposits may imitate the large-scale ones. Notably, the notion of scale-

independence and self-similarity also underlies the concept of fractality, which might explain why the lognormal bed-thickness distributions can be approximated by power-law functions. One is thus tempted to hypothesize that a variable with lognormal frequency distribution may be regarded as a kind of “imperfect fractal”.

If the assumption of a scale-independent geometrical similarity of volumetrically small and large beds deposited by similar process is correct, the various bed-thinning rates obtained from the outcrop datasets for different bed-thickness ranges can thus be stacked together according to their thickness ranges to represent the bulk thinning trend and pinchout geometry of a whole single “model” bed. From the point of their maximum thickness, the turbidites and tempestites would then appear to thin basinwards at a progressively lower rate, showing a concave-upward downflow thinning trend (Figs. 23, 27, 37 & 49).

A similar concave-upward trend of bed thinning has been documented by several previous studies, except for the most proximal, near-source bed segments, which tend to have fairly uniform thicknesses. This bed geometry can be referred to as “sigmoidal” and has earlier been deduced from long-distance correlations of small- to large-volume turbidites and tempestites (Rupke, 1976; Trincardi & Field, 1991; Murray et al., 2002; Talling et al., 2007a), as well as by the experimental and numerical studies of common and wave-supported density currents (Bonnecaze et al., 1993, 1995; Dade & Huppert, 1995; Gladstone et al., 1998; Hallworth & Huppert, 1998; Zhang et al., 1999; Pratson et al., 2000; Scully et al., 2002; Lamb et al., 2006). The deposit of a turbidity current in its most proximal, upstream part is expected to thicken quickly towards the flow’s zone of hydraulic jump, where the current would become fully depositional and tend to lose a large portion of its sediment load, while spreading the remaining load gradually in the downflow direction (see Engel, 1974; Lowe, 1982; Sadler, 1982; Zhang et al., 1999; Mulder & Alexander, 2001). The proximal bed segment with high and uniform thickness would then probably correspond to the depositional zone directly downflow from the hydraulic jump. Experiments by Kuenen (1951), Middleton (1967) and Lovell (1971) suggested that the deposition of a turbiditic current on a gradually flattening slope would commence in the less powerful tail part of the flow and subsequently advance towards the flow head. Consequently, the most proximal part of the deposit would tend to thicken downcurrent until the point at which the whole flow, except for a small region near its head, would be depositing sediment. The thickness of deposit would subsequently decrease in the downflow direction.

Some workers have managed to recognize the downflow-thickening “proximal limb” of turbidites (e.g., Meischner, 1962, 1964; Lovell, 1969; Eder, 1971; Sadler, 1982), but such documentations are relatively rare. As pointed out by Sadler (1982), there are at least three main reasons of this fact: (1) the most proximal outcrops of turbiditic systems are rare, because the basin proximal area is most often strongly uplifted and eroded; 2) the most proximal segments of turbidites tend to occur in channels or directly off their outlets, and



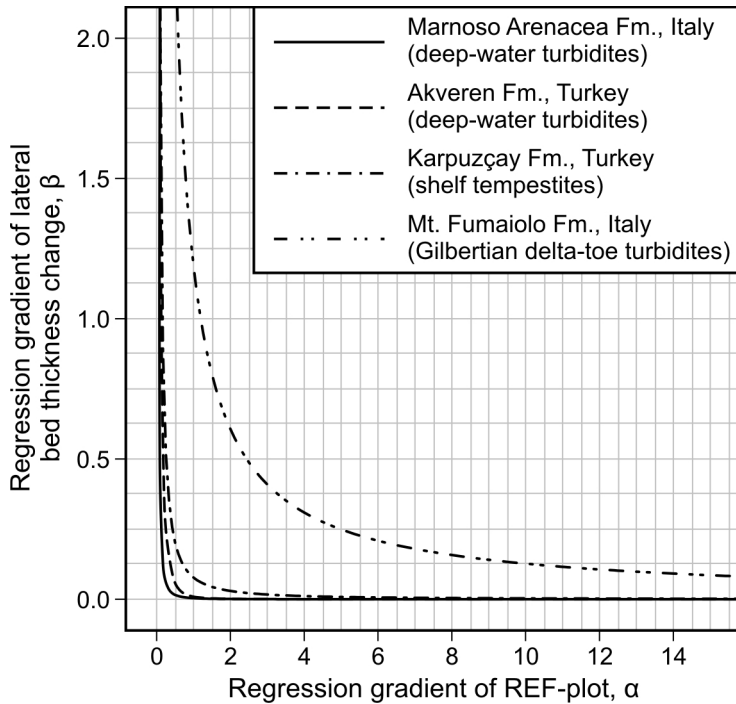
hence tend to be eroded by subsequent flows; and (3) the most proximal parts of turbidites may not necessarily be coarser-grained their thickest segments, and hence escape recognition.

No compelling evidence of a downflow thickening or thickness uniformity has been found in the thickest turbidites measured in the present study, where the maximum bed thickness measured was 130 cm in the Marnoso Arenacea Formation. However, Talling et al. (2007a) measured beds thicker than 130 cm in this formation and recognized cases of downflow thickening, apart from the gradual downflow thinning of the vast majority of turbidites there. As pointed out by Sadler (1982), Amy & Talling (2006) and Talling et al. (2007a, b), there is no evidence of downflow thickening in relatively thin (<100 m or so) turbidites.

In the case of tempestites, their maximum bed thicknesses are expected to occur around the inner/middle shelf transition, because of the suspension and/or re-suspension of sand by wave-generated bottom currents (Zhang et al., 1999). Since the wave action at the seafloor declines with water depth, the thickness of storm deposit decreases seawards.

### **11.3. Downflow changes in grain size and facies**

The maximum grain size in the Marnoso Arenacea, Akveren and Karpuzçay formations decreases consistently downflow in concave-upward manner from the point of the maximum bed thickness measured (Figs. 23, 37 & 49). This trend is almost identical with the downflow decrease in bed thickness (see the next section). A similar decrease in the maximum grain size with down-current distance has been recognized in the turbidite successions of Slovenia (Engel, 1974; Sadler, 1982), the Rheinische Schiefergebirge and Harz Mountains of Germany (Sadler, 1982) and the Cloridorme Formation of Quebec, Canada (Parkash & Middleton, 1970). Because tractional bedforms are determined primarily by grain size and flow power (Allen, 1982; Harms et al., 1982), it can be expected that the internal structures of a sand bed deposited by current will be linked to specific grain-size ranges and bed thicknesses. For example, the lateral thinning and fining of turbidite sandstone beds is expected to be accompanied by a concurrent thinning or pinchout of the lower Bouma divisions. A similar tendency is expected to characterize tempestites (Fig. 7). Downflow profiles of the separate Bouma and tempestite divisions are of lenticular shape (Figs. 24, 37 and 49), a trend also suggested by Lowe (1982), Sadler (1982) and Allen (1985). However, systematic lateral observations and measurement in the individual beds do not show any obvious trend in the Bouma divisions (Figs. 19 & 35), which indicates that the lateral changes in Bouma divisions and their thicknesses can be far less irregular than it is predicted by textbook models (e.g., Allen, 1982).



**Fig. 51.** The relationship between the gradients of the REF-segments ( $\alpha$ -values) and the corresponding gradients of lateral bed thickness changes ( $\beta$ -values) is best expressed by a power-law function, implying fractality of the bivariate system. On this basis, the  $\beta$ -value can readily be derived from the corresponding  $\alpha$ -value established on the basis of vertical bed-thickness measurements (e.g., well logs or outcrop sections). The  $\beta/\alpha$  relationship appears to be similar for the two turbiditic systems studied, but is different for the tempestite succession and even more different for the delta-toe turbidites.

#### 11.4. Predicting the pinchout geometry of turbidites and tempestites

As pointed out in section 11.1, the advantage of a log-log EF-plot of lognormal data population is that the latter splits into “natural” subpopulations (recognized as approximately straight-line segments of the plot), each characterized by a different and approximately constant bed-thinning rate.

A possible disadvantage of a log-log EF-plot is that the “heavy” (high bed-thickness) tail of the frequency distribution is highlighted. This effect may not be a problem when it comes to a prospect evaluation, because the thicker beds would obviously contain more hydrocarbons and would also form “shoot-outs” that might cause leakage of the hydrocarbons. However, the thinner beds are generally more abundant in a turbiditic or tempestitic succession and may be of interest when it comes to an overall characterization and modelling of the reservoir. In such a case, the bed-thickness dataset should be plotted as thickness  $T$  values against the number of data smaller or equal to a particular  $T$ -value. This plot will be a curve similar to the-EF curves used in this study, but horizontally mirrored and highlighting more the low- $T$  part of the frequency distribution. This kind of “reversed” EF-plot is referred here to as the REF-plot.

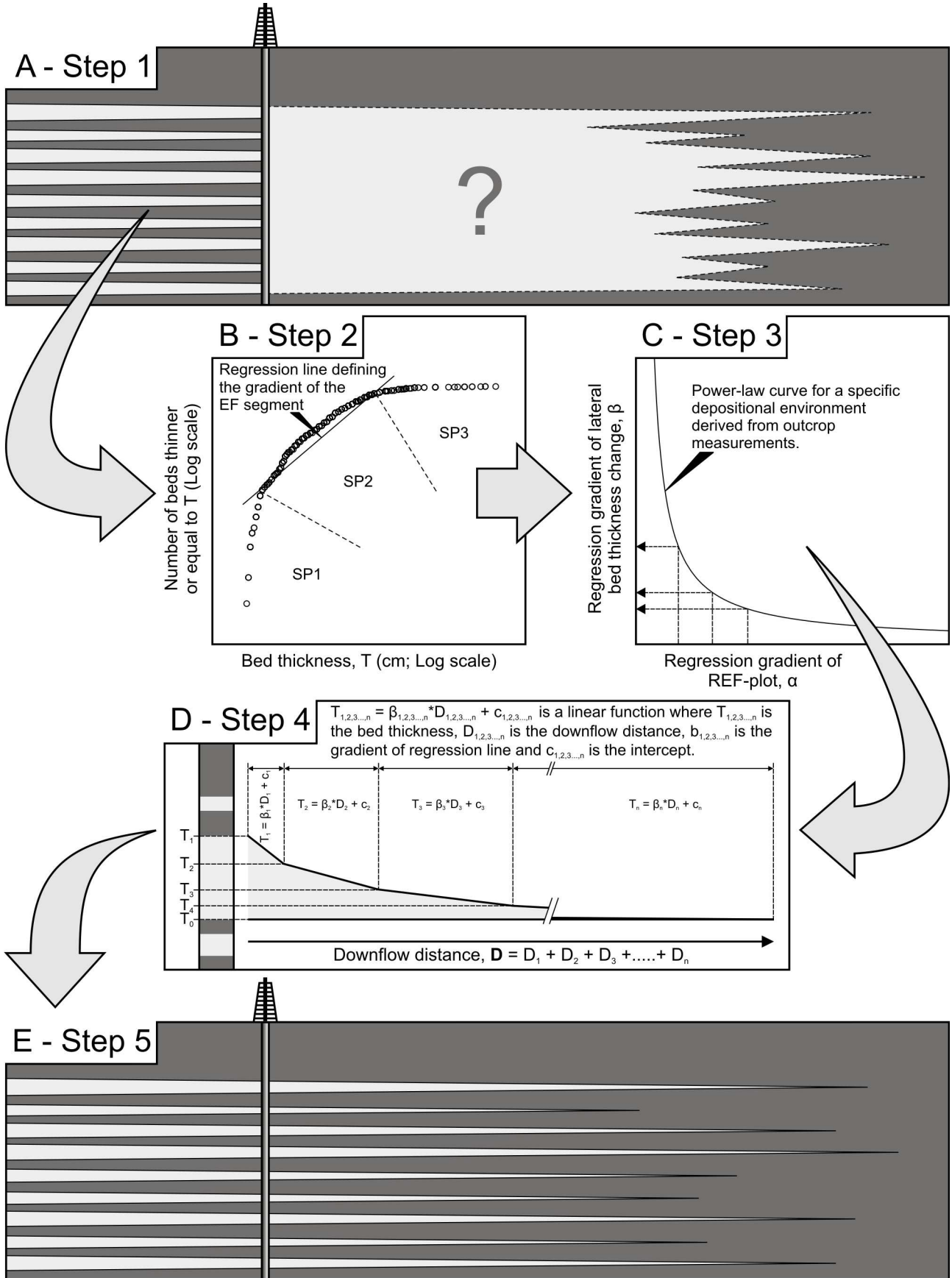
There is a close relationship between the bed-thickness ranges defined by the straight-line segments of log-log EF-plot (or log-log REF-plot, if used) and the downflow thinning rate of the beds, mathematically best expressed by a power-law function  $\beta = c \cdot \alpha^b$ , where  $\beta$  is the linear regression gradient of lateral bed-thinning trend for a particular bed-thickness range,  $\alpha$  is the linear regression gradient (or fractal number) of the corresponding EF-segment, and  $c$  and  $b$  are coefficients. This power-law function seems to approximate

best all the datasets in the present case, with some differences in coefficients  $c$  and  $b$ . A power-law relationship implies fractality (i.e., scale-independence and self-similarity), which means that the link between  $\beta$ -values and  $\alpha$ -values holds for any range of bed thicknesses. The turbidites of the Marnoso Arenacea Formation and Akveren Formation, though palaeogeographically and bathymetrically different, appear to be characterized by very similar power-law functions  $\beta=f(\alpha)$ , whereas the tempestites of the Karpuzçay Formation and the delta-toe turbidites of the Monte Fumaiolo Formation are characterized by distinctly different functions  $\beta=f(\alpha)$  (Fig. 51). This fact suggests that the  $\beta=f(\alpha)$  function may be system-specific when it comes to different depositional systems, or sedimentary environments.

**Method** – On the basis of the aforementioned statistical relationships, a simple five-step procedure for the estimation of lateral (downflow) turbidite and tempestite pinchouts from any given vertical succession is proposed. This method relies on the following assumptions: (1) the event beds, whether deep-water turbidites or mid-shelf tempestites, were deposited in an unconfined seafloor setting; (2) their general palaeoflow direction is known (from seismic sections/maps, well dipmeter data or palaeogeographic inferences); and (3) the thickness frequency distribution of beds measured in the available vertical succession (well cores) is lognormal, giving a segmented convex-upward on a log-log EF-plot (or REF-plot). The successive steps of the procedure are as follows (Fig. 52):

- *Step 1* – The thicknesses of sandstone beds in a well core are measured (Fig. 52A).
- *Step 2* – A log-log EF (or REF) plot is constructed for this dataset and the gradients ( $\alpha$ ) of its straight-line segments with the corresponding bed-thickness ranges are determined (Fig. 52B).
- *Step 3* – The lateral bed-thinning rate for a particular bed-thickness range is then derived from the  $\beta = f(\alpha)$  power-law function established for a given depositional system (Fig. 52C).
- *Step 4* – The lateral pinchout distance for every single bed in the measured (well-core) succession is calculated as the sum of distances corresponding to a given thickness range and the successive lower ranges, if any, as defined in *Step 2* on the basis of the EF (or REF) plot (Fig. 52D).
- *Step 5* – The net spatial pinchout geometry of the entire succession can be modelled on a bed-by-bed basis (Fig. 52E).

**Remarks** – The method developed here is tentative, because it is based on a pilot study and datasets from only a few formations. It should be verified through a wider range of similar detailed studies. For example, Browne et al. (1996; 2000) reported rapid thinning of thin beds (<35 cm) and gentle thinning of thick beds (35-60 cm) in a turbidite lobe of the Mt. Messenger Formation, northern Taranaki, New Zealand, which would appear to be inconsistent with the present study. Furthermore, a wider range of  $\beta = f(\alpha)$  relationships should be established for specific depositional systems (e.g., turbiditic channel levées, radial lobes and elongate lobes; regressive and transgressive offshore-transition environments). If this statistical method eventually proves to be valid, it will be of great value to the petroleum exploration and reservoir



**Fig. 52.** Figure showing a simple five-step procedure for the estimation of lateral (downflow) turbidite and tempestite pinchouts based on thickness data derived from any given vertical succession. **(A - Step 1)** The thickness of sandstone beds in a well core are measured **(B - Step 2)** A log-log EF (or REF) plot is constructed for this dataset and the gradients ( $\alpha$ ) of its straight-line segments with the corresponding bed-thickness ranges are determined. **(C - Step 3)** The lateral bed-thinning rate for a particular bed-thickness range is then derived from the  $\beta = f(\alpha)$  power-law function established for a given depositional system. **(D - Step 4)** The lateral pinchout distance for every single bed in the measured (well-core) succession is calculated as the sum of distances corresponding to a given thickness range and the successive lower ranges, if any, as defined in Step 2 on the basis of the EF (or REF) plot. **(E - Step 5)** The net spatial pinchout geometry of the entire succession can be modelled on a bed-by-bed basis.

---

modelling of sheet-like sandstone successions, such as the offshore-transition deposits (e.g., in the Tarbert Fm., Sognefjord Fm., Fensfjord Fm. and Flett Fm.) and numerous turbiditic successions in the North-West European Continental Shelf (e.g., see Glennie, 1998).

### 11.5. Bed-top undulations

The top surfaces of the measured turbidites and tempestites appear to show broad, low-amplitude to subtle morphological changes, referred to here as the “bed-top undulations”. Their wavelengths are up to 300 m and their amplitudes are relatively low (5-20 cm), but reaching 60 cm in the thickest beds (Figs. 22, 36 & 48). Statistical analysis by means of the Fourier transform indicates that they are non-random and their spatial cyclicity is significant. The waveforms decrease in amplitude and wavelength with the decreasing bed thickness in the downcurrent direction (Figs. 23, 37 & 49). As the bed thickness decreases, the waves appear to show increasingly more “random noise” and become more difficult to define in mathematical terms.

These waveforms are not associated with any particular stratification type or bed division and appear to be little more than simple lateral undulations in the bed thickness. They are visually unrecognizable in outcrop sections and – to the best of the present author’s knowledge – no similar features have been previously reported from either turbidites or tempestites.

The origin of these bed-top undulations is unknown, particularly since that they occur in both turbidite and tempestite beds. Turbidity currents and density-modified geostrophic currents are likely to behave similarly when it comes to internal density layering and interaction of ambient water. It is possible, therefore, that some large internal waves, or Kelvin-Helmholtz instabilities (Nemec, 1995), were generated at the top surfaces of these currents and affected the spatial distribution of sand deposited from the current. In short, the origin and hydrodynamic significance of the bed-top undulations remains to be studied.

### **11.6. Thickness changes normal to palaeoflow axis**

The turbidite lobe beds measured in the Kusuri Formation in the Boyabat Basin, north-central Turkey, were deposited in a narrow (<20 km) “piggyback” basin and the compensational stacking of the turbidite lobes there suggests semi-confinement. These beds, measured perpendicularly to the lobe axes, cannot thus be compared with the downflow measurements of unconfined turbidites in the Marnoso Arenacea Formation or the Akveren Formation. Notably, the lateral thinning trend of a bed segment measured perpendicularly to the general palaeoflow direction in the Marnoso Arenacea Formation does not differ from the downflow thinning trends of the other beds (Fig. 25). The depositional lobes in the latter formation were probably radial, with the turbidity currents spreading both frontally and sideways in a similar manner. The depositional lobes in the Kusuri Formation were elongate, with the frontal spreading of the turbidity currents far exceeding their sideways expansion.

## 12. Conclusions

Lateral changes in the thickness and internal sedimentary characteristics of sheet-like turbidite and tempestite beds have been studied for the purpose of determining the beds' thinning rate and pinchout geometry. Selected outcrops of the Marnoso Arenacea Formation (classical turbidites of depositional fan lobes), the Monte Fumaiolo Formation (bottomset turbidites of Gilbert-type delta), the Akveren Formation (turbidites of a shelf-fed, non-channelized axial system), the Kusuri Formation (turbidites of small depositional fan lobes), and the Karpuzçay Formation (offshore-transition tempestites) have been studied. Most of the outcrop sections were parallel to the palaeoflow direction. More than 3760 closely-spaced (2-10 m) measurements of the thickness of nearly 150 turbidite and tempestite beds have been collected over lateral distances of up to nearly 500 m. The statistical methods of exceedence frequency plot and least-square regression have been used to identify lateral bed-thinning trends.

The turbidite thicknesses in the Marnoso Arenacea Formation follow a segmented lognormal frequency distribution, allowing several subpopulations (or thickness classes) to be distinguished. The lateral thinning trend of the majority of the measured bed portions, ranging in thickness from 2.4 to 128 cm and 50 to 410 m in lateral extent, can be satisfactorily approximated by a linear function. However, there is a spectrum of regression coefficients (regression line gradients), indicating that the overall thinning trend is nonlinear. The relationship between the maximum bed thicknesses of the measured bed segments and their thinning gradient is negative and statistically significant ( $R^2 = 80.7\%$ ). The spectrum of thinning rates, when stacked according to the decreasing thickness classes, indicates that the downflow pinchout geometry of a "model" turbidite bed is a concave-upward function of distance. Turbidite beds measured in outcrops perpendicular to the palaeoflow direction show a thinning trend similar to that in the downflow direction, except for a much lower gradient in the thickest, most proximal part of "model" bed. An analogous concave-upward lateral trend is shown of the relationship between the maximum grain size and mean thickness of the beds. The individual Bouma divisions have lenticular pinchout geometries, as can be inferred from lateral facies changes. The bed tops appear to have gentle undulations with wavelengths of up to 100 m and amplitudes from less than 10 cm to ~60 cm, both decreasing with the decreasing bed thickness.

The thicknesses of delta-toe turbidites measured in the Monte Fumaiolo Formation are only slightly better approximated by a Gaussian frequency distribution than by lognormal distribution. These beds are short wedges (<70 m in downflow extent) with relatively steep thinning gradients and a concave-upward thinning trend. There are no well-defined undulations at their tops.

Lognormal frequency distribution characterizes also turbidite thicknesses in the Akveren Formation. The bed segments measured are 1.5-32 cm thick and have lateral extent of 68 to 484 m. More than half of these

bed segments are best approximated by a linear thinning trend, whereas the other beds are better approximated by a negative-growth exponential function. Also here, the bed-thinning gradients form a wide spectrum, implying an overall nonlinear thinning trend. Many beds appear to thicken in the downflow direction, which is attributed to a partial ponding of turbidity currents in basin-floor synclines related to blind thrusts. Their lateral thinning gradients of bed segments correlate with the segments' maximum thicknesses. This relationship is negative for the downflow thinning beds ( $R^2 = 67.8\%$ ) and positive for the downflow thickening beds ( $R^2 = 78.2\%$ ). The lateral thinning of beds occurs at a higher gradient than their thickening. When the gradients are stacked together according to the bed-segment thickness classes derived from the frequency plot, both the thinning and the thickening "model" beds appear to have a concave-upward lateral thickness trend. The individual Bouma divisions have lenticular, thickening-to-thinning downflow geometry. Grain size decreases exponentially, much like the overall bed thickness. Also here, Fourier analysis has revealed bed-top undulations, cyclic in some beds and chaotic in others, with wavelengths of up to nearly 300 m and amplitudes of 5-40 cm, both decreasing with the decreasing bed thickness.

Tempestite bed segments measured in the Karpuzçay Formation range in thickness from 0.3 to 40 cm and have lateral extent of up to 310 m. Their thickness frequency distribution is lognormal, much like that of the turbidites. The seaward thinning trend of more than half (62 %) of the bed segments is satisfactorily approximated by a linear function, but is negative-growth exponential the others. The bed segments here show a much wider spectrum of thinning gradients than is the case for turbidites, and also the number of bed-thickness classes recognizable from the frequency plot is higher. Linear correlation between regression gradients and class mean bed thicknesses is qualitatively recognizable, but appears to be statistically insignificant ( $R^2 = 41.4\%$ ), probably because the amount of data here is relatively small. The spectrum of gradients, when stacked according to the thickness classes, indicates a nonlinear, concave-upward thinning trend of a "model" tempestite bed. The thinning rate (regression gradient) thus increases with the decreasing bed thickness. The individual bed divisions are inferred to have a lenticular downflow geometries. Grain size shows no obvious downflow change in the individual measured bed segments, but decreases exponentially from the thicker to thinner segments, much like in the lobe turbidites. Cyclic bed-top undulations are relatively well-pronounced in the tempestites, despite their small thicknesses, showing wavelengths of up to 50 m and amplitudes of 5-25 cm. These waveforms are smaller and increasingly chaotic in the thinnest beds.

The lobe turbidites in the Kusuri Formation were measured in an outcrop section nearly 200 m long, transverse to the palaeoflow direction (or lobe axis). Also, the compensational stacking of elongate turbiditic lobes in the narrow basin implies flow semi-confinement, which means that the dataset may not be comparable with the datasets from the other, unconfined turbiditic lobes. The bed-thickness dataset has lognormal frequency distribution, and the exceedence frequency plot allows several bed-thickness classes to



be distinguished. Lateral thinning trends of beds cannot be satisfactorily defined by linear regression trendlines, making the pinchout geometries unpredictably and difficult to model.

On the basis of the results, a tentative statistical method has been developed for thickness analysis of sheet-like sandstone beds, which allows the pinchout distance of every bed in a turbiditic or tempestitic succession encountered in the subsurface to be predicted and the net spatial pinchout of the bed succession to be modelled. The lognormal exceedence frequency plot obtained from lateral bed-thickness measurements in a given sedimentary succession appears to be similar to that obtained from the measurement of bed thicknesses in a vertical log. This means that the former plot can satisfactorily be approximated by the latter plot (e.g., based on measurements from well cores). The relationship between the gradients ( $\alpha$ ) of the straight lines approximating lognormal exceedence frequency plot and the corresponding gradients ( $\beta$ ) of lateral bed-thinning trend is a power-law function. On this basis, the  $\beta$ -value can readily be derived from the corresponding  $\alpha$ -value for a particular bed-thickness range (class). The relationship  $\beta = f(\alpha)$  appears to be similar for the two unconfined turbiditic systems studied, but is different for the tempestite succession and even more different for the delta-toe turbidites. A wider range of depositional systems (e.g., turbiditic channel levées, prodelta turbidites, crevasse splays) should thus be studied in order to establish the  $\beta$  vs.  $\alpha$  relationship characteristic of particular sedimentary environments.



## References

- Aigner, T. and Reineck, H.-E., 1982. Proximality trends in modern storm sands from the Helegoland Bight (North Sea) and their implications for basin analysis. *Senckenbergiana marit.*, 14, 183-215.
- Al Ja'Aidi, O.S., McCaffrey, W.D. and Kneller, B.C., 2004. Factors influencing the deposit geometry of experimental turbidity currents: implications for sand-body architecture in confined basins. In: Lomas, S.A. and Joseph, P. (Editors), *Confined turbidite systems*. Geological Society of London, Special Publication, 222, pp. 45-58.
- Alexander, J. and Mulder, T., 2002. Experimental quasi-steady density currents. *Marine Geology*, 186, 195-210.
- Allen, J.R.L., 1982. *Sedimentary Structures: Their Character and Physical Basis, Volume II*. Elsevier, Amsterdam, 663 pp.
- Allen, J.R.L., 1985. *Principals of Physical Sedimentology*. Allen & Unwin, London, 272 pp.
- Amy, L.A., McCaffrey, W.D. and Kneller, B.C., 2004. The influence of a lateral basin-slope on the depositional patterns of natural and experimental turbidity currents. In: Joseph, P. and Lomas, S.A. (Editors), *Deep-Water Sedimentation in the Alpine Basin of SE France: New perspectives on the Grbs d'Annot and related systems*. Geological Society of London, Special Publication, 221, pp. 311-330.
- Amy, L.A. and Talling, P.J., 2006. Anatomy of turbidites and linked debrites based on long distance (120 x 30 km) bed correlation, Marnoso Arenacea Formation, Northern Apennines, Italy. *Sedimentology*, 53, 161-212.
- Argnani, A. and Ricci Lucchi, F., 2001. Tertiary silicoclastic turbidite systems of the Northern Apennines. In: G.B., V. and I.P., M. (Editors), *Anatomy of an Orogen: the Apennines and Adjacent Mediterranean Basins*. Kluwer Academic, Amsterdam, pp. 327-350.
- Aydın, M., Demir, O., Özçelik, Y., Terzioğlu, N. and Satır, M., 1995a. A geological revision of Inebolu, Devrekani, Ağlı and Küre areas: new observations on Paleotethys-Neotethys sedimentary successions. In: Erler, A., Tuncay, E., Bingöl, E. and Örçen, S. (Editors), *Geology of the Black Sea Region*. General Directorate of Mineral Research and Exploration (MTA), Ankara, pp. 33-38.
- Aydın, M., Demir, O., Serdar, H.S., Özaydin, S. and Harput, B., 1995b. Tectono-sedimentary evolution and hydrocarbon potential of the Sinop-Boyabat Basin, North Türkiye. In: Erler, A., Tuncay, E., Bingöl, E. and Örçen, S. (Editors), *Geology of the Black Sea Region*. General Directorate of Mineral Research and Exploration (MTA), Ankara, pp. 254-263.
- Baas, J.H. and Best, J.L., 2002. Turbulence modulation in clay-rich sediment-laden flows and some implications for sediment deposition. *Journal of Sedimentary Research*, 72, 336-340.
- Baas, J.H. and Best, J.L., 2007. The dynamics of turbulent, transitional and laminar clay-laden flow over a fixed current ripple. *Sedimentology*, online doi:10.1111/j.1365-3091.2007.00916.x.
- Baas, J.H., McCaffrey, W.D., Haughton, P.D.W. and Choux, C., 2005. Coupling between suspended sediment distribution and turbulence structure in a laboratory turbidity current. *Journal of Geophysical Research*, 110, C11015, online doi:10.1029/2004JC002668.
- Barnsley, M., 1988. *Fractals Everywhere*. Academic Press, Boston, 396 pp.
- Bartolin, C., Gehin, C. and Stanley, D.J., 1972. Morphology and recent sedimentation of the Western Alboran Basin in the Mediterranean Sea. *Marine Geology*, 13, 159-224.
- Beattie, P.D. and Dade, W.B., 1996. Is scaling in turbidite deposition consistent with forcing by earthquakes? *Journal of Sedimentary Research*, 66, 909-915.
- Belderson, R.H. and Laughton, A.S., 1966. Correlation of some Atlantic turbidites. *Sedimentology*, 7, 103-116.
- Bentley, S.J., Keen, T.R., Blain, C.A. and Vaughan, W.C., 2002. The origin and preservation of a major hurricane event bed in the northern Gulf of Mexico: Hurricane Camille, 1969. *Marine Geology*, 186, 423-446.

- Boggs, S., 2001. Principles of Sedimentology and Stratigraphy, 3rd edition. Prentice-Hall Inc., New Jersey, 726 pp.
- Bonnecaze, R.T., Hallworth, M.A., Huppert, H.E. and Lister, J.R., 1995. Axisymmetric particle-driven gravity currents. *Journal of Fluid Mechanics*, 294, 93-121.
- Bonnecaze, R.T., Huppert, H.E. and Lister, J.R., 1993. Particle-driven gravity currents. *Journal of Fluid Mechanics*, 250, 339-369.
- Bornhold, B.D. and Pilkey, O.H., 1971. Bioclastic turbidite sedimentation in Columbus Basin, Bahamas. *Geological Society of America Bulletin*, 82, 1341-1354.
- Bornhold, B.D. & Prior, D.B. 1990: Morphology and sedimentary processes of the subaqueous Noeick River delta, British Columbia, Canada. In: Colella, A. and Prior, D.B. (Editors), *Coarse-grained Deltas*. Int. Assoc. Sedimentol. Special Publication, 10, 169-181.
- Bouma, A.H., 1962. *Sedimentology of some Flysch Deposits: A Graphic Approach to Facies Interpretation*. Elsevier, Amsterdam, 168 pp.
- Brenchley, P.J., Pickerill, R.K. and Stromberg, S.G., 1993. The role of wave reworking on the architecture of storm sandstone facies, Bell Island Group (Lower Ordovician), eastern Newfoundland. *Sedimentology*, 40, 359-382.
- Browne, G.H., McAlpine, A. and King, P.R., 1996. An outcrop study of bed thickness, continuity and permeability in reservoir facies of the Mt Messenger Formation, North Taranaki. In: Anonymous (Editor), 1996 New Zealand petroleum conference, proceedings; confronting the issues 1996; an international perspective; Vol. 2. New Zealand Ministry of Commerce. Wellington, New Zealand, pp. 154-163.
- Browne, G.H., Slatt, R.M. and King, P.R., 2000. Contrasting styles of basin-floor fan and slope fan deposition: Mount Messenger Formation, New Zealand. In: Bouma, A.H. and Stone, C.G. (Editors), *Fine-grained turbidite systems*. AAPG Memoir 72/SEPM Special Publication 68, pp. 143-152.
- Bourgeois, J., 1980. A transgressive shelf sequence exhibiting hummocky stratification; the Cape Sebastian Sandstone (Upper Cretaceous), southwestern Oregon. *Journal of Sedimentary Research*, 50, 681-702.
- Cacchione, D. and Wunsch, C., 1974. Experimental study of internal waves over a slope. *Journal of Fluid Mechanics*, 66, 223-239.
- Carey, S., Sigurdsson, H. and Sparks, R.S.J., 1988. Experimental studies of particle-laden plumes. *Journal of Geophysical Research*, 95, 15314-15328.
- Carlson, J. and Grotzinger, J.P., 2001. Submarine fan environment inferred from turbidite thickness distributions. *Sedimentology*, 48, 1331-1351.
- Castro, I.P. and Snyder, W.H., 1993. Experiments of wave breaking in stratified flow over obstacles. *Journal of Fluid Mechanics*, 255, 195-211.
- Chen, C. and Hiscott, R.N., 1999. Statistical analysis of facies clustering in submarine-fan turbidite successions. *Journal of Sedimentary Research*, 69, 505-517.
- Choux, C.M. and Druitt, T.H., 2002. Analogue study of particle segregation in pyroclastic density currents, with implications for the emplacement mechanisms of large ignimbrites. *Sedimentology*, 49, 907-928.
- Conolly, J.R. and Ewing, M., 1967. Sedimentation in the Puerto Rico Trench. *Journal of Sedimentary Petrology*, 37, 44-59.
- Dade, W.B. and Huppert, H.E., 1995. A box model for non-entraining, suspension-driven gravity surges on horizontal surfaces. *Sedimentology*, 42, 453-471.
- Dade, W.B., Lister, J.R. and Huppert, H.E., 1994. Fine-sediment deposition from gravity surges on uniform slopes. *Journal of Sedimentary Research*, A64, 423-432.
- Dean, W.E. and Anderson, R.Y., 1967. Correlation of turbidite strata in the Pennsylvanian Haymond Formation, Marathon region, Texas. *Journal of Geology*, 75, 59-75.
- DeCelles, P.G. and Giles, K.A., 1996. Foreland basin systems. *Basin Research*, 8, 105-123.
- Dott, R.H. and Bourgeois, J., 1982. Hummocky stratification; significance of its variable bedding sequences, *Geological Society of America Bulletin*, 93(8), 663-680.

- Dreyer, T., Færseth, R., Alkan, H., Larsen, E., Puigdefábregas, C., Alayğut, D., Karpuz, M.R. and Nemec, W., in prep. Stratigraphy, tectonics and depositional systems of the Antalya Basin. *Sedimentary Geology*.
- Duke, W.L., 1985. Hummocky cross-stratification, tropical hurricanes, and intense winter storms. *Sedimentology*, 32, 167–194.
- Duke, W.L., Arnott, R.W.C. and Cheel, R.J., 1991. Shelf sandstones and hummocky crossstratification: new insight on a stormy debate. *Geology*, 19, 625–628.
- Dumas, S. and Arnott, R.W.C., 2006. Origin of hummocky and swaley cross-stratification – The controlling influence of unidirectional current strength and aggradation rate. *Geology*, 34, 1073–1076.
- Dzuleński S., Książkiewicz, M. and Kuenen, P.H., 1959. Turbidites in flysch of the Polish Carpathian Mountains. *Bulletin Geological Society of America*, 70, 1089-1118.
- Dzuleński, S. and Walton, E.K., 1965. *Sedimentary features of flysch and greywackes*. Elsevier Publishing Co., Amsterdam.
- Edbrooke, S.W. and Browne, G.H., 1996. An outcrop study of bed thickness and continuity in thin-bedded facies of the Whakataki Formation at Whakataki Beach, East Wairarapa. In: Anonymous (Editor), *Institute of Geological and Nuclear Sciences Science Report*. Institute of Geological & Nuclear Sciences. Lower Hutt, New Zealand, pp. 18.
- Eder, F.W., 1971. Riff-nahe detritische Kalke bei Balve im Rheinischen Schiefergebirge. *Göttinger Arb. Geol. Palaont.*, 10, 66.
- Edwards, D.A., Leeder, M.R., Best, J.L. and Pantin, H.M., 1994. On experimental reflected density currents and the interpretation of certain turbidites. *Sedimentology*, 41, 437-461.
- Engel, W., 1974. *Sedimentologische Untersuchungen im Flysch des Beckens von Ajdovščina (Slovenien)*. *Göttinger Arb. Geol. Palaont.*, 16, 65.
- Enos, P., 1969. Anatomy of a flysch. *Journal of Sedimentary Petrology*, 39, 680-723.
- Ewing, M., Aitken, T. and Eitrem, S., 1968. Giant ripples in the Madagascar Basin. *Trans. Am. Geophys. Union*, 49, 218-232.
- Fildani, A., Normark, W.R., Kostic, S. and Parker, G., 2006. Channel formation by flow stripping: large-scale scour features along the Monterey East Channel and their relation to sediment waves. *Sedimentology*, 53, 1265-1287.
- Feder, J., 1988. *Fractals*. Plenum Publishing Co., New York, 283 pp.
- Felix, M. and Peakall, J., 2006. Transformation of debris flows into turbidity currents: mechanisms inferred from laboratory experiments. *Sedimentology*, 53, 107-123.
- Flood, R.D., 1988. A lee wave model for deep-sea mudwave activity. *Deep-Sea Research*, 35(6), 973-983.
- Folland, G.B., 1992. *Fourier Analysis and Its Applications*, Brooks/Cole Publishing Co., 448 pp.
- Fox, P.J., Heezen, B.C. and Harian, A.M., 1968. Abyssal antidunes. *Nature*, 220, 470-472.
- Fralick, P., 1999. Paleohydraulics of chute-and-pool structures in a Paleoproterozoic fluvial sandstone. *Sedimentary Geology*, 125, 129-134.
- Gandolfi, G., Paganelli, L. and Zuffa, G.G., 1983. Petrology and dispersal directions in the Marnoso Arenacea Formation (Miocene, northern Apennines). *Journal of Sedimentary Petrology*, 53, 493–507.
- Gladstone, C., Phillips, J.C. and Sparks, R.S.J., 1998. Experiments on bidisperse, constant-volume gravity currents: propagation and sediment deposition. *Sedimentology*, 45, 833-843.
- Glennie, K.W., 1998. *Petroleum Geology of the North Sea*. 4th Edition, Blackwell Science, Oxford, 453 pp.
- Görür, N., Oktay, F.Y., Seymen, I. and Şengör, A.M.C., 1984. Palaeotectonic evolution of the Tuzgölü basin complex, Central Turkey: sedimentary record of a Neotethyan closure. In: Dixon, J.E. and Robertson, A.H.F. (Editors), *The Geological Evolution of the Eastern Mediterranean*. Geological Society of London Special Publication, 17, pp. 467-482.
- Görür, N. and Tüysüz, O., 2001. Cretaceous to Miocene palaeogeographic evolution of Turkey: implications for hydrocarbon potential. *Journal of Petroleum Geology*, 24, 119-146.
- Gray, T.E., Alexander, J. and Leeder, M.R., 2005. Quantifying velocity and turbulence structure in depositing sustained turbidity currents across breaks in slope. *Sedimentology*, 52, 467–488.

- Griggs, G.B., Carey, A.G. and Kulm, L.D., 1969. Deep-sea sedimentation and sediment-fauna interaction on Cascadia Abyssal Plain and in Cascadia Channel. *Deep-Sea Research*, 16, 157-170.
- Grossheim, V.A., 1961. The feasibility of long distance, horizon-by-horizon correlation of flysch sections ("teleconnection"). *Akad. Nauk SSSR Izv. Ser. Geol. (Trans. Am. Geol. Inst. Rept.)*, 1962, 41-48.
- Grossheim, V.A. and Vassoevich, N.B., 1960. A study of the lithologic variation in the flysch deposits. *Obshch. Ispytateley Prirody Byull., Otdel Geol., Moscow*, 35, 68-81.
- Hallworth, M.A. and Huppert, H.E., 1998. Abrupt transitions in high-concentration, particle-driven gravity currents. *Physics of fluids*, 10(5), 1083-1087.
- Hand, B.M., Middleton, G.V. and Skipper, K., 1972. Antidune cross-stratification in a turbidite sequence, Cloridorme Formation, Gaspé, Quebec. *Sedimentology*, 18, 135-138.
- Haq, B.U., Hardenbol, J. and Vail, P.R., 1988. Mesozoic and Cenozoic chronostratigraphy and cycles of sea-level change. In: Wilgus, C.K. et al. (Editors), *Sea-level Changes - An Integrated Approach*. SEPM Special Publication, 42, pp. 71-108.
- Harms, J.C. and Fahnestock, R.K., 1965. Stratification, bed forms, and flow phenomena (with an example from the Rio Grande). In: Middleton, G.V. (Editor), *Primary Sedimentary Structures and their Hydrodynamic Interpretation*. SEPM. Special Publication, 12, pp. 84-115.
- Harms, J.C., Southard, J.B., Spering, D.R. and Walker, R.G., 1975. Depositional environments as interpreted from primary sedimentary structures and stratification sequences. *Society of Economic Paleontologists and Mineralogists, SEPM Short Course 2*, Dallas, 153 pp.
- Harms, J.C., Southard, J.B. and Walker, R.G., 1982. Structures and sequences in clastic rocks. *Society of Economic Paleontologists and Mineralogists, Short Course 9*, 249 pp.
- Hayes, M.O., 1967. Hurricanes as geologic agents; case studies of Hurricane Carla, 1961 and Cindy, 1963. *Univ. Texas Bureau Economic Geology Rept. Inv.*, 61, pp. 56.
- Hesse, R., 1965. Herkunft und transport der sedimente im bayerischen Flyschtrogl. *Deutch. Geol. Gesell. Zeitschr.*, 116, 403-426.
- Hesse, R., 1974. Long-distance continuity of turbidites: possible evidence for an Early Cretaceous trench-abyssal plain in the East Alps. *Geological Society of America Bulletin*, 85, 859-870.
- Hesse, R., 1982. Cretaceous-Palaeogene Flysch Zone of the East Alps and Carpathians: identification and plate-tectonic significance of 'dormant' and 'active' deep-sea trenches in the Alpine-Carpathian Arc. *Geological Society of London, Special Publication*, 10, 471-494.
- Hesse, R., Rashid, H. and Khodabakhsh, S., 2004. Fine-grained sediment lofting from meltwater-generated turbidity currents during Heinrich events. *Geology*, 32, 449-452.
- Hirayama, J. and Nakajima, T., 1977. Analytical study of turbidites, Otadai Formation, Boso Peninsula, Japan. *Sedimentology*, 24, 747-779.
- Hiscott, R.N., 1994. Loss of capacity, not competence, as the fundamental process governing deposition from turbidity currents. *Journal of Sedimentary Research*, A64, 209-214.
- Howe, J.A., 1996. Turbidite and contourite sediment waves in the northern Rockall Trough, North Atlantic Ocean. *Sedimentology*, 43, 219-234.
- Hsü, K.J., 1989. *Physical principles of sedimentology. A readable textbook for beginners and experts*. Springer-Verlag, New York, 233 pp.
- Hsü, K.J., 2004. *Physics of sedimentology: textbook and reference*. Springer-Verlag, Berlin, 240 pp.
- Johnson, G.L. and Schneider, E.D., 1969. Depositional ridges in the North Atlantic. *Earth Planet. Sci. Lett.*, 6, 416-422.
- Johnson, H.D. and Baldwin, C.T., 1996. Shallow clastic sea. In: Reading, H.G. (Editor), *Sedimentary Environments; Processes, Facies, and Stratigraphy*. Blackwell Science, Oxford, U.K., pp. 232-280.
- Kahane, L.H., 2001. *Regression Basics*, Sage, London, 202 pp.
- Kane, I.A., Kneller, B.C., Dykstra, M., Kassem, A. and McCaffrey, W.D., 2007. Anatomy of a submarine channel-levee: An example from Upper Cretaceous slope sediments, Rosario Formation, Baja California, Mexico. *Marine and Petroleum Geology*, doi:10.1016/j.marpetgeo.2007.1001.1003.
- Kao, T.W., Pan, F. and Renouard, D., 1985. Internal solitons on the pycnocline: generation, propagation, and shoaling and breaking over a slope. *Journal of Fluid Mechanics*, 159, 19-53.

- Karl, H.A., Cacchione, D.A. and Carlson, P.R., 1986. Internal-wave currents as a mechanism to account for large sand waves in Navarinsky Canyon head, Bering Sea. *Journal of Sedimentary Petrology*, 56, 706-714.
- Kaymakçı, N., Duermeijer, C.E., Langereis, C., White, S.H. and Van Dijk, P.M., 2003. Palaeomagnetic evolution of the Çankırı Basin (central Anatolia, Turkey): implications for oroclinal bending due to indentation. *Geological Magazine*, 140, 343-355.
- Kelling, G. and Mullin, P., 1975. Graded limestone and limestone-quartzite couplets: possible storm deposits from the Moroccan Carboniferous. *Sedimentary Geology*, 13, 161-190.
- Kenyon, N.H. and Belderson, R.H., 1973. Bedforms of the Mediterranean undercurrent observed with side-scan sonar. *Sedimentary Geology*, 9, 77-99.
- Kerr, R.C., 1991. Erosion of a stable density gradient by sedimentation-driven convection, *Nature*, 353, 423-425.
- Kneller, B.C. and Branney, M.J., 1995. Sustained high-density turbidity currents and the deposition of thick massive sands. *Sedimentology*, 42, 607-616.
- Kneller, B.C. and Buckee, C., 2000. The structure and fluid mechanics of turbidity currents: a review of some recent studies and their geological implications. *Sedimentology*, 47, 62-94.
- Kneller, B.C. and McCaffrey, W.D., 2003. The interpretation of vertical sequences in turbidite beds; the influence of longitudinal flow structure. *Journal of Sedimentary Research*, 73, 706-713.
- Kolla, V., Eittreim, S., Sullivan, L., Kostecki, J.A. and Burckle, L.H., 1980. Current-controlled abyssal microtopography and sedimentation in Mozambique Basin, southwest Indian Ocean. *Marine Geology*, 34, 171-206.
- Komar, P.D., 1976. *Beach Processes and Sedimentation*. Prentice-Hall, Englewood Cliffs (N.J.), 429 pp.
- Kuenen, P.H., 1951. Properties of turbidity currents of high density. In: Hough, J.L. (Editor), *Turbidity Currents*, SEPM Special Publication, 2, pp. 14-33.
- Kuenen, P.H., 1957. Sole markings of graded graywacke beds. *Journal of Geology*, 65, 231-258.
- Lamb, M.P., Toniolo, H. and Parker, G., 2006. Trapping of sustained turbidity currents by intraslope minibasins. *Sedimentology*, 53, 147-160.
- Larsen, E., 1999. The Karpuzçay Formation (Late Serravellian - Early Messinian) in the western part of the Manavgat Basin, southwestern Turkey: sedimentological analysis of a shore-derived turbiditic apron. M.Sc. Thesis, University of Bergen, Bergen, 130 pp.
- Larsen, E., 2003. – Stratigraphic architecture of littoral to neritic clastic wedges, Ph.D. Thesis, University of Bergen, Bergen, Norway, 272 pp.
- Larsen, E., Ilgar, A., Wathne, E., Özaksoy, V. and Nemeč, W., 2008. Facies assemblages and depositional architecture of the İhtiyarlı fan-delta complex in the Manavgat Basin. MS in prep.
- Leren, B.L.S., 2003. Late Cretaceous to Early Eocene sedimentation in the Sinop-Boyabat Basin, north-central Turkey: facies analysis of turbiditic to shallow-marine deposits. M.Sc. Thesis, University of Bergen, Bergen, 141 pp.
- Levene, H., 1960. In: Olkin, I. et al. (Editors), *Contributions to Probability and Statistics: Essays in Honor of Harold Hotelling*, Stanford University Press, 278-292 pp.
- Lewis, K.B., Collot, J.-V. and Lallemand, S.E., 1998. The dammed Hikurangi Trough: a channel-fed trench blocked by subducting seamounts and their wake avalanches (New Zealand - France GeodyNZ Project). *Basin Research*, 10, 441-468.
- Lilliefors, H.W., 1967. On the Kolmogorov-Smirnov Test for Normality with Mean and Variance Unknown, *Journal of the American Statistical Association*, 62, 399-402.
- Longhitano, S.G. and Nemeč, W., 2005. Statistical analysis of bed-thickness variation in a Tortonian succession of biocalcarenic tidal dunes, Amantea Basin, southern Calabria, Italy. *Sedimentary Geology*, 179, 195-224.
- Lovell, J.P.B., 1969. Tyee Formation: a proximity in turbidites. *Journal of Sedimentary Petrology*, 39, 935-953.
- Lovell, J.P.B., 1971. Control of slope on deposition from small scale turbidity currents: experimental results and possible geological significance. *Sedimentology*, 17, 81-88.

- Lowe, D.R., 1982. Sediment gravity flows; II, Depositional models with special reference to the deposits of high-density turbidity currents. *Journal of Sedimentary Petrology*, 52, 279-297.
- Lowe, D.R., 1988. Suspended-load fallout rate as an independent variable in the analysis of current structures. *Sedimentology*, 35, 765-776.
- Lowe, D.R. and Guy, M., 2000. Slurry-flow deposits in the Britannia Formation (Lower Cretaceous), North Sea: a new perspective on the turbidity current and debris flow problem. *Sedimentology*, 47, 31-70.
- Lüthi, S., 1981. Experiments on non-channelized turbidity currents and their deposits. *Marine Geology*, 40, M59-M68.
- Malinverno, A., 1997. On the power law size distribution of turbidite beds. *Basin Research*, 9, 263-274.
- Malinverno, A., Ryan, W.B.F., Auffret, G.A. and Pautot, G., 1988. Sonar images of the path of recent failure events on the continental margin off Nice, France. *Geological Society of America, Special Paper*, 229, 59-75.
- McBride, E.F., 1962. Flysch and associated beds of the Martinsburg Formation (Ordovician), Central Appalachians. *Journal of Sedimentary Petrology*, 32, 39-91.
- Meischner, D., 1962. Rhenar Kalk und Posidonienkalk im Kulm des nordöstlichen Rheinisches Schiefergebirges und der Kohlenkalk von Schreufa (Eder). *Abhess. Landesam Bodenforsch.*, 39, 1-47.
- Meischner, D., 1964. Allodapische Kalke, Turbidite in riffnahen Sedimentationsbecken. In: Bouma, A.H. and Brouwer, A. (Editors), *Turbidites, Developments in Sedimentology 3*. Elsevier, Amsterdam, pp. 156-191.
- Middleton, G.V., 1967. Experiments on density and turbidity currents. III. Deposition of sediment. *Canadian Journal of Earth Sciences*, 4, 475-505.
- Middleton, G.V., 1993. Sediment deposition from turbidity currents. *Annual Review Earth Planetary Sciences*, 21, 89-114.
- Middleton, G.V. and Hampton, M.A., (1973). *Sediments Gravity Flows: Mechanics of Flow and Deposition*, In: Middleton, G.V. and Bouma, A.H. (Editors), *Turbidity and Deep Water Sedimentation*, Pacific Section SEPM, 1-38.
- Middleton, G.V. and Hampton, M.A., (1976). *Subaqueous Sediment Transport and Deposition by Sediment Gravity Flows*, In: Stanley, D.J. and Swift, J.P. (Editors), *Marine Sediment Transport and Environmental Management*, John Wiley, New York, 197-218.
- Middleton, G.V. and Neal, W.J., 1989. Experiments on the thickness of beds deposited by turbidity currents. *Journal of Sedimentary Petrology*, 59(2), 297-307.
- Morris, S.A., Kenyon, N.H., Limonov, A.H. and Alexander, J., 1998. Downstream changes of large-scale bedforms in turbidites around the Valencia channel mouth, north-west Mediterranean: implications for paleoflow reconstruction. *Sedimentology*, 45, 365-377.
- Morton, R.A., 1981. Formation of storm deposits by wind-forced currents in the Gulf of Mexico and the North Sea. In: Nio, S.D. (Editor), *Holocene Marine Sedimentation in the North Sea Basin*. International Association of Sedimentology, Special Publication, 5, pp. 385-396.
- Mulder, T. and Alexander, J., 2001. The physical character of subaqueous sedimentary density flows and their deposits. *Sedimentology*, 48, 269-299.
- Murray, C.J., Lee, H.J. and Hampton, M.A., 2002. Geostatistical mapping of effluent-affected sediment distribution on the Palos Verdes shelf. *Continental Shelf Research*, 22, 881-897.
- Murray, C.J., Lowe, D.R., Graham, S.A., Martinez, P.A., Zeng, J., Carroll, A., Cox, R., Hendrix, M., Heubeck, C., Miller, D., Moxon, I.W., Sobel, E., Wendebourg, J. and Williams, T., 1996. Statistical analysis of bed-thickness patterns in a turbidite section from the Great Valley Sequence, Cache Creek California. *Journal of Sedimentary Petrology*, 66, 900-908.
- Mutti, E. and Ricci Lucchi, F., 1972. Turbidites of the Northern Apennines: introduction to facies analysis. *International Geology Review*, 20, 125-166.
- Myrow, P.M. and Hiscott, R.N., 1991. Shallow-water gravity-flow deposits, Chapel Island Formation, southeast Newfoundland, Canada. *Sedimentology*, 38, 935-959.
- Myrow, P.M. and Southard, J.B., 1996. Tempestite deposition. *Journal of Sedimentary Research*, 66(5), 875-887.



- Nakajima, T. and Satoh, M., 2001. The formation of large mudwaves by turbidity currents on the levees of the Toyama deep-sea channel, Japan Sea. *Sedimentology*, 48, 435-463.
- Nemec, W., 1990. Aspects of sediment movement on steep delta slopes. In: Colella, A. and Prior, D.B. (Editors), *Coarse-grained Deltas*. Int. Ass. Sedimentol. Special Publication, 10, 29-73.
- Nemec, W., 1995. The dynamics of deltaic suspension plumes. In: Oti, M.N. and Postma, G. (Editors), *Geology of Deltas*. A.A. Balkema, Rotterdam, pp. 31-93.
- Nikishin, A.M., Korotaev, M.V., Ershov, A.V. and Brunet, M.-F., 2003. The Black Sea basin: tectonic history and Neogene-Quaternary rapid subsidence modelling. *Sedimentary Geology*, 156, 149-168.
- NIST/SEMATECH, 2007. E-Handbook of Statistical Methods. <http://www.itl.nist.gov/div898/handbook/>.
- Normark, W.R., Hess, G.R., Stow, D.A.V. and Bowen, A.J., 1980. Sediment waves on the Monterey Fan levee: a preliminary physical interpretation. *Marine Geology*, 37, 1-18.
- Okay, A.I. and Şahintürk, Ö., 1997. Geology of the Eastern Pontides. In: Robinson, A.G. (Editor), *Regional and Petroleum Geology of the Black Sea and Surrounding Regions*. AAPG Memoir, 68, pp. 291-311.
- Okay, A.I. and Tüysüz, O., 1999. Tethyan sutures of northern Turkey. In: Durand, B., Jolivet, L., Horváth, F. and Séranne, M. (Editors), *The Mediterranean Basins: Tertiary Extension within the Alpine Orogen*. Geologic Society of London, Special Publication, 156, pp. 475-515.
- Ori, G.G. and Friend, P.G., 1986. Sedimentary basins, formed and carried piggyback on active thrust sheets. *Geology*, 12, 475-478.
- Pantin, H.M. and Leeder, M.R., 1987. Reverse flow in turbidity currents: the role of internal solitons. *Sedimentology*, 34, 1143-1155.
- Parkash, B., 1970. Downcurrent changes in sedimentary structures in Ordovician turbidite greywackes. *Journal of Sedimentary Petrology*, 40, 572-590.
- Parkash, B. and Middleton, G.V., 1970. Downcurrent textural changes in Ordovician turbidite greywackes. *Sedimentology*, 14, 259-293.
- Parker, G. and Izumi, N., 2000. Purely erosional cyclic and solitary steps created by flow over a cohesive bed. *Journal of Fluid Mechanics*, 419, 203-238.
- Picha, F. and Niem, A.R., 1974. Distribution and extent of beds in flysch deposits, Ouachita Mountains, Arkansas and Oklahoma. *Journal of Sedimentary Petrology*, 44(2), 328-335.
- Piper, D.J.W., Hiscott, R.N. and Normark, W.R., 1999. Outcrop-scale acoustic facies analysis and latest Quaternary development of Hueneme and Dume submarine fans, offshore California. *Sedimentology*, 46, 47-78.
- Piper, D.J.W. and Savoye, B., 1993. Processes of late Quaternary turbidity current flow and deposition on the Var deep-sea fan, north-west Mediterranean Sea. *Sedimentology*, 40, 557-582.
- Potter, P.E. and Scheidegger, A.E., 1966. Bed thickness and grain size: graded beds. *Sedimentology*, 7, 233-240.
- Pratson, L.F., Imran, G., Parker, G., Syvitski, J.P.M. and Hutton, E., 2000. Debris flows vs. turbidity currents: a modeling comparison of their dynamics and deposits. In: Bouma, A.H. and Stone, C.G. (Editors), *Fine-grained Turbidite Systems*. AAPG Memoir 72/SEPM Special Publication 68, pp. 57-72.
- Ricci Lucchi, F., 1981. The Miocene Marnoso Arenacea turbidites, Romagna and Umbria Apennines, International Association of Sedimentologists Excursion Guidebook, 2nd European Regional Meeting, Tripoli, pp. 231-303.
- Ricci Lucchi, F., 1986. The Oligocene to Recent foreland basins of the northern Apennines. In: Allen, P.A. and Homewood, P. (Editors), *Foreland Basins*. Int. Assoc. Sedimentol. Special Publication, 8, pp. 105-139.
- Ricci Lucchi, F. and Valmori, E., 1980. Basin-wide turbidites in a Miocene, over-supplied deep-sea plain: a geometrical analysis. *Sedimentology*, 27, 241-270.
- Robinson, A.G., Rudat, J.H., Banks, C.J. and Wiles, R.L.F., 1996. Petroleum geology of the Black Sea. *Marine and Petroleum Geology*, 13, 195-223.
- Rona, P.A., 1969. Linear 'lower continental rise hills' off Cape Hatteras. *Journal of Sedimentary Petrology*, 39, 1132-1141.

- Rothman, D.H. and Grotzinger, J.P., 1996. Scaling properties of gravity-driven sediments. *Non-linear Processes Geophys.*, 2, 178-185.
- Rothman, D.H., Grotzinger, J.P. and Flemings, P., 1994. Scaling in turbidite deposition. *Journal of Sedimentary Research*, A64, 59-67.
- Rukavina, N.A., 1965. Particle orientation in turbidites: theory and experiment. Ph.D. Thesis, University of Rochester, Rochester, N.Y., 123 pp.
- Rupke, N.A., 1976. Sedimentology of very thick calcarenite-marlstone beds in a flysch succession, southwestern Pyrenees. *Sedimentology*, 23, 43-65.
- Ryan, T.A. Jr. and Joiner, B.L., 1976. Normal Probability Plots and Tests for Normality, Technical Report, Statistics Department, The Pennsylvania State University. (Available from Minitab Inc.)
- Ryan, W.B., Workum, F. and Hersey, J.B., 1965. Sediments in the Tyrrhenian Abyssal Plain. *Geological Society of America Bulletin*, 76, 1261-1282.
- Sadler, P.M., 1982. Bed-thickness and grain size of turbidites. *Sedimentology*, 29, 37-51.
- Scheidegger, A.E. and Potter, P.E., 1965. Textural studies of graded bedding. Observation and theory. *Sedimentology*, 5, 289-304.
- Schmincke, H.-U., Fisher, R.V. and Waters, A.C., 1973. Antidune and chute and pool structures in the base surge deposits of the Laacher See area, Germany. *Sedimentology*, 20, 553-574.
- Scott, R.W., Fee, D., Magee, R. and Laali, H., 1978. Epeiric depositional models for the Lower Cretaceous Washita Group, North-Central Texas. *Univ. Texas Bureau Economic Geology Rept. Inv.*, 94, pp. 23.
- Scully, M.E., Friedrichs, C.T. and Wright, L.D., 2002. Application of an analytical model of critically stratified gravity-driven sediment transport and deposition to observations from the Eel River continental shelf, Northern California. *Continental Shelf Research*, 22, 1951-1974.
- Seguret, M., Moussine-Pouchkine, A., Gabaglia, G.R. and Bouchette, F., 2001. Storm deposits and storm-generated coarse carbonate breccias on a pelagic outer shelf (South-East Basin, France). *Sedimentology*, 48, 231-254.
- Şengör, A.M.C., 1987. Tectonics of the Tethysides: orogenic collage development in a collisional setting. *Annual Review Earth Planetary Sciences*, 15, 213-244.
- Sestini, G., Bruni, P. and Sagri, M., 1986. The flysch basins of the Northern Apennines: a review of facies and of Cretaceous-Neogene evolution, *Mem. Soc. Geol. It.*, 31, 87-106.
- Shanmugam, G., 1996a. High density turbidity currents: are they sandy debris flows? *Journal of Sedimentary Research*, 66, 2-10.
- Shanmugam, G., 1996b. Perception vs reality in deep-water exploration. *World Oil*, 217, 37-41.
- Shanmugam, G., 1997. The Bouma Sequence and the turbidite mind set. *Earth-Science Reviews*, 42, 201-229.
- Shanmugam, G., 2000. 50 years of the turbidite paradigm (1950s-1990s): deep water processes and facies models - a critical perspective. *Marine and Petroleum Geology*, 17, 285-342.
- Shanmugam, G., Bloch, R.B., Damuth, J.E. and Hodgkinson, R.J., 1997. Basin-floor fans in the North Sea: sequence stratigraphic models vs sedimentary facies: Reply. *American Association of Petroleum Geologists Bulletin*, 81, 666-672.
- Shanmugam, G., Damuth, J.E. and Moiola, R.J., 1985. Is the turbidite facies association scheme valid for interpreting ancient submarine fan environments? *Geology*, 13, 234-237.
- Shanmugam, G. and Moiola, R.J., 1995. Reinterpretation of depositional processes in a classic flysch sequence (Pennsylvanian Jackfork Group), Ouachita Mountains, Arkansas and Oklahoma. *American Association of Petroleum Geologists Bulletin*, 79, 672-695.
- Shanmugam, G. and Moiola, R.J., 1997. Reinterpretation of depositional processes in a classic flysch sequence (Pennsylvanian Jackfork Group), Ouachita Mountains, Arkansas and Oklahoma: Reply. *American Association of Petroleum Geologists Bulletin*, 81, 476-491.
- Shapiro, S.S. and Wilk, M.B., 1965. An Analysis of Variance Test for Normality (Complete Samples), *Biometrika*, 52, 591-611.
- Sinclair, H.D., 1992. Turbidite sedimentation during Alpine thrusting: the Taveyannaz Sandstones of eastern Switzerland. *Sedimentology*, 39, 837-856.

- Sinclair, H.D. and Cowie, P.A., 2003. Basin-floor topography and the scaling of turbidites. *The Journal of Geology*, 111, 277-299.
- Sinclair, H.D. and Tomasso, M., 2002. Depositional evolution of confined turbidite basins. *Journal of Sedimentary Research*, 72(4), 451-456.
- Skene, K.I., Piper, D.J.W. and Hill, P.S., 2002. Quantitative analysis of variations in depositional sequence thickness from submarine channel levees. *Sedimentology*, 49, 1411-1430.
- Smith, R. and Møller, N., 2003. Sedimentology and reservoir modelling of the Ormen Lange field, mid Norway. *Marine and Petroleum Geology*, 20, 601-613.
- Snedden, J.W. and Nummedal, D., 1991. Origin and geometry of storm-deposited sand beds in modern sediments of the Texas continental shelf. *International Association of Sedimentology, Special Publication*, 14, 283-308.
- Snedden, J.W., Nummedal, D. and Amos, A.F., 1988. Storm- and fair-weather combined flow on the Central Texas Continental Shelf. *Journal of Sedimentary Petrology*, 58, 580-595.
- Southard, J.B. and Cacchione, D., 1972. Experiments on bottom sediment movement by breaking internal waves. In: Swift, D.J.P., Duane, D. and Pilkey, O. (Editors), *Shelf Sediment Transport: Process and Pattern*. Dowden, Hutchinson, and Ross, Stroudsburg (Pa.), pp. 83-97.
- Sparks, R.S.J., Bonnez, R.T., Huppert, H.E., Lister, J.R., Hallworth, M.A., Mader, H. and Phillips, J.C., 1993. Sediment-laden gravity currents with reversing buoyancy. *Earth and Planetary Science Letters*, 114, 243-257.
- Storms, J.E.A., Weltje, G.J., van Dijke, J.J., Geel, C.R. and Kroonenberg, S.B., 2002. Process-response modeling of wave-dominated coastal systems: simulating evolution and stratigraphy on geological timescales. *Journal of Sedimentary Research*, 72, 226-239.
- Stow, D.A.V. and Bowen, A.J., 1980. A physical model for the transport and sorting of fine-grained sediments by turbidity currents. *Sedimentology*, 27, 31-46.
- Stow, D.A.V. and Shanmugam, G., 1980. Sequence of structures in fine-grained turbidites; comparison of recent deep-sea and ancient flysch sediments. *Sedimentary Geology*, 25, 23-42.
- Sun, T. and Parker, G., 2005. Transportational cyclic steps created by flow over an erodible bed. Part 2, Theory and numerical simulation. *Journal of Hydraulic Research*, 43, 502-514.
- Swift, D.J.P., Parsons, B.S., Foyle, A. and Oertel, G.F., 2003. Between beds and sequences: stratigraphic organization at intermediate scales in the Quaternary of the Virginia coast, USA. *Sedimentology*, 50, 81-111.
- Sylvester, Z., 2007. Turbidite bed thickness distributions: methods and pitfalls of analysis and modelling. *Sedimentology*, online doi: 10.1111/j.1365-3091.2007.00863.x.
- Taki, K. and Parker, G., 2005. Transportational cyclic steps created by flow over an erodible bed. Part 1, Experiments. *Journal of Hydraulic Research*, 43, 488-501.
- Talling, P.J., 2001. On the frequency distribution of turbidite thickness. *Sedimentology*, 48, 1297-1329.
- Talling, P.J., Amy, L.A. and Wynn, R.B., 2007a. New insight into the evolution of large-volume turbidity currents: comparison of turbidite shape and previous modelling results. *Sedimentology*, online doi: 10.1111/j.1365-3091.2007.00858.x, 1-33.
- Talling, P.J., Amy, L.A., Wynn, R.B., Blackbourn, G. and Gibson, O., 2007b. Evolution of turbidity currents deduced from extensive thin turbidites: Marnoso Arenacea Formation (Miocene), Italian Apennines. *Journal of Sedimentary Research*, 77, 172-196.
- Tamura, T. and Masuda, F., 2005. Bed thickness characteristics of inner-shelf storm deposits associated with a transgressive to regressive Holocene wave-dominated shelf, Sendai coastal plain, Japan. *Sedimentology*, 52, 1375-1395.
- Trincardi, F. and Field, M.E., 1991. Geometry, lateral variation, and preservation of downlapping regressive shelf deposits: eastern Tyrrhenian Sea margin, Italy. *Journal of Sedimentary Petrology*, 61(5), 775-790.
- Vassoevich, N.B., 1948. *Le flysch et les methodes de son etude*. Gostoptekizdat, Moscow, 216 [French translation].
- Vrolijk, P.J. and Southard, J.B., 1997. Experiments on rapid deposition of sand from high-velocity flows. *Geoscience Canada*, 24, 45-54.

- Walker, R.G., 1965. The origin and significance of the internal sedimentary structures of turbidites. *Proc. Yorks. Geol. Soc.* 35, pp. 1–32.
- Walker, R.G., 1978. Deep-water sandstone facies and ancient submarine fans: models for exploration for stratigraphic traps. *American Association of Petroleum Geologists Bulletin*, 62, 932-966.
- Walker, R.G., 1979. Shallow marine sands. In: Walker, R.G. (Editor), *Facies Models*. Geoscience Canada, Reprint Series 1, pp. 75-89.
- Wathne, E., Larsen, E., Nemec, W., Alçiçek, M.C., Ilgard, A. and Helland, O.M., 2008. The Katirıneği and Asar fan-delta complexes in Manavgat Basin: facies architecture of small shoal-water deltas recording forced and normal regressions. MS in prep.
- Wheatcroft, R.A. and Borgeld, J.C., 2000. Oceanic flood layers on the northern California margin: large-scale distribution and small-scale physical properties. *Continental Shelf Research*, 20, 2163-2190.
- Wheatcroft, R.A. and Drake, D.E., 2003. Post-depositional alteration and preservation of sedimentary event layers on continental margins, I. The role of episodic sedimentation. *Marine Geology*, 199, 123-137.
- Wheatcroft, R.A., Stevens, A.W., Hunt, L.M. and Milligan, T.G., 2006. The large-scale distribution and internal geometry of the fall 2000 Po River flood deposit: Evidence from digital X-radiography. *Continental Shelf Research*, 26, 499-516.
- Woods, A.W., Bursik, M.I. and Kurbatov, A.V., 1998. The interaction of ash flows with ridges. *Bull Volcanol*, 60, 38–51.
- Wunsch, C., 1969. Progressive internal waves on slopes. *Journal of Fluid Mechanics*, 35, 131-144.
- Wynn, R.B., Masson, D.G., Stow, D.A.V. and Weaver, P.P.E., 2000a. Turbidity current sediment waves in subsurface sequences. In: Bouma, A.H. and Stone, C.G. (Editors), *Fine-grained turbidite systems*. AAPG Memoir 72/SEPM Special Publication 68, pp. 299-306.
- Wynn, R.B., Weaver, P.P.E., Ercilla, G., Stow, D.A.V. and Masson, D.G., 2000b. Sedimentary processes in the Selvage sediment-wave field, NE Atlantic: new insights into the formation of sediment waves by turbidity currents. *Sedimentology*, 47, 1181-1197.
- Wynn, R.B., Weaver, P.P.E., Masson, D.G. and Stow, D.A.V., 2002. Turbidite depositional architecture across three inter-connected deep-water basins on the Northwest African Margin. *Sedimentology*, 49, 669–695.
- Yılmaz, Y., Tüysüz, O., Yiğitbaş, E., Genç, Ş.C. and Şengör, A.M.C., 1997. Geology and tectonic evolution of the Pontides. In: Robinson, A.G. (Editor), *Regional and Petroleum Geology of the Black Sea and Surrounding Regions*. AAPG Memoir, 68, pp. 183-226.
- Yokokawa, M., Masuda, F. and Endo, N., 1995. Sand particle movement on migrating combined-flow ripples. *Journal of Sedimentary Research*, A65, 40-44.
- Zattin, M., Picotti, V. and Zuffa, G.G., 2002. Fission-track reconstruction of the front of the Northern Apennine thrust wedge and overlying Ligurian Unit. *American Journal of Science*, 302, 346–379.
- Zeng, J. and Lowe, D.R., 1997. Numerical simulation of turbidity current flow and sedimentation: II. Results and geological applications. *Sedimentology*, 44, 85-104.
- Zhang, Y., Swift, D.J.P., Fan, S., Niedoroda, A.W. and Reed, C.W., 1999. Two-dimensional numerical modeling of storm deposition on the northern California shelf. *Marine Geology*, 154, 155–167.

# **APPENDIX**

*Thickness versus Distance plots*



### Key:

b - regression gradient

n - number of measurements

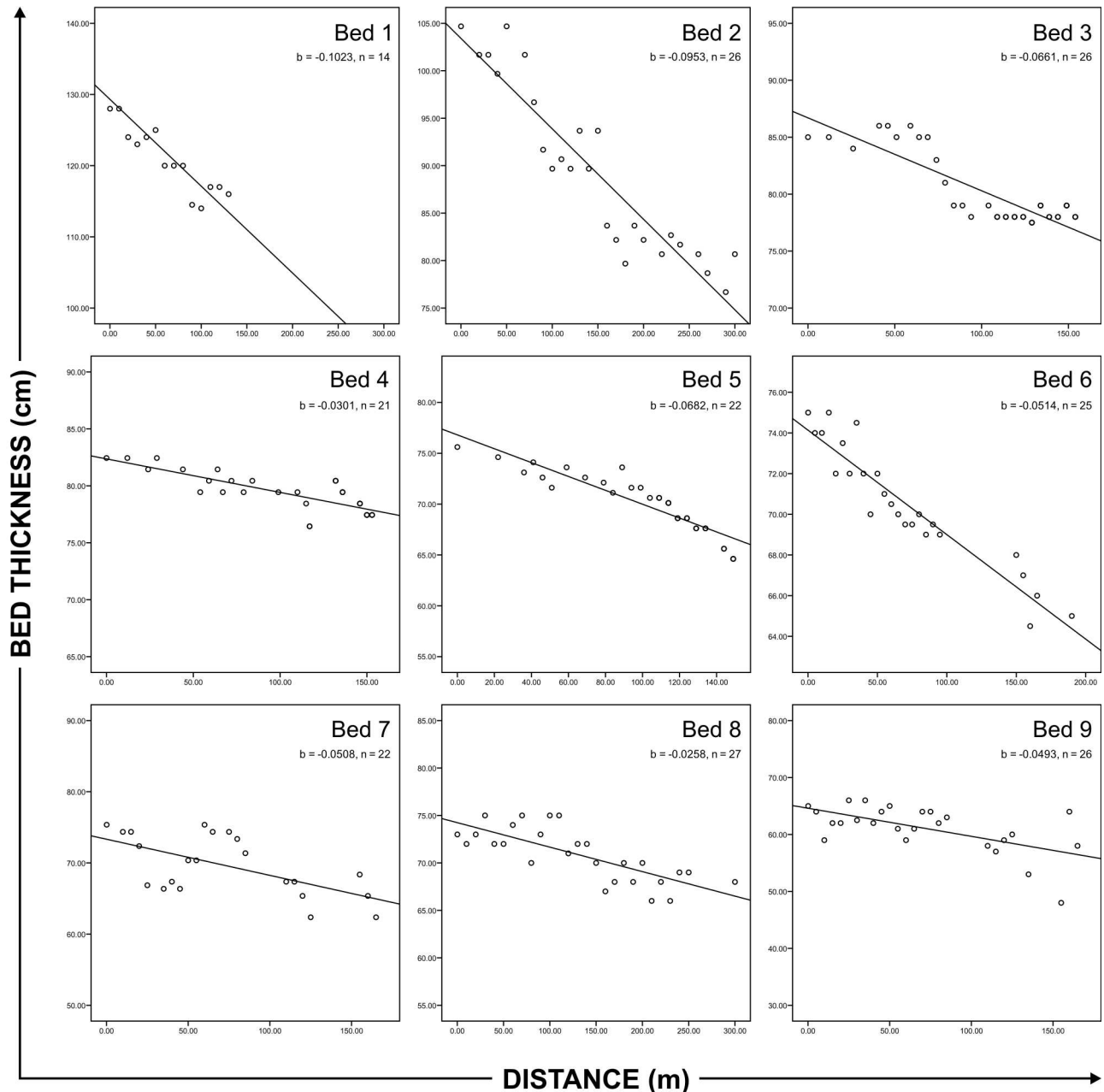
Bed numbering is consistent with that used in the text and figures.

## Marnoso Arenacea Formation

Beds measured parallel to depositional dip

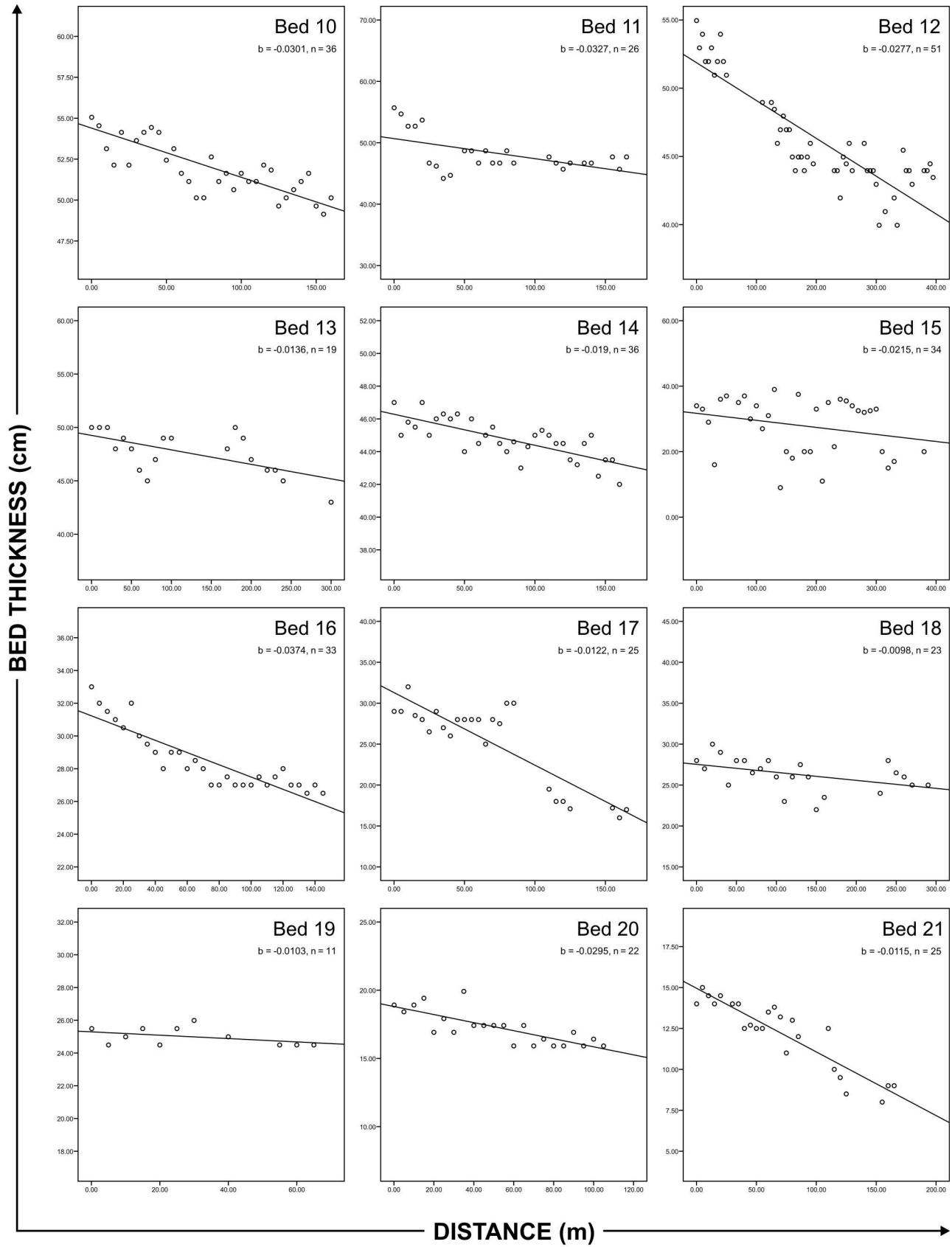
Number of beds: 50

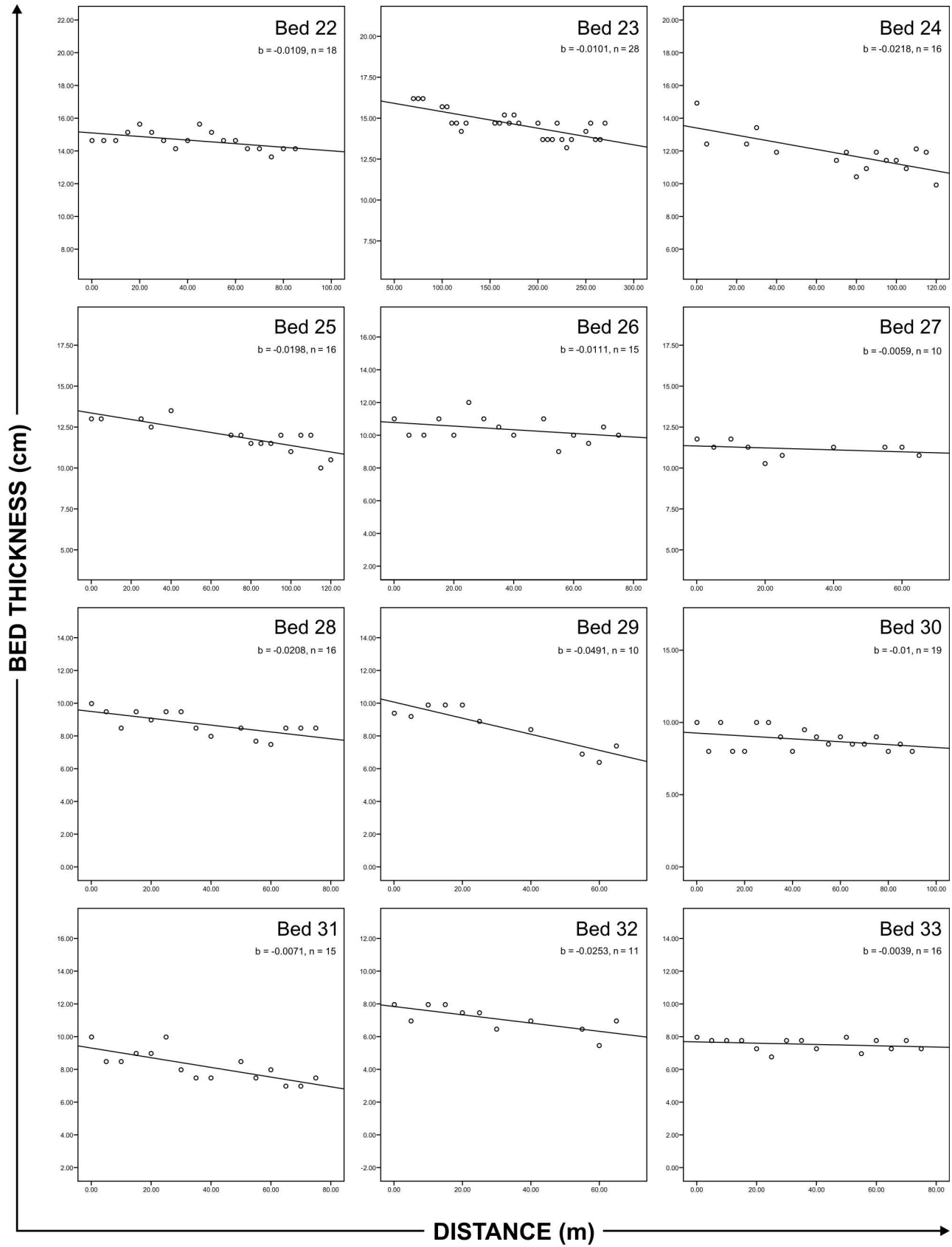
Number of measurements: 1767

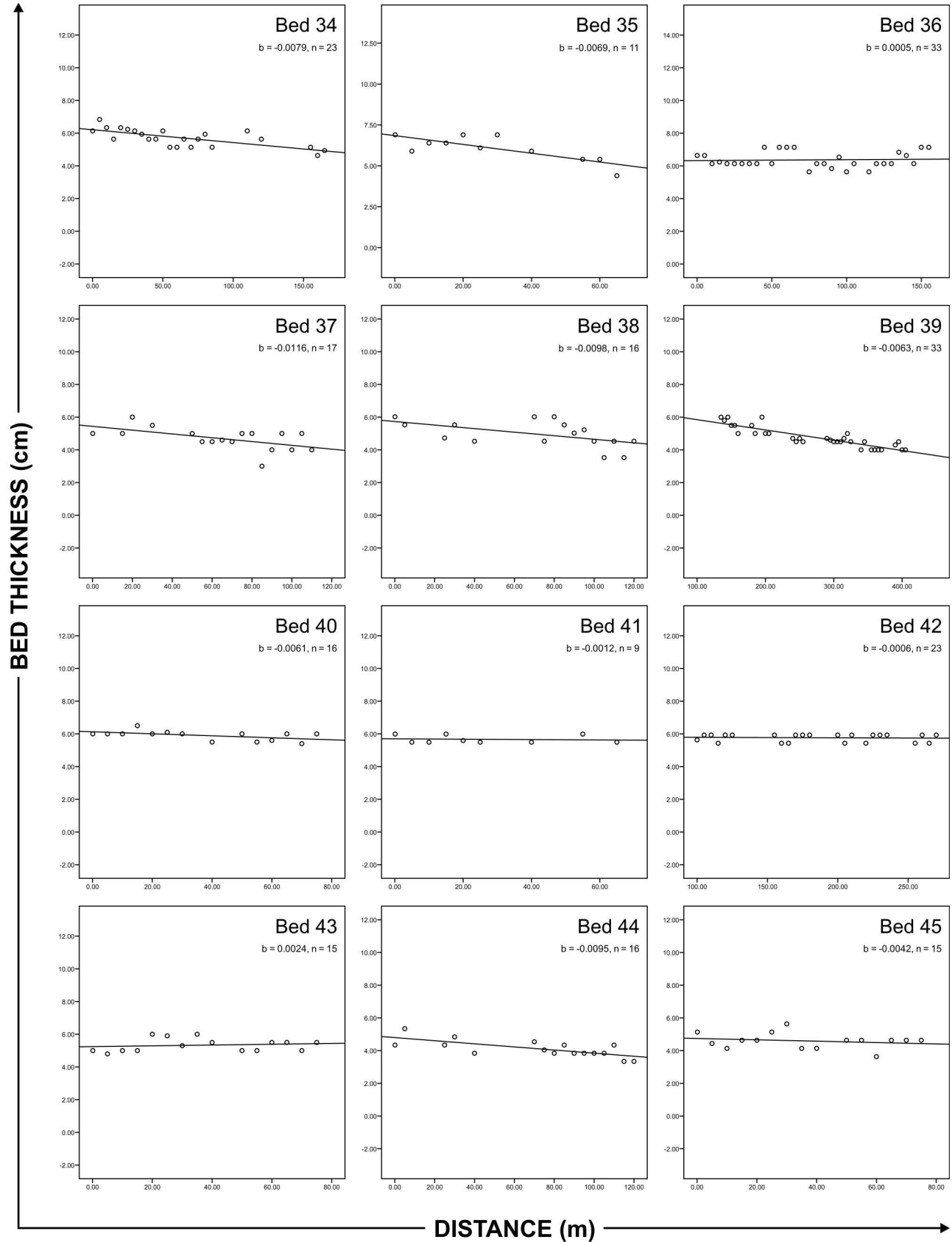


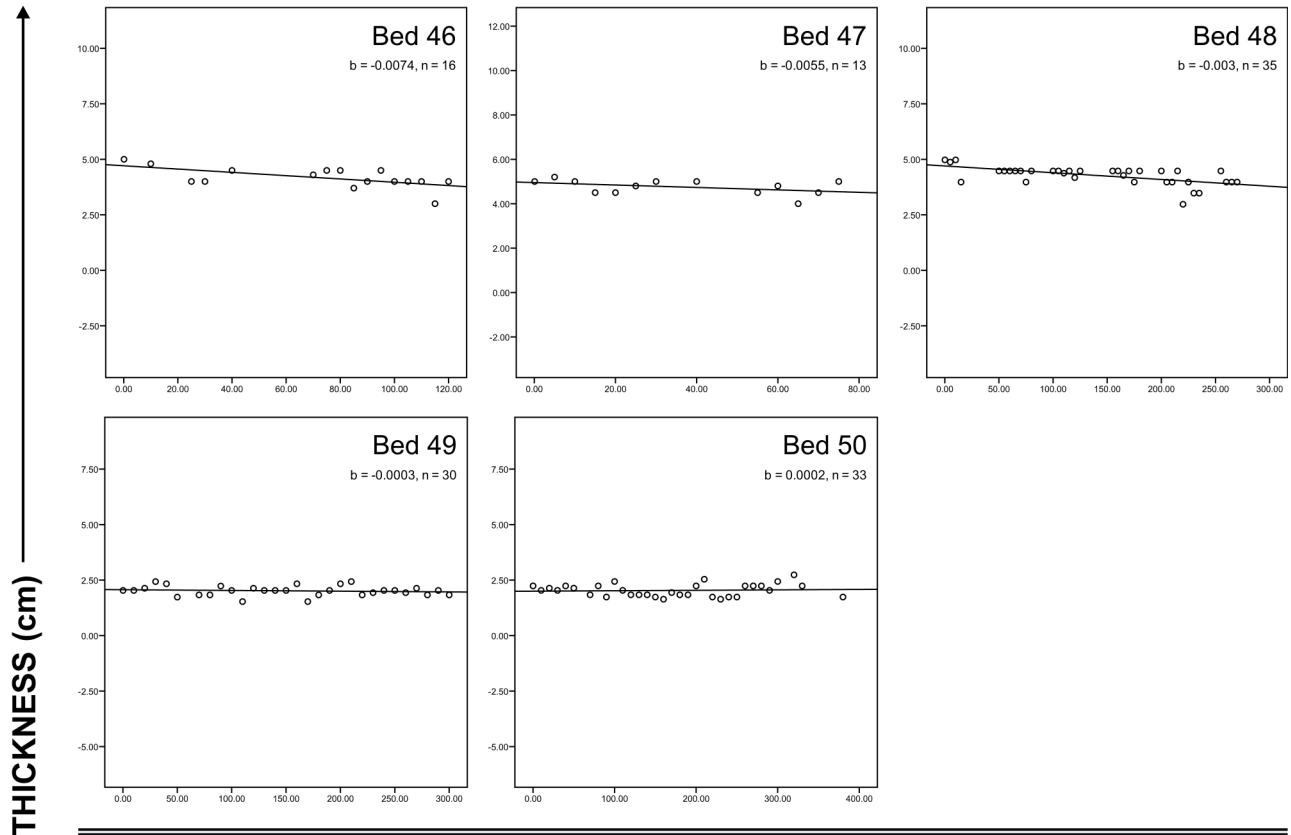








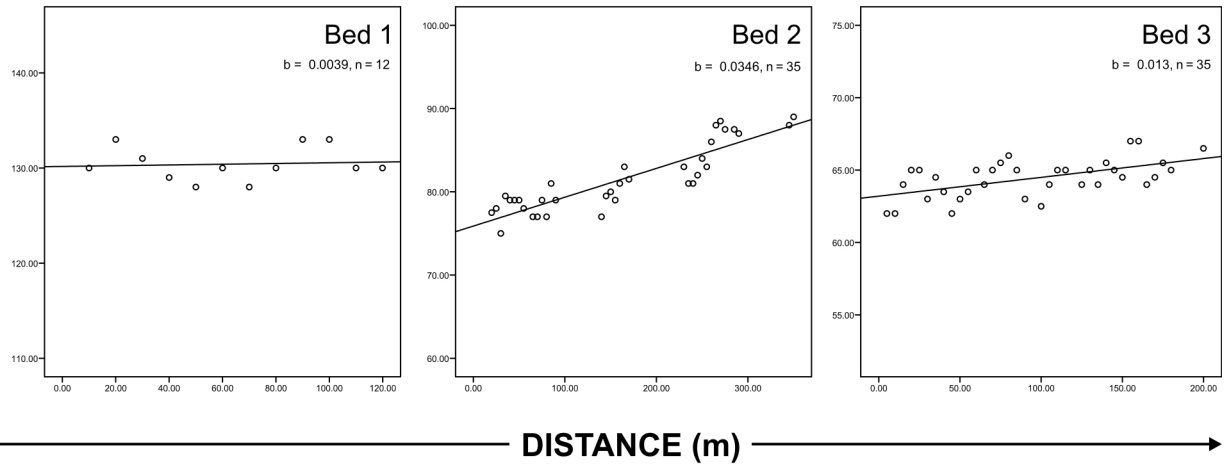




# Marnoso Arenacea Formation

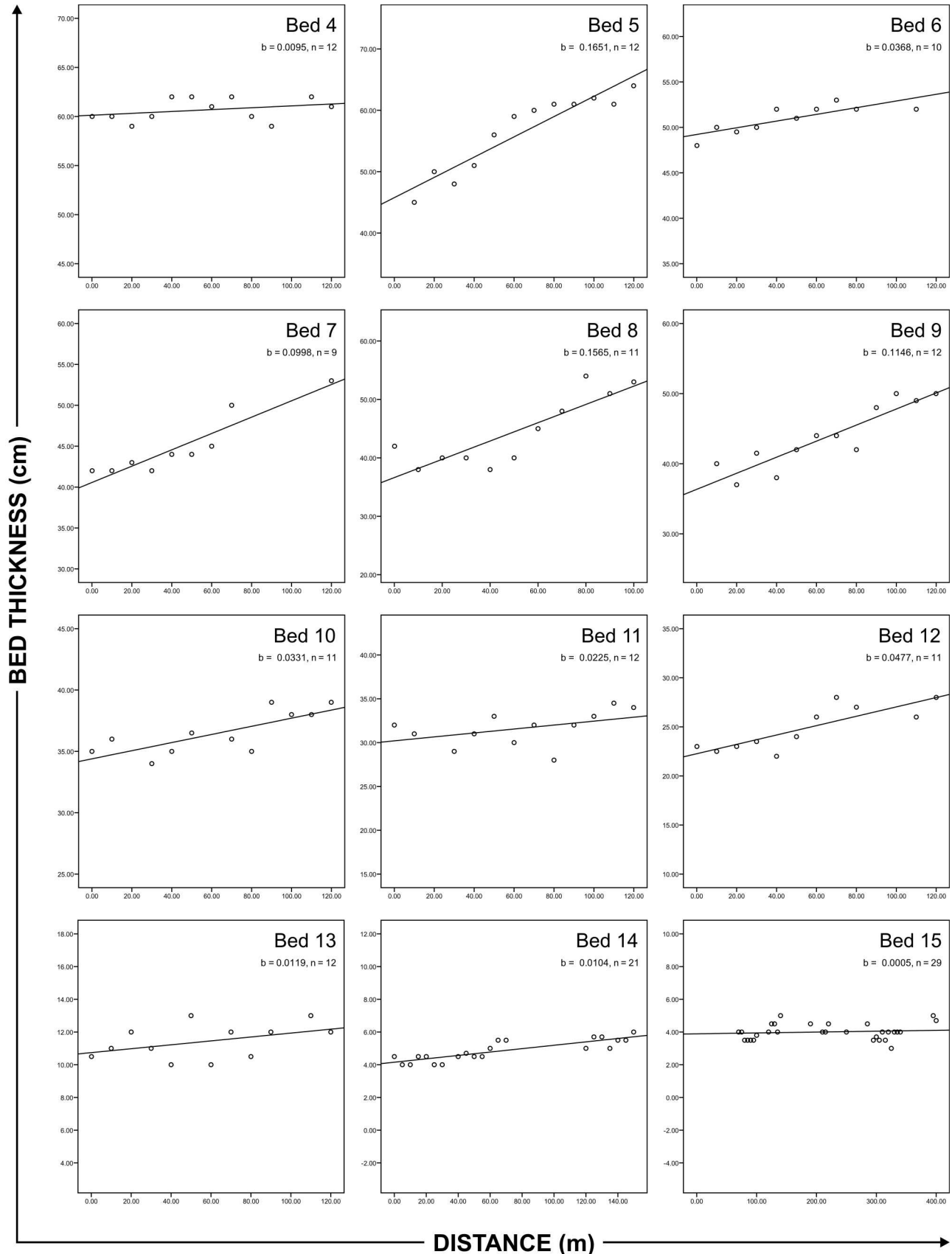
Beds measured perpendicular to depositional dip

Number of beds: 15  
 Number of measurements: 245



BED THICKNESS (cm)

DISTANCE (m)





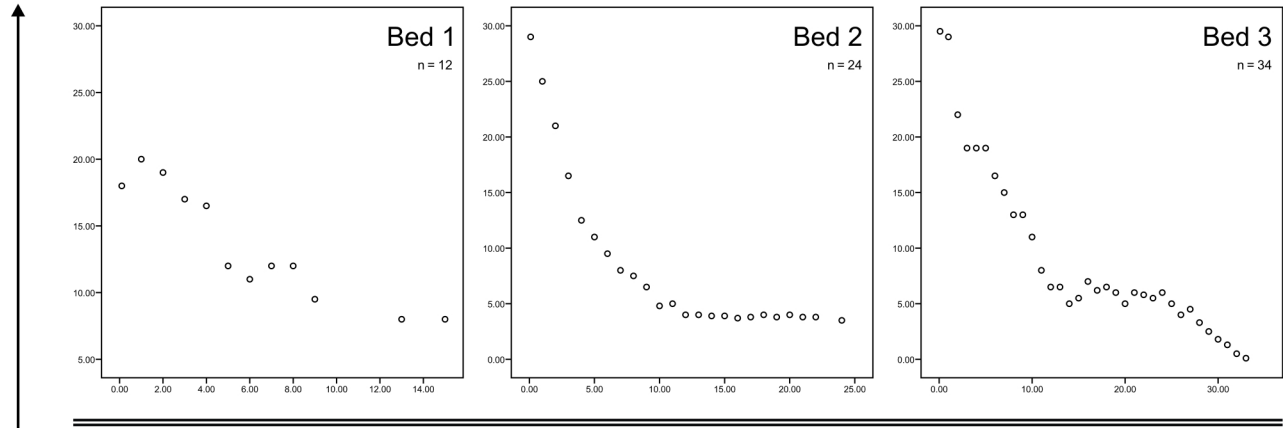
# Monte Fumaiolo Formation

Beds measured parallel to depositional dip

Number of beds: 3

Number of measurements: 70

Beds follow exponential (nonlinear) trends



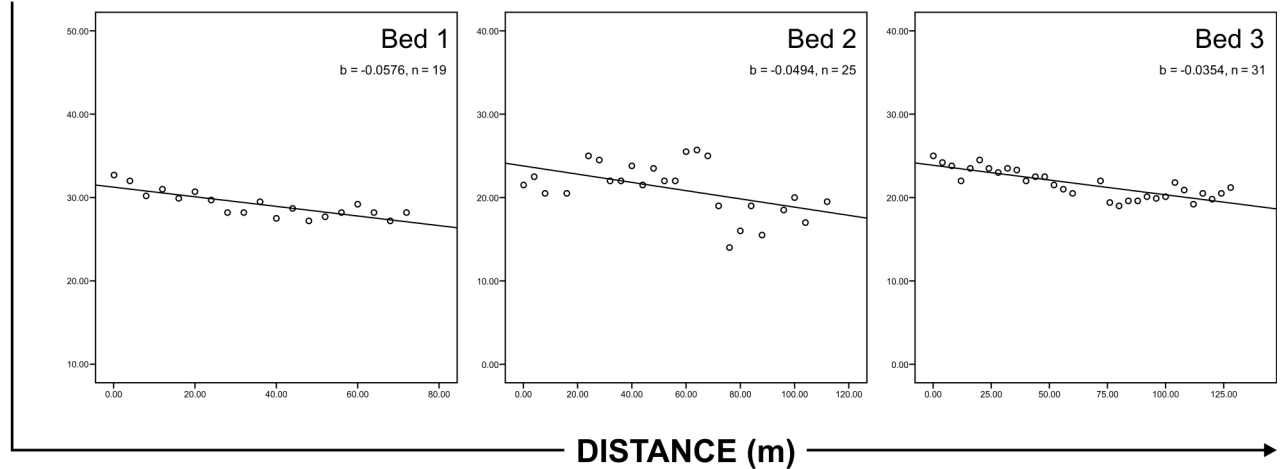
BED THICKNESS (cm)

# Akveren Formation

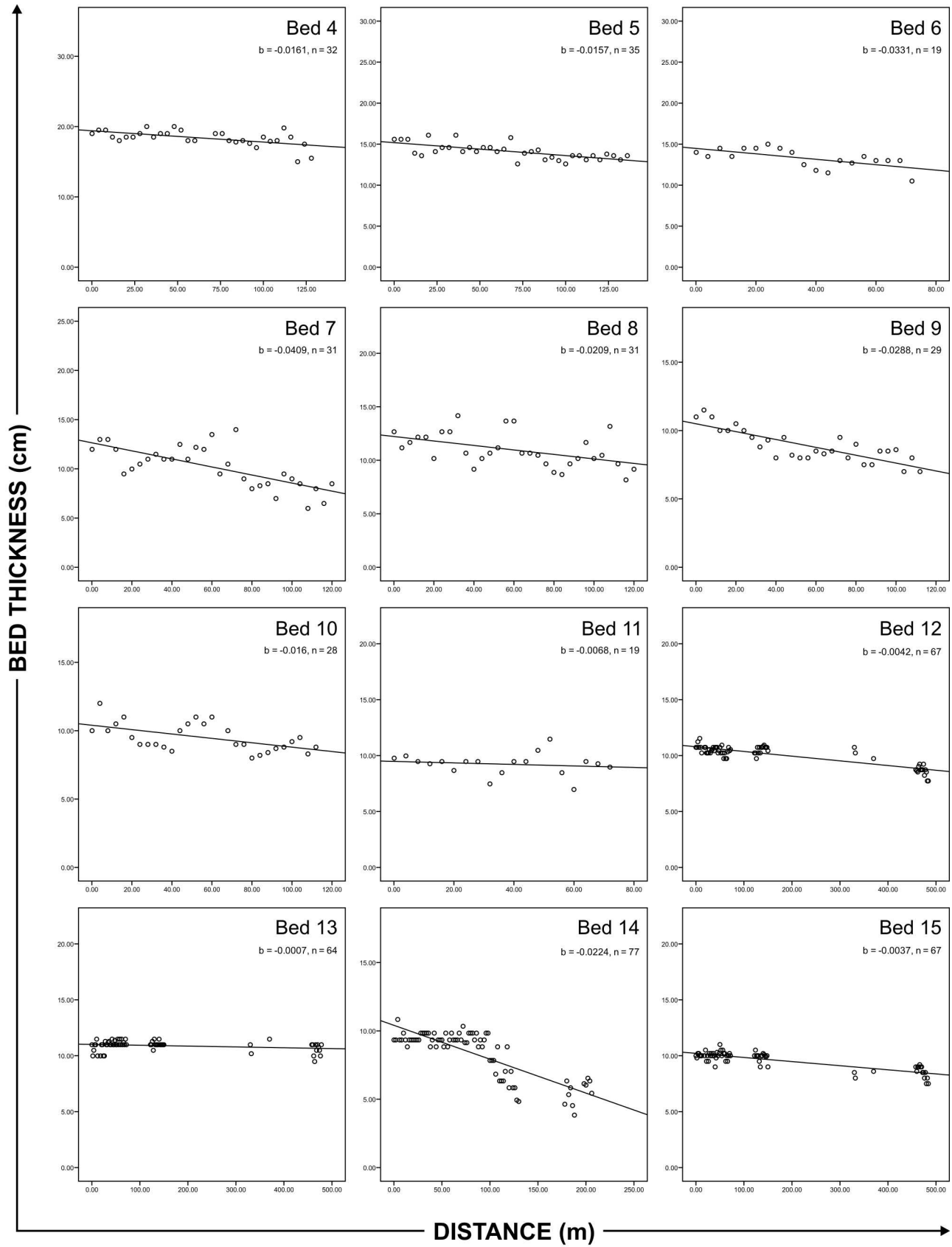
Beds measured parallel to depositional dip

Number of beds: 40

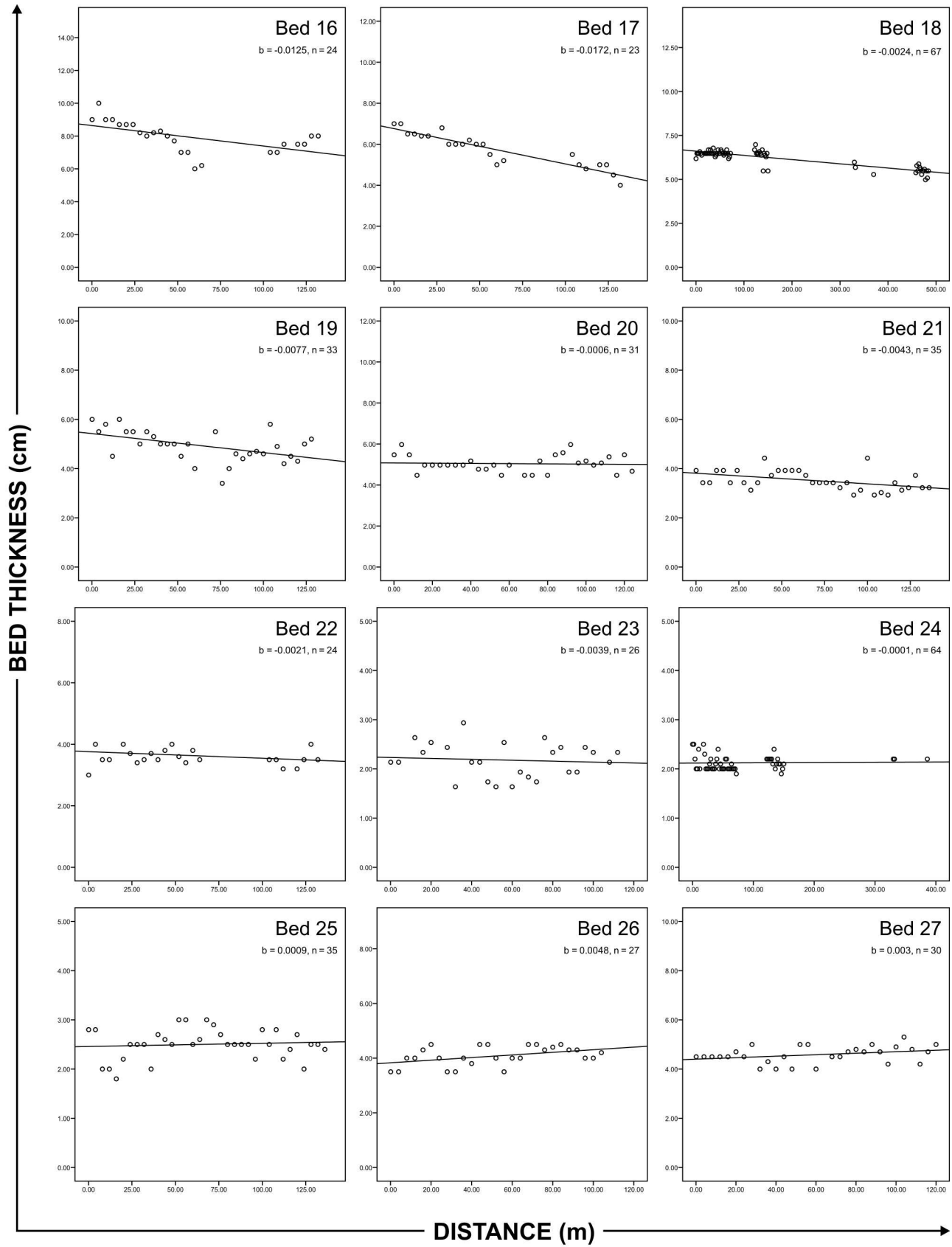
Number of measurements: 1157

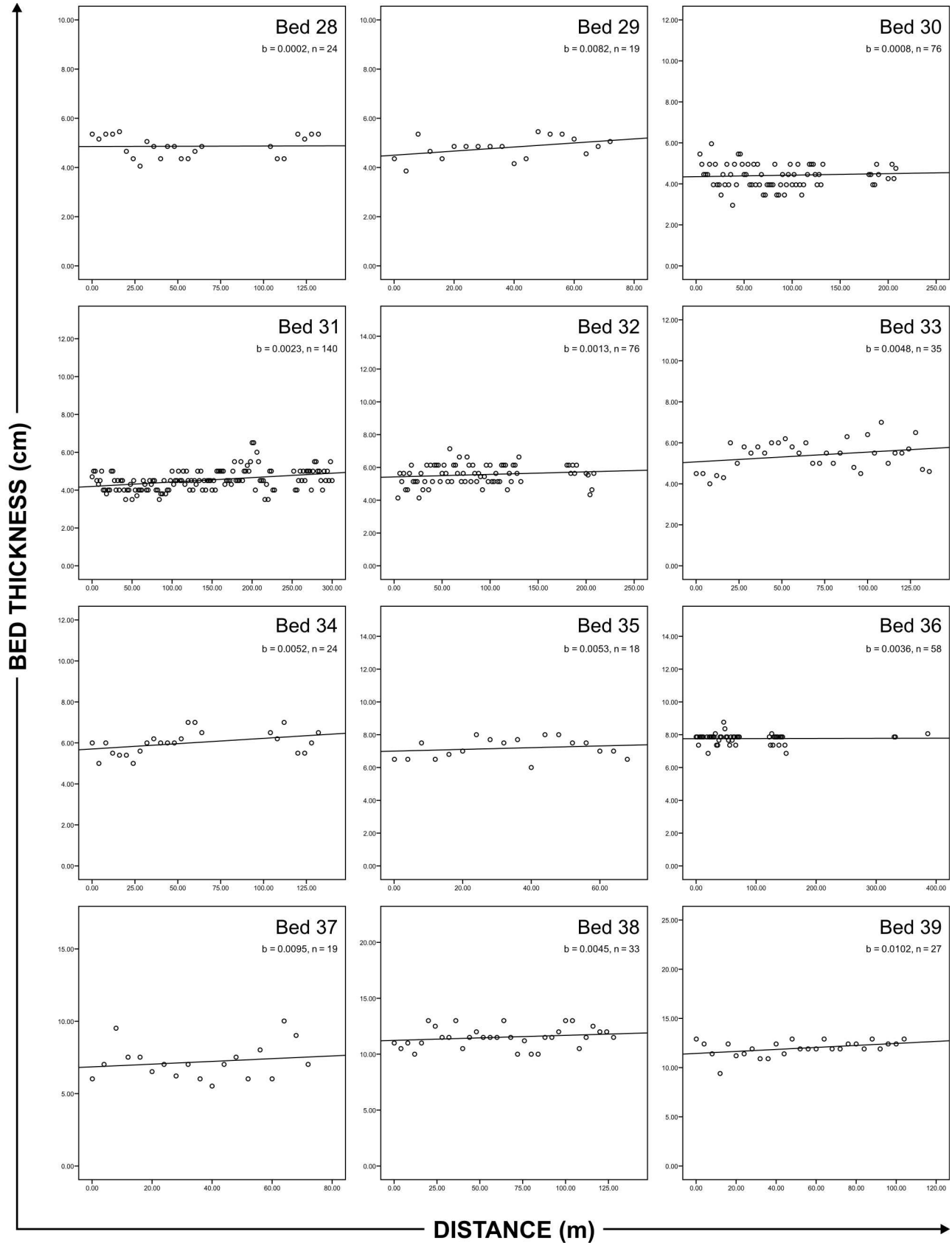


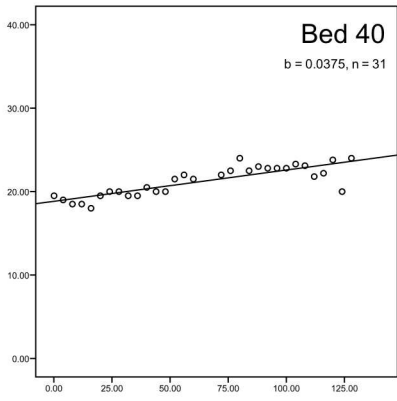
DISTANCE (m)









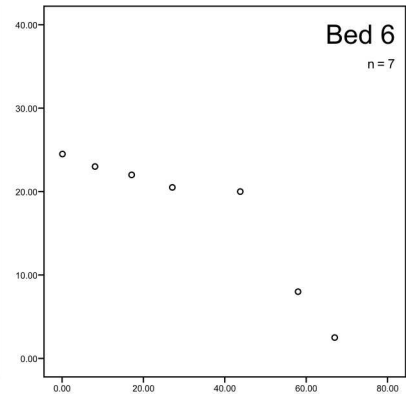
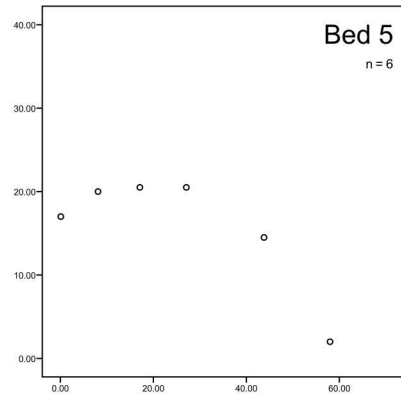
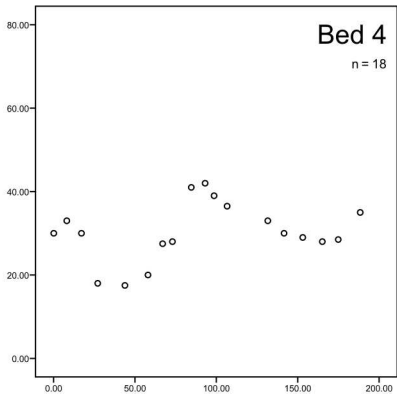
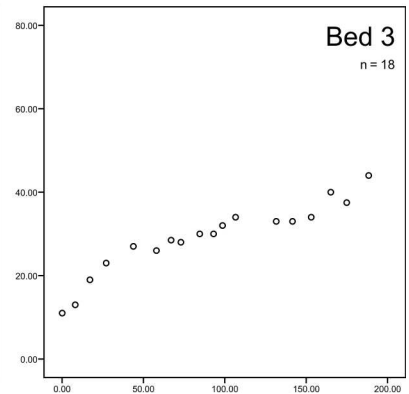
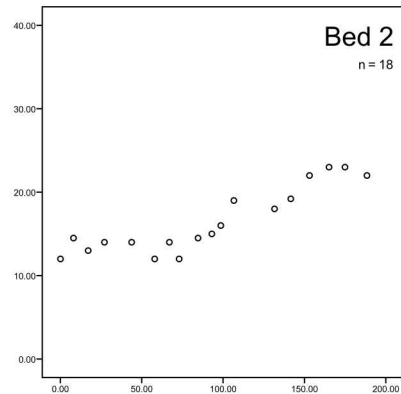
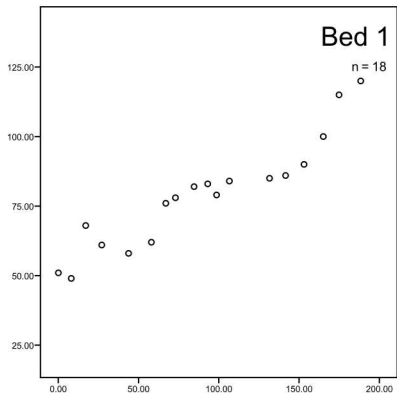


# Kusuri Formation

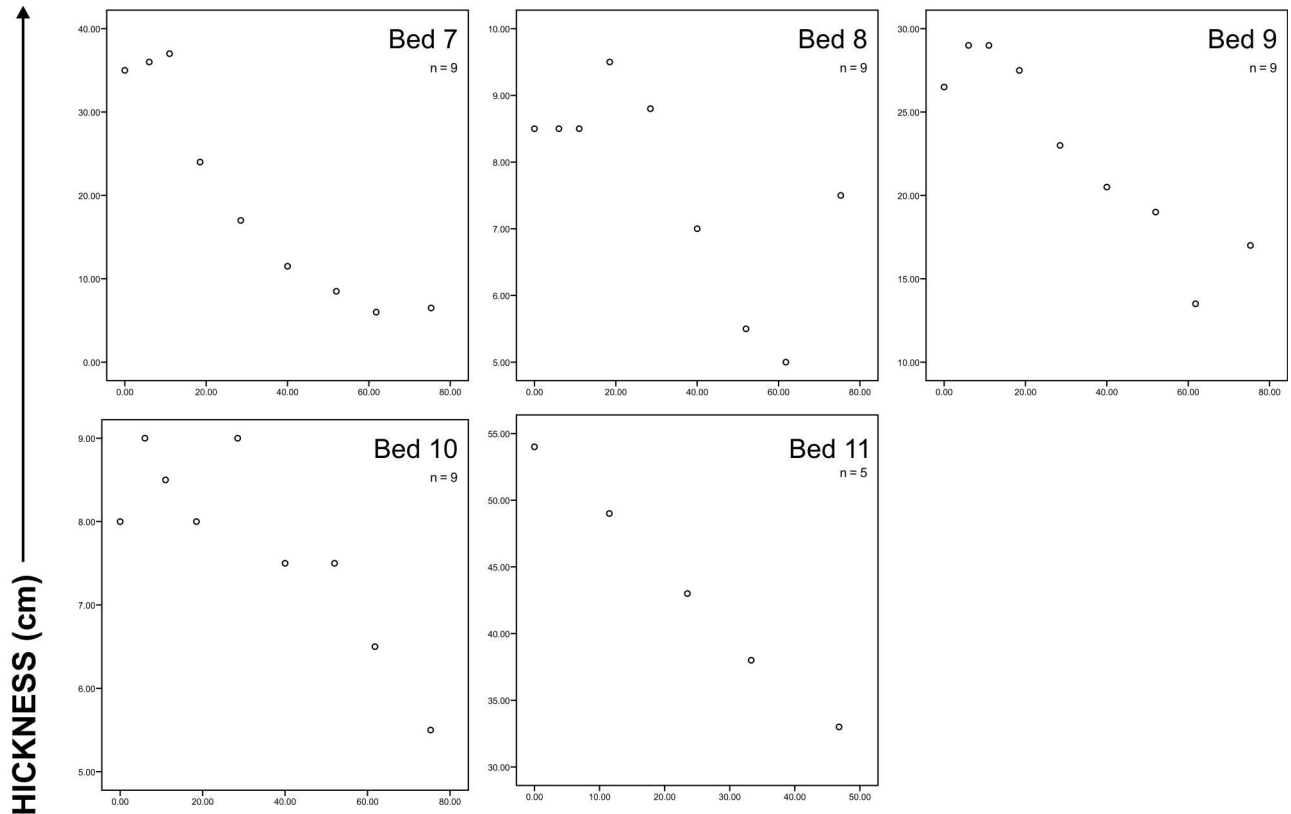
Beds measured perpendicular to depositional dip

Number of beds: 11  
Number of measurements: 126  
Beds follow nonlinear trends

BED THICKNESS (cm)



DISTANCE (m)



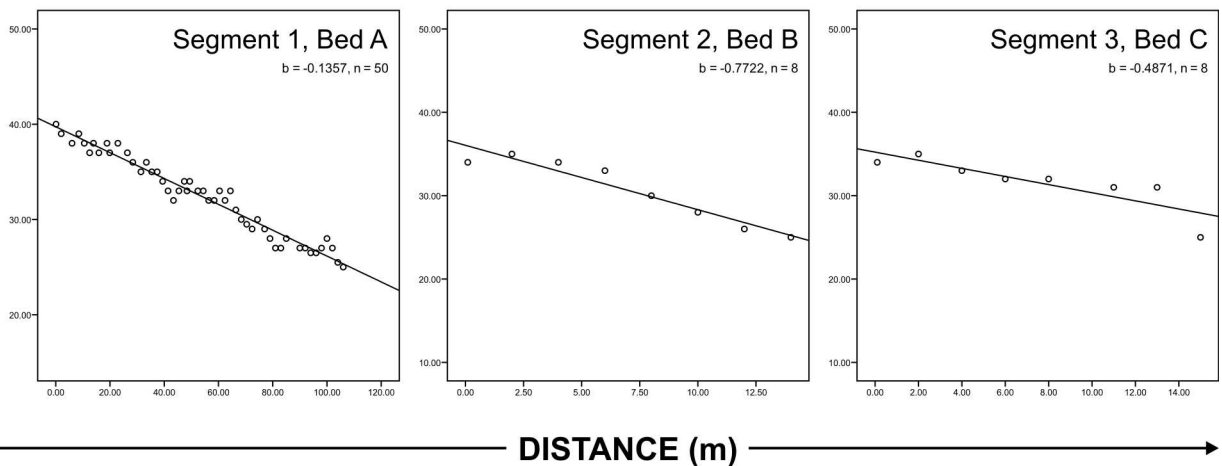
## Karpuzçay Formation

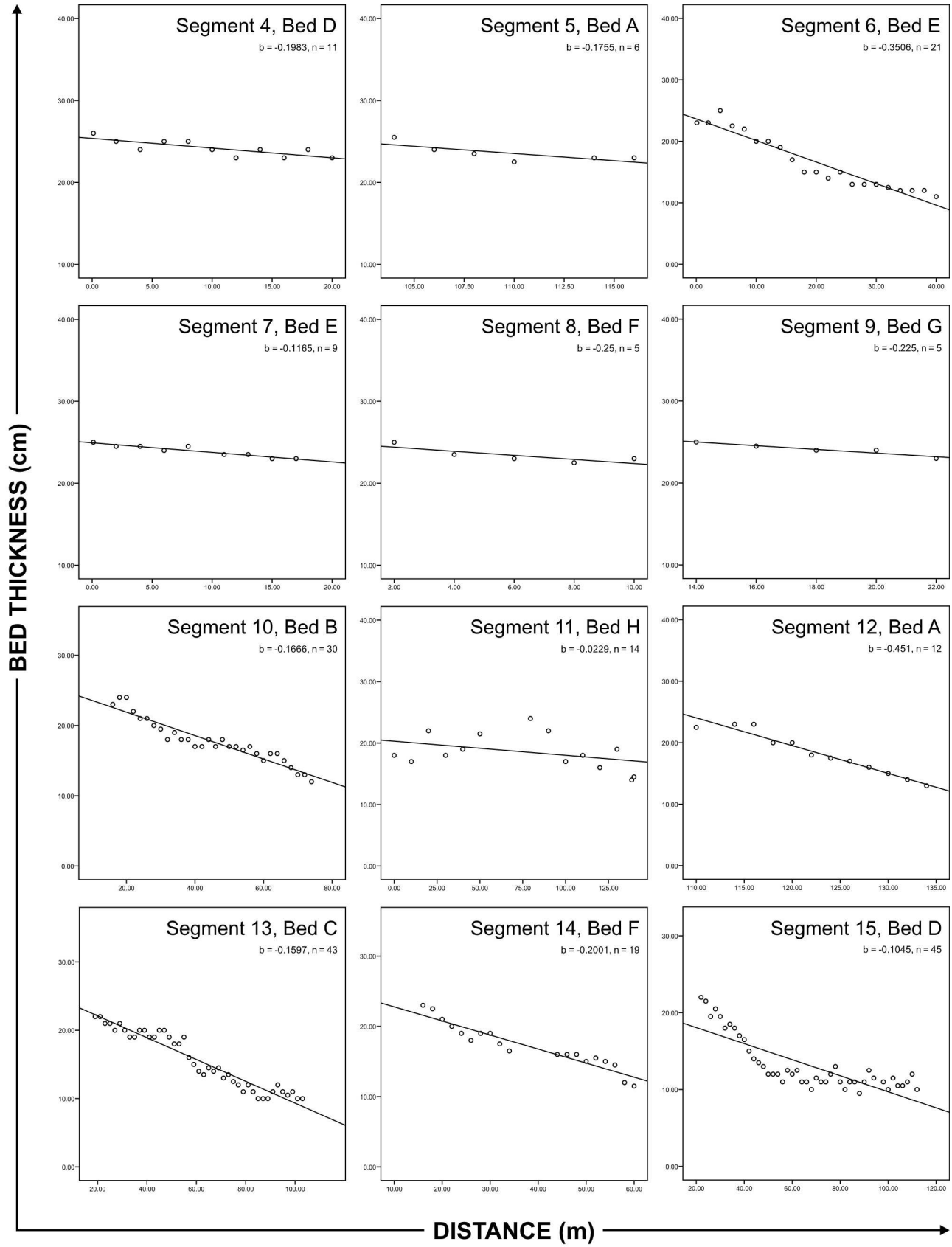
Beds measured parallel to depositional dip

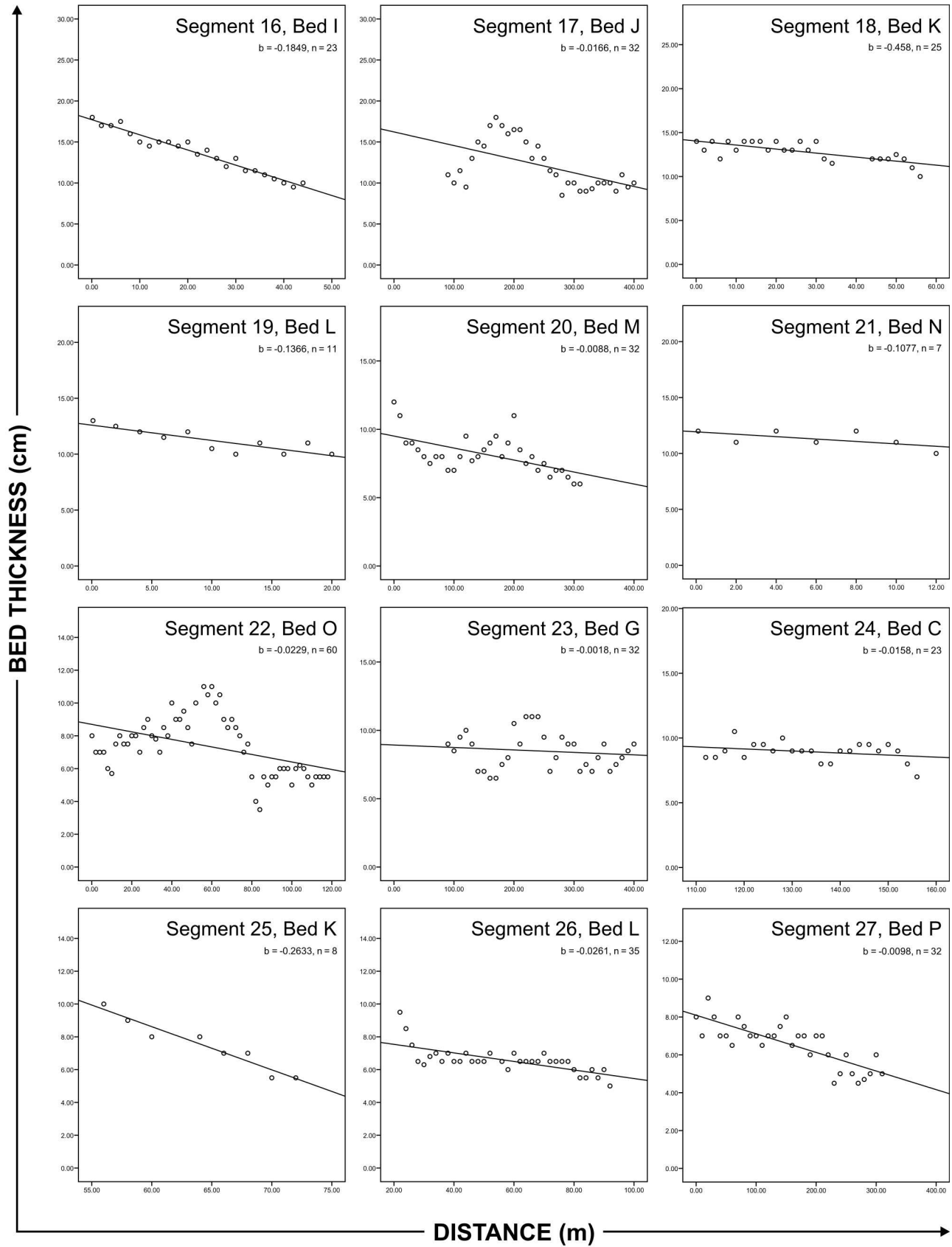
Number of beds: 21

Number of measurements: 637

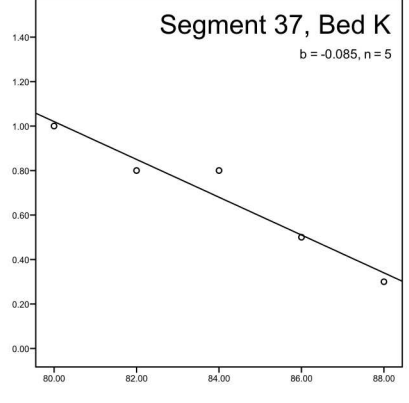
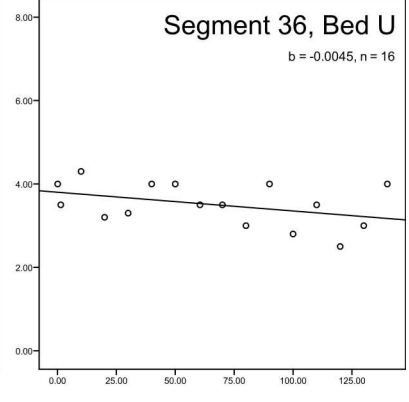
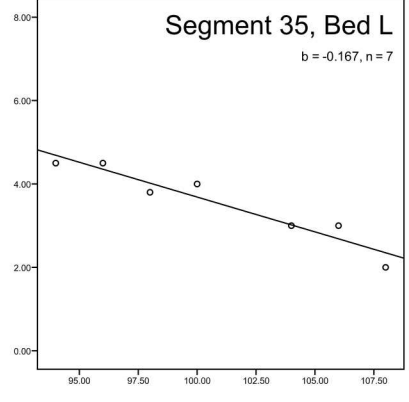
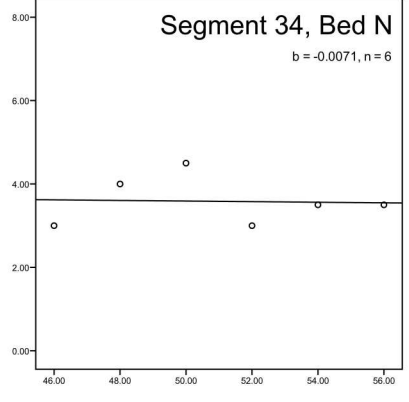
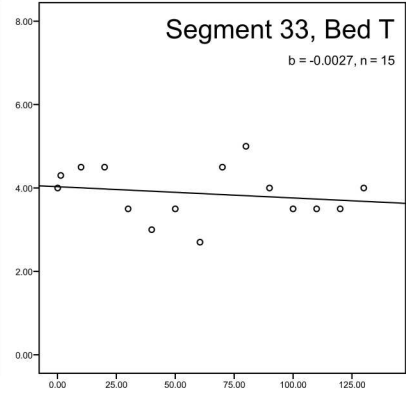
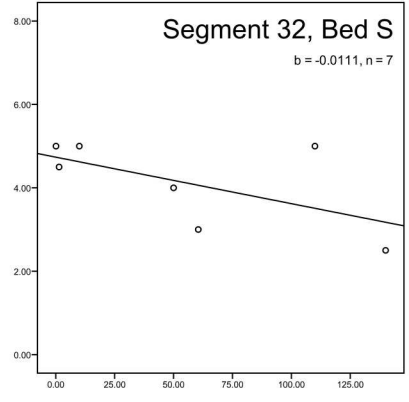
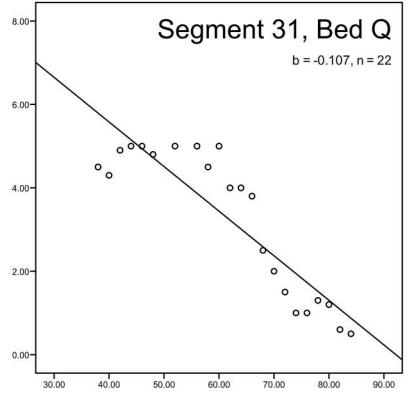
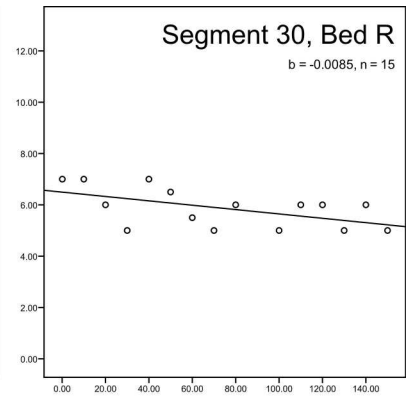
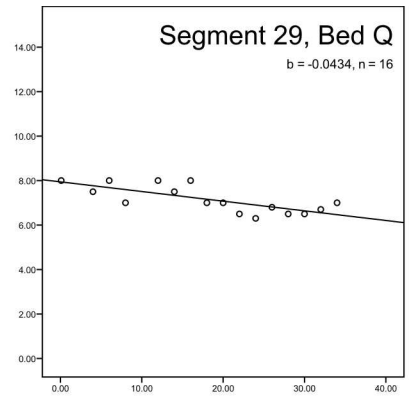
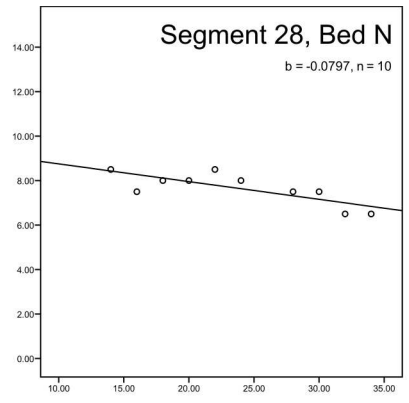
Beds have been segmented due to spanning a wide range of thicknesses - see section 10.2.3. for further explanation. Segment numbers correspond to those given in Fig. 45; capital letters denote beds from which the segments are derived.







BED THICKNESS (cm)



DISTANCE (m)